A CALIBRATION METHODOLOGY FOR ENERGY DISPERSIVE X-RAY FLUORESCENCE MEASUREMENTS BASED UPON SYNTHETICALLY GENERATED REFERENCE SPECTRA

A Thesis
Presented to
The Academic Faculty

by

Rutchanee Gullayanon

In Partial Fulfillment
of the Requirements for the Degree
Doctor of Philosophy in the
School of Electrical and Computer Engineering

Georgia Institute of Technology
December 2011

A CALIBRATION METHODOLOGY FOR ENERGY DISPERSIVE X-RAY FLUORESCENCE MEASUREMENTS BASED UPON SYNTHETICALLY GENERATED REFERENCE SPECTRA

Approved by:

Professor Thomas E. Michaels,
Committee Chair
School of Electrical and Computer Engineering
Georgia Institute of Technology

Professor George Vachtsevanos
School of Electrical and Computer Engineering
Georgia Institute of Technology

Professor Thomas E. Michaels,
Advisor
School of Electrical and Computer Engineering
Georgia Institute of Technology

Professor Gisele Bennett
School of Electrical and Computer Engineering
Georgia Institute of Technology

Professor Jennifer E. Michales
School of Electrical and Computer Engineering
Georgia Institute of Technology

Professor Massimo Ruzzene
School of Electrical and Computer Engineering
Georgia Institute of Technology

Date Approved: 12 August 2011

To my beloved grandparents ...

ACKNOWLEDGEMENTS

First and foremost, I am heartily thankful to my advisor, Prof. Thomas E. Michaels, whose encouragement, guidance, and support from the initial to the final stages of this research enabled me to develop an understanding of the subject. Throughout this research, Prof. Michaels has provided valuable advice to potential methodologies for solving problems. He has always been a wonderful mentor when I was feeling discouraged and an incredible advisor when I needed guidance. He has also been a wonderful supporter for seeking industrial sponsors for necessary samples, equipment, and information required to complete this study.

This research would not have been possible without the assistance of Dr. Martin A. Rudat (INVISTA^{TM}) who has provided essential information regarding the fluorochemical application on carpet manufacturing line, the current method of determining the fluorochemical concentration employed by the carpet industry, and information about the chemical properties of suitable taggants to be added to the fluorochemical solutions. Dr. Rudat also provided the carpet samples tagged with specific levels of taggants for use in the research.

I am grateful for Dr. Robert Shannon (Bruker AXS, Inc.) who has provided the technical support and knowledge to understand and maximize the capabilities of both XRF instruments employed in this research. This information was critical to identify optimal measurement settings required for the trace analysis of taggant constituents in carpet samples. Additionally, his information helped to indicate the limitation in which the XRF instruments could be used for on-line applications.

This project is made possible through support from NASA, Carpet and Rug Industry (CRI), and the state of Georgia, with the coordination of the support by Mr.

Lloyd Starks. NASA has provided both XRF instruments for use in the duration of this research. The CRI and the state of Georgia provided funding for the first two years of this research project.

I would like to also thank Shaw Industries, Inc. for providing the Georgia Tech research team the first-hand experience of the certified chemical burn test for determining the fluorochemical constituents on carpet fibers. Additionally, Shaw also provided an assortment of commercial carpet samples to aid in determining the factors affecting XRF measurements. In addition, J+J/Invision has kindly allowed us to observe the actual carpet manufacturing process, especially for the fluorochemical application, which enabled us to accurately evaluate potential locations for the on-line fluorochemical measurement system using XRF.

My deepest appreciation to my committee members, Prof. Jennifer E. Michaels, Prof. George Vachtsevanos, Prof. Gisele Bennett, and Prof. Massimo Ruzzene, for taking the time from their busy schedule to serve on my thesis committee and provide valuable comments on my work. Each member has provided feedback that was essential to improve the quality of this research.

Lastly, I offer my regards to my family, friends, and colleagues who supported me in many ways during the completion of the project.

TABLE OF CONTENTS

DEDICATION v

ACKNOWLEDGEMENTS vii

LIST OF TABLES xiii

LIST OF FIGURES xvii

LIST OF SYMBOLS OR ABBREVIATIONS xxiii

SUMMARY xxv

I INTRODUCTION 1

II X-RAY FLUORESCENCE (XRF) 7

2.1 XRF Principles 7

2.1.1 X-ray Scattering 9

2.1.2 Absorption 11

2.1.3 Secondary Enhancement 12

2.2 XRF Spectrum Components 13

2.3 XRF instruments 15

2.3.1 Wavelength-Dispersive X-ray Fluorescence (WDXRF) . . . 16

2.3.2 Energy-Dispersive X-ray Fluorescence (EDXRF) 18

2.4 XRF Qualitative Analysis 19

2.5 XRF Quantitative Analysis 23

2.5.1 Spectrum Analysis 24

2.5.2 Matrix Correction (Calibration) 27

2.6 Sample Preparation in XRF Calibration 31

2.7 Current Advances and Challenges in Real-time XRF Analysis . . . 33

III MEASUREMENT METHODOLOGY 37

3.1 Hardware Equipment 37

3.1.1 XRF Instrumentation 38

3.1.2 Three-axis Scanner 39
3.2 Software 40
3.2.1 Data Acquisition Software 40
3.2.2 Signal Processing Software 41
3.2.3 Automation Software 43
3.3 Sample Preparation and Chemical Taggants 44
3.4 XRF Measurement Setup 47
3.5 Preliminary Results 49
3.5.1 X-ray Tube Voltage 49
3.5.2 X-ray Tube Current 50
3.5.3 Primary Beam Filter 50
3.5.4 Measurement Time 54
3.5.5 Measurement Numbers 55
3.5.6 Other Factors 58
IV DATA ANALYSIS AND SIGNAL PROCESSING 63
4.1 Noise and LLD Analysis 64
4.2 Signal Smoothing Algorithms 66
4.2.1 Fourier Transform Method 67
4.2.2 Moving Average Smoothing Algorithm 68
4.2.3 Savitsky and Golay Polynomial Filters 70
4.2.4 Low-Statistics Digital Filter 72
4.3 Background Elimination Algorithms 77
4.3.1 Peak Stripping Method 78
4.3.2 Envelope Method 79
4.3.3 Morphological Operators 82
4.4 Peak Searching Algorithms 85
4.5 Curve Fitting Methods 86
4.6 Peak Area Determination 90

V CALIBRATION RESULTS 93
5.1 Solution Calibration 94
5.2 Carpet Calibration 102
5.3 Multiple Taggant Calibration 106
VI SYNTHETICALLY GENERATED ARTIFICIAL XRF SPECTRA . . . 111
6.1 Measurement Time 111
6.2 Primary Beam Filter 113
6.3 XRF Continuum Matching 114
6.4 Synthetic Peak Generation 120
6.5 Practical Example 123
VII RECOMMENDATIONS FOR CARPET INDUSTRY APPLICATIONS 131
VIII CONCLUSIONS AND RECOMMENDATIONS FOR FUTURE WORK 143
8.1 Conclusions 143
8.2 Recommendations for Future Work 146
APPENDIX A CHARACTERISTIC PEAK EVALUATIONS 147
APPENDIX B PERFORMANCE EVALUATION: MEASUREMENT NUMBERS 159
APPENDIX C PERFORMANCE EVALUATION: CONTINUOUS SCANS 171
APPENDIX D FLUOROCHEMICAL DISTRIBUTION ANALYSIS 177
APPENDIX E SYNTHETIC PEAK CALIBRATION PROCEDURE . . . 195
REFERENCES 203

LIST OF TABLES

1 XRF instrument comparison 20

2 Primary beam filters installed on S1 TRACeR 38

3 Rb intensity counts from Rb-tagged carpet and fluorochemical solution samples with various measurement times 56

4 Default instrument and measurement settings 61

5 Measurement settings for XRF noise analysis 65

6 Measurement noise analysis for carpet samples in Rb peak region . . 65

7 Savitsky-Golay coefficients for $r = 2$ and $r = 3$ and filter width $= 2m+1$ 71

8 Effectiveness of smoothing algorithms on an XRF spectrum 77

9 Recommended XRF signal processing algorithms for the fluorochemical concentration measurements on carpet fibers 91

10 Zn solution calibration data 96

11 ANOVA results for Zn solution calibration 97

12 Rb solution calibration data 99

13 ANOVA results for Rb solution calibration 99

14 Mo solution calibration data 101

15 ANOVA results for Mo solution calibration 102

16 Carpet calibration sample symbols 103

17 Targeted Rb and F concentration on MAR-995 series carpets 104

18 Calibration measurements for MAR-995-BMK carpets 105

19 ANOVA results for MAR-995-BMK carpet series 105

20 ANOVA results for MAR-995-3.5-LPB carpet series 105

21 ANOVA results for MAR-995-6.0-FRB carpet series 106

22 Fe aqueous solution XRF measurements 107

23 Cu aqueous solution XRF measurements 107

24 Fe-Cu aqueous solution and their corresponding XRF measurements . 108

25 Carpet density definition 121

26 Signal processing algorithms and their corresponding parameters used to generate synthetic spectra 124

27 Actual Rb concentration in stock solution and the peak counts resulting from background matched to LPB carpet 125

28 Total background intensity counts in Rb K_α region for an actual LPB carpet and the stock solution samples resulting from background matched to LPB carpet 126

29 Targeted and actual fluorochemical (F) and its translated taggant (Rb) concentration on LPB carpets using AATCC test 128

30 Performance evaluation for synthetic peak generation for MAR-995-LPB carpet series without AATCC correction 129

31 Performance evaluation for synthetic peak generation for MAR-995-LPB carpet series with AATCC correction 129

32 Recommended measurement time for fluorochemical measurements . 138

33 Recommended measurement and instrument settings for fluorochemical measurement on carpet fibers using S1 TRACeR 140

34 Cu characteristic peak in Cu-tagged aqueous solution using TRACeR II 150

35 Zn characteristic peak in Zn-tagged aqueous solution using TRACeR II 151

36 Rb characteristic peak in Rb-tagged aqueous solution using TRACeR II 152

37 Rb characteristic peak in Rb-tagged aqueous solution using S1 TRACeR 153

38 Rb characteristic peak in Rb-tagged fluorochemical solution 154

39 Rb characteristic peak in Rb-tagged MAR-995-BMK carpet series . . 155

40 Rb characteristic peak in Rb-tagged MAR-995-6.0-FRB carpet series 156

41 Rb characteristic peak in Rb-tagged MAR-995-3.5-LPB carpet series 157

42 Average relative standard deviation of the mean for carpet MAR-995-BMK series 161

43 Average relative standard deviation of the mean for carpet MAR-995-FRB series 162

44 Average relative standard deviation of the mean for carpet MAR-995-LPB series 163

45 XRF measurements from the scanning approach 172

46 Scanning measurements from carpet pairs with different concentrations 174

47 Calibration results for carpet MAR-995-BMK series 179

48 Calibration results for carpet MAR-995-FRB series 180

49 Calibration results for carpet MAR-995-LPB series 181

50 Actual Rb concentration in stock solution and the peak counts resulting from background matched to BMK carpet 195

51 Targeted and actual fluorochemical (F) and its translated taggant (Rb) concentration on BMK carpets using AATCC test 198

52 Performance evaluation for synthetic peak generation for MAR-995-BMK carpet series without correction 198

53 Performance evaluation for synthetic peak generation for MAR-995-BMK carpet series with correction 199

54 Actual Rb concentration in stock solution and the peak counts resulting from background matched to FRB carpet 199

55 Targeted and actual fluorochemical (F) and its translated taggant (Rb) concentration on FRB carpets using AATCC test 201

56 Performance evaluation for synthetic peak generation for MAR-995-FRB carpet series without correction 201

57 Performance evaluation for synthetic peak generation for MAR-995-FRB carpet series with correction 202

LIST OF FIGURES

1 XRF generation diagram 8

2 XRF transition energy diagram 10

3 XRF interaction at the sample level 11

4 Major components in a typical XRF spectrum 13

5 Example of characteristic peaks from two elements that interfere with each other 21

6 Example of a small characteristic peak of Zr in an EDXRF spectrum with a large background continuum 22

7 Matrix correction algorithms for XRF 28

8 Signal processing functions within Matlab XRF GUI program 42

9 Database function in Matlab XRF GUI program 42

10 Calibration function in Matlab XRF GUI program 43

11 Liquid, filter paper, and carpet samples ready for XRF measurements 47

12 XRF instrumentation bench top setup for analysis of small samples . 48

13 XRF instrumentation setup for real-time carpet analysis 49

14 Effect of primary beam filter for Al(38μm) 51

15 Effect of primary beam filter with Al(38μm) on an actual carpet sample spectrum 52

16 Effect of primary beam filter for Al(300μm) and Ti(25μm) 53

17 Effect of primary beam filter with Al(300μm) and Ti(25μm) on an actual carpet sample spectrum 53

18 Rb peaks detected for different measurement times 55

19 Measurement time vs. Rb peak intensity 57

20 Performance comparison for Rb-tagged BMK carpets 57

21 Performance comparison for Rb-tagged 3.5-LPB carpets 58

22 Performance comparison for Rb-tagged 6.0-LPB carpets 59

23 Performance comparison for 100ppm Rb from various carpet types . . 60

24 Effect of Fourier transform and lowpass filter with cutoff frequencies=0.05, 0.10, and 0.15 Hz 69

25 Effect of the moving average filter channel $2m + 1$ on noise reduction and peak distortion 70

26 Effect of the Savitsky-Golay polynomials smoothing algorithms with polynomial degree = 2, 3 and channel width = 3, 5, 10, 25 channels . 72

27 Effect of the low-statistics digital filters with channel width (f)=3, 5, 10, 25 and M=10, A=75, and r=1.3 74

28 Effect of the low-statistics digital filters with base degree (M)=5, 10, 15 and f=5, A=75, and r=1.3 74

29 Effect of the low-statistics digital filters with cut-off (A)= 50, 75, 100 and channel width=5, M=10, and r=1.3 75

30 Effect of the low-statistics digital filters with slope sensitivity (r) = 0.5, 1.0, 1.3, 1.8 and channel width=5, M=10, A=75 75

31 Comparison of smooth spectra resulting from Fourier transformation, moving average, Savitsky-Golay polynomials, and low-statistics digital filter 77

32 Effect of the peak stripping method with neighbor distance (w) = 1, 3, 5, and 10 80

33 Effect of the peak stripping method with the number of iterations = 100, 500, 1000, and 2000 80

34 Effect of background elimination algorithm using the envelop method with window channel width m = 50, 100, 200, and 500 82

35 Effect of background estimation using morphological operators with data structure segment S = 5, 10, 25, and 50 84

36 Result from applying a top-hat filter to a smoothed XRF spectrum for peak identification 87

37 Fitted Gaussian peak for a Rb K_α peak from a carpet sample 89

38 Location for Zn, Rb, and Mo characteristic peaks on an XRF spectrum 94

39 Zn solution calibration XRF spectra 95

40 Zn solution calibration XRF spectra (Zoomed view) 96

41 Zn solution calibration curve 97

42 Rb solution calibration spectra 98

43 Rb solution calibration spectra (Zoomed view) 98

44 Rb solution calibration curve 99
45 Mo solution calibration spectra 100
46 Mo solution calibration spectra (Zoomed view) 101
47 Mo solution calibration curve 102
48 Secondary enhancement and absorption effects between Fe and Cu . . 109
49 Measured and synthetic XRF spectra for 200 ppm Rb solution for various measurement times 112
50 Error Residuals for 200 ppm Rb solution for measurement time factor 113
51 Synthetic spectra generated for Filter No. 1 (300 μm Al and 25 μm Ti) using H_2O sample 115
52 Synthetic spectra generated for Filter No. 3 (200 μm Al 25 μm Ti 75 μm Cu) using H_2O sample 116
53 Synthetic spectra generated for Filter No. 5 (38 μm Al) using H_2O sample 117
54 XRF spectra obtained from various samples characteristics 118
55 Synthetic MAR-995-BMK spectrum generated from water solution . . 119
56 Synthetic Shaw spectrum generated from 100ppm Rb-tagged fluorochemical solution 119
57 Comparison for characteristic peaks obtained from three 50ppm Rb-tagged carpet types 120
58 Synthetic spectra generated from the BMK carpet sample as reference to match the FRB and LPB carpet series 122
59 Results from matching Rb-tagged fluorochemical samples to the blank LPB carpet 125
60 Synthetic and actual Rb K_α peak from carpet and stock solution for 25 ppm Rb 127
61 Synthetic and actual Rb K_α peak from carpet and stock solution for 50 ppm Rb 127
62 Synthetic and actual Rb K_α peak from carpet and stock solution for 100 ppm Rb 128
63 XRF spectra from different carpet samples 132
64 Possible energy channel range in XRF spectra for ideal chemical taggant 133

65 Fluorochemical application and recommended XRF locations during carpet manufacturing process 135

66 Effects of all primary beam filters equipped in S1 TRACeR on a typical carpet spectrum 136

67 Effect of the measurement time on the XRF measurement accuracy . 138

68 Measurement variation with relation to measurement numbers 139

69 Fluorochemical distribution profile from spray application 140

70 Measurement numbers and measurement accuracy analysis for carpet MAR-995-BMK series with no taggant 160

71 Measurement numbers and measurement accuracy analysis for carpet MAR-995-BMK series with 25ppm Rb 164

72 Measurement numbers and measurement accuracy analysis for carpet MAR-995-BMK series with 50ppm Rb 164

73 Measurement numbers and measurement accuracy analysis for carpet MAR-995-BMK series with 100ppm Rb 165

74 Measurement numbers and measurement accuracy analysis for carpet MAR-995-6.0-FRB with no taggant 165

75 Measurement numbers and measurement accuracy analysis for carpet MAR-995-6.0-FRB with 25ppm Rb 166

76 Measurement numbers and measurement accuracy analysis for carpet MAR-995-6.0-FRB with 50ppm Rb 166

77 Measurement numbers and measurement accuracy analysis for carpet MAR-995-6.0-FRB with 100ppm Rb 167

78 Measurement numbers and measurement accuracy analysis for carpet MAR-995-3.5-LPB with no taggant 167

79 Measurement numbers and measurement accuracy analysis for carpet MAR-995-3.5-LPB with 25ppm Rb 168

80 Measurement numbers and measurement accuracy analysis for carpet MAR-995-3.5-LPB with 50ppm Rb 168

81 Measurement numbers and measurement accuracy analysis for carpet MAR-995-3.5-LPB with 100ppm Rb 169

82 Continuous scanning setup using two carpet samples with different chemical taggant to detect inconsistencies in taggant distribution (Two numbers in the parenthesis correspond to the scanning length for carpet tagged with 0 and 50 ppm of Rb, respectively) 173

83 Fluorochemical distribution profile from spray application 178

84 Fluorochemical distribution profile for carpet MAR-995-BMK series with no taggant 182

85 Fluorochemical distribution profile for carpet MAR-995-BMK series with 25ppm Rb 183

86 Fluorochemical distribution profile for carpet MAR-995-BMK series with 50ppm Rb 184

87 Fluorochemical distribution profile for carpet MAR-995-BMK series with 100ppm Rb 185

88 Fluorochemical distribution profile for carpet MAR-995-3.5-FRB series with no taggant 186

89 Fluorochemical distribution profile for carpet MAR-995-3.5-FRB series with 25ppm Rb 187

90 Fluorochemical distribution profile for carpet MAR-995-3.5-FRB series with 50ppm Rb 188

91 Fluorochemical distribution profile for carpet MAR-995-3.5-FRB series with 100ppm Rb 189

92 Fluorochemical distribution profile for carpet MAR-995-6.0-LPB series with no taggant 190

93 Fluorochemical distribution profile for carpet MAR-995-6.0-LPB series with 25ppm Rb 191

94 Fluorochemical distribution profile for carpet MAR-995-6.0-LPB series with 50ppm Rb 192

95 Fluorochemical distribution profile for carpet MAR-995-6.0-LPB series with 100ppm Rb 193

96 Results from matching Rb-tagged fluorochemical samples to the blank BMK carpet 196

97 Synthetic and actual Rb K_α peak from carpet and stock solution for 25 ppm Rb 197

98 Synthetic and actual Rb K_α peak from carpet and stock solution for 50 ppm Rb 197

99 Synthetic and actual Rb K_α peak from carpet and stock solution for 100 ppm Rb 198

100 Results from matching Rb-tagged fluorochemical samples to the blank FRB carpet 199

101 Synthetic and actual Rb K_α peak from carpet and stock solution for 25 ppm Rb 200

102 Synthetic and actual Rb K_α peak from carpet and stock solution for 50 ppm Rb 200

103 Synthetic and actual Rb K_α peak from carpet and stock solution for 100 ppm Rb 201

LIST OF SYMBOLS OR ABBREVIATIONS

A	Height of a Guassian peak, group = math.
AATCC	American Association of Textile Chemists and Colorists.
ANOVA	Analysis of variance.
AXIL	Analytical X-ray Analaysis by Iterative Least-squares.
CRI	Carpet and Rug Institute.
EDXRF	Energy-dispersive x-ray fluorescense.
FP	Fundamental parameter calibration method.
FWHM	Full width at half maximum.
IUPAC	International Union of Pure and Applied Chemistry.
LLD	Lower limit of detection.
ppm	Parts per million.
WDXRF	Wavelength-dispersive x-ray fluorescence.
XRF	X-ray fluorescence.
$\bar{I}_b$	Average background intensity.
χ^2	Objective function for least-squares curve fitting procedure.
$\chi^2_{\mathbf{NORM}}$	Normalized χ^2 for determining the goodness of fit for a fitted function.
$\hat{y}$	Estimated spectrum value.
μ_a	Mass absorption coeffifient for element a.
ρ_a	Density of material a.
ρ_{car}	Density of a carpet.
σ_b	Standard deviation of a set of XRF background measurements.
b	Width of a Gaussian peak.
c	Location of a Gaussian peak maximum.
C_n^m	Concentration of element n in sample m.
E	Energy channel (KeV).

$filt$	Primary beam filter.
$G(x)$	Gaussian peak profile.
I	X-ray intensity (counts).
I_b	Background intensity.
I_p	Characteristic peak intensity.
I_{inst}	XRF instrument source current.
P_n^m	Net peak area of the characteristic peak for element n in sample m.
t_m	Measurement time.
V_{inst}	XRF instrument source voltage.
x	Spectrum (energy) channel index.
x_a	Thickness of material a.
y	Spectrum value.
y^*	Smoothed spectrum.

SUMMARY

This research proposes a new methodology for determining the amount of fluorochemicals on carpet fibers by measuring the amount of taggant in fluorochemicals using X-ray fluorescence (XRF). Fluorochemicals, which are applied during the carpet manufacturing process, are important for their use as a soil resist and stain blocker. Currently, a chemical burn test certified by the American Association of Textile Chemists and Colorists (AATCC), referred to as AATCC test method 187-2007, is used to ensure that the proper amount of fluorochemicals has been applied. This is an off-line test, whereas an on-line test would greatly improve the efficiency of this application step during the manufacturing of carpet. However, presently no method exists to directly measure the amount of fluorine actually applied on carpet fibers in real-time on the manufacturing floor. XRF methods offer promise as one possible measurement method; however, fluorine is not directly measurable using portable XRF instruments. Thus, a taggant has to be included in the fluorochemicals that is measurable via XRF but not adverse to their intended function.

The proper choice and use of a taggant is complicated because XRF spectra are unique not only to the chemical and physical properties of the samples, but also to a specific XRF instrument and its operational settings. Further, XRF measurement accuracy depends on the physical and chemical similarities between reference and unknown samples as well as the effectiveness of the calibration and signal processing algorithms. For most XRF applications, calibration specimens are required to relate peaks in the energy spectrum to concentrations of specific elements of interest. For the carpet application, a typical set of calibration specimens would include samples with

varying tagged fluorochemical concentrations for each carpet type to be measured. However, since carpet mills typically manufacture hundreds of different carpet styles, it is not feasible to fabricate a complete set of calibration standards for all carpets that are manufactured.

Instead, this research introduces a methodology to synthetically generate reference spectra using XRF spectra from standard fluorochemical stock solution samples and from base carpet samples for each carpet type to be tested. Thus, actual, physical standards are not required for each carpet type or style. Accomplishing this is still a challenging problem because XRF spectra contain a background continuum and characteristic peaks from all the materials in the carpet fibers and backing, and spectral shapes also change with physical construction of the carpet.

This research consisted of three phases. The first phase of this research was to review XRF principles to understand different factors of XRF spectra. XRF spectra were generated and the essential interactions that contribute unique feature to its XRF spectra were studied. Then, signal processing algorithms suitable for real-time signal processing were reviewed and a recommended set of algorithms and their corresponding parameters were identified to use for the remaining part of the research. The second phase of this research studied all measurement factors that affect XRF spectra such as measurement time and the number of measurements. An appropriate set of instrument settings, including X-ray tube voltage, X-ray tube current, and primary beam filter, for potential on-line measurement use was also determined in this phase. Additionally, chemical taggant performance was also evaluated in this stage and rubidium (Rb) was identified as a potential taggant to be used to identify fluorochemical concentration. The third and last phase of this research compared accuracy of complete XRF calibration with the industry standard AATCC test to show results are an acceptable alternative to the AATCC test.

Results from this research showed that the synthetically generated XRF spectra

alone were not always sufficient to guarantee the confidence interval required by the certified AATCC test. Thus, it is recommended that for on-line implementation, burn test results should be used to create a historical data base for each carpet type to reduce margin of error for calibrations generated from the synthetic spectra. In summary, the primary contribution of this research are:

- Provided an on-line measurement tool for measuring the fluorochemical concentration on carpet samples
- Introduced a new concept of how XRF measurements can be used on unconventional types of samples, i.e. uneven texture and various characteristics, without extensive sample preparation for calibration
- Introduced an alternative methodology to the fundamental parameter method to perform XRF calibration when there is a lack of reference samples and instrument parameters are not available
- Provided mathematical models for adjusting XRF spectra based on changes in
  - X-ray tube voltage
  - X-ray tube current
  - Measurement time
  - Primary beam filter
- Demonstrated the efficacy of the synthetic spectra methodology on actual carpet samples by comparing fluorochemical concentrations deduced from XRF measurements to AATCC burn test results

CHAPTER I

INTRODUCTION

For decades, carpet manufacturers have applied fluorochemical solutions to carpet fibers to protect them from foreign substances such as stain and soil, and to extend the life cycle of their carpets. To ensure repellent properties of carpet to foreign substances, the American Association of Textile Chemists and Colorists (AATCC) has certified a chemical burn test to verify the fluorochemical content on carpet fibers. This test, however, is performed off-line and can take several hours at best when performed on-site. Many carpet manufacturers send their random carpet samples out to professional laboratories to perform this test. These off-site tests can take weeks to obtain the results. This study presents a methodology which employs X-ray fluorescence (XRF) technology to develop a near real time measurement system for actively determining the fluorochemical concentration on carpet fibers during the manufacturing process. Such a measurement system can determine the fluorochemical concentration within minutes, allowing manufacturers to effectively adjust the amount of fluorochemical solution applied to the carpets on a near real time basis.

The carpet industry has used the application of fluorochemical solutions, all of which have the same essential element, fluorine (F), to create a physical barrier against foreign substances on carpet fibers. This solution is generally applied during the carpet manufacturing process as an "after treatment," [1] (after the carpet is already dyed and sewn together and before a latex compound is applied to the back of the carpet). This "after treatment" is a continuous process that is commercially applied as either a spray or foam, and is followed by a dwell period at an elevated temperature of approximately 275°F [1] to enhance the bonding of fluorocarbon molecules with the

carpet fibers. The spray application of the fluorochemical solution is primarily used in the manufacturing of residential carpets while the foam application is mostly used for commercial carpets. Although methods developed in the research are applicable to either application method, this study mainly focuses on samples prepared using the spray application method.

Fluorochemicals are primarily applied to carpets for soil resistance. Many fluorochemicals have the benefit of providing some stain resistance, some are good for both stain and soil resistance. The fluorochemicals have to be carefully applied on carpet fibers with proper penetration depth and chemical concentration. The required fluorochemical penetration into the carpet pile decreases as the density of the carpet increases, typically covering approximately 20-50% of the carpet pile height [1]. Similarly, the quantity of fluorochemical solution applied to the carpet is also determined by the carpet density; as the density of the carpet increases, the required quantity of fluorochemicals also increases. The fluorochemical concentration on carpet fiber is a primary factor affecting the repellent capability of carpets. Too small of a amount of fluorochemical solution on the carpet fibers reduces the ability of treated carpets to repel dirt and stain. However, an excessive amount of fluorochemicals can create an undesirable condition in which the carpet fibers attract dirt and stain.

Besides the fluorochemical concentration on carpets, the stain-repellent ability of carpets also relies on factors such as the non-fluorinated segment of the fluorochemical molecule, the orientation of the fluorocarbon tail, the distribution of fluorochemicals, and the geometry of the carpet [1]. Among these factors, only the distribution and concentration of the fluorochemicals, which can be controlled by the carpet manufacturing process and measured using XRF technology, are the main focus in this study. Due to their odorless and colorless properties, fluorochemicals cannot be detected online by conventional sensors. Instead, AATCC approved a standard chemical burn test (method 187-2007) for verifying the fluorochemical concentration and distribution

on carpet fibers.

The AATCC test is performed off-line on randomly selected carpet samples. This test measures the concentration of fluorochemicals by determining the amount of elemental fluorine on the carpet fibers. This test is capable of measuring fluorine concentrations between 100-1000 parts per million (ppm)[2]. Carpet fibers are removed from the carpet sample with a scalpel or razor blade and weighed. Then, the weighed carpet fiber is burned in an oxygen combustion flask and the released hydrogen fluoride is absorbed into a sodium hydroxide solution. The fluorine content is measured as dissolved sodium fluoride at a constant pH and ionic strength using a fluoride ion activity electrode and a specific ion meter[2]. Due to the complicated procedures involved, the precision and accuracy of this test vary between different laboratories and operators.

The AATCC 187-2007 test is time-consuming. Typically, if performed at a production site, the test can be completed and the results obtained in several hours. However, due to the lack of equipment and personnel, carpet manufacturers routinely send their random carpet samples to an off-site professional laboratory, and obtaining results can take several weeks. Because of the slow response time for performing the AATCC 187-2007, a large quantity of carpets that do not meet product specifications might be manufactured and subsequently shipped to customers or installed in buildings. This is an added cost burden to the carpet mills as they often have to recall and replace defective products, and the cost can be millions of dollars each year. Therefore, carpet manufacturers desire a near real time measurement system of the fluorochemical concentration and distribution on carpet fibers.

To develop a near real time measurement system for the fluorochemical concentration and distribution on carpet fibers, research reported here utilizes XRF to determine the fluorochemical concentration during carpet manufacturing processes. XRF, a non-destructive, analytical technique that is widely used in many industries as a

process control tool, is capable of determining chemical compositions both qualitatively and quantitatively by measuring radiation characteristic to elements in the composition. During XRF measurements, the sample is irradiated by polychromatic radiation from an X-ray tube that excites the elements in the sample so that they emit radiation at specific characteristic energy levels. This secondary emitted radiation consists of several spectral lines with different wavelengths and intensities. For quantitative analysis, both the wavelength and the intensity of the emitted radiation must be measured and translated to elemental concentrations.

Due to instrument limitations, most portable XRF instruments are not capable of detecting fluorine, the essential element in fluorochemicals. As a result, fluorochemicals may be combined with a taggant, a chemical tagging material, to assist with measuring fluorochemical concentration on carpet fibers using XRF. The amount of taggant included in the fluorochemicals should be maintained at a minimum to be cost effective. However, low-concentration taggants are not easily interpreted by XRF. When properly calibrated, taggant concentration is a proxy for the fluorine level on carpet fibers, which in turn represents fluorochemical concentration, creating a possible way to measure fluorochemical concentrations on carpet fibers using XRF.

XRF measurements are sensitive to many factors, including the chemical concentration of elements, the physical properties of samples, the influence of other elements presented in the sample (also known as the inter-element effects), instrument settings, and measurement parameters. These factors can alter the recorded intensity and the overall shapes of the measured XRF spectra. Due to these sensitivities, classical calibration methodologies require calibration samples with the same physical properties as the unknown samples. Therefore, the reference sample preparation can be a time-consuming, expensive, and inconvenient part of the procedure, impeding the use of XRF as a quality control tool in carpet manufacturing and many other applications.

To minimize the number of reference samples that must be fabricated in each

calibration set, the traditional approaches studied in many publications suggest the use of fundamental parameter calibration methods that incorporate instrument parameters in the calibration equations derived from the actual physics of how XRF is generated. Although these methods are reported in many publications to be a success in performing calibration using minimal reference samples [3, 4], most of these fundamental instrument parameters are proprietary and are known only to the instrument manufacturers. Additionally, XRF manufacturers charge their customers substantial fees for their software that incorporates these instrument parameters, making XRF not an affordable measurement tool for quality control in relatively low-cost industries such as carpet manufacturing.

This research attempts to resolve this problem by establishing a methodology for XRF calibration using a minimal set of reference carpet samples without the need for any knowledge of the XRF instrument parameters. Methodology developed in this research considers the following aspects of XRF calibration and measurement: sample preparation, measurement procedures, signal processing, and XRF calibration. The sample preparation and measurement procedures recommend a set of procedures for both the reference and carpet samples as well as a set of measurement settings to obtain XRF spectra necessary for subsequent analysis. Next, the signal processing algorithms, which include generation of synthetic XRF spectral peaks from carpet samples of interest using only XRF spectra from reference samples, process and extract necessary peak area information for the calibration process. Finally, the calibration stage performs XRF calibration using information extracted from synthetic XRF spectra.

This research is expected to contribute several benefits to the XRF field, especially in the carpet industry. Among them, the main benefit is the successful development of a near real time fluorocarbon measurement system to be used in conjunction with

the traditional AATCC test for determining fluorochemical concentration and distribution on carpet fibers. With the methodology presented here, the fluorochemical concentration analysis time can be significantly reduced from hours or weeks down to a matter of minutes. As a more general contribution, this methodology can further reduce the number of reference samples that must be prepared for the XRF calibration procedure, creating more opportunities for the use of XRF in other applications where fabricating calibration samples is expensive or impossible.

CHAPTER II

X-RAY FLUORESCENCE (XRF)

First introduced in 1928 by Glocker and Schreiber by using the so-called cold excitation method that uses the radiation of an X-ray tube [5], X-ray fluorescence (XRF) determines chemical compositions of a material both qualitatively and quantitatively by measuring the characteristic radiation. The emission of the characteristic radiation for every element in the periodic table is completely independent of the type of chemical bonds which enables accurate measurements of all elements that exist in a given sample. XRF can provides a fairly uniform detection sensitivity across a large portion of the periodic table and is applicable to a wide range of concentrations, from 100% to a few ppm.

This chapter first establishes the basic knowledge of XRF, which explains the physics including the generation of XRF spectra and major characteristic of a typical XRF spectrum. Next, this chapter summarizes several signal processing algorithms suitable for performing real time analysis that can effectively extract information of interest from XRF spectra. Finally, empirical calibration techniques, which do not require any knowledge of the instrument parameters, are described. The XRF technique can be utilized to rapidly analyze sample chemical compositions without destroying the samples; however, it has several limitations, which will be discussed at the end of this chapter.

2.1 XRF Principles

As shown in Figure 1, when high-energy X-rays or gamma rays bombard onto a sample, one or more electrons from one of the inner orbital shells of the atom can be dislodged resulting in an excited atom with a vacancy in the inner orbital shell.

The ejected electron is called a "photoelectron" and the interaction is referred to as the "photoelectric effect". The atom regains stability by filling the vacancy left in the inner orbital shell with an electron from a higher energy orbital shell in the atom, releasing a fluorescent X-ray, the energy of which is equal to the characteristic radiation equivalent to the energy difference between the two orbital shells involved.

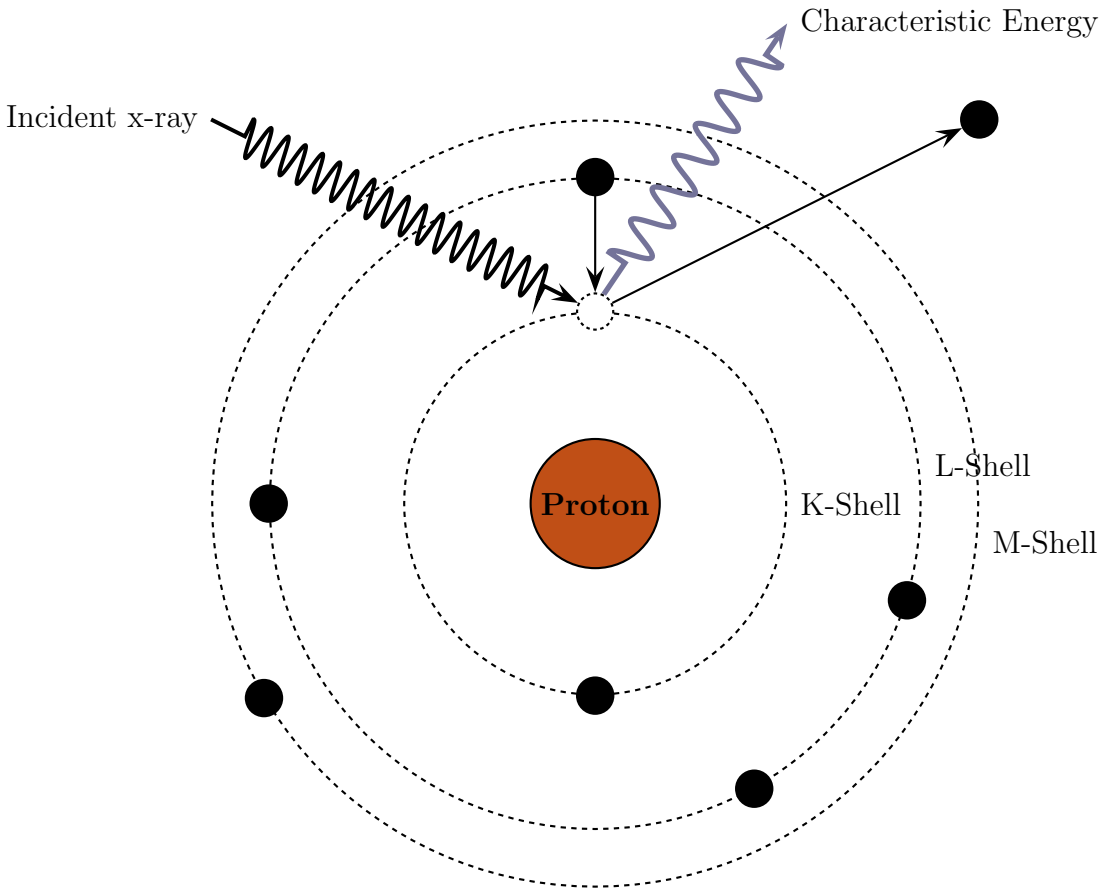

Figure 1: XRF generation diagram

Each element in the periodic table is clearly defined by its atomic number Z or by the number of its electrons in a neutral state. The binding energies or the energy levels in every element are different and unique to that element. As a result, if an electron of an inner shell is ejected by the irradiation of energy, an electron from a higher shell can fall into its vacancy by releasing an amount of energy unique to the

difference between the energy levels involved in the atom, such radiation is called the *characteristic X-rays*.

There are only a limited number of ways in which the electrons from higher energy orbitals can fill the vacancies in the lower energy orbitals. Figure 2 shows some major transitions that give rise to different types of characteristic radiation. The horizontal lines represent the energy level in the atom while the arrows show the possible transitions. The main transitions are given names: an L to K transition is traditionally called K_α, an M to K transition is called K_β, an M to L transition is called L_α, and so on. Each of these transitions yields a fluorescent photon with a characteristic energy equal to the difference in energy of the initial and final orbitals. The wavelength of this fluorescent radiation can be calculated from Planck's Law:

$$\lambda = \frac{hc}{E} \tag{1}$$

where λ and E are the wavelength and energy of the fluorescent radiation, and h and c are the Planck constant and the speed of light, respectively. A complete discussion of transition energies can be found in the article by J. A. Bearden [6].

In addition to the emission of the characteristic radiation, several other X-ray interactions also occur during the bombardment of an atom with X-rays as illustrated in Figure 3. These interactions include X-ray scattering, X-ray absorption, and secondary effects. In the following subsection, each of these interactions is described in detail. These interactions alter the overall appearance of the XRF spectrum, so it is vital to understand how these interaction occur when analyzing XRF spectra.

2.1.1 X-ray Scattering

X-ray scattering occurs when the incident X-ray collides with one of the electrons of the absorbing element. Where this collision is elastic, no energy is lost in the collision process, the scattering is said to be *coherent* (Rayleigh) scattering. Since no energy change is involved, the coherently scattered radiation will remain the same wavelength

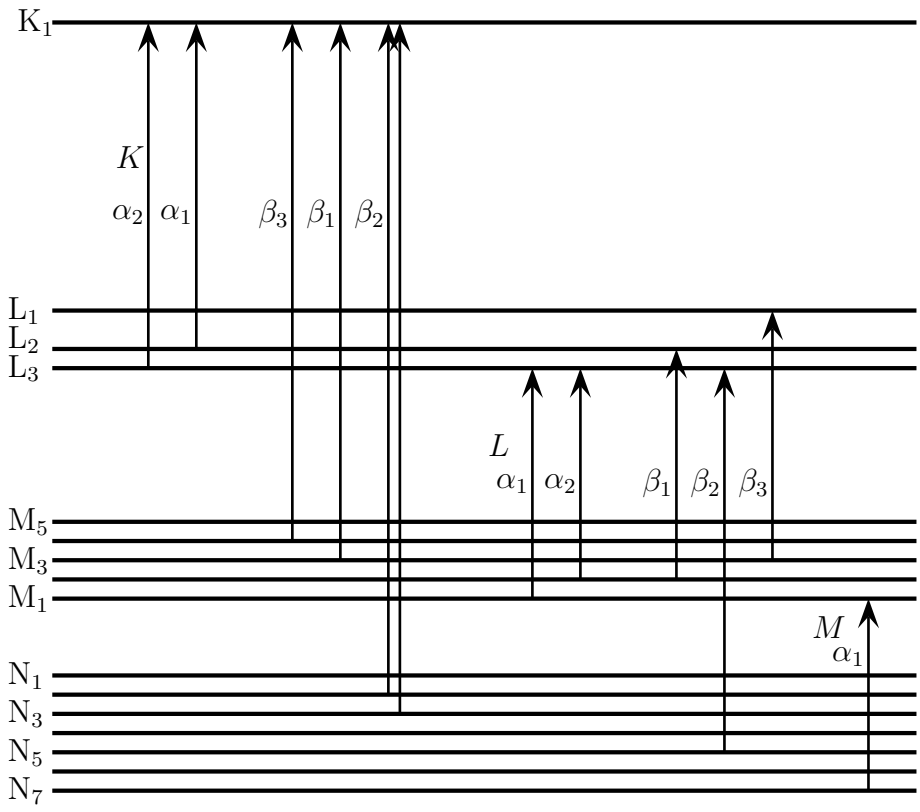

Figure 2: XRF transition energy diagram

as the incident beam. During the collision processes, the scattered photons can also give up a small part of their energy, especially where the electron with which the photon collides is only loosely bound. In this instance, the scattering is said to be *incoherent* (Compton) scattering and the wavelength of the incoherently scattered photon will be greater than the wavelength of the incident X-ray.

In many XRF sample preparation procedures, it is recommended that the analysis samples should be prepared to be as smooth as possible because an increase in roughness on the sample surface can cause an increase in Compton scattering. Because the incoherently scattered photons contain greater wavelength than the incident X-ray, they increases background continuum counts in the lower energy channels. When synthetically generating an XRF spectrum from one type of sample to apply to another,

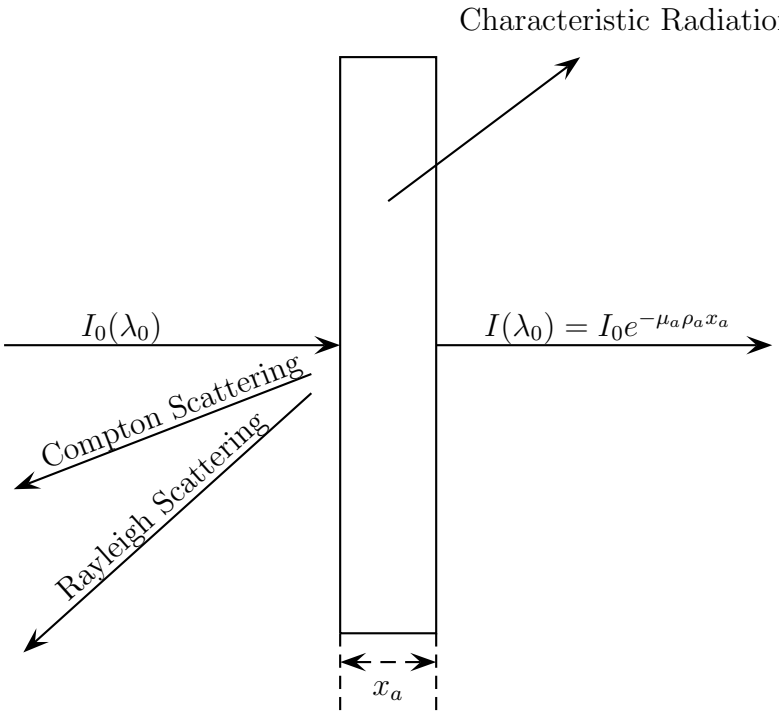

Figure 3: XRF interaction at the sample level

sample surfaces have to be considered to take into account the effects of Compton scattering.

2.1.2 Absorption

When a beam of X-ray photons falls onto a sample, it acts as an absorber and a number of different processes may occur. The more important of these are illustrated in Figure 3 and can be described as the following: when a monochromatic beam of radiation of wavelength λ_0 and intensity I_0 is incident on an sample of thickness x_a and density ρ_a, absorption occurs as a function of depth such that only a certain fraction (I/I_0) of the radiation may pass through any given thickness segment of the sample.

The probability of X-ray absorption is a function of path length through a sample

and is given by Beer's Law for X-rays [7]:

$$I(\lambda_0) = I_0 \exp^{(-\mu_a \rho_a x_a)} \tag{2}$$

where I is the X-ray intensity transmitted through a thickness x_a of a material of density ρ_a. The parameter μ_a is the mass absorption coefficient, which is a function of the atomic number (Z) and the energy (or wavelength) of the X-ray.

Studies have been done to determine the mass absorption coefficients of different materials [8]. It is worth mentioning in this section that when plotting the absorption profile (μ_a/ρ_a) against excitation energy of X-rays of an element, one can observe several sharp discontinuities in the profile. These discontinuities are referred to as the *absorption edges*. At higher energies (shorter wavelengths) than the edge, the incoming photons have enough energy to cause the ejection of orbital electrons from its shell. On the other hand, if lower energies (longer wavelength) than the edge, the photons do not have sufficient energy to cause the ejection of any electrons from that specific orbital in the atom.

2.1.3 Secondary Enhancement

During the emission of the characteristic radiation, it is possible that the first release of radiation contains enough energy to be absorbed by another element within the sample, resulting in excitation of this secondary element and a second release of characteristic radiation. This effect is called *secondary enhancement*. To initiate the excitation of a secondary element, the characteristic radiation from the first element has to be more than or equal to the absorption edge of the secondary element.

If designed wisely, the secondary enhancement can help with the detection of low-concentration taggants embedded in carpet samples. On the contrary, unwanted secondary enhancement can altered the predicted concentration of the element of interest. When choosing a chemical taggant to combine with a fluorochemical solution to apply to carpets, other elements present in carpet fibers and backings should be

considered to either avoid or take advantage of secondary effects.

2.2 XRF Spectrum Components

The X-ray interactions mentioned above contribute to the release of photoelectrons from the atoms. These photoelectrons are detected and registered in XRF instruments based on detection at specific wavelengths or energies. Figure 4 shows a typical XRF spectrum generated from a carpet with taggant applied and the stock fluorochemical solution. These spectra differ in overall shape, but both consist of four major components: characteristic peaks, a continuum of background radiation, Compton peak, and an anode target peak. To effectively evaluate XRF spectra, the phenomena associated with each component should be well understood.

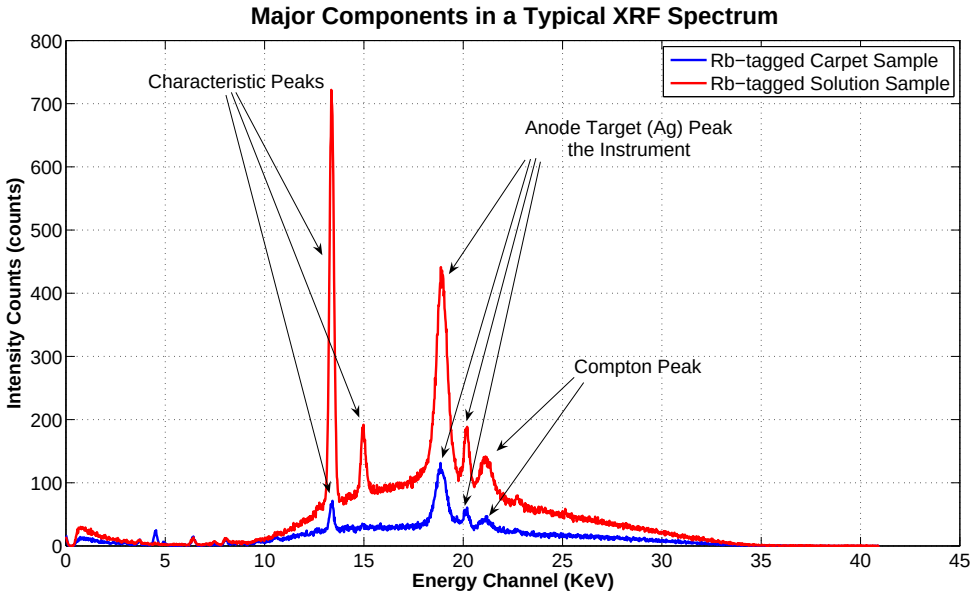

Figure 4: Major components in a typical XRF spectrum

Characteristic Peaks The characteristic peaks are the most important feature in an XRF spectrum. The intensity counts for an element's characteristic peaks can directly be translated to the chemical concentration of this element. The characteristic peak of a particular X-ray line has a Lorentz distribution [9]. The

peak profiles observed at the semiconductor detector are the convolution of this Lorentz distribution with nearly Gaussian detector response function, giving rise to what is known as Voigt profile [10]. Because the Lorentz peak width is in the order of only 10 eV for elements with atomic number lower than 50 while the width of the detector response function is in the order of 160 eV, a Gauss function is an adequate approximation of the line profile [11].

Compton Peak The Compton peak is produced from incoherent scattering of X-ray radiation from the excitation source and is present in the spectrum of every sample. Normalizing the characteristic energy peak to the Compton peak can reduce problems with matrix effects that vary among samples.

Anode Target Peak X-ray beam from a typical commercial EDXRF instrument is created by applying a high-voltage power source to a cathode and an anode materials. During this process, X-ray photons from the cathode material, which is the source of the energy electrons, strike the anode material. Some of these photons carry enough energy to eject an electron from the anode target. When these ejected electrons leave the tube, they carry the energy unique to anode target materials and when detected by the instrument detector, the energy carried by these electrons are registered as an anode target peak.

Background Continuum Aside from all the peaks mentioned above, the remaining spectra in Figure 4 are considered the background continuum. The continuum in XRF spectra are mainly a result of the coherent and incoherent scattering of the excitation radiation by the sample [9]. Therefore, the shape of the continuum can be very complex and depends both on the initial shape of the excitation spectrum and on the sample composition. In addition, the continuum can also have contributions from the deceleration of the incident X-rays due to the atomic electrons of the elements in the sample. This type of continuum is

referred to as the *white radiation* or the *Bremsstrahlung*. When using XRF for the measurements of low concentration substances, a major problem is the significant amount of incoherent scattering. Such scattering affects the detected signal in a highly variable way.

2.3 XRF instruments

Commercially available XRF instruments can be categorized into two types: energy-dispersive (EDXRF), and wavelength-dispersive (WDXRF) XRF spectrometers. Although they are similar in their operational principles, EDXRF and WDXRF are different in the technique used to measure the characteristic radiation and the intensities emitted by the fluorescent X-ray photons. While WDXRF instruments measure the wavelengths released by the X-ray photons, which is inversely proportional to their energy, EDXRF instruments directly measure the energy of the fluorescent X-ray photons. By measuring the wavelengths or the energies released by fluorescent X-ray photons, a specific element in the sample can be identified. Furthermore, for a particular energy channel of fluorescent X-rays emitted by an element in the sample, the number of fluorescent X-ray photons per unit time, generally referred to as peak intensity or count rate, can be related to the elemental concentration in the sample.

XRF instruments consist of three basic parts: the excitation source, the sample holding chamber, and the data collection and processing unit [7]. The excitation source generates primary radiation to excite the elements of the sample; this can be done a number of ways. The most straight forward and safest approach is irradiation using X-rays from an X-ray tube [12] where a high voltage is applied between a heated cathode (i.e. a filament) and a suitable anode material. Electrons in the tube accelerate from the heated cathode material and strike the anode to produce X-rays. The sample holding chamber holds the specimen in a precisely defined position during analysis with respect to the X-ray source and a detector. This unit is more critical

in the case of WDXRF where the specimen presentation unit sets proper angles for the detection mechanism. The data collection and processing unit is responsible for counting the X-ray photons of various wavelengths or energies detected from the sample.

2.3.1 Wavelength-Dispersive X-ray Fluorescence (WDXRF)

Wavelength-dispersive spectrometers are constructed based on Moseley's law, showing that the reciprocal of the wavelength of a characteristic radiation for any given element is directly related to the square of the atomic number [9],

$$\frac{c}{\lambda} = k(Z - \sigma)^2, \tag{3}$$

Where c is the speed of light, λ is the wavelength, Z is the atomic number, k is a constant for a particular spectral series, and σ is a screening constant for the repulsion correction due to other electrons in the atom. These wavelengths are well documented for all elements in the periodic table [13]. By measuring the wavelengths of the characteristic radiation, one can infer the atom from which it originated.

WDXRF analyzers use an X-ray source to excite a sample. X-rays that have wavelengths that are characteristic to the elements within the sample and are emitted in all directions. A single material crystal or other diffraction device is placed in the way of the X-rays coming off the sample. An X-ray detector is position where it can detect the X-rays that are diffracted and scattered off the crystal. Depending on the spacing between the atoms of the crystal lattice, the diffractive device, and its angle in relation to the sample and detector, specific wavelengths directed at the detector can be controlled. The angle can be changed in order to measure elements sequentially, or multiple crystals and detectors may be arrayed around a sample for simultaneous analysis.

The main difference between WDXRF and EDXRF is in the detection mechanism. In WDXRF, the X-ray energies are separated by means of a diffracting crystal and a

detector that are placed in positions complying with Bragg's law of diffraction [7]:

$$n\lambda = 2d\sin(\theta) \tag{4}$$

where λ is the wavelength, d is the spacing of the layers in the analyzing crystal, and θ is the incident angle of the photons. The layers of the analyzing crystal act like weak reflecting mirrors for the X-rays. Only if the path difference of the relected X-rays is a whole number of wavelengths does constructive interference occur. The placement of the analyzing crystal is either by turning of a goniometer, measuring the energies one after the other (sequential) or in fixed positions, measuring the energies all at the same time (simultaneous). In a sequential WDXRF spectrometer, the crystal is turned and the spectrum is measured sequentially, scanning the wavelengths by changing the 2θ angle. In a simultaneous WDXRF spectrometer, one or more detectors are placed at the certain angle for an element, and so it is possible to measure different elements simultaneously. In both cases, the elements and their concentration are identified by the spectral intensities.

Typically, WDXRF spectrometers can provide working resolutions between 5 eV and 20 eV depending on the instrument design [9]. The higher resolution of WDXRF provides advantages in reducing spectral overlaps and background noise. As a result, complex samples can be more accurately characterized with increased detection limit and sensitivity. However, the additional optical components of a WDXRF system, especially the diffraction crystal and collimators, means that it suffers from greatly reduced efficiency. Typically this is compensated for by high powered X-ray sources, which can have a significant impact on cost and ease of use. The additional optical components of WDXRF also effect the cost, and make for WDXRF a relatively expensive instrument.

2.3.2 Energy-Dispersive X-ray Fluorescence (EDXRF)

In contrast to WDXRF, EDXRF spectrometers are relatively simple and inexpensive. However, the lower limit of the working resolution typically ranges from 150 eV to 300 eV, depending on the type of detector employed in the instrument [9]. In an EDXRF spectrometer, the incident X-ray photons interact to produce a specific number of electron hole pairs based upon Moseley's law. The charge produced is collected by the detector to produce a voltage pulse proportional to the original X-ray photon energy. Thus, when a range of photon energies are incident upon the detector, an equivalent range of voltage pulses is produced at the detector output. These voltage pulses are then sorted through to produce a histogram representation of the X-ray energy spectrum.

EDXRF instruments use the proportional characteristics of a suitable detector to produce a distribution of voltage pulses proportional to the spectrum of photon energies from the sample. Early EDXRF spectrometers employed gas proportional counters and scintillation as a means of detecting and processing energy emitted from the X-ray photons. However, they had limited counting capacity and, hence, this initially limited the use of EDXRF based instruments. It wasn't until the 1960's and early 1970's that electronics had developed to the point that high-resolution detectors, such as lithium drifted silicon, Si(Li), could be made and installed in commercial devices. Computers are also a necessity to collect and process data from EDXRF detectors. With an EDXRF system, an entire spectrum is acquired virtually simultaneously, so that elements from across most of the periodic table can be detected within a few seconds.

Unlike WDXRF, the EDXRF excitation source is often optimized to increase the overall peak-to-background count ratio. Filters made of various elements may be placed between the source and sample to increase the excitation of the element of interest or reduce the background in the region of interest. The X-ray source utilized

in EDXRF spectrometers to excite the sample can be configured in one of two ways. The first way is direct excitation where the X-ray beam is pointed directly at the sample. The second way uses a secondary target, where the source points at the target, the target element is excited and fluoresces, and then the target fluorescence is used to excite the sample. There are several ways to improve the performance of EDXRF instruments including the selection of tube anode material, variation of tube voltage, use of primary beam filters, and the use of secondary targets. The selection of the tube anode material is typically chosen at the time of the instrument purchase in view of a specific intended application.

The major differences between WDXRF and EDXRF spectrometers shown in Table 1 are a good guideline to select the appropriate XRF instrument type for a particular application. In the near-real-time measurements of fluorocarbon content on carpet fibers, EDXRF instruments are selected for their inexpensive, multi-element analysis, and fast measurement capabilities. The two most important factors in selecting the XRF spectrometer are the cost and the portability of the system. Due to the relatively low cost of products manufactured in the carpet industry, the instrument chosen should not add a large component to the manufacturing cost. Furthermore, the system should be portable to permit moving it across the manufacuting floor to acquire measurements from different locations.

2.4 XRF Qualitative Analysis

The main objective in the XRF qualitative analysis is to be able to identify whether an element is present or not in a sample to a high degree of certainty. When performing the qualitative analysis on an XRF spectrum, the main objective is to be able to detect any characteristic peaks present in the sample above the background. To achieve this, the acquired XRF spectrum is first processed to reduce measurement noise. Then, the background continuum is removed to expose any small characteristic peaks. Finally,

Table 1: XRF instrument comparison

Category	EDXRF	WDXRF
Resolution	Low (150 - 300 eV)	High (5 - 20 eV)
Spectral Overlap	High	Low
Background Continuum	High	Low
Source (Energy) Efficiency	Low	High
Excitation Efficiency	High	Low
Scanning Speed	Fast	Slow
Number of Elements measured at a time	Multiple	Single
Price	Cheap	Expensive
Portability	Portable	Desktop Units

a peak search process is used to locate and evaluate the peak for legitimacy [14]. This is considered a crucial process in detecting small characteristic peaks embedded in a noisy count background. All of these signal algorithms will be discussed in detail in Chapter 4.

In the EDXRF qualitative analysis, two challenges arise due to the nature of the instrument. The first challenge that results directly from low resolution detectors is peak interference, which alter the overall peak appearance. The second challenge is the presence of a high background continuum in EDXRF spectra, which prevents the detection of small characteristic peaks from low concentration elements. An example of peak interference is shown in Figure 5, where the characteristic peaks of two elements are partially overlapped, causing the height and width of each peak to alter. Peak interference can result in one broader peak instead of two individual peaks, making it impossible to detect individual elements. Many research studies in EDXRF address the peak interference problem at the signal processing stage [14, 15]; however, characteristic peaks present in a typical carpet sample are well separated. This is because carpet samples, which contain mostly carbon-based materials, have a limited number of elements above the detection range lower limit of the EDXRF instrument used in this study, i.e., atomic number 22 (Ti). As a result, characteristic peaks

typically present in a carpet sample are well separated such that peak interference is usually not a major concern.

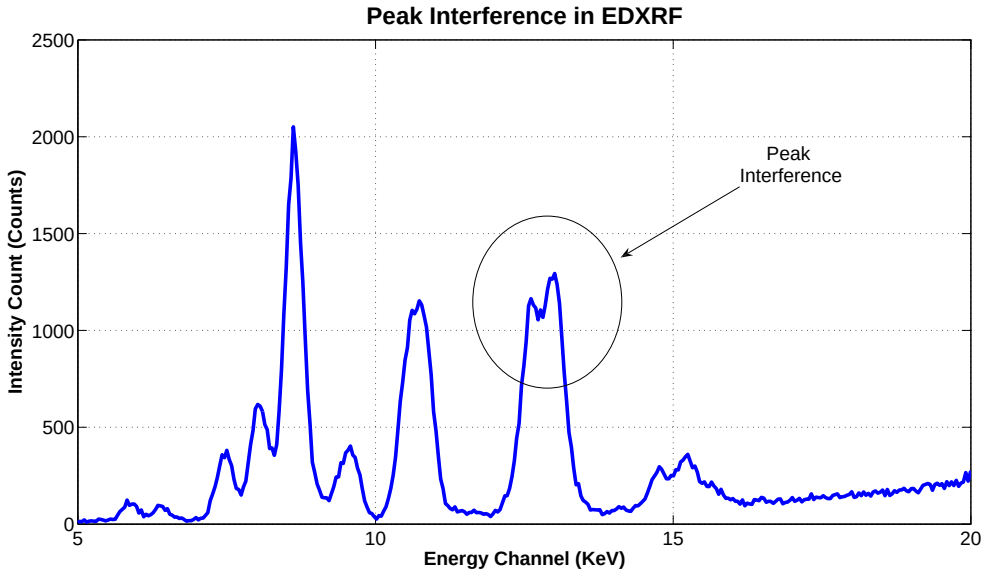

Figure 5: Example of characteristic peaks from two elements that interfere with each other

The presence of a large background continuum in XRF spectra can conceal small characteristic peaks, and as a result, this limits the minimum concentration of taggant that can reliably detected. Figure 6 illustrated a characteristic peak of a 20 ppm of Zirconium (Zr) in a carpet sample. The height of this characteristic peak is very similar to those from measurement noise surrounding it, making this peak difficult to be detected both by visual examination or by using a peak search algorithm. Such challenges directly impact this study since the lowest taggant concentration corresponding to the smallest peak detectable determines the minimum standard amount of chemical taggant the manufacturer is required to add to the fluorochemical solution.

To calculate the minimum chemical concentration detectable by a particular XRF instrument, this study will refer to the expression "Lower Limit of Detection"(LLD), which is used in XRF literature to refer to the lowest net peak intensity of an element

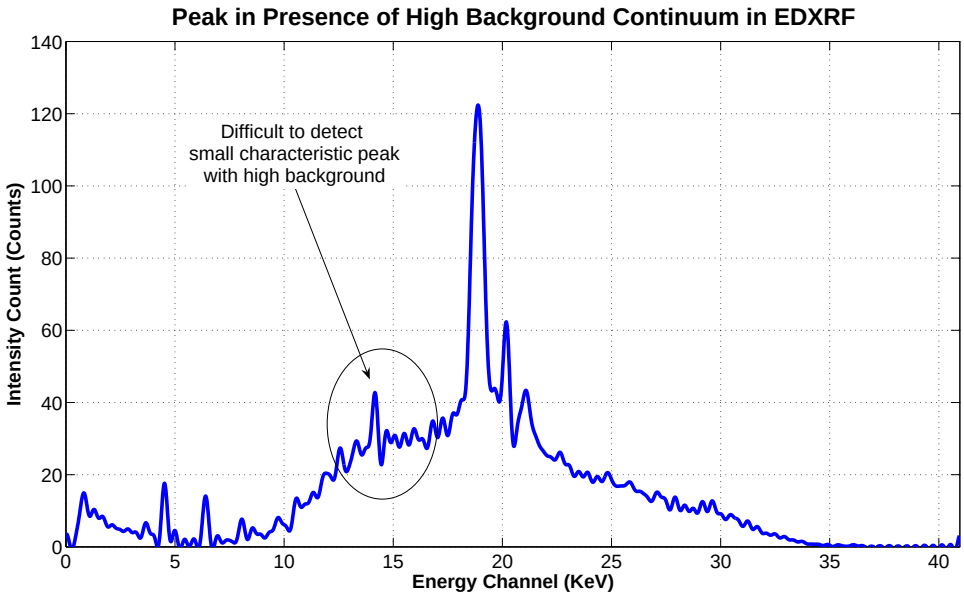

Figure 6: Example of a small characteristic peak of Zr in an EDXRF spectrum with a large background continuum

that can be detected by an XRF spectrometer to a 3 sigma confidence level, which is the standard employed by most manufactures and recommended by IUPAC [16]. In practice, a set of XRF measurements from a blank sample are acquired and processed to determine the corresponding average background intensity, $\bar{I}_b$, and the counting errors, σ_b. Assuming that the counting statistics follow a Gaussian distribution, the LLD measurable from a specific sample is 3.0 sigma (99.7%) above the average background count intensity when

$$LLD = \bar{I}_b + 3.0\sigma_b. \tag{5}$$

Thus, for a characteristic peak of intensity I_p to be considered significant, the minimum peak intensity has to be

$$I_p \geq \bar{I}_b + 3.0\sigma_b. \tag{6}$$

2.5 XRF Quantitative Analysis

Quantitative XRF analysis provides a means of mapping the measured XRF spectra to the actual chemical composition of the sample. When a sample that contains element A is irradiated by a primary X-ray source, fluorescent X-rays from element A are generated. The intensity of these fluorescent X-rays is dependent on the concentration of element A in the sample. The higher the concentration of element A, the higher will be the count intensity in its corresponding energy channel. Thus, if the fluorescent X-ray intensity and concentration of an element contained in a standard sample are both known, then a calibration can be established to determine the concentration of element A from its fluorescent X-ray count intensity. Obtaining this calibration function is the main objective of all quantitative XRF analysis methods.

Quantitative analysis has traditionally entailed a two-step process: spectrum analysis and matrix corrections. The spectrum analysis is used to eliminate unwanted background noise and extract the net peak area and intensity of spectra peaks from elements present in the sample. Next, these peak area and intensity results, from a collection of reference samples, are used in a matrix correction algorithm to resolve any peak interferences and to determine the relationship between net peak areas for each element and their corresponding chemical concentrations. This matrix correction algorithm is essentially the final calibration for relating XRF spectral results to elemental concentrations present in the sample.

Since the late 1980's, several research studies have been published on automated XRF spectrum analysis algorithms. The intent has been to develop software to assist technicians in XRF quantitative analysis. For example, the QXAS software developed by the International Atomic Energy Agency (IAEA) uses an Analytical X-ray Analysis by Iterative Least-squares (AXIL) method, in which the net peak information is obtained by fitting measured spectra with mathematical functions tailored to specific elements using a nonlinear least-squares strategy [17]. In 1998, SAX (Software for the

Analysis of XRF spectra) was developed to improve upon the QXAS software when peak overlap conditions were encountered, by using an empirical energy-dependent peak-shape function to resolved overlapped spectra peaks [18]. Other software systems, such as XRFAES [15] and AXIS [19], were developed to address secondary enhancement and absorption issues, for which a fundamental parameter method was used. Since each of these automated XRF spectrum analysis systems address different sample and spectrum conditions, none of these perform perfectly in all scenarios [17, 18]. Generally, for a specific application, appropriate algorithms and software must be carefully selected by an experienced operator to obtain optimum calibration results.

2.5.1 Spectrum Analysis

Spectrum analysis is especially critical in EDXRF compare to WDXRF because of the relatively low resolution of the solid-state detectors employed. As a result, many signal analysis algorithms published in this field focus on analyzing data obtained from energy-dispersive instruments [9]. Spectrum analysis can be divided into four steps: (1) spectrum smoothing, (2) background elimination, (3) peak search methods, and (4) net peak area determination. Each step plays a vital part in extracting important information from XRF spectra. The accuracy of an XRF measurement greatly depends upon the skill of the operator in selecting the optimum set of signal analysis algorithms for each of the above steps.

2.5.1.1 Smoothing Algorithms

The goal of most smoothing algorithms is to maximize signal intensity by reducing the background noise level. This process is generally achieved by reducing individual data points that may be associated with background noise. Specifically, points that are higher than immediately adjacent points. This reduces noise and truer data values are obtained. Signal averaging and filtering are other strategies often used to reduce

background noise. While the smoothing algorithms can effectively reduce random noise in the measurements, they can also potentially be over aggressively applied, thereby distorting spectral peak data.

The following list of smoothing algorithms are studied in this research and each is described in Chapter 4.

- Fourier transform method
- Moving average smoothing algorithm
- Savitskey and Golay polynomial filter
- Low-statistics digital filter

2.5.1.2 Background Removal

In XRF quantitative analysis, the relevant information is contained in the characteristic spectral peaks and the background continuum is considered a nuisance. Eliminating the continuum can improve the accuracy of the net peak area determination. There are generally two methods to eliminate the background continuum in XRF spectra. The first method directly eliminates the background using a heuristic approach while the second method estimates the background using a set of analytical functions [7].

For first method, the continuum is removed from spectra by applying a suitable filter with minimal or no knowledge of the actual XRF background which makes it more suitable for real-time analysis because it is computationally less demanding. This method, as applied to this research, is further described in Chapter 4.

In the second method, the continuum is modeled using various analytical functions which are least-squares fitted to segments of background spectrums. Modeling the continuum involves using analytical functions tailored to represent the various excitation conditions and widths of regions in the XRF spectrum. Because a the large

number of processes contribute to the background for any specific spectrum, it is virtually impossible to find a single mathematical equation that adequately describes the entire background[9]. For this reason, the spectrum is split into sections and one of the following types of polynomial expressions are often applied to each range.

- Linear polynomials (recommended for 2-3 KeV wide spectrum segments):

$$I_B(i) = a_0 + a_1(E(i) - E_0) + a_2(E(i) - E_0)^2 + \cdots + a_k(E(i) - E_0)^k \qquad (7)$$

- Exponential polynomials (recommended for 2-16 KeV wide spectrum segments):

$$I_B(i) = a_0 \exp\left[a_1(E(i) - E_0) + a_2(E(i) - E_0)^2 + \cdots + a_k(E(i) - E_0)^k\right] \qquad (8)$$

where $I_b(i)$ and $E(i)$ are the background intensity and the energy in KeV of channel i, respectively. E_0 is a suitable reference energy, typically the middle of the fitting range. $a_0, a_1, \ldots, a_k$ are the fitting parameters.

In addition, the background can also be estimated using other types of polynomials such as orthogonal polynomials [20] and Bremsstrahlung model [7]. However, these approaches are complex, computationally intensive and tedious to implement. They require a knowledge of instrument parameters which is not always available and thus were not considered for this study.

Therefore, the heuristic approach was selected for this research because of its feasibility for use in the intended application, and it is further described in Chapter 4.

2.5.1.3 Peak Search Algorithms

Several peak search algorithms have been developed for the automatic peak localization in an XRF spectrum. Nearly all algorithms follow the same general procedure where the original spectrum is transformed into a form that emphasizes the peak like structures and reduces the continuum, followed by a decision making step to determine

the validity of the detected peak [9]. Common peak search algorithms differ mainly in the choice of a pre-processing function. Some use the first and second derivative of the spectrum while others use some form of a correlation filter, i.e., convolution of the original spectrum with a filter that approximates the shape of XRF characteristic peaks [21, 22, 23, 9]. Specific peak search algorithms used in this research are further described in Chapter 4.

2.5.1.4 Peak Area Determination

In both WDXRF and EDXRF, the concentration of an element is proportional to the number of counts under the characteristic peak after correcting for the background continuum. In WDXRF, the acquisition of the entire peak profile is very time-consuming and usually the count rate is measured at the peak maximum instead. In EDXRF, the net peak area of an isolated peak can be calculated by integrating the continuum-corrected spectrum over the region of the characteristic peak. This method provides accurate results when applied correctly to isolated peaks [22]. However, its practical use is limited by the peak interferences in EDXRF. Because of this restriction, simple peak integration can only be applied in a limited number of applications where elemental concentrations are high and isolated well above the background noise level. Other peak integration methods have been studied by Hertogen et al. in 1974 [24]. These are computationally intensive and most useful when there is strong peak-to-peak interference. They were not considered in this study because peak-to-peak interference was not encountered. Specific peak area determination algorithms used in this research are further described in Chapter 4.

2.5.2 Matrix Correction (Calibration)

A matrix correction step is used after raw count data are smoothed and peak areas are calculated. This step is essentially a final calibration to obtain the best estimate of elemental concentrations from processed energy spectrum versus count data. Matrix

corrections can be categorized as two types: *empirical methods* and *fundamental parameter (FP) methods*. These methods along with sub-categories of each type are displayed in Figure 7. The matrix correction methods are displayed with simple empirical methods on the right side and more complicated parameter based methods on the left. The highlighted path is the simplest approach suitable for real-time analysis and this what is utilized in this study.

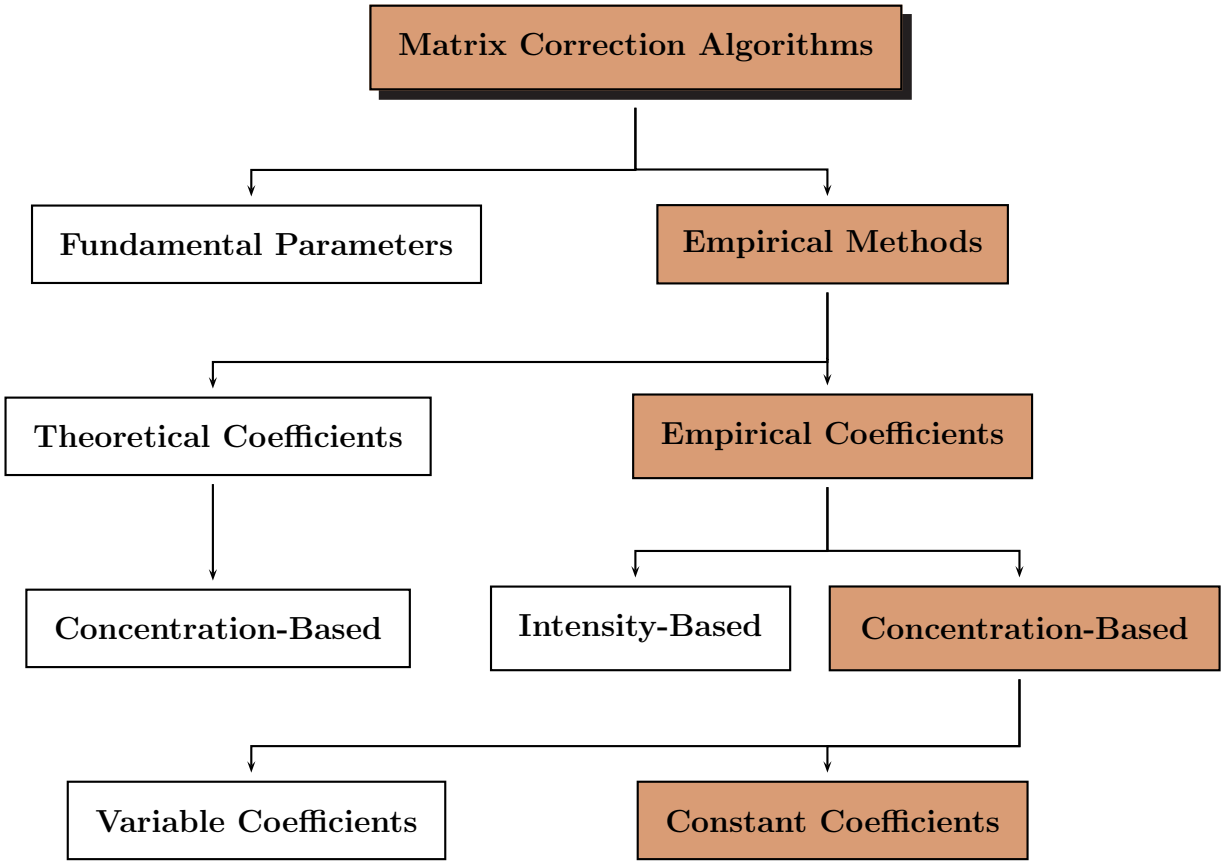

Figure 7: Matrix correction algorithms for XRF

The simpler empirical method may be constructed without any XRF principles which would require knowledge of instrument and material parameters. The empirical method produces a calibration curve to determine the chemical concentration for

elements in the sample from processed XRF energy count data. Two empirical methods widely used in commercially available XRF instruments are the Lucas-Tooth and Price [25] and Lucas-Tooth and Pyne [26] calibration algorithms. The Lucas-Tooth and Pyne algorithm uses a non-linear interpolation step to correct for inter-element interactions; whereas, the Lucas-Tooth and Price uses linear interpolation. Inter-element interactions are caused when the XRF intensity from one element is absorbed by, or enhanced by, another element.

The simpler Lucus-Tooth and Price matrix correction algorithm is used for most commercial XRF applications and was used in this study. The general equation includes terms to translate measured intensity to elemental concentrations and also to correct for inter-element effects as shown in Equation 9.

$$C_n^m = \alpha_n + P_n^m \left(\kappa_0 + \sum_x \kappa_x P_x^m \right) , \tag{9}$$

where n and m are the number of calibration samples and the number of elements present in the samples, respectively, C_n^m is the chemical concentration of the element n in the sample m, and P_n^m is the net peak area of the element n in the sample m. The variables κ and α represent the constants to be determined by the calibration process. Using regression to analyze n elements in a sample, requires at least $n + 2$ standard samples, and for optimal calibration results, a least-squares fitting method is normally adopted.

Although the empirical methods are mathematically simple, they require a large number of reference standards with chemical and physical properties similar to those of the unknown samples. The preparation of the calibration standards is the critical step in the calibration process. This step must be carried out with great care, and all standard samples must be prepared in exactly the same manner as the unknown sample. Thus, the same sample preparation steps and experimental conditions must be used for both standards and unknown samples. This requirement for sample preparation limits many potential uses for XRF in practical applications. The focus

for this research is to relax the sample preparation requirements, making it easier to implement in real-world applications.

In contrast to empirical methods, another type of matrix correction method is the fundamental parameter (FP) method which was first introduced by Sherman in 1955 [27]. Other popular FP-based calibration methods include those studied by Criss [28] and Rousseau[29]. These methods utilize knowledge of instrument and material parameters such as theoretical X-ray beam intensity, beam and detector angles, inter-element effects, and spectral background to estimate elemental concentrations. The FP models are computationally demanding and impractical for near real-time applications; however, FP methods require as little as one reference sample to produce acceptable calibration results. Further, the reference sample does not have to exactly match the properties of the unknown sample.

Due to the mathematical simplicity of empirical methods and the small number of calibration standards required for the FP methods, researchers have focused their efforts toward the development of semi-empirical matrix correction algorithms to combine the strengths of empirical and FP methods. Specifically, these combine the mathematical models from the empirical methods with theoretical coefficients obtained from instrument parameters. These type of matrix correction methods have been an on-going research area for XRF spectral analysis since mid the 1960's. Researches such as Criss and Birk [30, 31, 13], de Jongh [32], Lachance and Traill [33], and Rasberry and Heinrich [34] have developed various semi-empirical algorithms for the matrix correction step. Although the complication of mathematical models is somewhat reduced from the full FP method, this semi-empirical method often requires reference samples consisting of pure elements, which are generally very difficult to obtain. The semi-empirical methods were not considered for this study because we had no knowledge of the actual instrument parameters, as these were not available from the manufacturer.

Lastly, another set matrix correction algorithms has been developed which also fall into the computationally intensive category. These new algorithms, often referred to as the *direct mapping method*, directly relate the net peak areas of elements present in the sample to the corresponding concentrations. Any inter-element interactions are corrected without the need for additional mathematical models. Direct mapping methods studied include the partial least-squares method (PLS) [35, 36] and artificial neural network (ANN) methods [37, 38, 39]. Because of the number of calculations that must be performed to implement direct mapping methods, they are not suited for real-time applications and were not utilized in the study.

2.6 Sample Preparation in XRF Calibration

XRF Analysis using empirical methods requires a large number of reference standards with similar physical and chemical properties as the unknown samples. In many real-world applications, preparation for these standards is expensive and time consuming, which impedes the application of XRF as a tool in many quality control processes. To reduce sample preparation costs, many industrial applications have adopted one of the following six methodologies to prepare reference samples [40].

Calibration-Standard Methods This is the most common standards preparation method. Various standard samples with physical and chemical properties are manufactured. The elemental intensity from samples is compared with that from standards which have the closest physical form and chemical composition as the unknown sample.

Internal Standardization The calibration-standard method involves using the characteristics of known elements which exist in the samples or by adding a known amount of a secondary element whose concentration can be quantified. Such elements are referred to as internal standard elements and these should have excitation, absorption and enhancement characteristics similar to those

of the target elements to measure in the samples. This calibration function involves determining the intensity ratio of the target element to this internal standard element. In many cases, the Compton peak within a specified energy range is a suitable choice for the internal standard element.

Matrix-Dilution Methods The matrix of all samples is diluted to a composition such that the effect of the matrix is determined by measurements made on the diluent rather than on the matrix. This method is best suited for liquid samples.

Thin-Film Methods The samples are made so thin that absorption-enhancement effects substantially disappear. For this method to provide suitable calibration results, the samples must be smooth and the unknown elements must be near the surface.

Standard Addition and Dilution Methods The elemental concentration is altered quantitatively in the preparation of the reference samples. The matrix is the same for each reference sample and also matches that of the unknown samples. The intensity of the analyte lines are measured and a calibration curve is established. For the case of lighter atomic weight elements, it may not be possible to directly measure the element of interest. In such cases a taggant that is measurable may be added to the element of interest where the ratio of the taggant concentration to the element concentration is consistent for all the reference and unknown samples.

Mathematical Corrections Absorption-enhancement effects are corrected mathematically by the use of influence coefficients for each element present in the samples. Influence coefficients are generally determined experimentally from reference samples. The basic assumption is that the XRF intensity at a particular wavelength will in some way be affected by each element in the sample.

This method requires a extensive reference sample set along with the knowledge of all elements present in both the reference and unknown samples.

2.7 Current Advances and Challenges in Real-time XRF Analysis

The use of both WDXRF and EDXRF based instruments has increased steadily over the years due to improvements in these systems and the rapid and non-destructive nature of the measurements. WDXRF based instruments can measure all elements in the periodic table from Beryllium (Be) to Uranium (U)[41]. Important application areas include geological and materials research, and process control in the mining, cement, chemical, ceramic, semiconductor, petrochemical, and metallurgical industries. Analysis using WDXRF instruments is time consuming and not suitable for portable instruments because the measurements are often made in a vacuum chamber. However, compared to EDXRF, WDXRF is capable of detecting lighter elements and generating higher energy resolution within the XRF spectra. Thus, EDXRF based instruments are used in applications that require rapid response time and portability. Usage areas for EDXRF based instruments include environmental, industrial, pharmaceutical, forensic, and scientific research applications[42].

There are many challenges in using XRF as a quality and process control tool in industrial applications[42]. Some of the factors that must be addressed include sampling conditions, sensitivity, accuracy, measurement and maintenance costs, etc. Additionally, EDXRF spectra interpretation is tedious because of the sensitivity of XRF spectra to the sample preparation steps and the overall measurement accuracy to the skill in applying signal analysis procedures. Unfortunately, there is no standard methodology for controlling the quality of information obtained from XRF spectra[43]. Any variations in sample preparation, measurement procedures, or the use of signal processing algorithms, can drastically affect the final analytical results. As a result, in applications where it is not possible to prepare uniform samples, EDXRF is often

used as only a complementary tool to assist in implementing a more quantitative measurement methodology. Specifically, it is often used as a screening tool to sort or determine which samples should be selected for more thorough examination. Example areas for using XRF as a screening tool include semiconductor manufacturing, mineral and mining process control, and the art authentication.

In semiconductor manufacturing industries, many companies utilize portable EDXRF instruments as an in-line screening tool to ensure the level of Restriction of Hazardous Substances (RoHS) substances in their manufacturing processes[44, 45] as well as determining the crystallographic structure and surface roughness in the ultra-thin barrier layers for ULSI applications[46, 47]. However, concerns remain regarding the calibration and sensitivity of XRF instruments, because it is not always possible to obtain quantifiable measurement results due to a lack of suitable calibration standards. Thus, as discussed previously, a rapid pass/fail test using a portable EDXRF instrument is performed during the manufacturing process to eliminate as many defect materials passing through the production line as possible. Then, further destructive chemical analysis are performed on subsets of the questionable materials to quantify concentration levels. Regardless of these limitations, the use of EDXRF as an in-line screening tool can both lower costs and obtain faster results. However, EDXRF systems still require a semi-skilled operator with a sound understanding of the measurement fundamentals, equipment capabilities and the likely composition of materials involved in the process[48].

XRF is also used as a process control tool in the mineral and mining industries. In these industries, the determination of mineralogy prior to material extraction in an open-pit mine is an important step for routing the material to the appropriate processing stream. An on-line continuous scanning system utilizing XRF was developed to measure the mineral content of the materials by measuring the sample dust and cuttings during the drilling process [49]. For this application, XRF is an acceptable

alternative to laboratory assays. XRF samples were easily prepared in a powder form that was consistent with the unknown samples.

Another area where portable EDXRF instruments are widely used is as an art authentication tool. Most objects being analyzed include paintings, manuscripts, sculptures, etc. EDXRF instruments are popular in this type of application because of their portability and rapid analysis capability. However, using portable EDXRF instruments as a non-destructive methodology to quantitatively authenticate art objects is challenging due to the inhomogeneous, layered nature of these objects[50]. As a result, portable EDXRF instruments are often used for field analysis to distinguish the differences between the outer two or three layers of paint. Objects with more complex paint layer structures are difficult to analyzed using XRF, and hence, require more thorough laboratory analysis that is often destructive in nature, e.g., PIXE[51].

Other examples where EDXRF methods have been used include the following:

- NASA utilizes XRF to read nanocodes[52]. These are "chemical bar codes", that can be incorporated in the outer paint layer or applied to the surface layer of a material, thereby serving as an alternative to standard part-marking processes. This new method makes it possible to apply a visually transparent bar code to the outer surface of parts.

- Carpet and Rug Institute (CRI) developed a certified test criteria, known as a gold, silver or bronze seal of approval (SOA), for carpet extractors using portable EDXRF spectrometers[53].

- WDXRF is utilized in conjunction with other measurement methods, such as XRD, to simplify the analysis of foodstuffs and pharmaceutical raw materials. The combined measurement methods extend from lighter elements such as sodium (Na) to uranium (U)[54].

- Crime laboratories utilize XRF as a tool to differentiate elemental composition of gunshot residues from various types of smooth-bore and rifled-bore guns, and also for detecting the presence of bodily fluids at crime scenes[55, 56].

Although the main attraction of the XRF technology is its rapid response time to analyze chemical constituents in a given sample, few of the aforementioned applications have successfully developed a truly automated, real-time analysis tool that takes full advantage of XRF technology. Applications employing XRF as a on-line screening tool are often limited to those that can produce calibration samples to represent all chemical and physical variations of their products. This requirement is possible for certain manufacturing process such as semiconductor manufacturing process, where the manufacturing parts are of standard sizes, and the mineral and mining process, where the samples can be easily prepared in the powder form for XRF analysis.

Many industries manufacture products with slight variations customized to meet the needs of their customers. Such is the case in the carpet industry where new carpet styles are routinely introduced, each with a different physical appearance which can alter measurements recorded by XRF instruments. Physically manufacturing XRF calibration samples for each type of carpet is not practical or cost effective. This is the challenge this study has focused on, and successful solution would allow XRF to be used as an effective, rapid quality control instrument in the carpet and other industries. In the carpet industry, its use would reduce or eliminate the need for expensive, time consuming off-line tests that are currently used to determine chemical compositions.

CHAPTER III

MEASUREMENT METHODOLOGY

This chapter describes XRF instrumentation and measurement procedures, which directly impact the precision and accuracy of XRF measurements. The XRF measurements in this research involve several essential components. Each component is described in the following sections. The first section describes all hardware instruments involved in this research. The next section discusses all software related to this study. Then, different types of experimental samples and their corresponding preparation procedures are discussed including a chemical taggant, which is added to assist XRF measurements. The final portion of this chapter presents a set of measurement factors, which influence XRF measurements in carpet applications. Analysis of these measurement factors has lead to recommended settings for making carpet measurements for fluorochemical analysis using portable XRF instrumentation. Methods introduced will be used throughout the rest of the study unless otherwise stated.

3.1 Hardware Equipment

The near real time XRF measurement system designed for the carpet industries consist of two main components; a portable XRF instrument and a linear motion scanning system. The portable XRF instrument is utilized for taking XRF measurements and the scanner is the means of moving the XRF instrument across the carpet, either on the manufacturing floor or on specimens in the laboratory. Equipment details are discussed in the sections which follow.

3.1.1 XRF Instrumentation

The portable XRF instrument primarily used in this research is the S1 TRACeR manufactured by Bruker AXS (formally KeyMaster Technologies). This instrument consists of a miniature X-ray tube as a source, a silver (Ag) anode target, a Si-Pin detector, an interchangeable filter wheel, and a detachable vacuum chamber. This device is capable of generating a primary X-ray beam source up to 40 KeV in power and up to 15 μA in intensity. The acquired XRF spectra have a resolution of 20 eV per channel. This device is capable of detecting elements from Titanium (Ti) to Uranium (U) without the vacuum chamber and Magnesium (Mg) to Uranium (U) with the vacuum chamber attached. The penetration depth of S1 TRACeR is approximately 0.1 mm for steels and 1-2 mm for aluminum.

An interchangeable filter wheel with locations for five different filter types is built into the Bruker's S1 TRACeR portable instrument. Table 2 lists the specific filter types that were supplied with instrument used for this study. Note that the second filter is an empty slot for used when no filter is required.

Table 2: Primary beam filters installed on S1 TRACeR

Filter No.	Layer No. 1	Layer No. 2	Layer No. 3
1	Al (300 μm)	Ti (25 μm)	-
2	-	-	-
3	Al (200 μm)	Ti (25 μm)	Cu (75 μm)
4	Ti (25 μm)	Fe (50 μm)	Mo (50 μm)
5	Al (38 μm)	-	-

In addition to Bruker's S1 TRACeR XRF instrument, a TRACeR II manufactured by KeyMaster Technologies (acquired by Bruker in 2008) was also used in the early stages of this research. Similar to the S1 TRACeR, the TRACeR II also contains a miniature X-ray tube as the primary X-ray source and a silver (Ag) anode target capable of generating an X-ray beam up to 40 KeV with intensities up to 28μA. The

TRACeR II instrument did not have either vacuum chamber or interchangeable filter wheel capabilities. It was also subject to measurement fluctuations caused by internal heating when successive measurements were made. These measurement fluctuations were reported in the Master thesis by Laurent Mahuteau [57]. The TRACeR II was only utilized to qualitatively compare XRF results between the TRACeR II and S1 TRACeR instruments, and then for only small count intervals separated by a long period of time between measurements so as to prevent internal heating.

3.1.2 Three-axis Scanner

Final application of XRF measurements to measure fluorchemical content at a carpet manufacturing facility will require not only the portable XRF instrument, but also a device to consistently move the instrument across the carpet. To simulate this task in the laboratory, a three-axis, linear motion scanning system was constructed to control the position and the speed of the portable XRF instrument, resulting in a more accurate and more precise measuring system than could be obtained with hand held measurements. This scanner system is capable of positioning the XRF instrument over an area of 400×300 mm. This scanning system was used with two data acquisition methods; point-to-point and continuous.

The point-to-point measurement method is the standard method for taking XRF measurements for most applications, where discrete points on the sample are selected to collect XRF spectral data. This method is effective when a collection of data from several locations are combined to get an average reading.

The continuous measurement method is implemented by scanning the XRF instrument across the sample as count data is collected. This requires an XRF instrument which can accurately acquire counts over long time intervals. For the carpet application, when the XRF instrument is moved across a sample, the raw count rates versus position can be used to identify inconsistencies in the application of fluorochemical

compounds across the carpet. However, the moving speed of the XRF instrument must be slow enough to obtain a statistical number of counts at each carpet position. Guidelines for these type of measurements are established in this research.

3.2 Software

Three suites of software are utilized in this research to acquire data from the XRF instrument, process spectra obtained from a given sample, and automate the scanning system. In this section, each software suite is briefly described.

3.2.1 Data Acquisition Software

XRF spectra can be acquired from Bruker's XRF instruments through Bruker supplied software using either a PDA or PC platform. The software from both PDA and PC platforms are capable of recording XRF count data in a Bruker-specific data format (**.pdz* files). These specially formatted files contains valid count rate, and raw counts for each energy channel along with all instrument and XRF measurement parameters including instrument and ambient temperatures. The software also displays the XRF spectral plots with a limited number of custom viewing options that may be selected by the user. The Bruker formatted data are transportable between between the Bruker PDA and PC platforms.

Although Bruker's XRF software on both PDA and PC platforms can perform the same fundamental data acquisition functions, they each contains additional features that are unique to each platform. The PDA-based software is intended for rapid elemental analysis for several specialized applications. Further, the PDA-based software supplied by Bruker contains databases either specific to an intended XRF applications or to what has been requested by the customer. These databases enable the software to automatically identify elements present in samples using either an empirical or the fundamental parameter method.

The PC-based XRF software does not contain any databases that are appropriate

for identifying elemental constituents in carpet samples. However, the PC-based software is capable of creating custom XRF views, one of which is an overlay comparison of any two XRF spectra which was used extensively in this research.

The PC-based software may be used to store data in a generic XRF data file as a spreadsheet format. In addition, the PC-based software can also generate this spreadsheet format from any Bruker-specific XRF data file taken from the PDA-based software. The PC-based software was utilized as a the primary data acquisition software for this research to collect XRF measurements in a generic spreadsheet file format (**.csv*).

3.2.2 Signal Processing Software

The custom signal processing software used in this research is based upon Mathworks Matlab. A Matlab-based GUI program was developed to import XRF measurements in a spreadsheet format, eliminate any unwanted noise in the signals, extract necessary XRF counts, and perform XRF calibrations. This program was separated into three subcategories which were signal processing, database management, and calibration functions.

The signal processing GUI shown in Figure 8 provides the user a means to visually inspect and to automatically apply a sequence of signal steps to a collection of XRF spectra. This GUI included of all signal processing algorithms discussed in Chapter 4. In this GUI, multiple types of spectra resulting from either different processing algorithms or different data sets can be calculated and displayed in the same figure. The GUI is also capable of processing a large collection of XRF spectra based on a preselected set of signal processing algorithms. Results from this GUI can be stored for later import into the calibration GUI.

Figure 9 shows the GUI interface for database management. This GUI links to a MySQL database which stores elemental information, such as atomic number, atomic

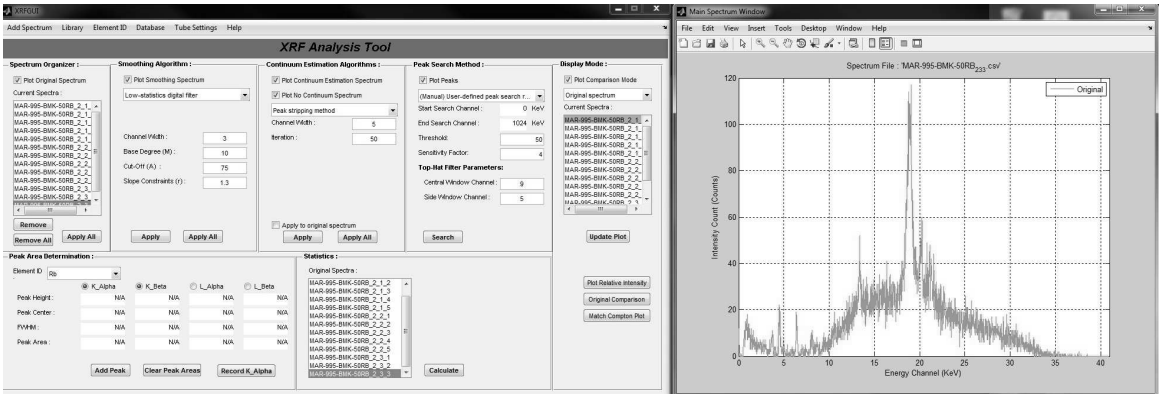

Figure 8: Signal processing functions within Matlab XRF GUI program

weight, density, and characteristic line energies, for elements from Al to Rn.

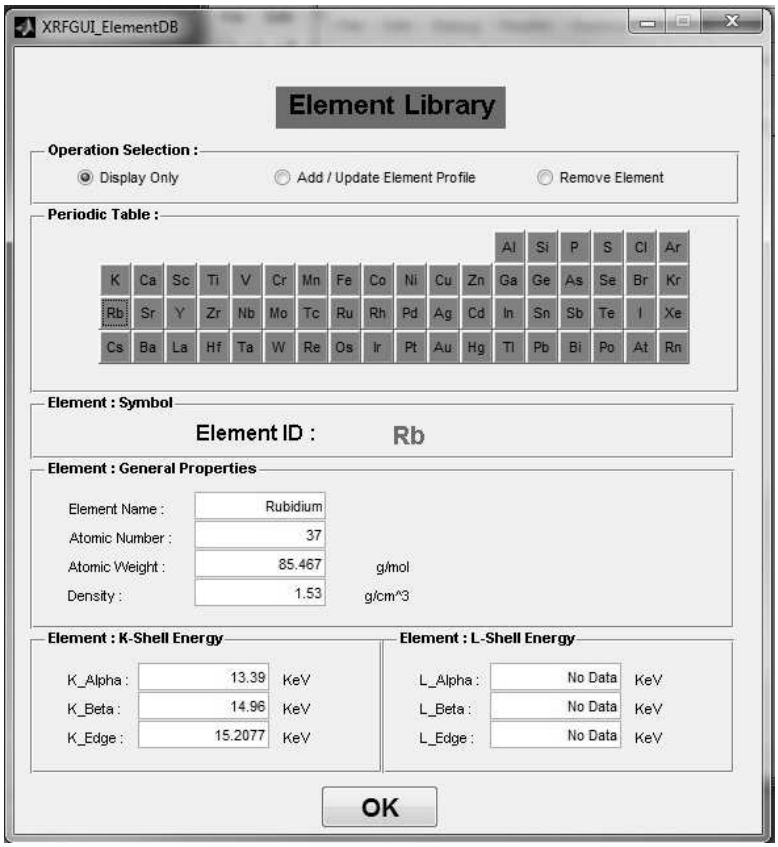

Figure 9: Database function in Matlab XRF GUI program

Figure 10 shows the calibration GUI which enables the user to add, edit, and remove calibration information for any particular sample type. For existing calibrations, the user can recalibrate carpet samples with a different set of signal processing

algorithms. The ability to easily modify existing calibrations is important for maintaining implementation flexibility for the intended carpet mill application.

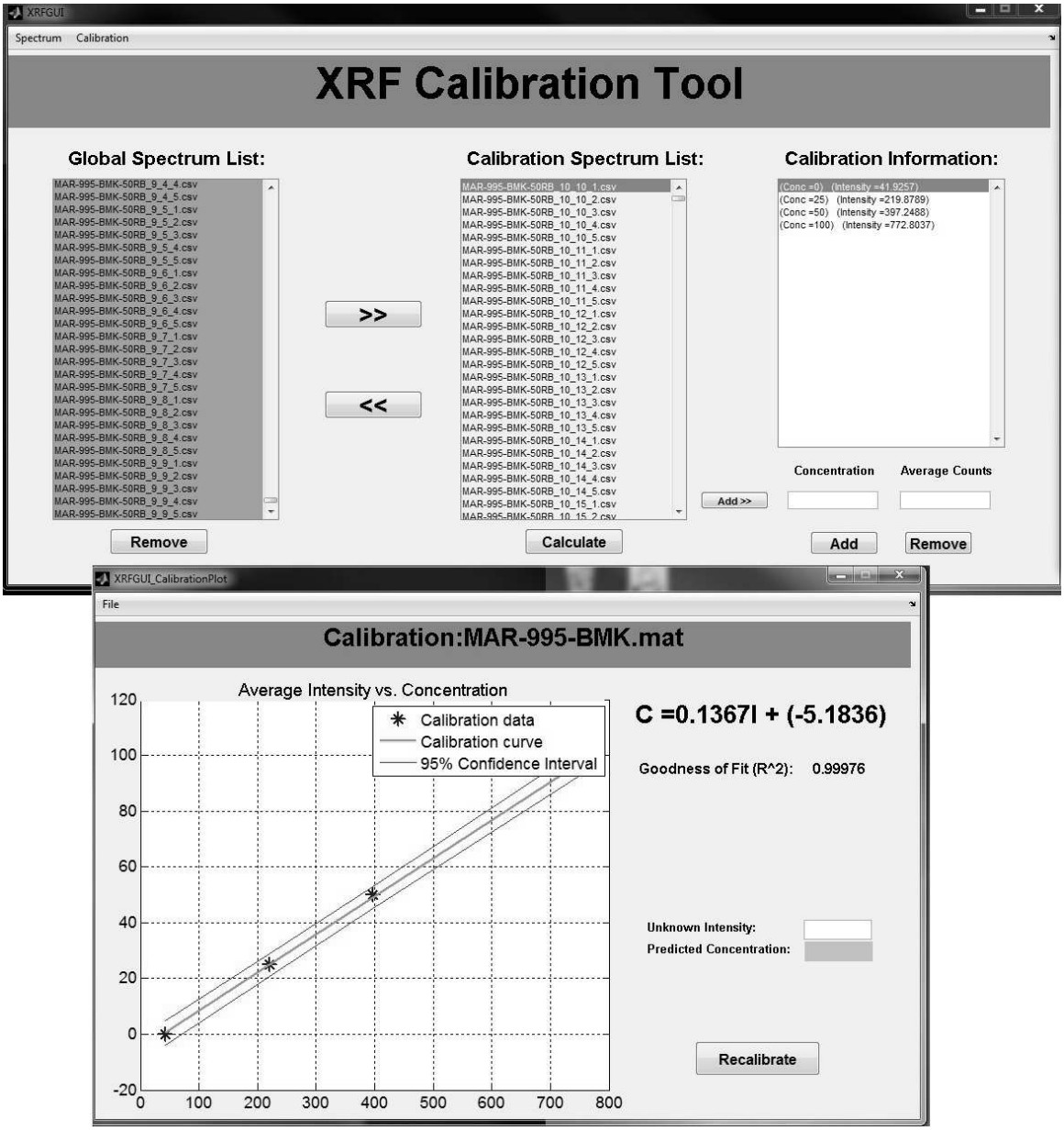

Figure 10: Calibration function in Matlab XRF GUI program

3.2.3 Automation Software

Automation software was developed to use the XRF instrument with a three-axis scanner to form an automated XRF system to acquire data from carpet samples.

However, XRF instrument software is proprietary, thus this research used AutoIt automation software [58] to synchronize XRF data collection with the motion of the scanner.

AutoIt is a freeware BASIC-like scripting language designing for automating Windows GUIs and scripting. It uses a combination of simulated keystrokes, mouse movements and window/control manipulation in order to automate tasks in a way not possible without writing a dedicated program that incorporates both XRF and scanner control aspects.

3.3 Sample Preparation and Chemical Taggants

XRF spectra are collected from three types of samples in this work; liquid solutions, filter papers, and carpet samples. Specimen were prepared using the same methodology whenever possible to reduce any discrepancies in the measured spectra. Unless otherwise stated, preparation for each sample type will follow the procedures described in the following sections. Prior to the introduction of these sample preparation procedures, the chemical taggant approach is further discussed.

The primary element in fluorochemicals, fluorine, is not measurable directly by portable XRF instruments. As a result, chemical taggants must be added to the fluorochemical solution to enable XRF measurements. The measurement of fluorine is then obtained by measuring the concentration of the chemical taggant. During this research, several chemical taggants were considered as potential candidates for measurement of the concentration of fluorochemicals on carpet samples. Some examples of possible taggants include Fe, Zn, and Rb. These taggants were initially selected based upon the economic factors as well as their chemical properties such as their solubility in fluorochemicals.

However, the chemical taggant utilized in the carpet application has to not only

be detectable by the XRF instrument, but also must not adversely affect the intended physical and chemical properties of the carpet. An ideal chemical taggant for fluorochemical determination should meet all of the following conditions.

- Within the detectable range of portable XRF instruments
- Inexpensive
- Conserve the physical and chemical properties of carpets and applied fluorochemicals
- Insoluble in water (this property enables carpet manufacturers to continuously monitor fluorochemical levels on carpet fibers even after carpets leave the manufacturing lines)

Aqueous-based and fluorochemical solution samples were prepared in the laboratory to meet the desired concentration standards for specific taggants under consideration. Then, 20ml of the solution was placed in 31mm diameter, double open ended X-Cell containers. The X-Cell containers were covered with a piece of thin film, Mylar© XRF film, which made from polyester with 0.25 mil (6μ) uniform thickness. The filled X-Cells were then positioned near the XRF spectrometer for measurement. When taking measurements for liquid samples, the XRF instrument was position upward with little or no air gap between the X-Cell containers and the instrument.

Filter paper samples were used to represent carpet samples of uniform texture and thickness. A smooth surface eliminates many of the effects of X-ray scattering that are normally seen in samples with a rough surface texture. To prepare filter paper samples, ten pieces of filter paper were first stacked together to create a 3mm uniform thickness sample. Then 30cc of prepared solution was applied to the center of the filter paper. Note that initial investigation showed that the taggants used in the study were completely dissolved in the aqueous-based solutions prior to application

on these samples. Hence, the releasing of liquid solution at the center of filter paper samples assures representative and even distribution of the chemical taggant where the XRF measurement will be made.

The majority of the samples analyzed in this research were from actual carpet samples. Due to the variety of commercially available carpet styles and the sensitivity of XRF measurements on these different styles, with different carpet materials, a procedure had to be developed for consistently preparing carpet samples. The first step was to remove any excess loose fibers on the sample that might result from the tufting processes during manufacturing or later cutting of the sample. Then the carpet samples were brushed in one direction. When the continuous scanning method was used, the brushing direction was aligned along the scan direction of the moving instrument.

This research used carpet samples to which taggants were applied from two sources: from a professional laboratory and blank carpet samples treated in the laboratory on Georgia Tech campus where this research was conducted. The professional laboratory produced carpet samples on a pilot manufacturing line, and fluorochemicals were applied using a commercial-grade spray applicator. The professional laboratory also perform the certified AATCC test to provide a benchmark comparison of the fluorine content on the samples to results determined from XRF measurements.

The carpet samples produced in Georgia Tech laboratory were prepared from samples cut from commercial carpets obtained from a carpet manufacturer. These carpet samples were cut into small pieces and soaked with specially prepared aqueous solutions of various chemical taggants and concentrations. The initial and final weight of each sample before and after the soaking process was measured to determine the amount of chemical taggant actually applied. Then the wet samples were place in an oven and baked at $450F$ for three hours to simulate a similar baking procedure in the typical carpet manufacturing process.

All prepared samples, both the filter paper and carpet pieces, were placed in clear plastic bags to prevent contamination to/from the XRF instrument. Figure 11 shows the three different types of samples used for the subsequent XRF measurements.

Figure 11: Liquid, filter paper, and carpet samples ready for XRF measurements

3.4 XRF Measurement Setup

This study used two different types of XRF measurement methodologies: upward bench top measurements where samples were placed above the XRF instrument on a fixed stand and an automation method where the XRF instrument was supported above the sample and aimed downwards during scans across the carpet. The upward bench top method was used primarily for small sample analysis and the downward automated method was primarily used for simulating the real-time XRF measurements that might later be made on large carpet samples. Both methodologies involved the same XRF instrument and data acquisition software. A three-axis scanner with automation software was used for the downward automation measurement method as was described previously in this chapter.

The bench top XRF instrumentation setup for small samples analysis is shown in

Figure 12. In this setting, the portable XRF instrument is positioned on a stand in an upright position. The X-ray beam is emitted upward and the sample is placed on top of the instrument. Because this configuration has air as the background above the sample, it is especially useful for the analysis of small and thin samples.

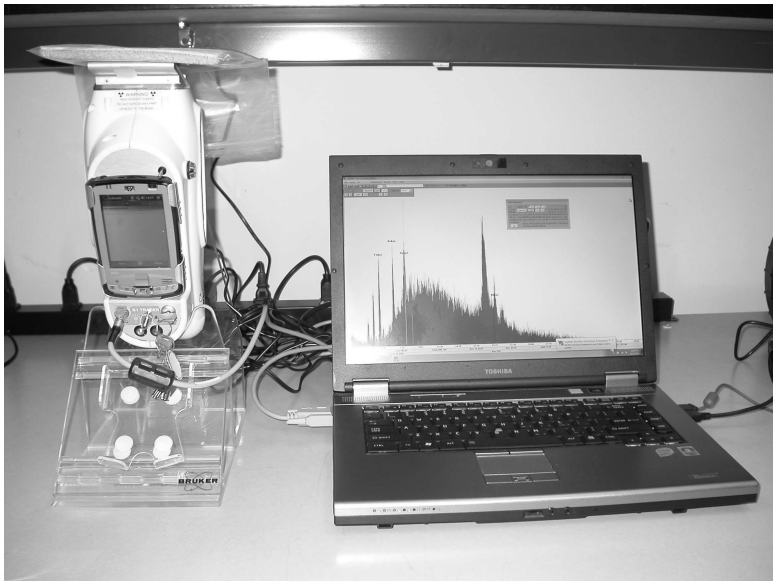

Figure 12: XRF instrumentation bench top setup for analysis of small samples

For the actual carpet inspection procedure, the XRF instrument was mounted on a three-axes manipulator with the incident X-ray beam aimed in a downward direction and the carpet sample was placed on a flat surface below the instrument. Figure 13 shows the typical setup for the downward carpet measurement method. This configuration was designed to simulate the actual use of XRF measurements in the carpet manufacturing process. The automated scanner constructed for this research models a measurement configuration which has been proposed by our research team for the eventual carpet mill application. Specifically, at the end of a typical carpet production line, the carpet is laid flat on the production floor for visual inspection by technicians for several minutes. This is the anticipated location where XRF measurements could be made on-line at a carpet production facility.

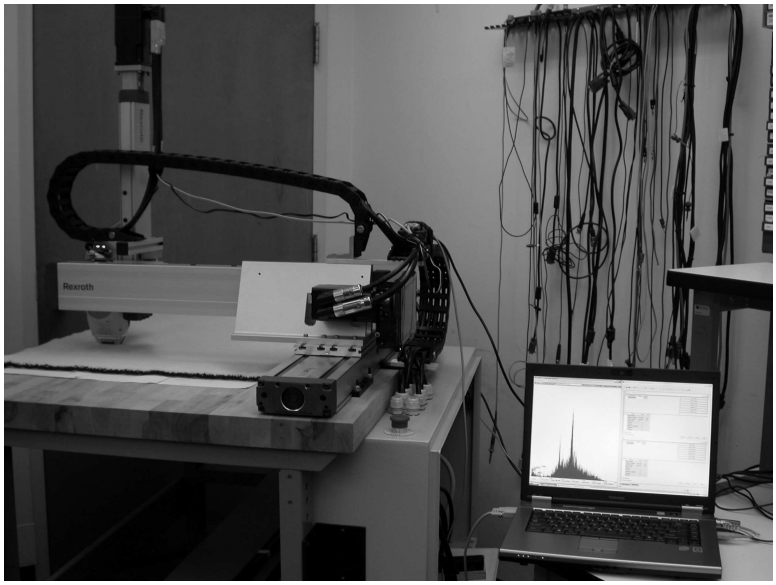

Figure 13: XRF instrumentation setup for real-time carpet analysis

3.5 Preliminary Results

XRF is essentially a comparative method, thus a standard set of measurement and sample preparation procedures need to be developed prior to attempting to measure taggant concentrations on carpet fibers. To accomplish this, all parameters affecting XRF measurements must be identified. This section explores different measurement and sample preparation factors that can affect measured XRF spectra and how each parameter alters the XRF spectra results.

3.5.1 X-ray Tube Voltage

The X-ray tube voltage is the primary excitation source for the portable XRF instrument. This voltage determines the energy of the primary source used to excite atoms in the sample. The tube voltage directly corresponds to the binding energy of the electrons which are knocked out of an atom. If the tube voltage is greater than the binding energy of an atom's electron in the K-shell, that electron can be knocked out of its orbit resulting in the K_α and K_β characteristic line pair for that atom. Similar events happen when X-ray tube voltage is greater than the binding energy of

an atom's electrons in the L-, M-, and N-shells.

To investigate the effects of the X-ray tube voltage on measured spectra, a series of samples were excited with tube voltages which were less than, equal to, and higher than the target element's absorption edge. The resulting XRF spectra were next visually inspected by comparing raw counts in energy regions less than, equal to, and higher than the element's absorption edge. From these studies, the X-ray tube voltages were determined for optimum analysis of atomic elements of interest.

3.5.2 X-ray Tube Current

The X-ray tube's current indicates the number of electrons generated by the X-ray source that subsequently excite the atoms in the sample. Ideally, the X-ray tube current should not affect the overall shape of measured XRF spectra but simply scale it in count amplitude. To prove this fact, a series of samples were excited using different X-ray tube currents. The overall XRF spectra were then visually compared by observing the raw counts from various energy regions of interest.

Although increasing X-ray tube current will subsequently increase the total counts obtained within a fixed time interval, current changes may dramatically increases the internal heat generated by the X-ray source inside the XRF instrument. Hence, this setting has to be carefully selected for real-time, long-term use of the XRF instruments. Proper duty cycle time has to be adjusted both to extend the life of the XRF instrument and to assure the instrument is always within the proper temperature range for accurate instrument calibration.

3.5.3 Primary Beam Filter

An optional thin metal film may be placed between the primary X-ray beam source and the sample. This is called the *primary beam filter*. The main role of this filter is to act as an absorber blocking radiation which normally contributes to the background continuum in the region of interest. Based on X-ray absorption theory described in

Section 2.1.2, this filter absorbs background radiation at energy levels equal to or greater than the absorption edge of the materials of the filter. According to Equation 2, the beam is also attenuated by the ratio I/I_0 as it passes through the filter material. The effects of different primary beam filters are examined next.

A primary beam filter with 38μm Al has the filter profile shown in Figure 14. The corresponding effect of this filter on the actual XRF spectrum is shown in Figure 15. This primary beam filter dramatically reduces the background continuum above the Al absorption edge (K_{edge} = 1.562 KeV). As the energy channel increases past this edge, the effect of this filter slowly decreases.

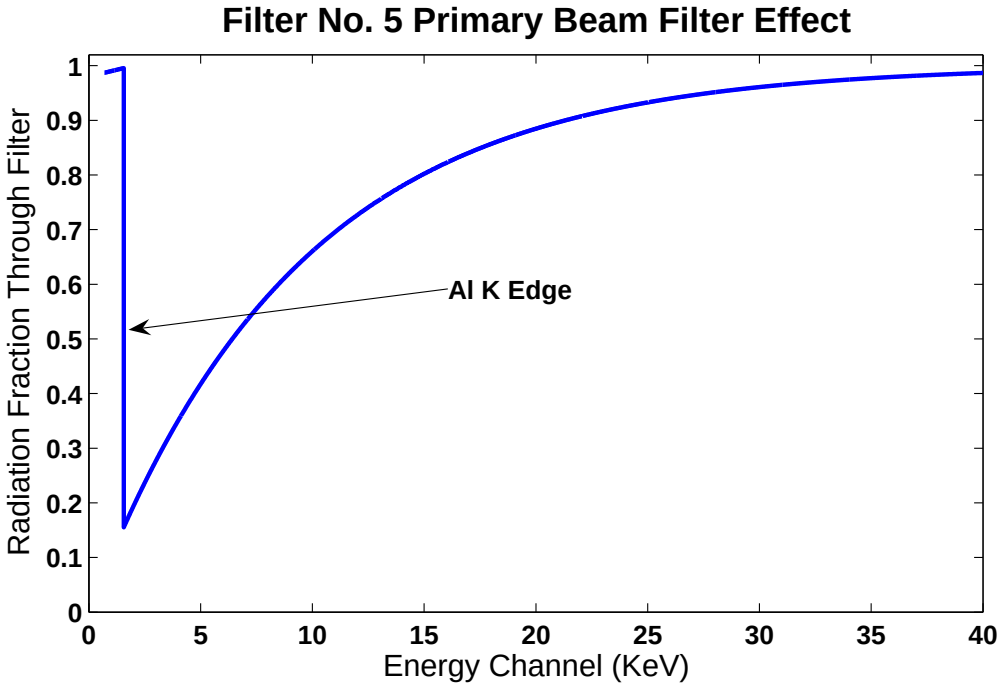

Figure 14: Effect of primary beam filter for Al(38μm)

Another example of a primary beam filter consisted of two elements: 300μm Al in the first layer and 25μm Ti and this filter was investigated as a second option. Similar to the single-element case above, each element in this filter is analyzed separately using Al absorption edge (K_{edge} = 1.562 KeV) and Ti absorption edge (K_{edge} = 4.965 KeV). The profile for each filter layer is plotted in the top two subplots of Figure

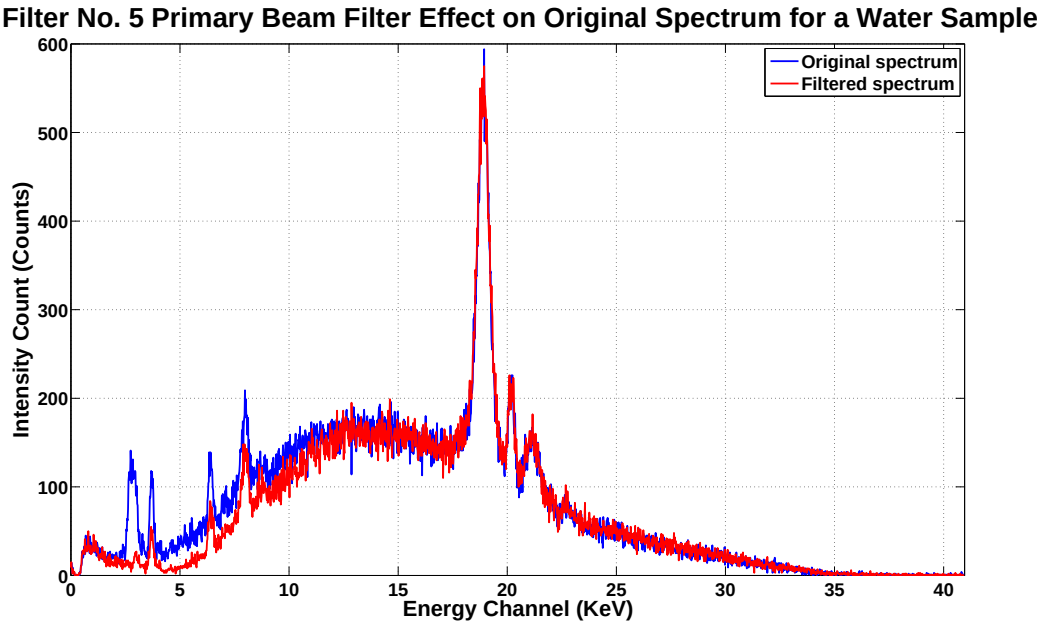

Figure 15: Effect of primary beam filter with Al(38μm) on an actual carpet sample spectrum

16. The combined effect of both elements is simply just the multiplication of the individual effects, which is plotted in the bottom subplot of Figure 16. The overall XRF spectrum after passing through this filter is plotted against its original signal as shown in Figure 17.

Similar to the first scenario with single element (Al) as a filter, the XRF spectrum background at the Al absorption edge ($K_{edge} = 1.562$ KeV) is significantly reduced. Furthermore, due to the second layer of element in the filter, the background is reduced again near the absorption edge of Ti ($K_{edge} = 4.965$ KeV).

The degree to which a filter reduces the intensity of the fluorescence radiation from the sample is much more difficult to estimate accurately due to the loss of X-ray intensity through scattering. For this reason, the optimal filter thickness was determined experimentally from choices in the XRF instrument, and found to be the first primary beam filter from those listed in Table 2 (Al(300μm) and Ti(25μm)). This filter is the preferable since it is capable of reducing carpet background significantly

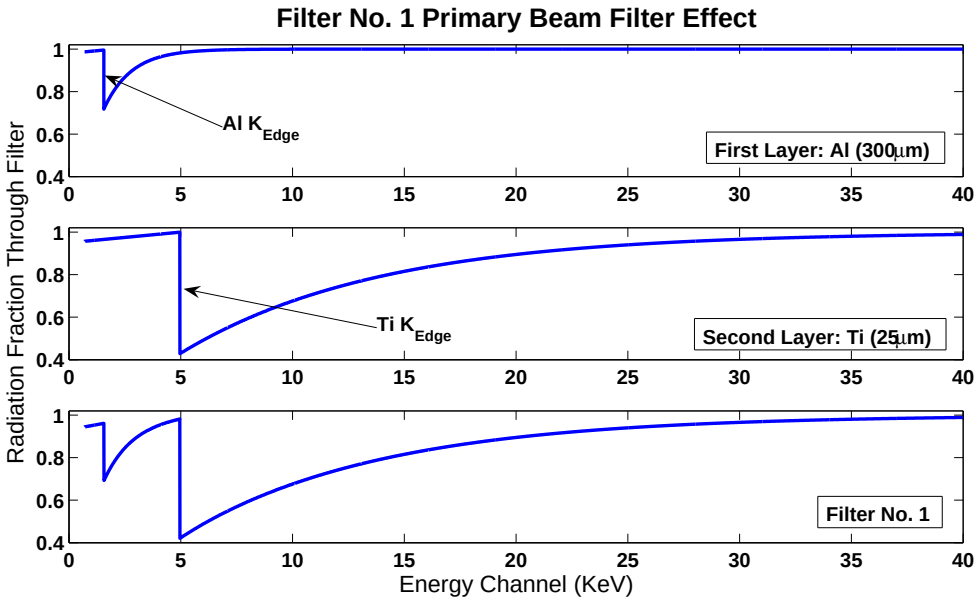

Figure 16: Effect of primary beam filter for Al(300μm) and Ti(25μm)

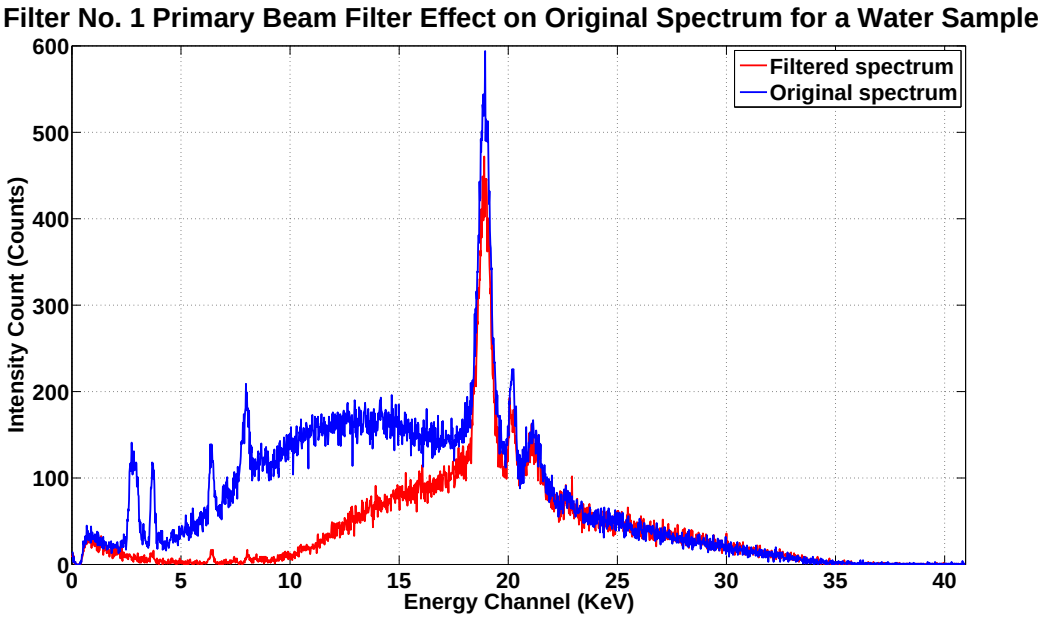

Figure 17: Effect of primary beam filter with Al(300μm) and Ti(25μm) on an actual carpet sample spectrum

in the lower energy channels of interest in this study. Specifically, the background radiation is significantly reduced, thereby leaving spectra peaks from taggants visible for subsequent analysis.

3.5.4 Measurement Time

XRF intensity counts are collected through the accumulation of the total number of photoelectrons detected by the XRF instrument throughout the entire measurement time. Hence, each XRF measurement (I_{raw}) is directly proportional to the measurement time (t_m):

$$I_{raw} \propto t_m \tag{10}$$

Since photoelectrons generated from any element in the sample are also directly proportional to the concentration of the element in the sample, photoelectrons from major constituents are generally more in quantity than those collected from other trace elements in the sample. As a result, when performing XRF measurements, the longer the measurement time, raw counts from major elements will be more prominent than other trace elements. Thus it is a challenge to detect trace elements of interest, in low concentrations, especially when the sample surface is rough so as to generate a noisy background continuum in the XRF spectra, and carefully balancing measurement time with other measurement parameters is very important to obtain consistent results.

To determine the relationship between the measurement time and the XRF intensity collected from the instrument, two types of samples were used: aqueous solutions and carpet samples. A total of four samples were used: two carpet samples and two aqueous solutions samples, each tagged with 200 and 400 ppm Rb. Each sample was measured using the S1 TRACeR XRF instrument for a duration of 10 through 60 seconds at intervals of 10 seconds. For each time interval, ten measurements were taken and the average of the Rb peaks were calculated from the XRF measurements. An example of Rb peaks collected from the 200 ppm, aqueous-based solution using different measurement times are plotted in Figure 18.

From Figure 18, one can observe that the overall XRF spectral appearance is the

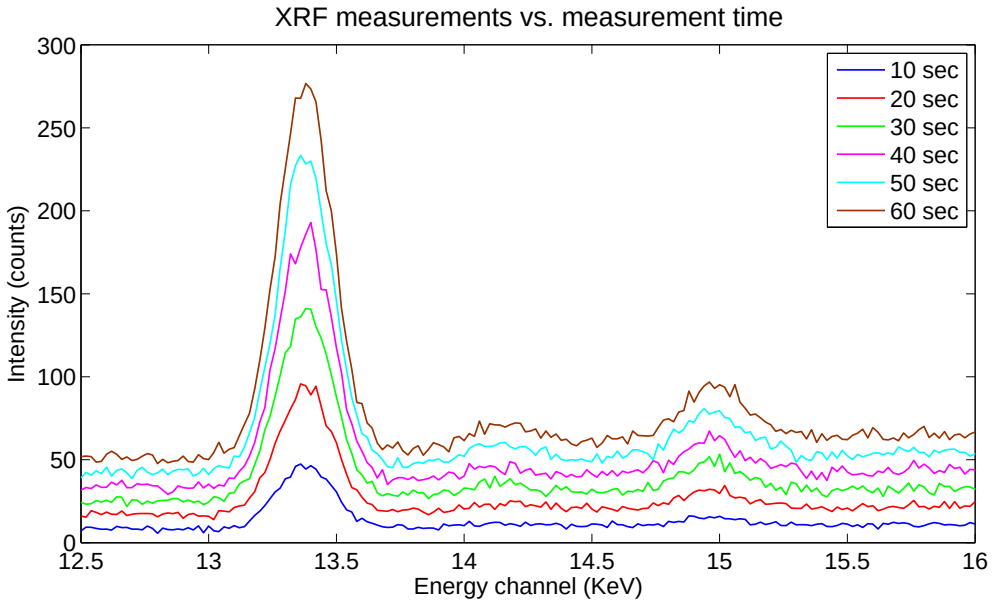

Figure 18: Rb peaks detected for different measurement times

same for the various measurement times. The difference is primarily the intensity count level. Table 3 summarizes the Rb peak counts collected from various sample materials with different Rb-tagged fluorochemical concentrations and measurement times. The relative standard deviation (RSD) is the standard deviation of the Rb counts of ten measurements made on a single sample at the same measurement time.

In Figure 19, the average Rb raw counts are plotted against the measurement time for the four samples tested. From this figure, one can observe that the relationship between measurement time and the intensity counts are linearly proportional for each sample. However, the slopes are dependent on both the specimen type and Rb concentration and do not directly scale with changes in Rb concentration.

3.5.5 Measurement Numbers

Experimental data contains various types of noise, which create deviations in measurement data. To reduce this deviation, several measurements are collected from the same sample. To evaluate the effectiveness of the number of measurements versus the measurement deviation, relative standard deviation from specific samples are

Table 3: Rb intensity counts from Rb-tagged carpet and fluorochemical solution samples with various measurement times

Sample Name	Measurement Time (sec)	Rb Intensity (counts)	RSD (%)
200 ppm carpet	10 sec	564	3.26
	20 sec	1122	2.78
	30 sec	1682	2.51
	40 sec	2244	2.02
	50 sec	2780	1.72
	60 sec	2322	1.89
400 ppm carpet	10 sec	857	2.52
	20 sec	1708	2.95
	30 sec	2552	2.18
	40 sec	3400	1.75
	50 sec	4222	1.08
	60 sec	5060	0.97
200 ppm solution	10 sec	890	3.95
	20 sec	1823	2.51
	30 sec	2834	1.75
	40 sec	3698	1.16
	50 sec	4603	1.12
	60 sec	5615	1.42
400 ppm solution	10 sec	1483	2.45
	20 sec	3115	1.31
	30 sec	4667	1.38
	40 sec	6193	0.78
	50 sec	7723	1.22
	60 sec	9131	1.40

plotted against the number of measurements. Figure 20, 21, and 22 show the relationship between the number of measurements and the relative standard deviation of Rb raw intensity counts from three types of carpet samples applied with Rb-tagged fluorochemical solutions.

These results show that the number of measurements required to obtain the optimum balance between accuracy and number of measurements is both a function of carpet types and Rb concentration, however, for most cases, 25 to 50 measurements

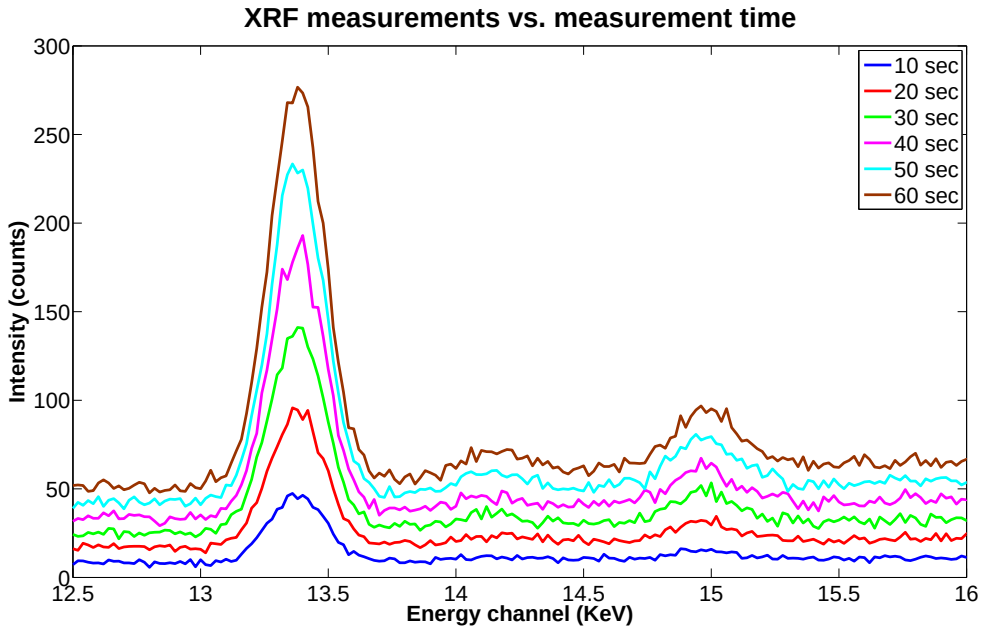

Figure 19: Measurement time vs. Rb peak intensity

are sufficient.

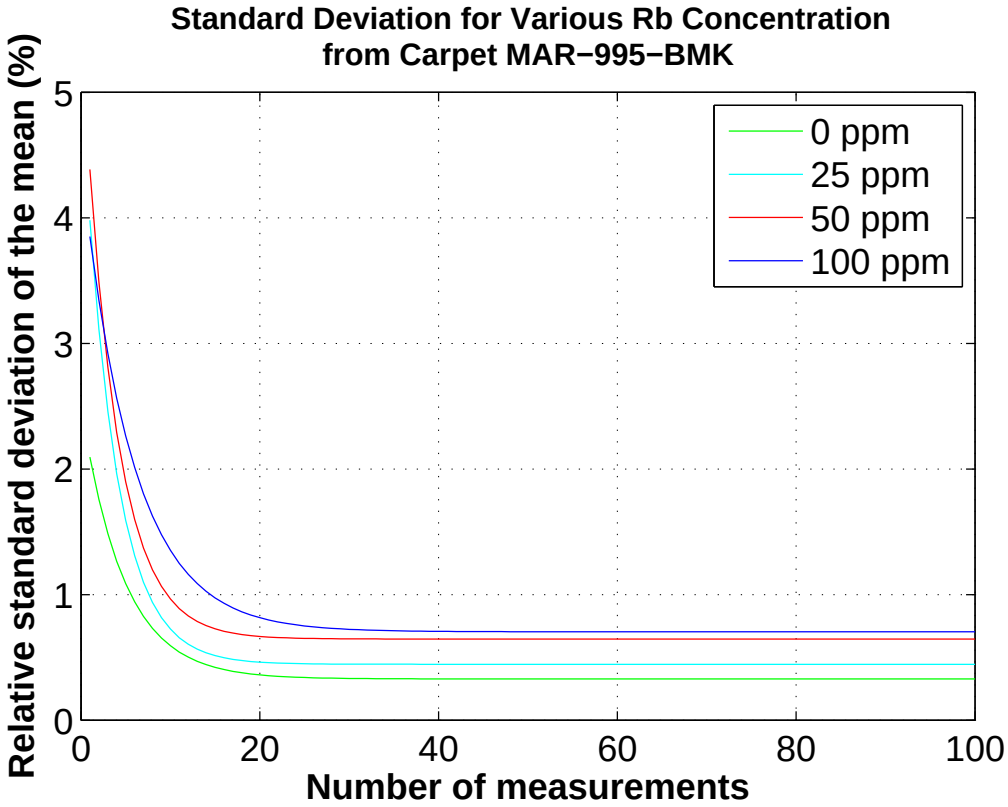

Figure 20: Performance comparison for Rb-tagged BMK carpets

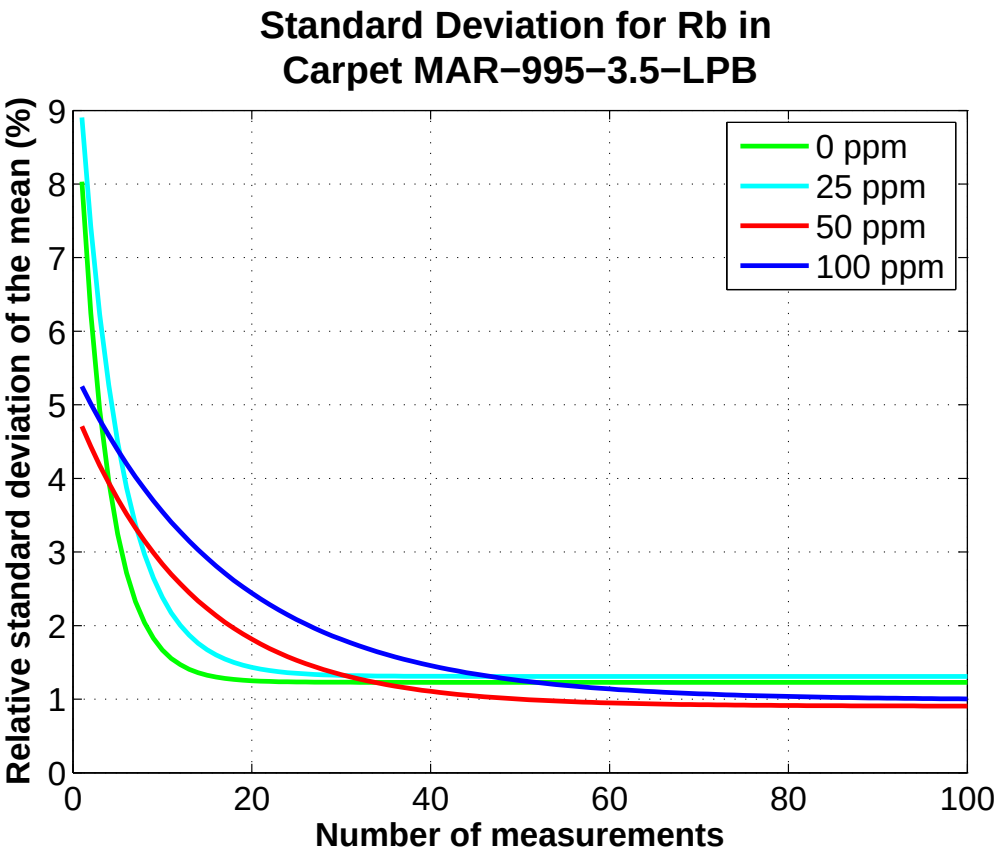

Figure 21: Performance comparison for Rb-tagged 3.5-LPB carpets

3.5.6 Other Factors

The distance between the sample and the XRF instrument affects the overall XRF measurements. This was discussed in Laurent Mahuteau's Master thesis [57]. Similar to the measurement time, it was found that the distance between the instrument and the sample does not alter the overall shapes of XRF spectra, rather it affects the intensity counts collected from the XRF instrument. Fortunately, the distance factor affects the older generations of XRF instrument such as Bruker's TRACeR II used in Mahuteau's work more than newer generation instruments such as S1 TRACeR used in this study. Bruker's S1 TRACeR is equipped with a safety mechanism preventing users from accidentally activating the instrument without a sample present to block the beam. This safety mechanism shuts off the instrument whenever counts collected

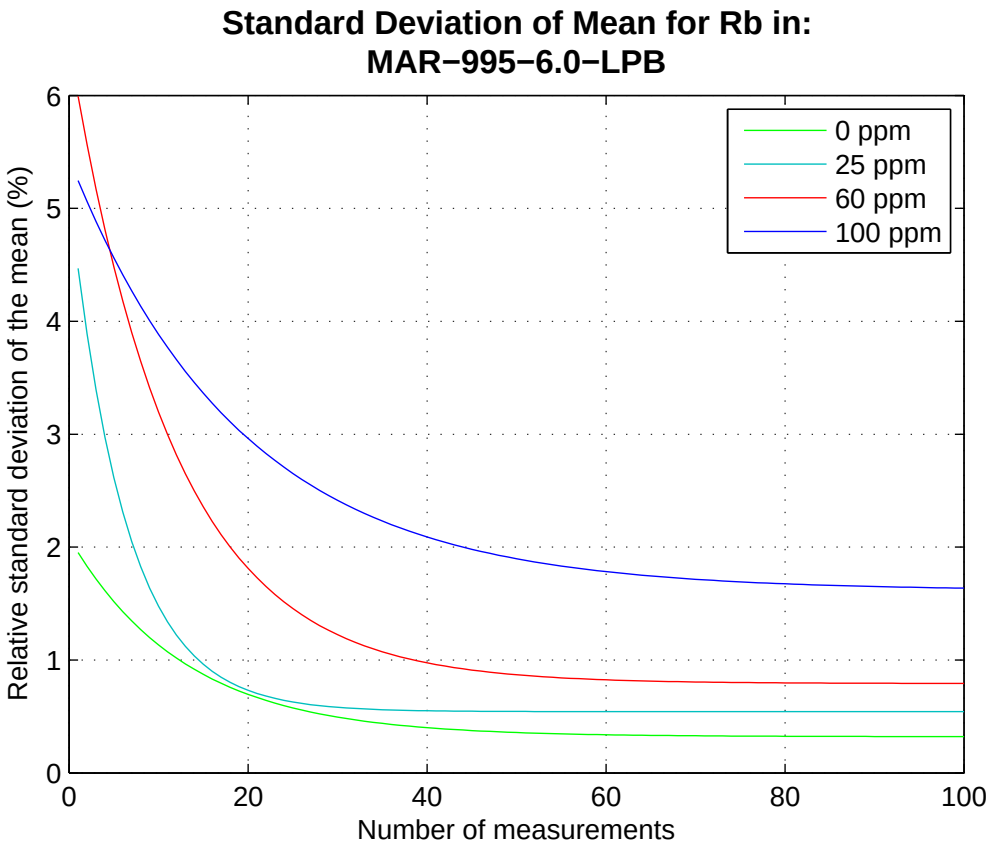

Figure 22: Performance comparison for Rb-tagged 6.0-LPB carpets

by the detector are lower than a certain threshold level, which implies that no sample is presented to the instrument. There is also a safety mechanism to shut off the instrument when the sample is greater than 5mm from the instrument.

The sample surface texture also affects the overall XRF measurement results. Any method of sample preparation must produce samples that are reproducible and which, for a certain calibration range, have similar physical properties including mass attenuation coefficient, density, particle size, and particle homogeneity. In addition, the sample preparation method must be affordable and must not introduce extra, significant systematic errors, for example the introduction of trace elements from contaminants in a diluent. Sample preparation is an all important factor in the ultimate accuracy of any XRF measurement.

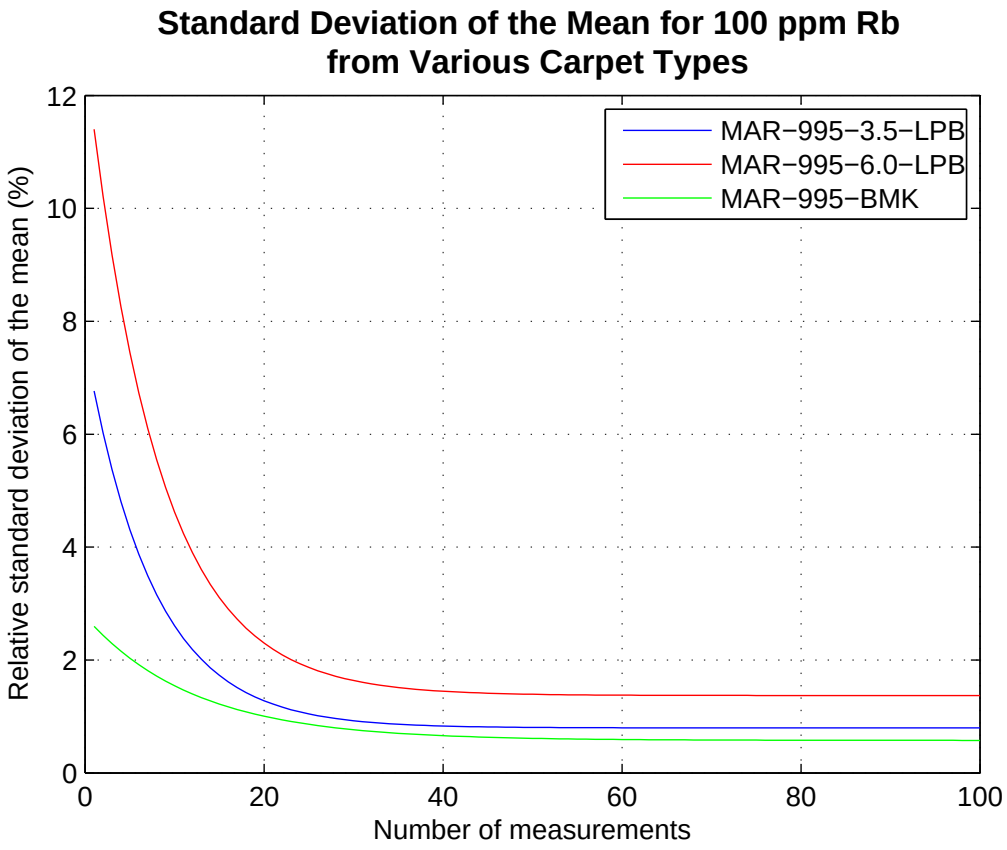

Figure 23: Performance comparison for 100ppm Rb from various carpet types

From the measurement factors studied in this chapter, a set of default measurement settings, shown in Table 4, are recommended for the near real time measurements of carpet and fluorochemical solution samples using Bruker's S1 TRACeR XRF instrument. These settings were selected so that the XRF instrument could sustain near continuous operation. The ten 30-second measurements per sample was selected to ensure a 5% relative standard deviation in measurement results from actual carpet samples.

Table 4: Default instrument and measurement settings

Category	Values
X-ray tube voltage	40 KeV
X-ray tube current	2.8 μA
Primary beam filter	Al (300 μm) Ti (25 μm)
Measurement time	30 s
Duty cycle	50 %
Measurement number	10

CHAPTER IV

DATA ANALYSIS AND SIGNAL PROCESSING

Signal processing is an important step in XRF analysis, especially in EDXRF, to accurately determine chemical constituents in a sample. The EDXRF spectra of the instruments used are generally complex due to sensitivity and channel resolution of semiconductors detectors. Powerful signal analysis tools are required to compute chemical concentration of samples for the complex spectra obtained from samples such as carpets. Selecting an appropriate set of signal processing algorithms for a specific application is typically performed by an experienced operator. This chapter evaluates several signal processing algorithms to determine a suitable set for the fluorochemical concentration analysis on carpet fibers.

Experimental measurement data always contain three types of uncertainties, which are *variability*, *measurement uncertainty*, and *vagueness* [21]. The variability of measurement data is typically observed from samples with slight physical variations such as the natural of uneven texture of typical carpets. The measurement uncertainty has contributions from the precision of the measurement and ignorance of the exact concentration in standard samples. Since collecting XRF spectrum data is a statistical process, independent count fluctuations exist on each energy channel and this gives the appearance of noise on the spectrum. This measurement noise needs to be removed in order to accurately apply XRF analysis to determine minute concentrations in complex samples, and is the main focus of this chapter. The vagueness is introduced by using a natural or professional language to describe an observation. For example, if the carpet is thick or loose. This type of uncertainty is generally characterized using fuzzy methods [21]; however, fuzzy methods were not included in

this work.

This chapter starts with the analysis of the measurement noise, which is the main factor to determine a nominal level of taggant concentration applied in the fluorochemical stock solution. Then a number of signal processing algorithms are discussed and their performance is evaluated for measuring the concentration of fluorochemicals on carpet specimens.

4.1 Noise and LLD Analysis

One of the fundamental problems when performing trace analysis with XRF spectra is estimating characteristic peak amplitude or area in the presence of background noise. The lower limit of detection (LLD) as described in Section 2.4 is a widely accepted standard utilized by many XRF practitioners. The LLD is the minimum peak amplitude that can be considered a statistically significant characteristic peak at any specific energy channel in the XRF spectrum, i.e., LLD is a function of background noise which may vary with energy. For this work, LLD is defined as 3.0 times the standard deviation of the background noise. Therefore, the first step in the XRF noise analysis is to determine the level of measurement noise, and its corresponding standard deviation, for a typical carpet sample in order to establish the nominal taggant concentration required for a candidate fluorochemical application.

To study the measurement noise, eight samples from four carpet types, each representing different manufacturing styles, were measured using Bruker's S1 TRACeR instrument with the XRF instrument settings listed in Table 5. These carpet samples were cut from carpet sections provided by a professional laboratory, where carpets were supplied to Georgia Tech with and without 25 ppm of Rb as a taggant. One blank and one Rb tagged carpet sample were tested for each of these carpet types. The carpet samples in Table 5 are arranged based on their carpet pile height and carpet density. Carpet No. 1 through 3 having the yarn density of approximately

45 oz per square yard and carpet No. 4 having the yarn density of 35 oz per square yard. These carpet samples are arranged with carpet No. 1 having the longest pile height of 0.88 inch to carpet No. 4 with the pile height of 0.30 inch.

Five measurements from each of the eight samples studied were obtained at the same measurement position on each sample and with the same instrument settings. Further, the samples were cut from the same general location across the carpet web for each carpet type. Intensity counts and standard deviations were calculated from measured XRF spectra for the energy range from 13.26 to 13.54 KeV, i.e., the energy range near the K_α characteristic peak of Rb. Results are shown in Table 6.

Table 5: Measurement settings for XRF noise analysis

Settings	Values
Tube voltage	40 KeV
Tube current	2.8 μA
Primary beam filter	Layer 1: Al (300 μm)
	Layer 2: Ti (25 μm)
Measurement time	30 sec
Measurement number	5
Taggant	Rb
Taggant channel range	13.26 - 13.54 KeV [59]

Table 6: Measurement noise analysis for carpet samples in Rb peak region

Carpet Sample No.	Yarn Density (oz/sy)	Pile Height (inch)	Average Background ($\bar{I}_b$)	Standard Deviation (σ_b)	LLD	Intensity Count from 25-ppm Rb-tagged Carpet
1	45-46	0.88	371	15.4	417	437
2	45-46	0.62	223	26.2	302	310
3	45-46	0.56	407	18.8	463	529
4	35	0.30	476	22.9	545	541

Two observations are made from the results in Table 6. The first observation regards the relationship between the physical characteristics of carpet samples and the total intensity count of the background over the selected energy range. Background

intensity counts are inversely proportional to the carpet pile height. No conclusion can be made for the relationship between yarn density and the net intensity counts due to the lack of carpet samples. The second observation regards the relationship between the physical characteristics of carpet samples and the total standard deviation calculated over the selected energy range. Specifically, there is no obvious correlation between the total standard deviation and carpet characteristics.

Based on the definition of LLD in Equation 5 and the results of Table 6, three out of four carpet types studied have LLD values low enough to statistically detect a concentration of 25 ppm Rb, which was applied to four of the eight samples. The 25 ppm Rb tagged carpet sample of the fourth carpet type resulted an average XRF intensity count of 541, which is slightly lower than the LLD value of 545. Thus, a minimum level of Rb that can be detected to a confidence level of 3.0 sigma is approximately 25 ppm. For carpet type No. 2, i.e., the least dense carpet type, 25 ppm of Rb can be detected to a confidence level of 3.2 sigma. The later value was determined by calculating the ratio of the Rb peak level in the 25 ppm tagged sample to the standard deviation of the noise background of the blank sample.

For the remaining of this chapter, four carpet samples tagged with 25 ppm Rb from each carpet type listed in Table 6 were used to study the performance of signal processing algorithms studied in this chapter. Five XRF measurements for each carpet sample were obtained using the instrument and measurement settings specified in Table 5.

4.2 Signal Smoothing Algorithms

Measurement data contain two types of noise, systematic and random [21]. The objective of the signal smoothing processes for XRF applications is to minimize random noise from a spectrum without distorting any characteristic peak amplitudes or

shapes. As mentioned in the previous section, the fundamental problem when performing trace analysis in XRF is to distinguish between small characteristic peaks and the background measurement noise. Sometimes the two can be partly distinguished on the basis of frequencies, e.g. signals may contains lower frequency components while random noise typically contains higher frequency components. This fact is the basis of most all filtering and smoothing algorithms [9].

4.2.1 Fourier Transform Method

The XRF spectra normally consists of three parts; a nearly constant component that is the continuum, the actual peak signal which is generally a lower to intermediate frequency component, and the random noise which is generally in a higher frequency range [60]. Thus, filtering out noise can be accomplished by applying a forward Fourier transformation from the XRF spectral domain to the amplitude versus frequency domain, filtering out higher frequency components, followed by applying an inverse Fourier transform back the the XRF spectral domain [9].

For any discrete spectrum $y(x)$, $x = 0, ..., n-1$, the discrete Fourier transform is defined as

$$Y(u) = \frac{1}{n} \sum_{x=0}^{n-1} y(x) e^{\frac{-j2\pi ux}{n}} \tag{11}$$

where $j = \sqrt{-1}$ and $u = 0, \ldots, n-1$. $Y(u)$ is a complex number that that contains both amplitude and phase information. Generally, if high frequency components are eliminated, random noise can be reduced without affecting the spectral peak shapes. Such filtering is accomplished by multiplying the Fourier transform with a suitable filter function $H(u)$:

$$Y^*(u) = Y(u)H(u) \tag{12}$$

A high frequency cutoff filter is one such example:

$$H(u) = \begin{cases} 1, & u \leq u_{th} \\ 0, & u > u_{th} \end{cases} \tag{13}$$

This filter sets the real and imaginary coefficients above a cutoff frequency, u_{th}, to zero. Finally, the inverse Fourier transformation shown below is used to transform from the frequency domain to the original XRF spectral domain.

$$y(x) = \sum_{u=0}^{n-1} Y(u) \exp\left(\frac{j2\pi ux}{n}\right) \tag{14}$$

Since multiplication in the Fourier domain is equivalent to convolution in the original domain, spectrum smoothing operations can also be done directly in the original XRF spectral domain. Specifically, this can be implemented as the convolution of the original XRF sptrum with a digital filter $h(x)$, which is the inverse Fourier transformation of $H(u)$. Consequently, the smoothed spectrum y^* can be directly calculated using the following equation.

$$y^*(x) = \frac{1}{N} \sum_{j=-m}^{m} h(j)y(x+j) \tag{15}$$

where N is a suitable normalization factor and the filter width is given by $2m+1$.

Figure 24 shows the results from applying a high frequency cutoff filter, with cutoff frequencies of 0.05, 0.10, and 0.15 Hz, to a Rb K_α peak from a 25 ppm Rb tagged carpet sample. The plotted region focuses on the Rb characteristic peak. A high frequency cutoff filter preserves the overall peak shapes while most of the random measurement noise is significantly reduced. The noise is decreased as the cutoff frequency decreases; however, a peak distortion is more pronounced as the cutoff frequency approaches 0 Hz.

4.2.2 Moving Average Smoothing Algorithm

A moving average filter, also known as box-car filter, is one of the simplest and most effective smoothing algorithms [21, 9]. Starting from a measured spectrum y,

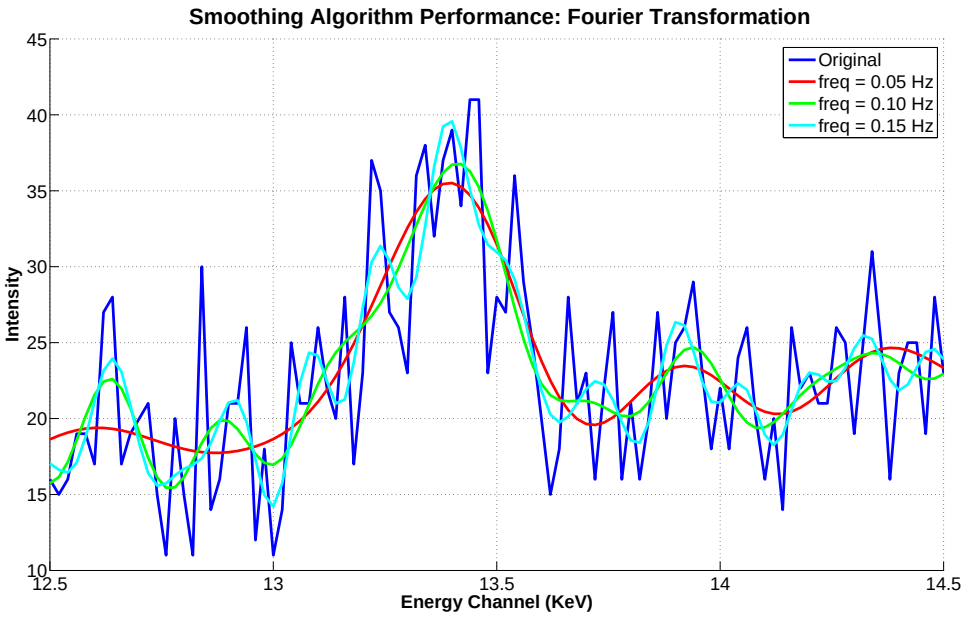

Figure 24: Effect of Fourier transform and lowpass filter with cutoff frequencies=0.05, 0.10, and 0.15 Hz

a smooth spectrum y^* is obtained by calculating the mean channel content around each channel x:

$$y^*(x) = \frac{1}{2m+1} \sum_{j=-m}^{+m} y(x+j) \tag{16}$$

Although this filter is mathematically simple, it introduces a considerable amount of peak distortion, which increases as the filter channel width $2m+1$ is increased. Figure 25 shows an example of the noise reduction and peak distortion results a moving average filter applied to XRF spectral data in the region near a Rb for filter widths of 3, 5, 10, and 25 energy channels.

The peak distortion effect of a moving average filter is generally undesirable for XRF spectral analysis. However, by placing more weight on the central channels and less weight on the end channels of the filter, smoothing can be accomplished with a reduced amount of peak broadening when compared to the standard moving average filter, and such filters are referred to as *weighted moving average* filters [21].

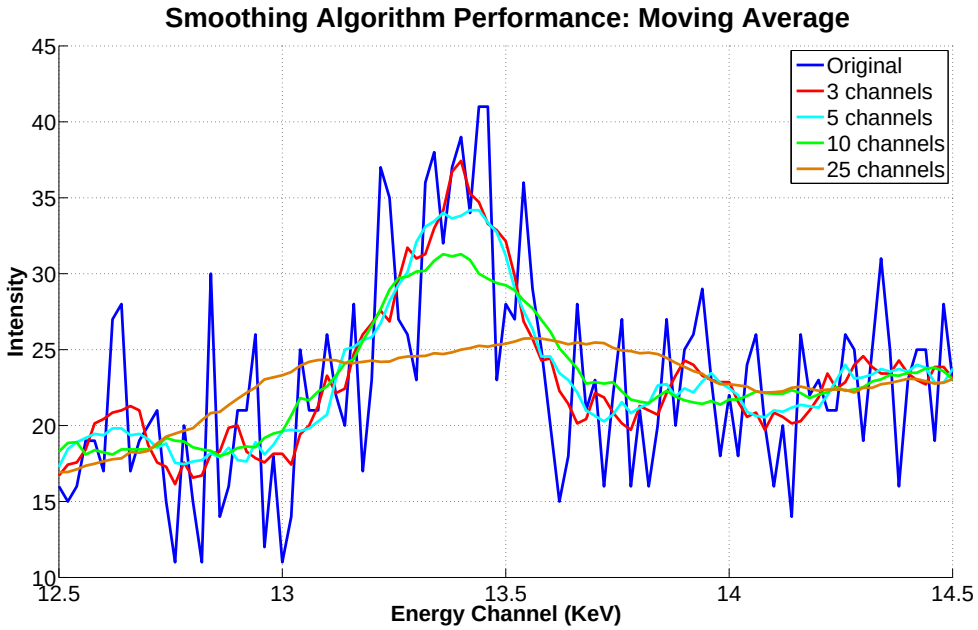

Figure 25: Effect of the moving average filter channel $2m + 1$ on noise reduction and peak distortion

4.2.3 Savitsky and Golay Polynomial Filters

Statistical fluctuations on a measured spectra near a characteristic peak of interest may also be reduced using a polynomial filtering method developed by Savitsky and Golay [9]. For this method, a best-fitting curve is drawn through the data points in the region of the spectral peak. This method is based on the fact that nearly all measured spectrum y can be modeled by a polynomial of some order r, i.e.,

$$y(x) = a_0 + a_1(x - x_0) + a_2(x - x_0)^2 \cdots + a_r(x - x_0)^r \tag{17}$$

where x is the energy channel index. Once the coefficients a_j are determined, the value of the polynomial at the central channel x_0 can be used as the smoothed data value:

$$y^* = y(x_0) = a_0 \tag{18}$$

When strictly applied, this method requires a least-squares fit to all the individual data points in the spectral range of interest. However, since all the energy channels

x are evenly spaced, this procedure may be implemented more efficiently as a convolution of the spectrum with a filter having appropriate weights [21, 9]. In general, fitting a spectrum y with a Savitsky-Golay polynomial of degree r and channel width of $2m+1$, the smoothed spectrum y^* can be written as

$$y^*(x) = \frac{1}{N_{rm}} \sum_{j=-m}^{j=m} C_{rm,j} y(x+j) \tag{19}$$

where N_{rm} and $C_{rm,j}$ are the normalization factor and the convolution integers, respectively. Both of these constants depend on the polynomial degree r and the filter half width m and are shown in Table 7.

Table 7: Savitsky-Golay coefficients for $r = 2$ and $r = 3$ and filter width $= 2m + 1$ [9]

		j ($C_{rm,j} = C_{rm,-j}$)												
m	N_{rm}	0	1	2	3	4	5	6	7	8	9	10	11	12
2	35	17	12	-3										
3	21	7	6	3	-2									
4	231	59	54	39	14	-21								
5	429	89	84	69	44	9	-36							
6	143	25	24	21	16	9	0	-11						
7	1105	167	162	147	122	87	42	-13	-78					
8	323	43	42	39	34	27	18	7	-6	-21				
9	2261	269	264	249	224	189	144	89	24	-51	-136			
10	3059	329	324	309	284	249	204	149	84	9	-76	-171		
11	805	79	78	75	70	63	54	43	30	15	-2	-21	-42	
12	5175	467	462	447	422	387	342	287	222	147	62	-33	-138	-253

The Savitsky-Golay smoothing algorithm was applied to the same XRF spectrum that was shown for the moving average filter in Figure 25 and results are shown in Figure 26 for polynomial degrees of 2 and 3 along and channel widths of 3, 5, 10, and 25 enegy channels. In comparison to the smooth spectra processed by the moving average algorithm, the Savitsky-Golay algorithm introduces less peak distortion for the same window channel width.

The peak distortion effect introduced by both the moving average and the Savitsky-Golay algorithms both depend on the ratio of filter width to peak width ratio [9].

However, for the Savitsky-Golay algorithm, when the filter width becomes wider than peak width, some oscillations can be observed near the characteristic peak boundaries [9].

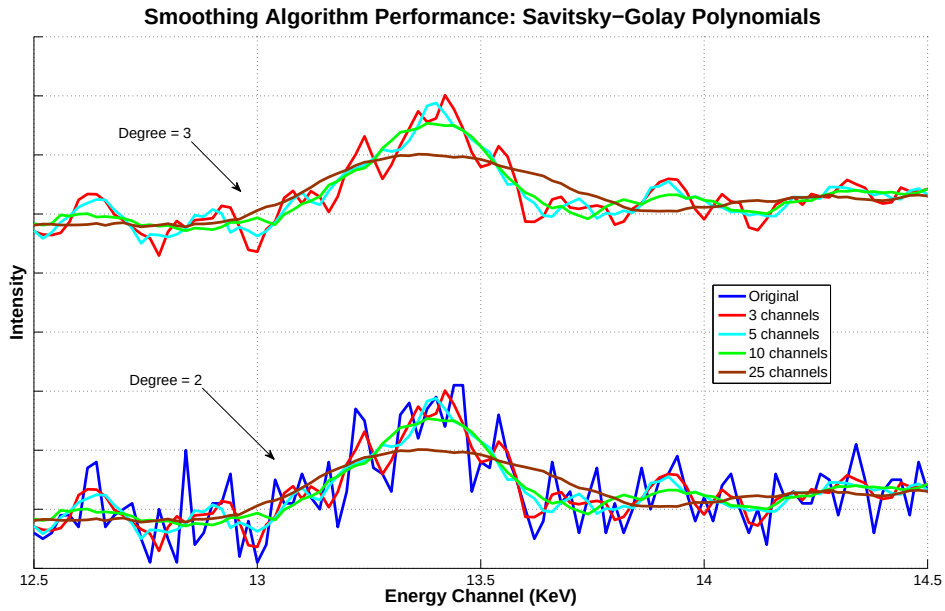

Figure 26: Effect of the Savitsky-Golay polynomials smoothing algorithms with polynomial degree = 2, 3 and channel width = 3, 5, 10, 25 channels

The Savitsky-Golay polynomial smoothing algorithm is an attractive method for on-line smoothing processing of XRF spectra not only because of its simple implementation procedure to produce the smoothed algorithm, but also its capability to simultaneously produce the second derivative of the smoothed spectrum without an additional processing step, which can be useful for peak identification process describing in the next section [9].

4.2.4 Low-Statistics Digital Filter

The low-statistics digital filter provides n-point mean smoothing of the data, primarily in areas with low counts, while avoiding the spreading of the bases of spectral peaks and the degrading of minima between peaks [61]. An adaptive n-point smoothing filter may be applied selectively to the low statistics regions of the spectrum between

peaks. Generally, the width of the interval is decreased as the channel counts increase. In addition, a slope fit to the smoothing interval is used to detect the onset of a peak, which may be used to reduce the interval to avoid the incorporation of the peak tail in the average for the smoothing interval.

The algorithm for the low-statistics digital filter may be used to produce a smoothed spectrum y, channel by channel, in a single pass. For each channel, i, the algorithm can be summarized by the following steps:

1. Contents from two adjacent windows, one on each side of the channel i with f channels wide, are summed to produce L (left) and R (right) side sums.

2. Both windows are reduced in width until the total sum $S = y + L + R$ falls below a minimum M, which sets the base degree of smoothing in regions of vanishing counts, or until two conditions are met

   - The sum $S < A\sqrt{y}$, where A is a constant
   - The slope $\frac{1}{r} \leq \frac{R+1}{L+1} \leq r$, where r is a constant.

3. Once the above conditions are satisfied, the average S/W is adopted as the channel count, where $W = 2f + 1$

The results from the applying the low-statistics digital filter on the same XRF spectrum with varying channel width (f), base degree (M), cut-off (A), and slope sensitivity (r) are shown in Figures 27 through 30. Figure 27 shows that random noise in the region of the peak is reduced and peak distortion is increased as the filter channel width (f) is increased. All other parameters (M=10, A=75, r=1.3), were held constant. Figure 28 shows that the base degree (M) determines how close to the top of the characteristic peak the algorithm can be applied and still conserve all the peak information. Figure 29 shows that the noise removed from the peak area is directly proportional to the cut-off (A). Further, aggressively removing random noise

increased the amount of the peak distortion. Figure 30 shows the effect of the slope sensitivity (r) in the smoothing process. The amount of smoothing decreases as the value of r approaches a value of 1.

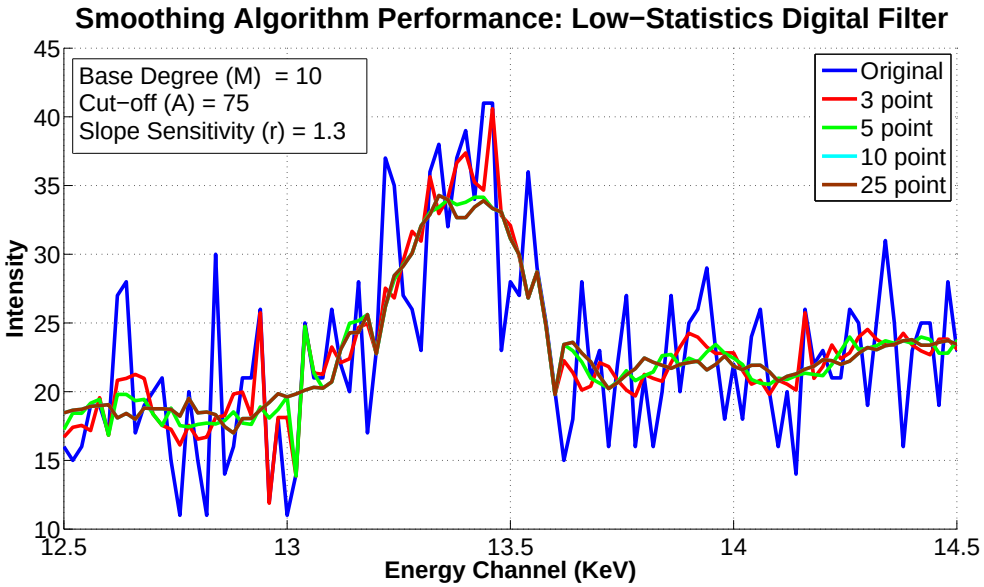

Figure 27: Effect of the low-statistics digital filters with channel width (f)=3, 5, 10, 25 and M=10, A=75, and r=1.3

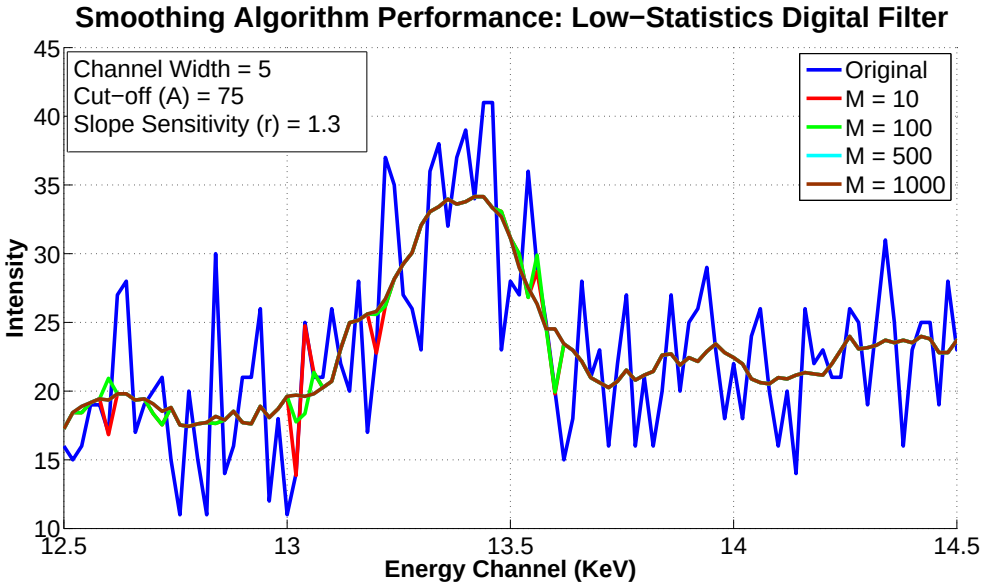

Figure 28: Effect of the low-statistics digital filters with base degree (M)=5, 10, 15 and f=5, A=75, and r=1.3

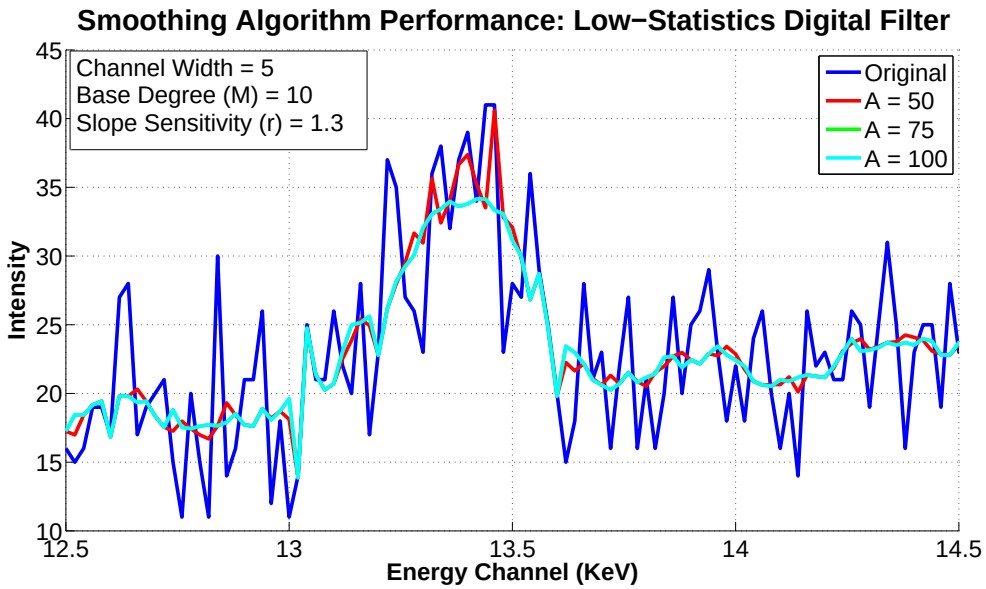

Figure 29: Effect of the low-statistics digital filters with cut-off (A)= 50, 75, 100 and channel width=5, M=10, and r=1.3

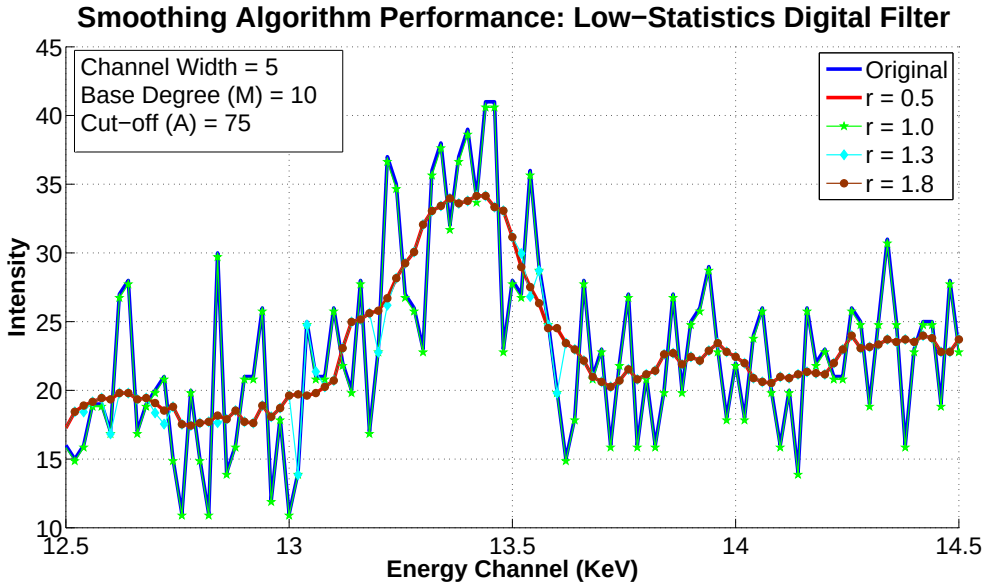

Figure 30: Effect of the low-statistics digital filters with slope sensitivity (r) = 0.5, 1.0, 1.3, 1.8 and channel width=5, M=10, A=75

Although the low-statistics digital filter has the advantage of conserving the original characteristic peak information while reducing random noise in the continuum region of the XRF spectra, determining the parameters for this algorithm is rather

heuristic [9]. From experimenting with Rb characteristic peaks from thirteen different carpet samples, the algorithm parameters resulting in the best noise reduction in the background continuum region while maintaining the most original characteristic peaks are with channel width $f = 3$, base degree $M = 10$, cut-off $A = 75$, and the slope sensitivity $r = 1.3$.

Figure 31 shows smoothed spectra from all of the smoothing algorithms described in this section using parameter values listed in Table 8 and statistics of each are list in Table 8. The effectiveness of each smoothing algorithm was determined by calculating the sum of squares of the differences between the smoothed spectrum and the actual spectrum shown in Equation 20. From these results listed in Table 8 and visual examination of curves in Figure 31, it is apparent that the Fourier transform and the moving average algorithms significantly reduce random measurement noise while the Savitsky-Golay and low-statistics filter algorithms are better candidates for preserving the original peak shapes. Further, the results shown in Table 8 show that the low-statistics digital filter out performs other smoothing algorithms in terms of peak preservation. However, visual inspection of results shown in Figure 31 suggests that the low-statistics filter still contains a great deal of measurement noise in the characteristic peak region. From these results, the Fourier transform method, which is the next best performance in peak preservation and noise reduction, was selected for future signal processing of XRF spectra in this research. The XRF spectrum analyzed in this section is processed using the Fourier transform method with a cutoff frequency of 0.10, and the resulting spectrum is presented in the next section as an example of the background elimination method.

$$\chi_s = \sum_{j=x1}^{x2} \left(y_{ref}(j) - y^*(j)\right)^2 \tag{20}$$

where $x1$ and $x2$ are the start and end channel indices for a given region of interest.

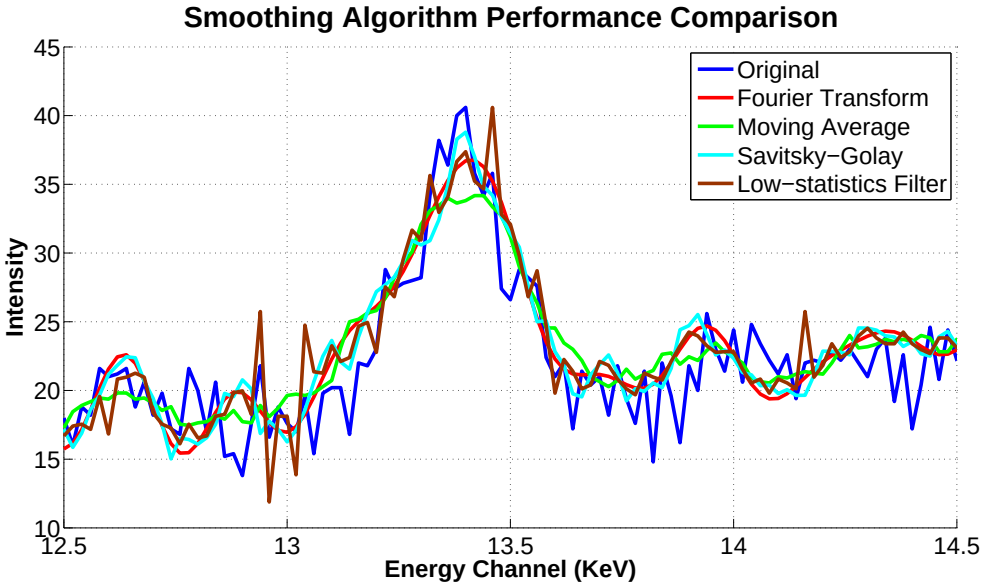

Figure 31: Comparison of smooth spectra resulting from Fourier transformation, moving average, Savitsky-Golay polynomials, and low-statistics digital filter

Table 8: Effectiveness of smoothing algorithms on an XRF spectrum

Algorithm	Algorithm Parameters	χ_s
Fourier Transform	$u_{th} = 0.10$	1982
Moving Average	$2m + 1 = 5$	2341
Savitsky-Golay	$r = 3$	2036
	$2m + 1 = 5$	
Low-statistics Filter	$f = 3$	1943
	$M = 10$	
	$A = 75$	
	$r = 1.3$	

4.3 Background Elimination Algorithms

In XRF analysis, the estimation and removal of the continuum on which the characteristic peaks are superimposed is a primary requirement. Under-estimation or over-estimation of the continuum can potentially introduce large errors in quantitative analysis, especially for small characteristic peaks. Continuum estimation methods, which are effectively heuristic approaches, must fulfill the following requirements: the method must be able to reliably estimate the continuum in all kinds of situations,

e.g., small isolated peaks on a high continuum as well as one peak in proximity to another peak, the method must permit processing of a large number of spectra efficiently, and the method needs to be nearly free of user-adjustable parameters [9]. This section investigates several background elimination algorithms to determine a suitable background elimination algorithm for the real-time XRF analysis of carpet samples.

4.3.1 Peak Stripping Method

The peak stripping method was originally designed for PIXE spectra, but also proved to be generally applicable for pulse-height spectra as shown by Clayton et al. in 1987 [9]. This method essentially compares the mean of the intensity counts between the neighboring channels, $y(x + w)$ and $y(x - w)$, and the current channel count $y(x)$. Here, w is the distance away from the current channel along the XRF spectrum energy axis. The general mathematical model for this method can be written as:

$$m(x) = \frac{y(x - w) + y(x + w)}{2} \tag{21}$$

This algorithm is applied as follows: Let $m(x)$ be the mean value of channel x. If $m(x)$ is smaller than the actual count $y(x)$ of this channel, then the content of channel x is replace by $m(x)$. This transformation is repeated until the background is reduced to an acceptable level.

The distance w can take any positive integer value. In fact, a study by Ryan et al. [61] suggests that the value for w should be twice the FWHM of the spectrometer at channel x resulting in a minimum iteration number of 24 to generate an acceptable continuum shapes when applied to PIXE spectra. During the last eight iteration cycles, w is progressively reduced by a factor of $\sqrt{2}$ to obtain a smooth continuum. Further, a difference algorithm for background elimination, known as the SNIP algorithm (Statistical Nonlinear Iterative Peak clipping) was also introduced by Ryan et al., which combined the low-statistics digital filter with the peak stripping method.

Because the peak stripping method tends to connect local minima, it is very sensitive to local fluctuations due to the random measurement noise [9]. Therefore, to avoid oscillations in a estimated background continuum, it is mandatory to smooth the spectra prior to application of the peak stripping method. The number of iterations depends on the width of characteristic peaks. When ideally applied, after an appropriate number of iterations, the continuum converges and a more or less smooth continuum results.

Figure 32 shows the estimated continuum using peak stripping methods for a constant iteration number of 2000 but when varying the neighboring distances from w =1 to 10. These results suggest that the continuum is over estimated if the intensity counts are just taken from the immediate neighbors on each side, which consequently reduces the precision of the net peak area determination. Figure 33 shows the estimated continuum using the peak stripping method for a constant neighbor distance of $w = 3$, but when varying the number iterations from 100 to 2000. With a small number of iterations, the continuum tends to be over-estimated and partial peak area information may be interpreted as being part of the continuum. However, a larger number of iterations results in longer signal processing times.

4.3.2 Envelope Method

The envelope method is another simple algorithm that requires no additional spectrum information to effectively remove the continuum counts from XRF spectra. In this method, the envelope of the points in a spectrum is plotted from beneath, i.e. the lower envelop limit of the continuum. Since the lines of XRF characteristic peaks are generally narrower than the continuum, the values at tangency points of the envelope can be considered equal to the background magnitude (noise is ignored) as is described next [62].

Two "movable" points, are displaced along the spectrum. The first point is the

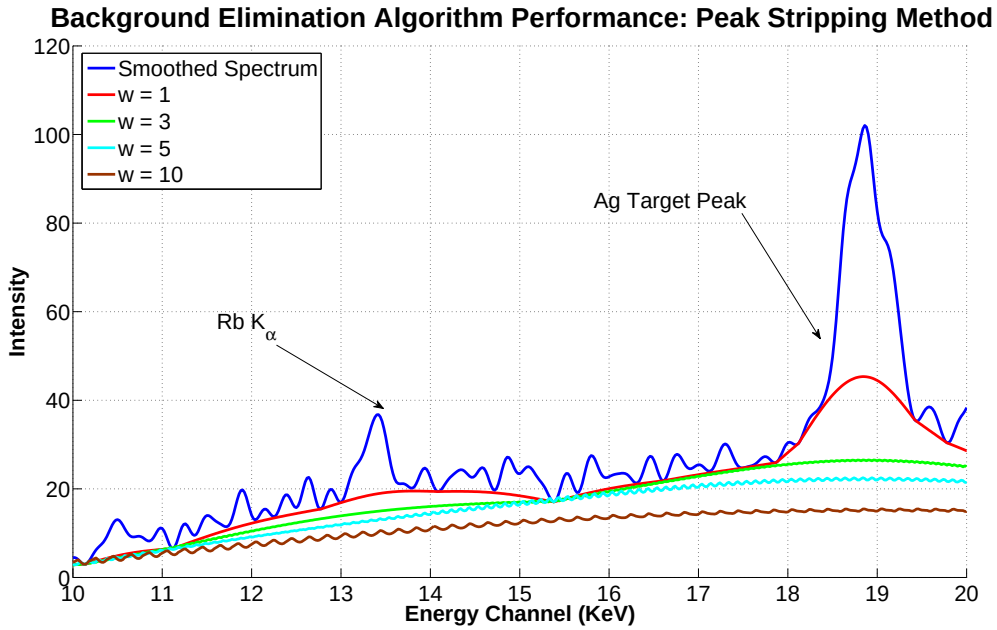

Figure 32: Effect of the peak stripping method with neighbor distance (w) = 1, 3, 5, and 10

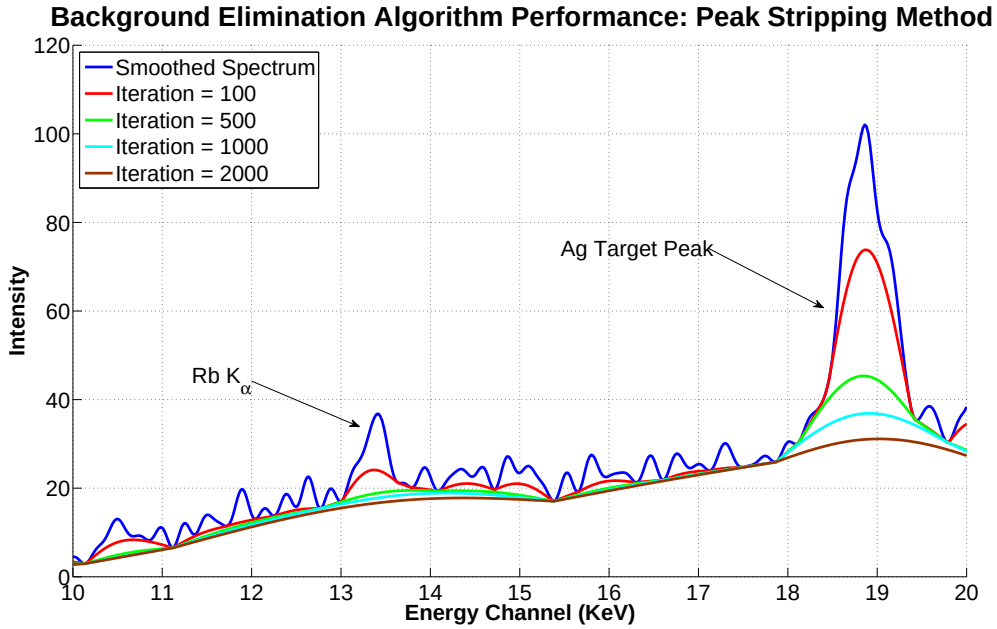

Figure 33: Effect of the peak stripping method with the number of iterations = 100, 500, 1000, and 2000

initial point of an experimental spectrum, and the second is its final value of a given channel width m (wider than a typical characteristic peak). A linear segment is drawn

between the movable points. If at least one point of the spectrum lies below this line, the second movable point is displaced to a spectral point with an index reduced by one. The second point moves along the spectrum until all of the spectral points falling within the interval between the two movable points lie above the linear segment. The first and second points found as a result of this procedure are considered to be the points along the envelope and these values are used to begin the next iteration.

In the next iteration, the position of the second movable point is assumed as the beginning of the continuum region under analysis, and the first movable point is repositioned there. Next, the second movable point is relocated m channels away toward the end of the spectrum thereby repeating the entire procedure all along the spectrum to obtain all the points of the envelope. Next, a parabolic spline is fit to the distinct neighboring points. Each parabola is generated based on three neighboring points to ensure the continuity, but the spline involves only the segment of the parabola that connects the final two points. The final estimated continuum is the concatenation of all the splines calculated for the entire spectrum.

Figure 34 shows the results from applying the envelop background elimination method to the same XRF spectrum used as the previous example. In this figure, four channel widths of 50, 100, 200, and 500 are applied to the spectrum and the corresponding estimated backgrounds are shown. Too large or too small of a value for the channel width generates under-estimated or over-estimated continuum, respectively. To effectively estimate the background of a given XRF spectrum, the channel width should be chosen slightly larger than the analyzing characteristic peak. In this example, the channel width of 100 channels (2 KeV), is sufficiently wider than the channel widths of both the Rb and the Ag peaks; thus, these peaks are eliminated and the background continuum is estimated correctly.

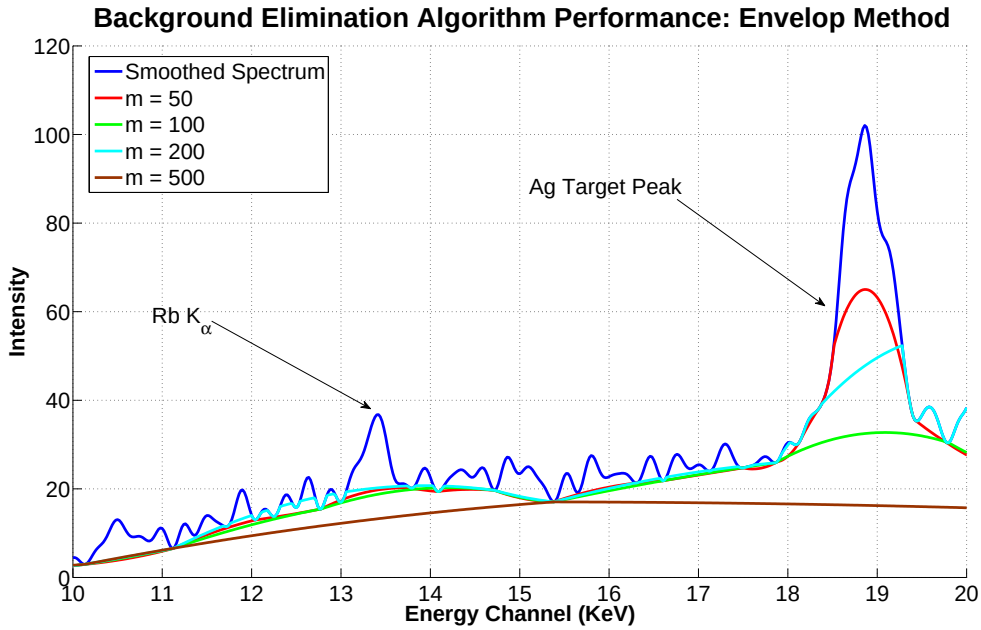

Figure 34: Effect of background elimination algorithm using the envelop method with window channel width $m = 50$, 100, 200, and 500

4.3.3 Morphological Operators

Background removal algorithm using morphological operators is a fast continuum elimination algorithm without peak distortion. This method does not required additional spectral information, and can be rapidly applied to on-line analysis of spectra [63]. The mathematical morphology method was developed in 1964 by Matheron and Serra as a nonlinear approach to image processing. As proposed by Antonio Brunetti [63], operators were utilized to cancel noise while conserving signal characteristics. Since the spectral information for XRF applications is one-dimensional, the following description of the morphological algorithm is only expressed in the one-dimensional sense.

This method can be thought of as an interaction of a signal spectrum f with one or more data structure sets m, which contain characteristic peak information. This interaction changes the original signal spectrum into a new form that is intended to be more expressive to the user. The morphological operators are local operators

defined in terms of intersection, union, difference, max, and min. The operation of the morphological operators on one-dimensional signals such as XRF spectra is simple [63]. The definitions given below for the morphological operators are restricted to only the one-dimensional signal case.

The morphological language is based on two basic operators: erosion and dilation, denoted by '$\oplus$' and '$\otimes$' operators, respectively. These operators are the complement of each other and are performed on the signal data f with length M and the structural data k with length N. The erosion and dilation operators are defined as the following:

$$(f \oplus k)(m) = \min_{n=0,...,M-N} (f(m+n) - k(n)), \text{for } m = 0, ..., M-N \quad (22)$$

$$(f \otimes k)(m) = \max_{n=0,...,N-1} (f(m-n) + k(n)), \text{ for } m = N-1, ..., M-1 \quad (23)$$

Performing an erosion followed by a dilation provides a new operator, the *opening*, while an erosion after a dilation builds another operator, the *closing*. The opening operation cancels small components of the signal and smooths internal contours, while the closing operator magnifies little components and smooths external contours.

Both the *opening* and the *closing* operators can be used for continuum removal. If the *open* operation is performed on a signal, the positive peaks with a base narrower than the structure data width S will be canceled. Similarly, if the *close* operation is performed on a signal, the the negative peaks with a base narrower than S will be canceled. Since XRF spectra contain only positive peaks, only the *open* operation is required. The data structure suitable for removing the background continuum is found to be a horizontal segment with S wide and zero intensities, i.e. $k(n) = 0$ for $n = 0, 1, 2, \ldots, S-1$ [63]. The overall background removal procedures using the morphological operators can be summarized as the followings:

1. Estimate the width of the interested characteristic peaks (S)

2. Define the structural element with zero intensities and the length S (i.e. $k(n) = 0$, for $n = 0, ..., S-1$)

3. Perform an open operation on the desired XRF spectrum using the structural element defined in the previous step

4. Perform an interpolation between data points from the spectrum in the previous step to obtain the estimated background continuum

Figure 35 shows the estimated continuum of the Rb-tagged XRF spectrum using morphological operators for a structure data segment $S = 5$, 10, 25, and 50. For this example, the segment length of 25 (0.5 KeV), which is approximately the FWHM of the Rb peak, effectively estimates the continuum without over or under estimate the Rb characteristic peak. This result confirms the study in [63] that the optimal segment S should be slightly larger than the FWHM of the analyzing peak, which suggests that the segment S should be chosen dynamically to suit different peaks targeted for analysis. This dependence of S on the FWHM can potentially introduces errors in XRF spectrum analysis as will be show in a later chapter for Rb characteristic peaks from different carpet styles with different FWHM values.

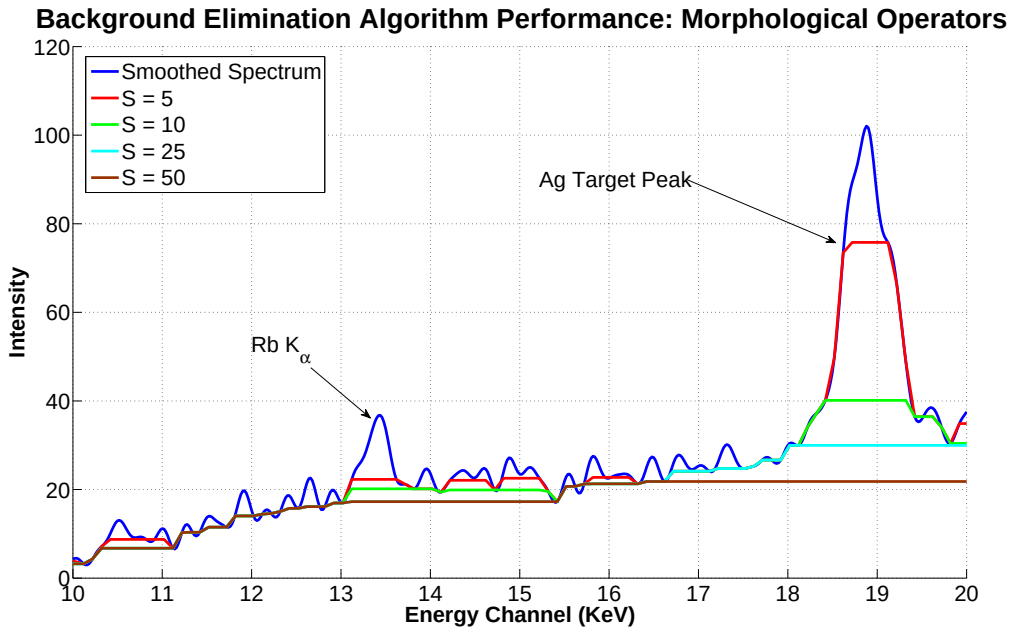

Figure 35: Effect of background estimation using morphological operators with data structure segment $S = 5$, 10, 25, and 50

4.4 Peak Searching Algorithms

Peak search procedures usually involve three steps: (1) transformation of the original spectrum so that background contributions are eliminated, peaks are readily locatable, and overlapping peaks are partially resolved, (2) a significance test and approximate location of the maximum for each peak, and (3) determination of a more accurate position estimate of peaks in the original spectrum. Various peak search algorithms mainly differ in the choice of the transformation. Some methods use the first and second derivative of the spectrum to locate local maxima. Other methods employ some form of correlation technique, which is basically the convolution of the original spectrum with a filter in order to emphasize the peaks.

The simplest and the most effective filters for XRF spectra belong to a group of zero-area rectangular filters [9]. An important representation of this group of filters is the "top-hat" filter, which has a central window with an odd number of channels and two side windows. The convolution of an X-ray spectrum with this kind of filter yields spectra in which the continuum is removed and the peaks are easily locatable. These filters have a central window with an odd number of channels w and two side windows each v channels wide. The value of the filter coefficients follows a zero-area constraint:

$$h(k) = \begin{cases} -\frac{1}{2v}, & -v - \frac{w}{2} \leq k < -\frac{w}{2} \\ \frac{1}{w}, & -\frac{w}{2} \leq k \leq +\frac{w}{2} \\ -\frac{1}{2v}, & +\frac{w}{2} < k \leq \frac{w}{2} + v \end{cases} \tag{24}$$

The filtered spectrum is obtained by the convolution of the original spectrum with this filter:

$$y'(i) = \sum_{k=-v-\frac{w}{2}}^{k=v+\frac{w}{2}} h(k)y(i+k) \tag{25}$$

The variance of the filtered spectrum is obtained by simple error propagation:

$$sy'(i)^2 = \sum_{k=-v-\frac{w}{2}}^{k=v+\frac{w}{2}} h^2(k)y(i+k) \tag{26}$$

If $y'(i)$ is significantly different from zero, a peak structure is found and the top of the peak can be approximately located by searching for the maximum. Thus, i corresponds to the position of a peak maximum in the original spectrum if the following conditions are satisfied:

$$y'(i) = rsy'(i)^2 \tag{27}$$

$$y'(i-1) \leq y'(i) > y'(i+1) \tag{28}$$

Typical values for the sensitivity factor r are between 2 and 4. Higher values result in the loss of small peaks; lower values cause background noise to be interpreted as peaks [9].

Figure 36 shows the filtered (convolved) spectrum from applying the top-hat filter to an XRF spectrum. The presence of the characteristic peak is clearly visible on the filtered spectrum. Once the peak is located, a more precise maximum for the location of the peak can be found by fitting a parabola or Gaussian over a few channels around the peak.

4.5 Curve Fitting Methods

The objective of curve fitting is to find a mathematical equation that describes XRF data for a range of the spectrum but is minimally influenced by random noise. The major considerations involved in implementing a curve fitting method include (1) choosing the fitting function, (2) selecting a "best fit" criteria, (3) implementing an optimizing algorithm, and (4) validation of results [64]. In this section, functions and procedures suitable for performing curve fitting for XRF characteristic peaks are investigated.

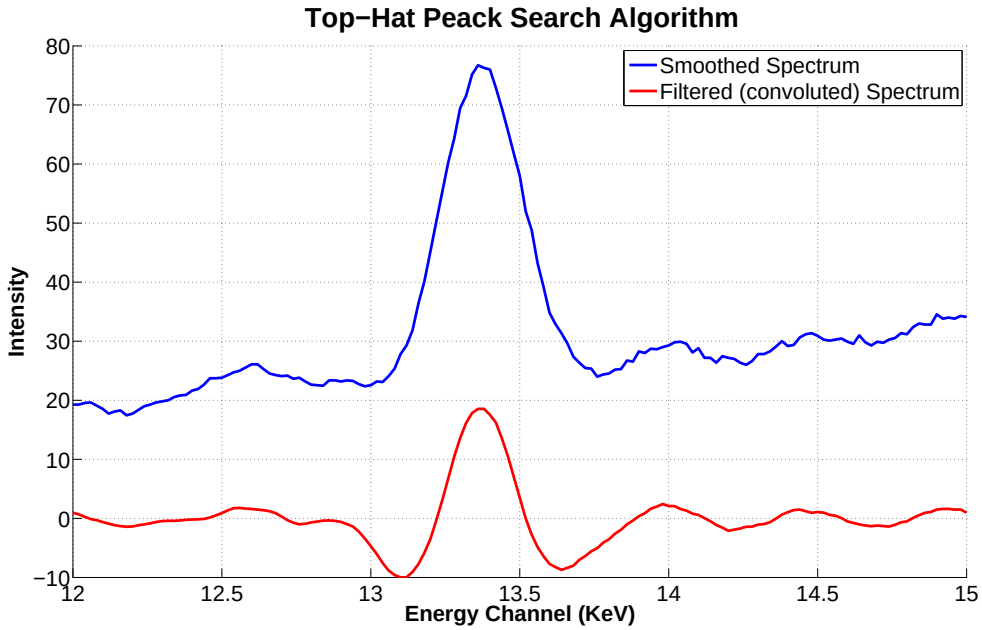

Figure 36: Result from applying a top-hat filter to a smoothed XRF spectrum for peak identification

Studies show that the response function of most solid-state detectors is predominantly Gaussian. However, when describing the curve for the K lines of high atomic number elements, such as Pb or U, the influence of the natural line shape becomes appreciable and the use of a more complicated Voigt profile is required [9, 11, 65, 22, 64, 10]. For health hazard reasons, the chemical taggants employed in fluorochemical measurements on carpet fibers are lower atomic number elements; thus, a Gaussian curve is sufficient for representing the characteristic peaks.

A Gaussian peak is characterized by three parameters: peak position, width, and height or area. XRF analysis utilizes peak area rather than peak height because the peak area directly relates to the number of X-ray photons detected by the instrument while the peak height depends on the instrument resolution [9]. The general form of a Gaussian peak profile $G(x)$ is given by

$$G(x) = A \exp\left[-\frac{(x-b)^2}{2c^2}\right] \tag{29}$$

where A is the peak height, b is the location of the peak maximum, and c is the

width of the Gaussian peak expressed in energy channels. The term FWHM in XRF analysis is related to c by a factor of $2\sqrt{2\ln(2)}$ or FWHM$= 2.35c$. The peak area is also related to the peak parameters by the relationship AREA$= A\sqrt{2\pi}c$.

The optimization criteria χ^2 commonly used to determine the suitability of Gaussian curve fitting in XRF, as well as other physical analysis problems, is defined as the weighted sum of squares of the differences between the model $\hat{y}$ and the measured spectrum y over a region of interest [9, 64]:

$$\chi^2 = \sum_j \frac{(\hat{y}(j) - y(j))^2}{\sigma_j^2} \tag{30}$$

where χ_j^2 is the variance of a data point j. The optimal values of the parameters are those for which χ^2 is minimal.

In many XRF applications, the optimization function χ^2 can be expressed as a linear function of the parameters of interest. For the example of applying a known chemical taggant, one can assume that the peak position c and width b of the chemical taggant are known so that only the height parameter A need to be determined. The complete mathematical expression for an XRF spectrum without background can be expressed as

$$\hat{y}(x) = A_1 G_1(x) + A_2 G_2(x) + \ldots + A_n G_n(x) \tag{31}$$

where A_j is the peak height of the j^{th} element in the sample and $G_j(i)$ is the Gaussian function for the j^{th} element with fixed parameters b and c for the x index. Solving for this fitting function for the minimum optimization criteria shown in Equation 20 is straight-forward and can be accomplished for most of the curve fitting problems in this study using this linear function.

A nonlinear fitting function must be used in XRF analysis when the location of characteristic peaks and/or their width parameters are uncertain. The Gaussian functions representing characteristic peaks in a spectrum are then replaced with nonlinear functions that are complicated to solve. Such nonlinear curve fitting problems are

typically solved using the following: pattern search methods, gradient search methods, and analytic solution methods. These nonlinear curve fitting processes most often slowly converge to a useful solution, making these unsuitable for near real time analysis [66, 64].

The last step in the curve fitting process is the validation of results. The χ^2 fitting criteria is a useful indicator which will be used in this study to report the quality for various least-squares fitting problems. For convenient, χ^2 is reported as "normalized chi-squared", that is divided by $(N - n)$ where N is the number of data points fitted and n is the number of free parameters. When normalized, $\chi^2 \approx 1$ indicates a "good" fit and $\chi^2 \gg 1$ is an indication of a systematic error.

A Rb K_α peak is fitted using the Gaussian peak profile defined in Equation 29 resulting in the fitted curve shown in Figure 37. Only the top half of the characteristic peak is used in the curve fitting to prevent any interference from the characteristic peak and background noise. Based on the fitting criteria χ^2_{NORM}, this Gaussian curve is fitted with $\chi^2_{\text{NORM}} = 2.31$, which is considered a reasonably good fit.

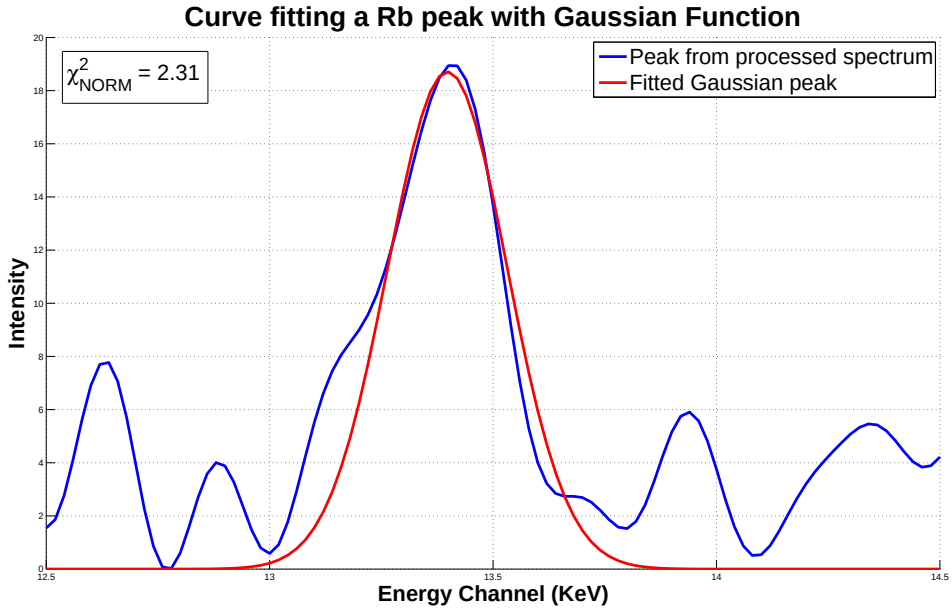

Figure 37: Fitted Gaussian peak for a Rb K_α peak from a carpet sample

4.6 Peak Area Determination

Peak area determination is a very important process in EDXRF spectroscopy. For many applications, quantitative analysis is customarily based on the peak area rather than a peak height measurements. The reason for this is that peak area is less sensitive to the influence of peak broadening (dispersion) mechanisms. These broadening effects, which arise from many sources, cause spectral peaks to be shorter, broader, and more unsymmetrical, but have little effect on the total area under the peak [9]. The peak area remains proportional to the total quantity of element detected by the instrument; therefore peak area remains proportional to the total quantity of substances whose counts are registered by the detector.

A simple approach for peak area determination, which is a direct consequence of the curve fitting procedure, is to calculate the parameters of a Gaussian function fit to the peak. The parameters calculated from the curve fitting process can be used directly to calculate the net peak area using the formula AREA= $A\sqrt{2\pi}c$, where A and c are the height and width of the fitted Gaussian curve. This method provides a good estimate for an isolated peak. Precautions should be taken when using this method to ensure that any peak overlapping and/or high background continuum are not present. Proper application of previous signal processing techniques are essential to obtain an accurate peak area determination from Gaussian function parameters.

Another straight forward method to obtain the net peak area of an isolated peak in an XRF spectrum consists of interpolating the continuum under the peak and summing the continuum-corrected channel contents in a window over the energy range of the peak. The classical way to handle this problem is to draw two vertical lines from the left and right bounds of the peak down to the x-axis and then to measurement the total area bounded by the spectrum curve, the x-axis, and the two vertical lines. This method is often called the *perpendicular drop method* [40].

After investigating several signal processing algorithms suitable for the near real

time XRF analysis, the algorithms listed in Table 9 and their corresponding listed parameters are recommended for the fluorochemical concentration measurement on carpet fibers.

Table 9: Recommended XRF signal processing algorithms for the fluorochemical concentration measurements on carpet fibers

Category	Algorithm	Parameters
Smoothing Algorithm	Fourier Transform	$u_{\text{th}} = 0.10$
Background Elimination	Peak Stripping	$w = 3$ Iteration = 1000
Peak Search Algorithm	Top-hat Peak Search	$v = 5$ $w = 9$ threshold = 50 $r = 4$
Curve Fitting Function	Gaussian Curve	$G(x) = A \exp\left[-\frac{(x-b)^2}{2c^2}\right]$
Goodness of Fit	χ^2_{NORM}	$\chi^2 = \frac{1}{N-n}\sum_j \frac{(\hat{y}(j)-y(j))^2}{\sigma_j^2}$
Peak Area Determination	Perpendicular Drop Method	

CHAPTER V

CALIBRATION RESULTS

XRF calibration, or matrix correction, algorithms play a major role in the accuracy of XRF measurements. Many studies on the calibration methods aim to resolve inter-element effects [33, 25, 26, 67, 68, 34], others aim to reduce the number of required reference samples by incorporating instrument and elemental parameters [32, 27, 30]. Since the main focus of this research is to synthetically generate reference spectra to use in the calibration process, the simplest yet effective calibration method is selected to be used in this study: the Lucas-Tooth and Price algorithm.

In this chapter, both single and multi-element calibrations were performed to determine the suitability and accuracy of the XRF calibration without synthetically generated spectra. For the single-element calibration method, which is the main focus for this study, both fluorochemical solutions and carpet samples were used to perform the calibration. The multi-element calibration on aqueous-based solution samples was also investigated to determine its suitability for future implementation.

To ensure the compatibility of the calibration results, identical measurement settings and signal processing algorithms were used for the remainder of this research unless otherwise stated. Specifically, the settings are listed in Table 4 and the processing algorithms in Table 9. The calibration results from this chapter are further compared to those obtained using synthetically generated reference spectra in Chapter 6.

5.1 Solution Calibration

In the solution calibration, three chemical taggants are selected from three energy regions in the XRF spectrum which have different backgrounds and noise interferences: zinc (Zn), rubidium (Rb), and molybdenum (Mo). Each taggant and its corresponding K-shell characteristic peaks are plotted in Figure 38. The XRF spectrum displayed in blue is measured from a bare carpet sample with filter No. 1 (300 μm Al and 25 μm Ti) and this is the baseline to which the tagged samples can be compared.

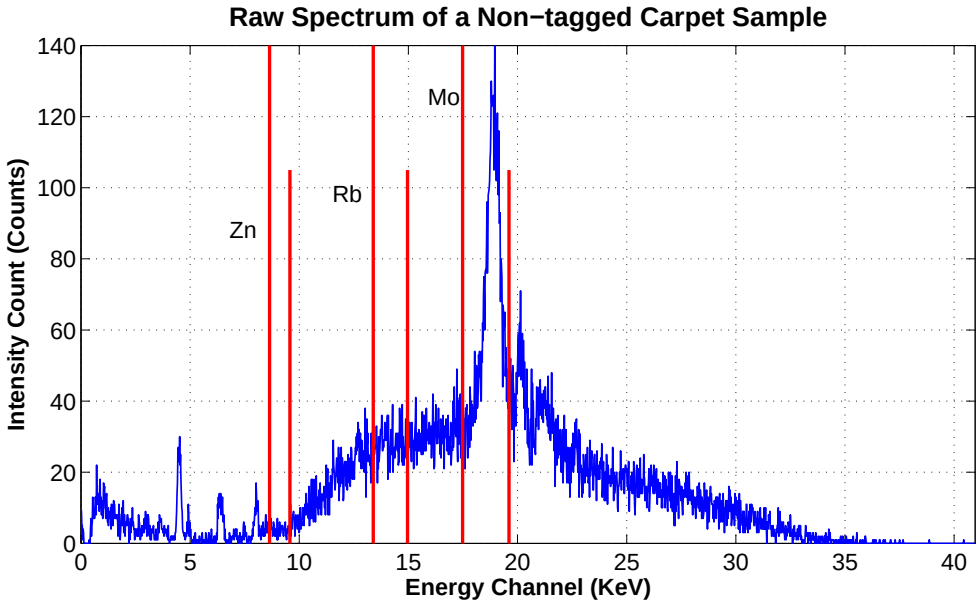

Figure 38: Location for Zn, Rb, and Mo characteristic peaks on an XRF spectrum

Each of these taggants represents a taggant from energy region in the XRF spectra where the presence of the background continuum is either minimal, moderate, or substantial. Regardless of the location of the characteristic peak for each taggant on the XRF spectrum, the background continuum is a major source of interference. In addition, these taggants might interfere with characteristic peaks or be affected by secondary enhancement effects from other low-atomic elements that are routinely present in carpet materials and backings. Since different carpet manufacturers employ

different materials for carpet backings, chemical taggants have to be carefully selected such that any interference or enhancement can be avoided, perhaps on an individual carpet basis.

Zinc (Zn) gives an example of a chemical taggant from the energy region where the XRF background continuum is minimal. The K_α and K_β energy channels belonging to Zn are at 8.64 and 9.57 KeV respectively. To investigate Zinc calibration without any interference from other elements, solution samples with eight different concentrations of zinc were used. Their average raw spectra are plotted in Figure 39. A closer look at both the K_α and K_β peaks of Zn are shown in Figure 40. The K_α and K_β peaks for Zn are located close to each other, and as the Zn concentration is increased, these two peaks become overlapped. Both the areas of the K_α and K_β peaks of Zn were calculated based on the signal analysis algorithms listed in Table 9 and the results are shown in Table 10.

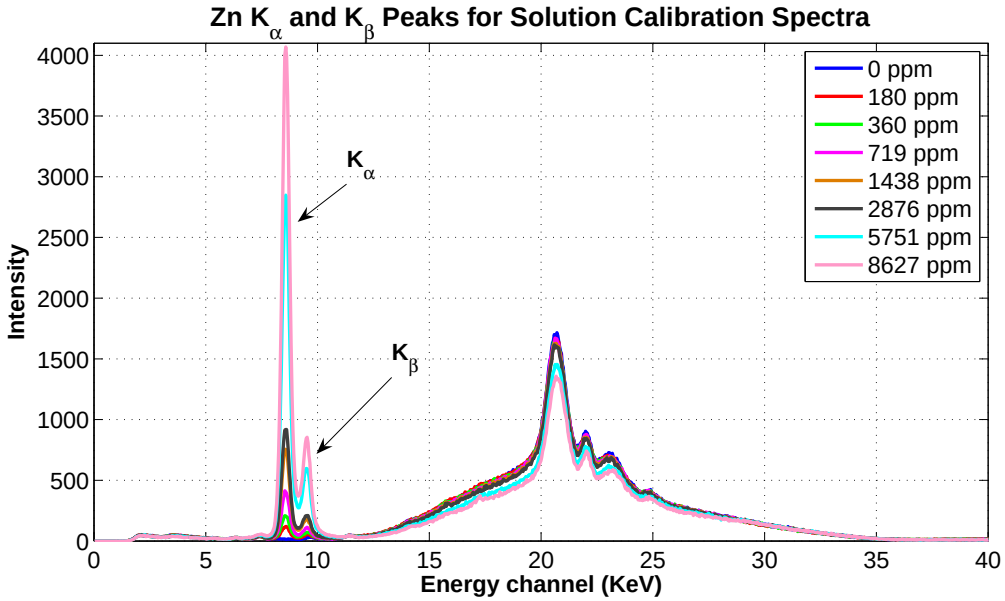

Figure 39: Zn solution calibration XRF spectra

Figure 41 shows the Zn solution calibration curve, $C = 0.21I - 45.80$, with a coefficient of determination of 1.00 and the 95% confidence interval bands. This is based on a straight line model $C = a_0 + a_1 I$, where the sums of squares was determined

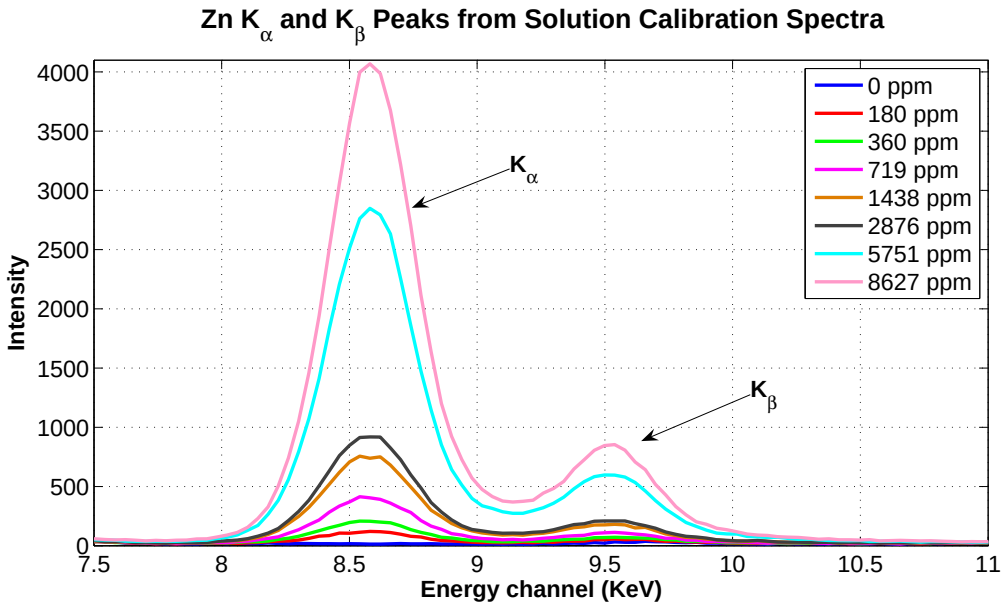

Figure 40: Zn solution calibration XRF spectra (Zoomed view)

Table 10: Zn solution calibration data

Zn Concentration (ppm)	K_α Peak Area (counts)	K_β Peak Area (counts)
0	65	17
180	885	37
359	1690	52
719	3390	87
1440	6510	150
2880	16800	362
5750	27500	599
8630	41900	904

by performing an analysis of the variance (ANOVA). The results from the ANOVA are displayed in Table 11.

Also shown in Figure 38, the rubidium (Rb) characteristic peaks are located at 13.39 and 14.96 KeV for K_α and K_β respectively. This region is at the base of the Compton peak region, which means, there is a continuously increasing background continuum in the region of the peaks as shown in Figure 42. From a closer look at these peaks in Figure 43, we observe that the starting slope for the background

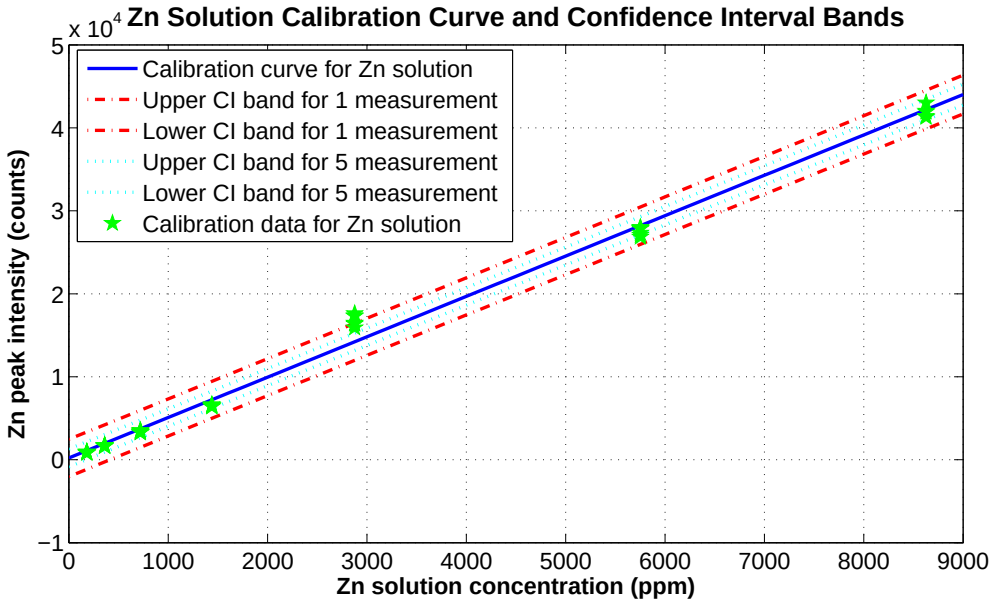

Figure 41: Zn solution calibration curve

Table 11: ANOVA results for Zn solution calibration

Sources of Variation	SS[1]	Dof[2]	MSS[3]
Total (SS_T)	2.86E+09	70	4.08E+07
Mean (SS_M)	1.07E+10	1	1.07E+10
Corrected for the mean (SS_{corr})	1.64E+09	69	2.37E+07
Factors (SS_{fact})	1.63E+09	1	1.63E+09
Residuals (SS_R)	8.22E+06	68	1.21E+05

continuum is almost constant, thus the Rb overall shapes of the characteristic peaks were unaltered by this gradual, constant slope.

Using the same signal processing algorithms as was used for the Zn calibration, the average Rb characteristic peak counts were obtained and these are listed in Table 12. From this calibration data, a calibration curve of $C = 0.13I - 14.83$ was obtain and plotted in Figure 44, along with the 95% confidence interval bands. A value of 1.00 was obtained for the coefficient of determination. The corresponding ANOVA

[1]Sum of squares
[2]Degree of freedom
[3]Mean sum of squares

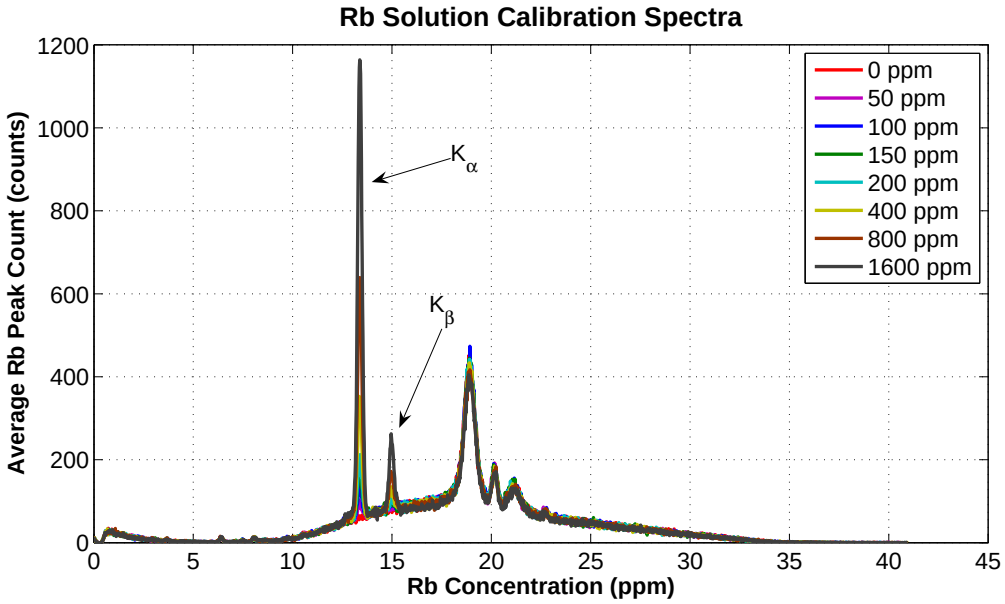

Figure 42: Rb solution calibration spectra

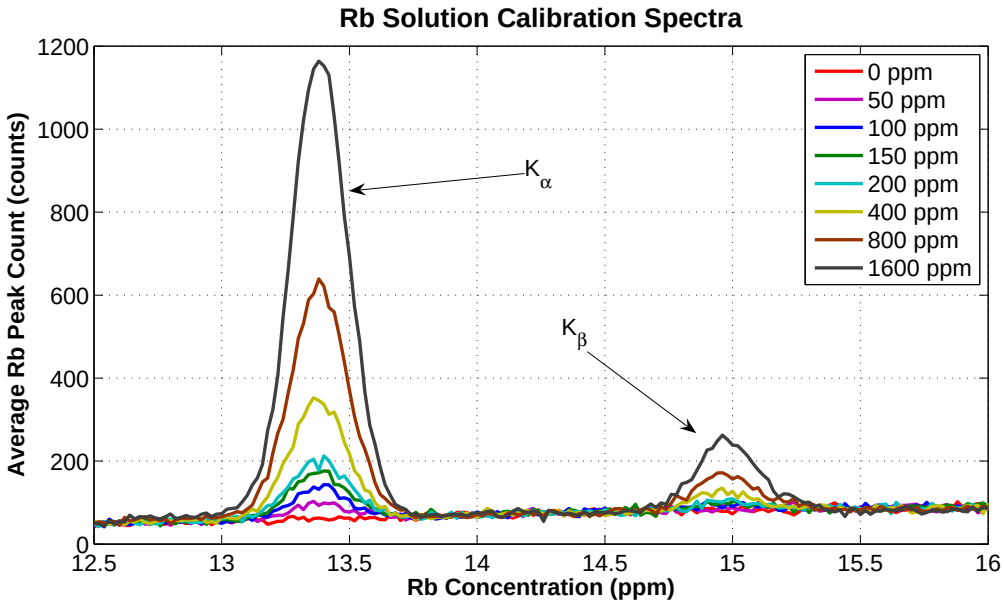

Figure 43: Rb solution calibration spectra (Zoomed view)

analysis is shown in Table 13. The background continuum does not affect Rb peak counts, which implies that the taggant within this region can be applied with a low concentration and still produce reliable results.

The characteristic peaks of molybdenum (Mo) are located at 17.48 and 19.61

Table 12: Rb solution calibration data

Rb Concentration (ppm)	K_α Peak Area (counts)	K_β Peak Area (counts)
0	61	13
50	428	74
100	834	283
150	1244	256
200	1808	307
400	3281	633
800	6625	1130
1600	12498	1780

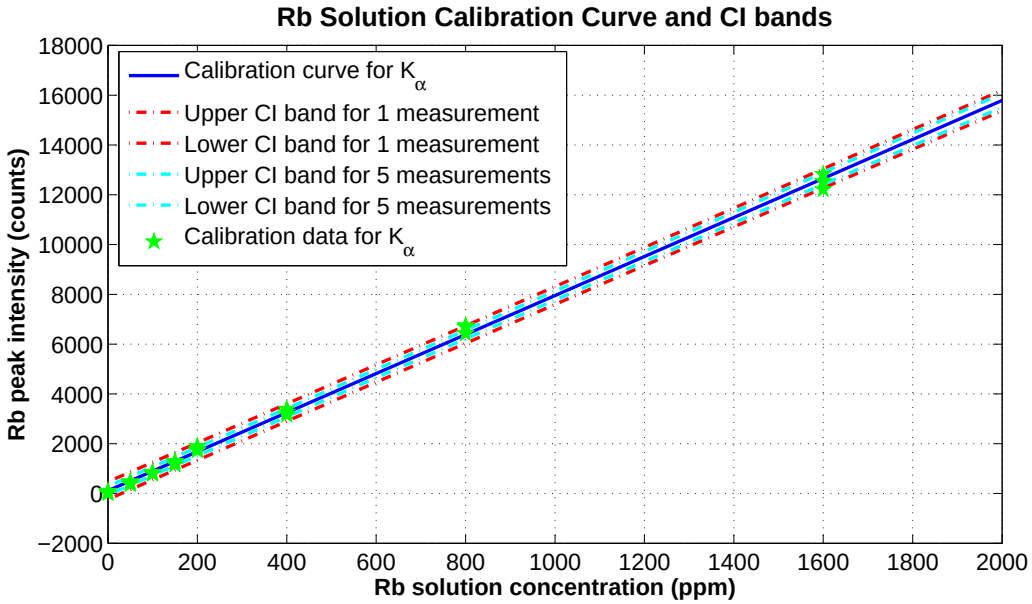

Figure 44: Rb solution calibration curve

Table 13: ANOVA results for Rb solution calibration

Sources of Variation	SS	Dof	MSS
Total (SS_T)	2.17E+08	100	2.17E+06
Mean (SS_M)	1.12E+09	1	1.12E+09
Corrected for the mean (SS_{corr})	1.27E+08	99	1.29E+06
Factors (SS_{fact})	1.27E+08	1	1.27E+08
Residuals (SS_R)	1.04E+05	98	1.06E+03

KeV for the K_α and K_β peaks, respectively. These peaks are near the center of Compton peak in the XRF spectrum (Figure 38). As one can observe from XRF spectra obtained from Mo solution (Figures 45 and 46), both Mo peaks interfere with the Compton peak. The calibration process for Mo can help determine if Compton peak interference affects measurement accuracies for a typical XRF spectrum.

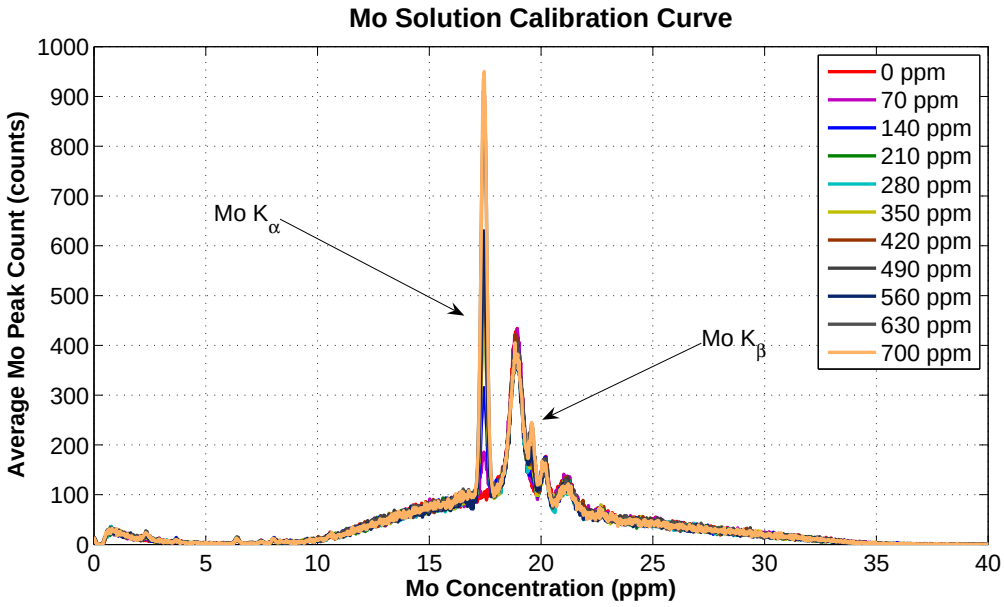

Figure 45: Mo solution calibration spectra

Using the same set of signal processing algorithms and parameters as was used for Rb and Zn, both K_α and K_β characteristic peak areas were determined for Mo and results are shown in Table 14. The resultant calibration curve for Mo solution is $C = 0.06I - 35.06$ with a fitting parameter of $R^2 = 0.90$. The calibration curve along with its 95 % confidence interval bands and the ANOVA analysis results are also shown in Figure 47 and Table 15, respectively. As we can see from these results, the interference from the Compton background decreases the overall accuracy of the calibration for Mo compared to Rb and Zn. Thus, to improve the taggant calibration in this region, a higher concentration of Mo would be required than would be required for either Rb or Zn.

The solution calibration results show how the XRF calibration accuracies depend

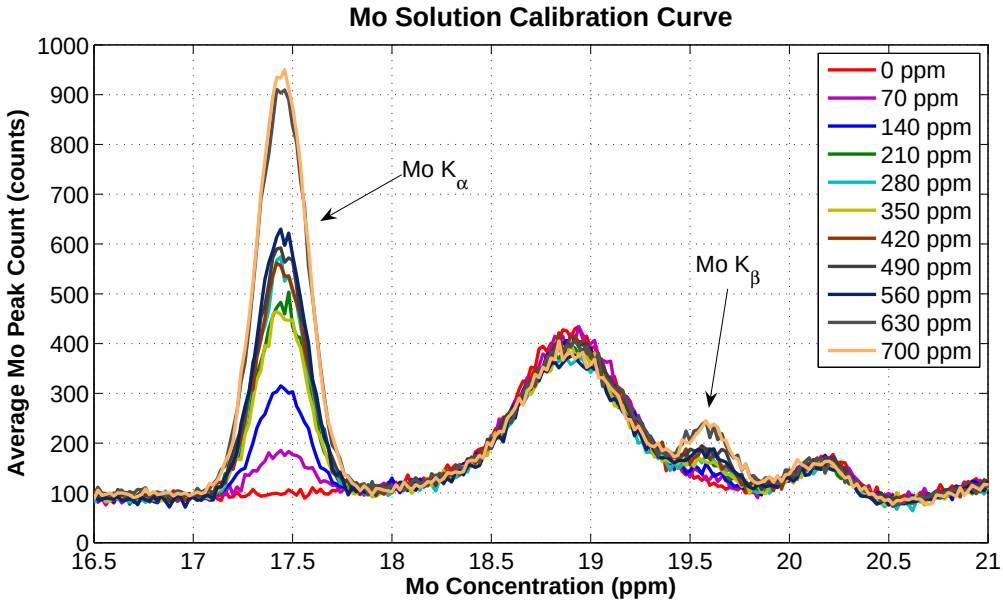

Figure 46: Mo solution calibration spectra (Zoomed view)

Table 14: Mo solution calibration data

Mo Concentration (ppm)	K_α Peak Area (counts)	K_β Peak Area (counts)
0	47	116
70	1190	137
140	2910	265
210	5600	543
280	6760	673
350	5300	499
420	6240	550
490	6690	812
560	7890	834
630	11800	1230
700	12600	1400

upon the XRF background continuum near the region of the taggant peaks. The Rb characteristic peaks are located at a region with a nearly constant background continuum, thus, the continuum does not interfere with the processed characteristic peak counts. The characteristic peaks for Mo, on the other hand, lie on a steeper slope of the Compton peak with also more background noise. Thus the overall processed

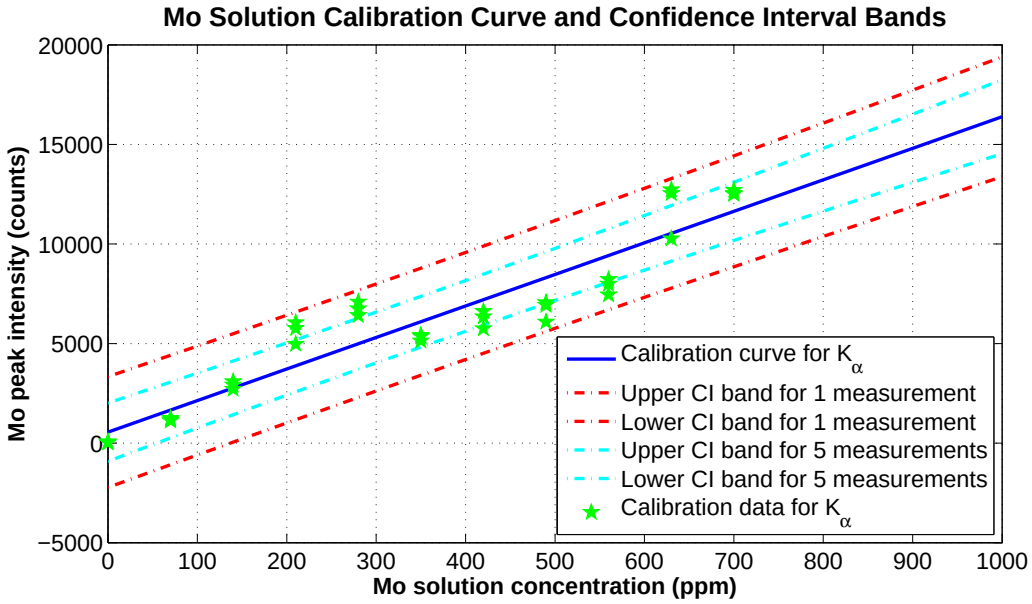

Figure 47: Mo solution calibration curve

Table 15: ANOVA results for Mo solution calibration

Sources of Variation	SS	Dof	MSS
Total (SS_T)	5.60E+08	100	5.60E+06
Mean (SS_M)	3.72E+09	1	3.72E+09
Corrected for the mean (SS_{corr})	1.51E+08	99	1.52E+06
Factors (SS_{fact})	1.35E+08	1	1.35E+08
Residuals (SS_R)	1.57E+07	98	1.61E+05

peak counts and calibration are not as good for Mo when the same XRF instrument parameters and filter settings are used for these experiments.

5.2 Carpet Calibration

Carpet fibers introduce non-uniformity to the samples, resulting in more X-ray scattering and higher background interference. The effects of this interference on the calibration process is studied in this section. Using the same signal processing algorithms and the calibration procedure as in the solution samples, the carpet calibrations were performed on three series of carpets, namely MAR-995-BMK, MAR-995-3.5-LPB, and MAR-995-6.0-FRB. The alphanumeric labels in the carpet names represent the

styles of each carpet and can be decoded using the description shown in Table 16. All of these carpet samples are virtually identical in their overall physical characteristics, the main differences are the carpet pile height and density.

Table 16: Carpet calibration sample symbols

MAR	file header
995	995 denier yarn
BMK	45 oz/sy Saxony-style carpet [6.0 turns per inch (tpi), standard straight-set Superba heat setting conditions, tufted on 1/8 gauge machine, pile height about 9/16 inch]
6.0, 3.5	twist (tpi)
FRB	Frieze style carpet [Standard texture-set Superba heat setting, 1/8 ga. machine, 7/8 inch pile height]
LPB	Loop style carpet [Standard texture-set Superba heat setting, 1/8 ga. machine, approx. 0.3 inch pile height]
0, 25, 50, 100	Targeted Rb level

Due to the unavailability of carpets with other taggants, only Rb-tagged carpets were used in this section. For each carpet sample, four levels of the fluorochemical (F) and taggant (Rb) concentration were chosen. Their corresponding targeted and actual concentration on carpets are listed in Table 17.

The measurement settings and the signal processing algorithms defined in Tables 4 and 9, were used for the XRF measurements and subsequent data analysis, respectively. For each of these carpet samples, measurements were made at several locations across the entire carpet sample to include any variations in the fluorochemical concentration due to locations and spray pattern variations of the applicators used by the manufacturer to apply the fluorochemicals. For each carpet style and concentration, a sample of 85×150mm was sectioned from the carpet with the long axis across

Table 17: Targeted Rb and F concentration on MAR-995 series carpets

Carpet Name	Targeted F (ppm)	Targeted Rb (ppm)	Actual F (ppm)	Expected Rb (ppm)
MAR-995-BMK-00	0	0	33	0
MAR-995-BMK-25	75	25	110	34
MAR-995-BMK-50	150	50	146	45
MAR-995-BMK-100	300	100	355	125
MAR-995-3.5-LPB-00	0	0	31	0
MAR-995-3.5-LPB-25	75	25	95	44
MAR-995-3.5-LPB-50	150	50	135	57
MAR-995-3.5-LPB-100	300	100	421	160
MAR-995-6.0-FRB-00	0	0	33	0
MAR-995-6.0-FRB-25	75	25	103	34
MAR-995-6.0-FRB-50	150	50	133	45
MAR-995-6.0-FRB-100	300	100	374	125

the web of the carpet. A grid of 17×30, with a 5mm separation between adjacent locations, was used to obtain the XRF spectra measurements for each of these carpet samples, and five measurements were recorded at each grid location. The remaining calibration process was identical to that used for the solution samples. The average peak intensity from all the measurements was calculated and results are listed Table 18. These values were next used to perform the carpet calibration for each of the corresponding carpet types.

The calibration curve for each carpet series was determined from the calibration data listed in Table 18. The resulting calibration curves for the BMK, LPB, and FRB carpet series are $C_{Rb} = 0.18I_{Rb} - 7.66$, $C_{Rb} = 0.19I_{Rb} - 12.44$, and $C_{Rb} = 0.53I_{Rb} - 18.62$, respectively. The coefficients of determination for these three types of carpets are 0.98, 0.97, and 0.96 for carpet types BMK, LPB, and FRB, respectively. The ANOVA analysis results for the BMK, LPB, and FRB carpet types are listed in Tables 19, 20, and 21, respectively.

Several factors contributed the inaccuracies of the carpet calibration results when

Table 18: Calibration measurements for MAR-995-BMK carpets

Carpet	Targeted Rb Concentration (ppm)	Actual Rb Concentration (ppm)	Rb K_α (counts)
MAR-995-BMK-00RB	0	0	42
MAR-995-BMK-25RB	25	34	184
MAR-995-BMK-50RB	50	45	338
MAR-995-BMK-100RB	100	125	718
MAR-995-3.5-LPB-00RB	0	0	29
MAR-995-3.5-LPB-25RB	25	44	98
MAR-995-3.5-LPB-50RB	50	57	173
MAR-995-3.5-LPB-100RB	100	160	330
MAR-995-6.0-FRB-00RB	0	0	43
MAR-995-6.0-FRB-25RB	25	34	196
MAR-995-6.0-FRB-50RB	50	45	380
MAR-995-6.0-FRB-100RB	100	125	692

Table 19: ANOVA results for MAR-995-BMK carpet series

Sources of Variation	SS	Dof	MSS
Total (SS_T)	6.65E+05	5100	1.30E+02
Mean (SS_M)	5.23E+08	1	5.23E+08
Corrected for the mean (SS_{corr})	2.55E+05	5099	5.00E+01
Factors (SS_{fact})	2.50E+05	1	2.50E+05
Residuals (SS_R)	4.46E+03	5098	8.74E-01

Table 20: ANOVA results for MAR-995-3.5-LPB carpet series

Sources of Variation	SS	Dof	MSS
Total (SS_T)	1.49E+05	5100	2.92E+01
Mean (SS_M)	1.27E+08	1	1.27E+08
Corrected for the mean (SS_{corr})	1.56E+05	5099	3.06E+01
Factors (SS_{fact})	1.54E+05	1	1.54E+05
Residuals (SS_R)	1.43E+03	5098	2.80E-01

compared to the solution samples. Besides the obvious carpet physical characteristics and the sample surface roughness differences, carpet samples also have an uneven

Table 21: ANOVA results for MAR-995-6.0-FRB carpet series

Sources of Variation	SS	Dof	MSS
Total (SS_T)	6.63E+05	5100	1.30E+02
Mean (SS_M)	5.48E+08	1	5.48E+08
Corrected for the mean (SS_{corr})	2.34E+05	5099	4.59E+01
Factors (SS_{fact})	2.24E+05	1	2.24E+05
Residuals (SS_R)	9.57E+03	5098	1.88E+00

taggant distribution across the samples as is reported in Appendix D. These inconsistencies in the taggant distribution are due to the difficulty in applying the taggant evenly during the carpet manufacturing process. The effects of this uneven distribution of taggant will have to be taken into consideration when performing carpet calibrations for the eventual real time use of XRF measurements in a carpet mill.

5.3 Multiple Taggant Calibration

Although the multi-element taggants are not the primary focus for this research, understanding the multi-element taggant calibration process can assist general understanding in the situations which contain inter element interferences, i.e., a secondary enhancement effect, between chemical taggants and other materials contained in carpets. The second enhancement effect, as discussed in Section 2.1.3, alters the linear relationship between the chemical concentration and the intensity counts from the characteristic peaks. If taggants are carefully choosen, this effect can help verify not just the taggant concentration on carpet samples, but also authenticate a specific fluorochemicals formula applied to the carpet fiber, e.g., both a soil resistant and stain blocker are often applied and a separate taggant could be used for each fluorochemical.

To study how additional taggants in the sample might affect the overall calibration results, we studied aqueous-based solution samples tagged with either iron (Fe), copper (Cu), or a combination of these two elements. The taggant concentration in each sample along with the corresponding Fe and Cu characteristic (K_α) peak

counts for single element solution samples are listed in Tables 22 and 23, respectively. These data are used to generate single element calibration curves for comparison purposes. Similarly, a set of solution mixtures of Fe and Cu samples were prepared with concentrations of each element as listed in Table 24.

Table 22: Fe aqueous solution XRF measurements

Iron (Fe) Solution	
Concentration (ppm)	Intensity (counts)
0	90
174	232
348	354
695	696
1390	1269
2780	2648
5560	5192
8340	8301

Table 23: Cu aqueous solution XRF measurements

Copper (Cu) Solution	
Concentration (ppm)	Intensity (counts)
0	82
175	656
349	1175
698	1733
1396	3846
2792	7181
5584	15220
8375	23570

The results reported next followed the same calibration process previously reported for single element taggants, only now a second element was added in the Lucas-Tooth and Price algorithm. The calibration curves for all four sets of data, single Fe, single Cu, Fe in presence of Cu, Cu in presence of Fe, are displayed in

Table 24: Fe-Cu aqueous solution and their corresponding XRF measurements

Concentration (ppm)		Intensity (counts)	
Iron (Fe)	Copper (Cu)	Iron (Fe)	Copper (Cu)
0	10000	177	24390
1000	9000	1589	20430
2000	8000	2873	17440
3000	7000	4145	14910
4000	6000	5571	11980
5000	5000	6583	9713
6000	4000	8235	7428
7000	3000	8826	5584
8000	2000	9903	3300
9000	1000	10700	1544
10000	0	10890	82

Figure 48. Because the K_α and K_β characteristic peaks for Cu are located at 8.05 and 8.9 KeV, respectively, which is greater than the absorption edge, K_{edge}, of Fe (7.13 KeV); part of the characteristic energy emitted by Cu is absorbed by Fe. This generates a secondary enhancement effect. Hence, the calibration curves for both Fe and Cu in the Cu-Fe mixture are non-linear, i.e., concave up and down respectively for Fe and Cu.

Although the multi-element taggants are not used in this study, the results obtained in this section demonstrate a potential benefit of using multiple-taggants on a single carpet samples to embed any codes within fluorochemical treatments, which might then assist carpet manufacturers by identifying the type and amount of two specific chemicals applied to a carpet. This may be especially useful when allowing manufacturers to easily determine, using XRF measurements, the brand and the amount of fluorochemicals, or stain blocker, present in a specific carpet.

All calibration results performed in chapter support the possibility of incorporating an XRF instrument as a part of the near real time measurement of the fluorochemical concentration on carpet fiber. However, these results must be compared to

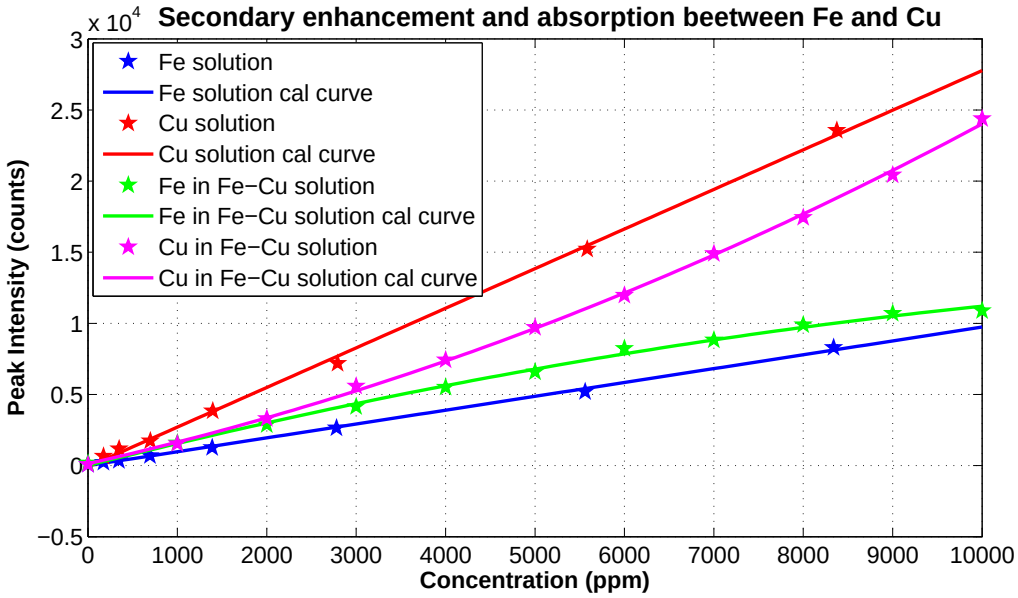

Figure 48: Secondary enhancement and absorption effects between Fe and Cu

the calibration results obtained from using artificial spectra as XRF calibration spectra to ensure that the results are still within the standard accepted by most carpet manufacturers. Specifically, since providing a set of calibration samples with varying taggant concentrations is not practical for every potential carpet type produced by a manufacturer.

CHAPTER VI

SYNTHETICALLY GENERATED ARTIFICIAL XRF SPECTRA

Previous chapters have identified several factors which can affect XRF measurements and have reported their effects on the measured XRF spectra. In this chapter, we combine effects of these factors to generate artificial XRF spectra for calibration purposes. Specifically, the following measurement factors are considered: measurement time (t_m), primary beam filter ($filt$), X-ray source current (I_{inst}), X-ray source voltage (V_{inst}), and carpet density (ρ_{car}). The synthetic XRF spectrum of an unknown sample with a desired taggant concentration, Γ, will be generated from a reference XRF spectrum from a known reference sample, Γ_0.

Since the artificial XRF spectra generated by the procedures proposed in this chapter are mainly for calibration purposes, only the three main components of the XRF spectra will be the discussed in this study: characteristic peaks of the desired element, the Compton peak, and XRF background. The characteristic peak of the desired element provides the actual peak counts used for the calibration process. The Compton peak provides an internal reference for comparing characteristic peaks information from different spectra. And finally, the overall XRF continuum provides information regarding the physical properties of the samples.

6.1 Measurement Time

Since the XRF counts per channel accumulate over time, the overall XRF counts per channel are expected to be linearly proportional to the measurement time. This relationship holds as long as the instrument stays stationary with respect to the

sample, or moving at a steady slow speed (< 3 cm/s), and can be written as

$$\Gamma = \frac{t_m^d}{t_m}\Gamma_0 \tag{32}$$

where t_m^d is the measurement time for the reference spectrum and t_m is the measurement time for the unknown sample. To illustrate this relationship, an XRF spectrum obtained from 200ppm Rb aqueous solution for a 30 second measurement time is used as a reference spectrum, Γ_0. Five additional synthetic spectra with measurement times of 10, 20, 40, 50, and 60 seconds are generated using Equation 32, and the results are plotted in Figure 49 against the actual XRF measurements.

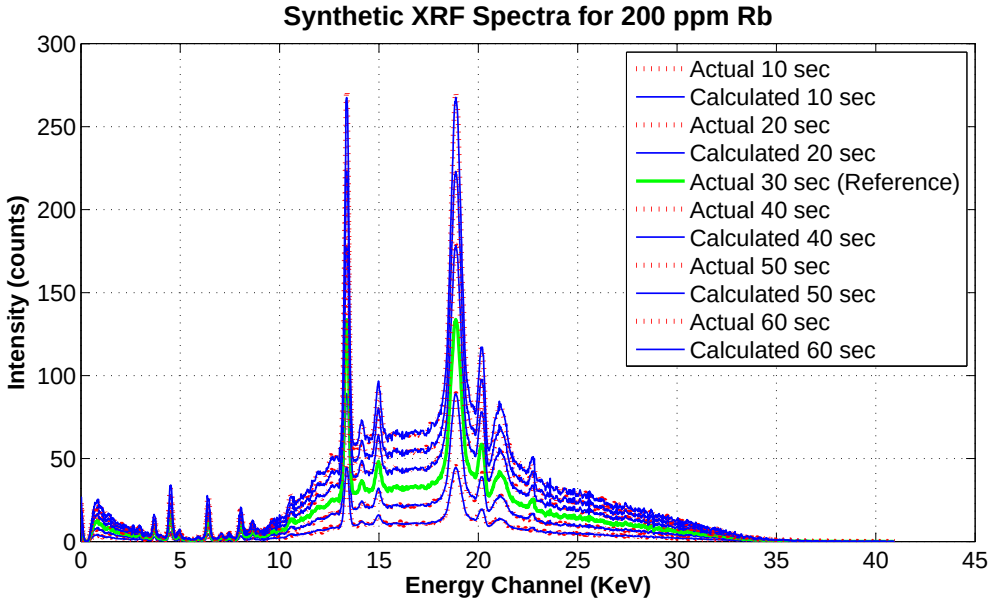

Figure 49: Measured and synthetic XRF spectra for 200 ppm Rb solution for various measurement times

The residual error plots between each set of the actual and synthetic spectra pairs are plotted in Figure 50. As we can observed from this plot, the residual increases as the measurement time increases. This increase in the residual is caused by the higher measurement noise observed from longer measurement times. Overall, the residual error betweem the synthetic and actual spectra are less than ± 5 counts for measurement time changes.

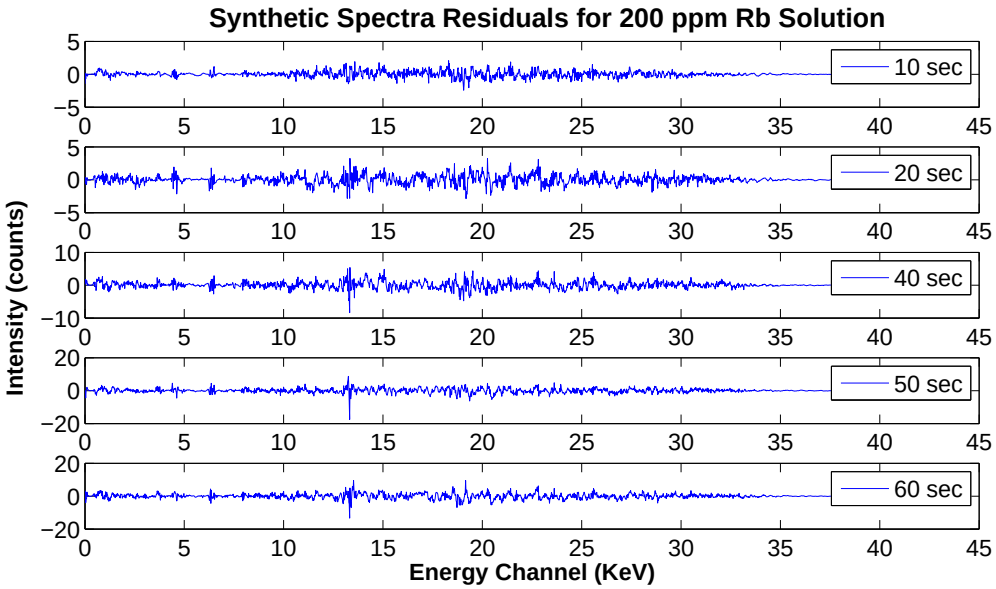

Figure 50: Error Residuals for 200 ppm Rb solution for measurement time factor

6.2 Primary Beam Filter

Section 2.1.2 discusses factors which affect X-ray absorption, which is a key element in determining the effect of any specific primary beam filter on an XRF spectrum. Often it is necessary to synthetically generate a specific XRF spectrum with a certain filter using another XRF spectrum that was generated using a different filter. Thus, it is important to have a model for any given filter that is placed in the primary beam path. Equation 2 may be modified with a constant, κ, to include the degree to which the fluorescence intensity is reduced by a single filter layer.

$$\frac{I}{I_0} = \kappa \exp^{(-\mu_a \rho_a x_a)} \tag{33}$$

To include all three filter layers present in each primary beam filter for S1 TRACeR, the overall fraction of XRF intensity that passes through the combined filter can be expressed as

$$\frac{I}{I_0} = \kappa \exp^{(\sum_{i=1}^{3}(-\mu_i \rho_i x_i))} \tag{34}$$

where κ includes the overall intensity absorbed by the filter, i.e. $\kappa = \kappa_1\kappa_2\kappa_3$. This constant can be easily determined by measuring a sample with and without the filter, and then by comparing the overall XRF spectrum outputs. Once the constant κ is determined, synthetic spectra Γ can be obtained by using the equation

$$\Gamma = \kappa \exp^{(\sum_{i=1}^{3}(-\mu_i\rho_i x_i))} \Gamma_0 \tag{35}$$

To illustrate this relationship, a blank aqueous solution sample was measured for 30 seconds using filters 1, 2, 3, and 5. Details regarding these filters can be found in Table 2. The XRF spectrum corresponding to the blank filter (No. 2) is used as the reference spectrum to generate synthetic spectra corresponding for those obtained from filters 1, 3, and 5. Figure 51, 52, and 53 show synthetic spectra for the aqueous sample from filters 1, 3, and 5, respectively. From these results, we can see that with the exception of energy channels 0-5 KeV, the synthetic spectra well represent the actual XRF spectra obtained using the corresponding primary beam filter. Thus, the absorption effects of various filters may be determined and results may be used to compensate/correct XRF energy spectra.

6.3 XRF Continuum Matching

XRF measurements are also sensitive to the physical characteristics of the samples. In the case of carpet samples, several physical characteristics distinguish one type of carpet from another. These characteristics include fiber density, backing materials, carpet pattern, pile height, yarn type, etc. These characteristics contribute to different XRF continuums as shown in Figure 54. Although each of the above carpet characteristic provides a different physical appearance to the carpet sample, they each also alter the density of the carpet sample. To simplify the problem, this study will treat all these carpet physical characteristic as one property, which is the carpet density.

In Figure 54, solution samples along with three types of carpets with different

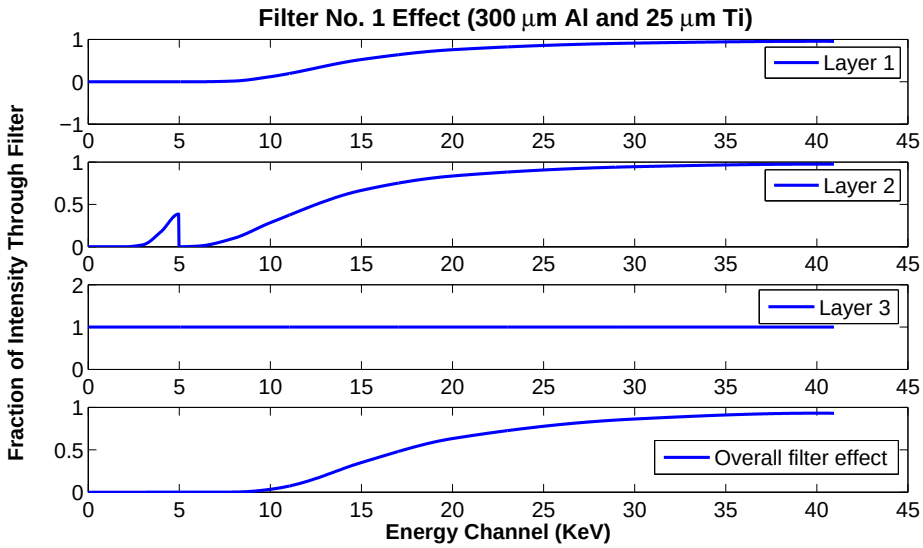

(a) Filter No. 1 absorption effect

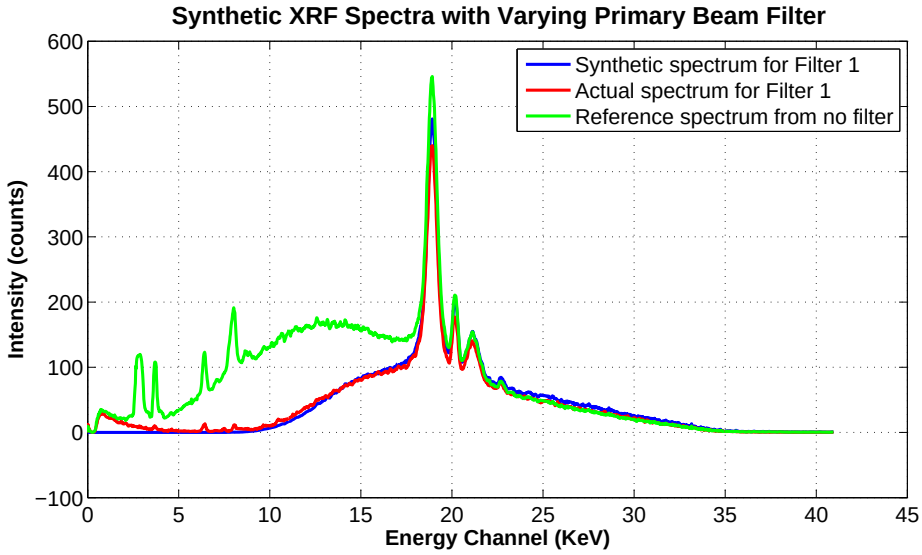

(b) Filter No. 1 effect on H_2O samples

Figure 51: Synthetic spectra generated for Filter No. 1 (300 μm Al and 25 μm Ti) using H_2O sample

Rb taggant concentrations were used for the synthetic background generation: MAR-995-BMK, MAR-995-3.5-LPB, and MAR-995-6.0-FRB. These carpets are all dyed light wool beige, treated with stain resist, then separately treated with anti-soil with the indicated taggant amount. The manufacturing procedure for these carpets were identical. Other variations in the physical characteristics of these carpet samples are

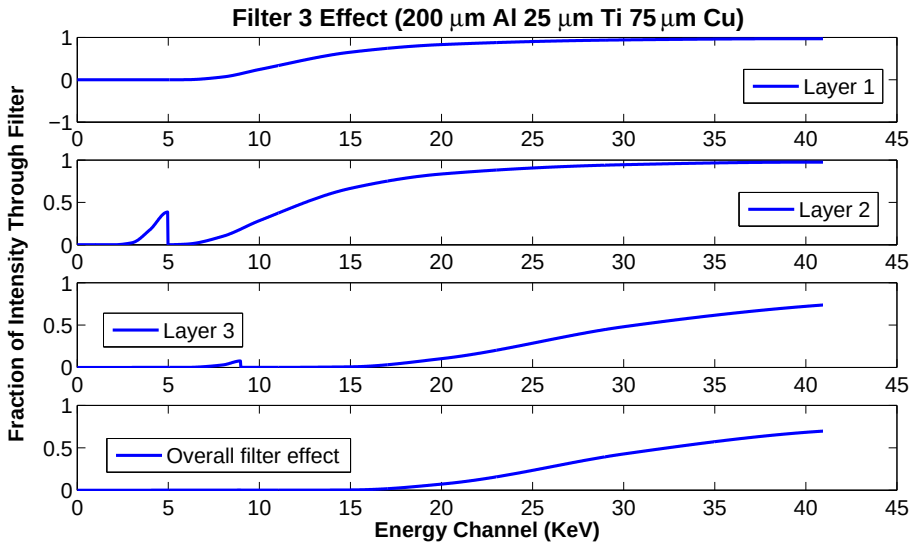

(a) Filter No. 3 absorption effect

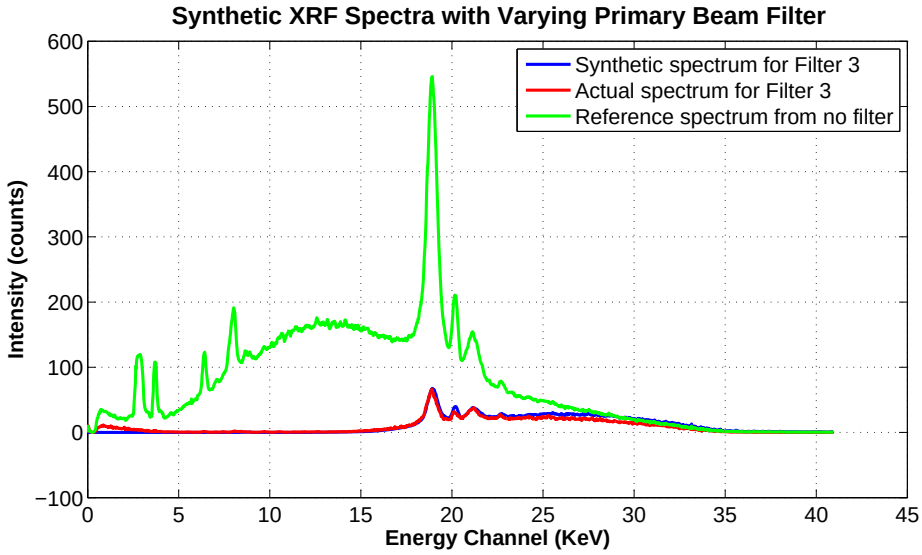

(b) Filter No. 3 effect on H_2O samples

Figure 52: Synthetic spectra generated for Filter No. 3 (200 μm Al 25 μm Ti 75 μm Cu) using H_2O sample

contained in the carpet names and can be decoded as indicated in Table 16.

To generate XRF spectra by matching continuums, two steps were used: first, the Compton peaks were matched, and secondly, the continuum background in a specific region of interest was matched. In the first process, the Compton peak for each spectrum is located and a parabolic curve is fit to the peak over an energy

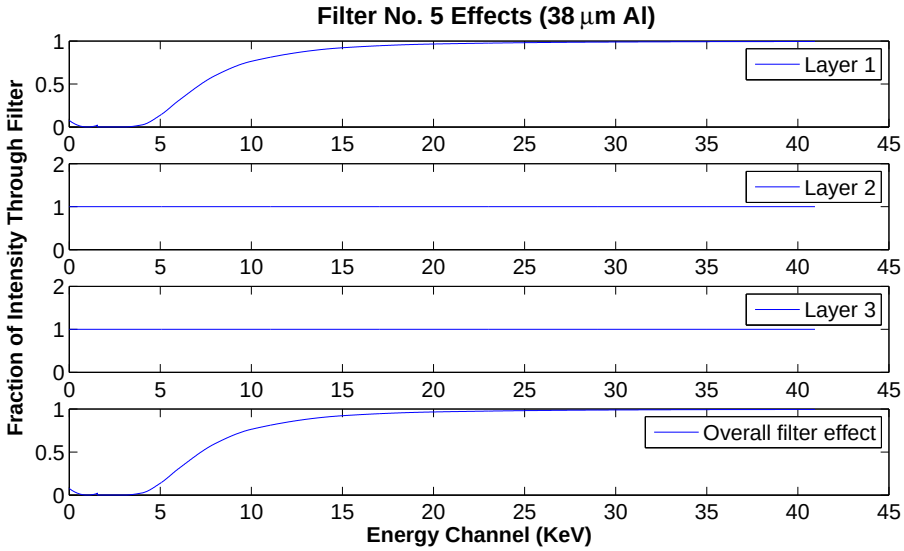

(a) Filter No. 5 absorption effect

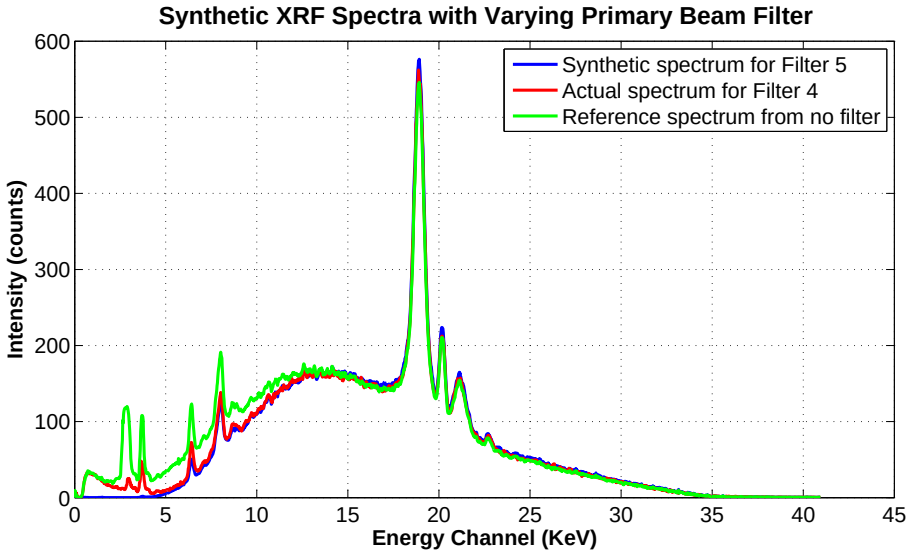

(b) Filter No. 5 effect on H_2O samples

Figure 53: Synthetic spectra generated for Filter No. 5 (38 μm Al) using H_2O sample

window which extended 0.2KeV from either side of the Compton peak. The ratio of the maximum value of the Compton peak was next used to transform the data count rate from one spectrum to another in this first correction step.

For the second step, the energy channel range around the characteristic peaks of interest is selected for the Rb-tagged carpet samples, this energy range corresponds

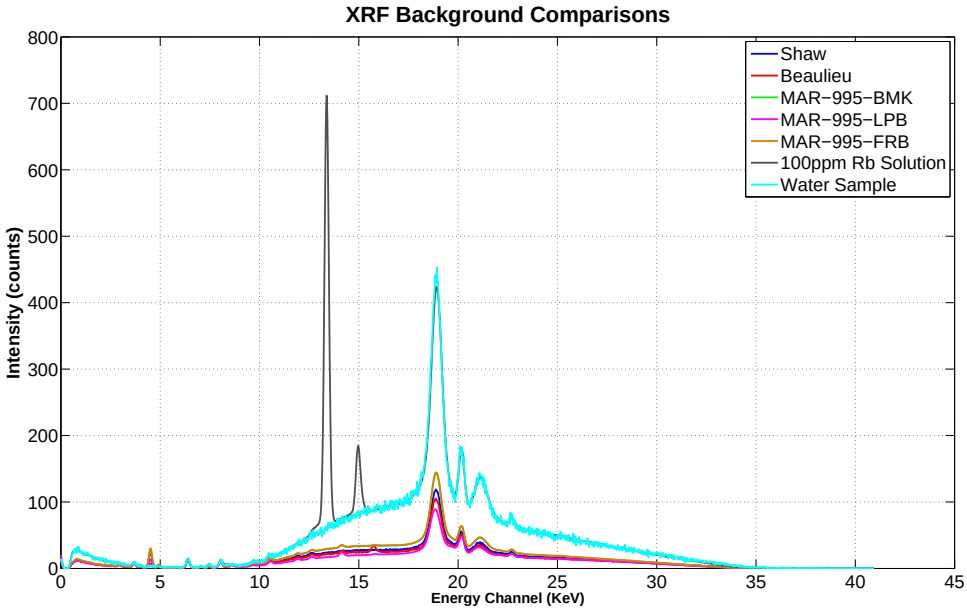

Figure 54: XRF spectra obtained from various samples characteristics

to energy channels from 10 to 16 KeV. To match the background continuum in this region, both spectra are first stripped of any characteristic peaks and fit to a cubic polynomial. The ratio of both continuum data within this energy range is then used as the correction factor for this second step.

Figure 55 and 56 show XRF continuum matching results for both synthetic generation of a spectrum and the actual measured spectrum for a commercial carpet sample, i.e., one by combining the solution calibration method with the known carpet background, and the other from actual fluorochemical solutions applied to carpet samples. In both cases, even after successful continuum matching from one spectrum to another, one can notice a spectral peak located at energy channel 4 KeV which is present in the actual spectrum, but did not exist in the synthetic spectrum. These cases are encountered when we generate a synthetic spectrum from a different carpet material. In this case, elements present in the reference carpet differ from the actual carpet to which we are attempting to generate a calibration spectrum and this effect produces spurious peaks. Thus, it is important that the reference blank carpet sample

closely match the final carpet type. Especially if the spurious peaks are located in near taggant peaks.

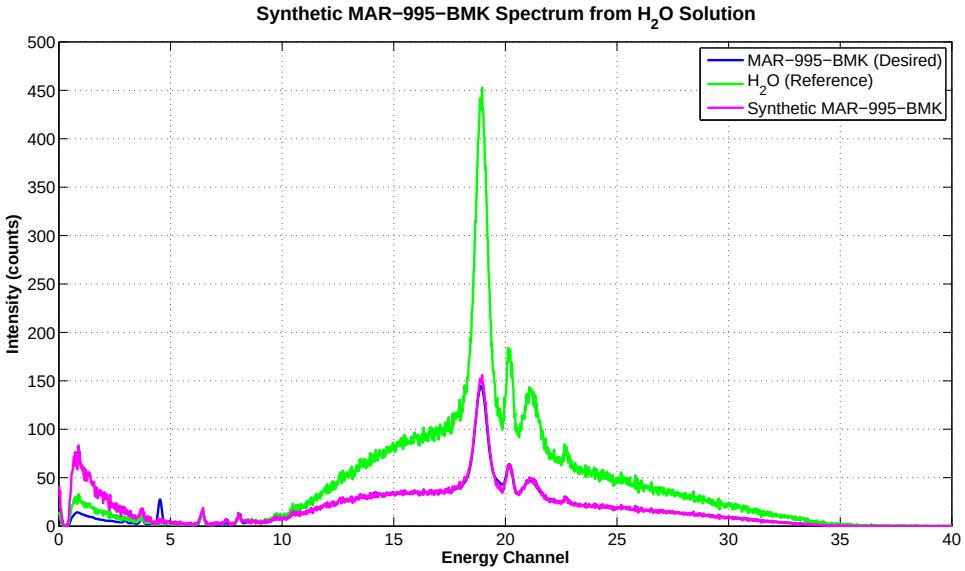

Figure 55: Synthetic MAR-995-BMK spectrum generated from water solution

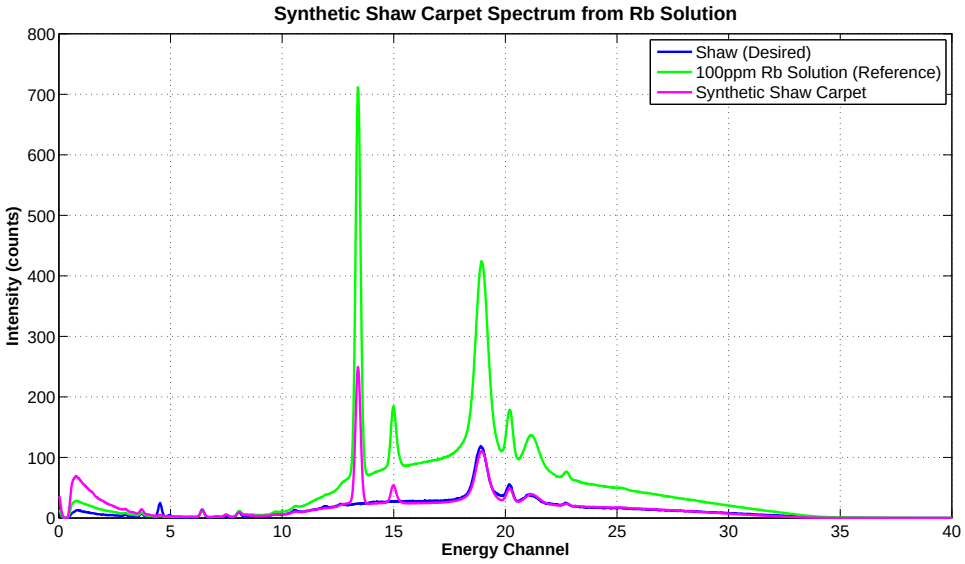

Figure 56: Synthetic Shaw spectrum generated from 100ppm Rb-tagged fluorochemical solution

6.4 Synthetic Peak Generation

In the previous section, XRF continuum matching strategies were developed. In this section, the properties of the characteristic peak from taggants will be altered slightly to account for peak to peak interference and inter-element effects. Specifically, characteristic peaks have different peak heights and peak widths when these effects exist. Fortunately, in the case of Rb peaks in stock solution and carpet samples studied to date, the characteristic peak height and width remain relatively constant as reported in Appendix A.

Figure 57 shows an example of the Rb characteristic peaks for three different 50 ppm Rb tagged carpet samples. The measurement settings used to obtain these spectra were the same for all the samples; however, the peak heights vary considerably between these samples. The peak area count from each carpet sample is calculate and display along with the density of each carpet and these results is listed in Table 25, where density is again defined by the product of the carpet pile height and the turns-per-in (τ).

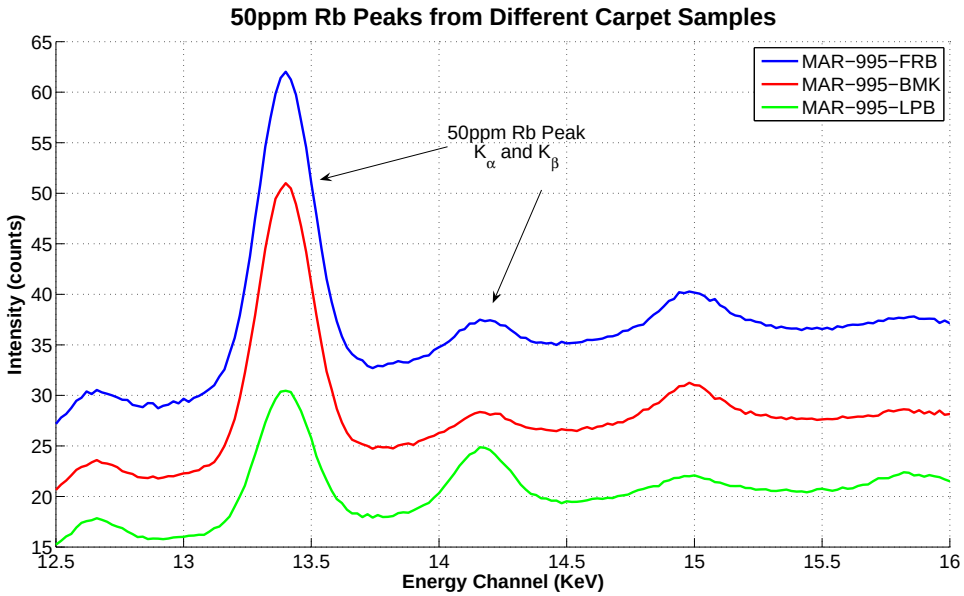

Figure 57: Comparison for characteristic peaks obtained from three 50ppm Rb-tagged carpet types

Table 25: Carpet density definition

Carpet	Pile Height	Turns-per-inch	Peak Count
FRB	0.88	6.0	385
BMK	0.56	6.0	342
LPB	0.30	3.5	176

Generating synthetic characteristic peaks involves two steps. The first step is to calculate the factor by which the peak area should be adjusted based on the compensation from the continuum matching process. Next, Gaussian peak parameters are calculated based on the element of interest and the adjusted peak areas from the first step.

The background intensity counts in the energy region corresponding to the peak of interest for both the blank carpet and for the reference samples, denoted by I_{B1} and I_{B0}, respectively, can be used to determine compensation values, a_1 and a_2, for the synthetic peaks using the following equation:

$$I_{B0} = \left[(a_1\tau)^2 + (a_2 h)\right] I_{B1}. \tag{36}$$

Note that this relationship is expressed in terms of carpet pile height, h, and turns-per-inch, τ. To solve for both parameters, two energy regions in both XRF spectra near the location of the characteristic peak of interest are selected. The relationship between the intensity counts in the characteristic peak areas from the reference sample, I_0, and the synthetic peak in the blank sample, I_1, can be then be expressed as:

$$I_1 = \frac{I_0}{\left[(a_1\tau)^2 + (a_2 h)\right]}. \tag{37}$$

The synthetic spectra for the FRB and LPB series were generated using the BMK carpet samples as a reference and results are plotted in Figure 58. As these results show, even after the carpet backing compensation, the synthetic peaks generated for the different carpet types do not perfectly match. Thus, a final step is needed to

correct taggant peaks in the synthetic spectra in order to obtain the best possible calibration results.

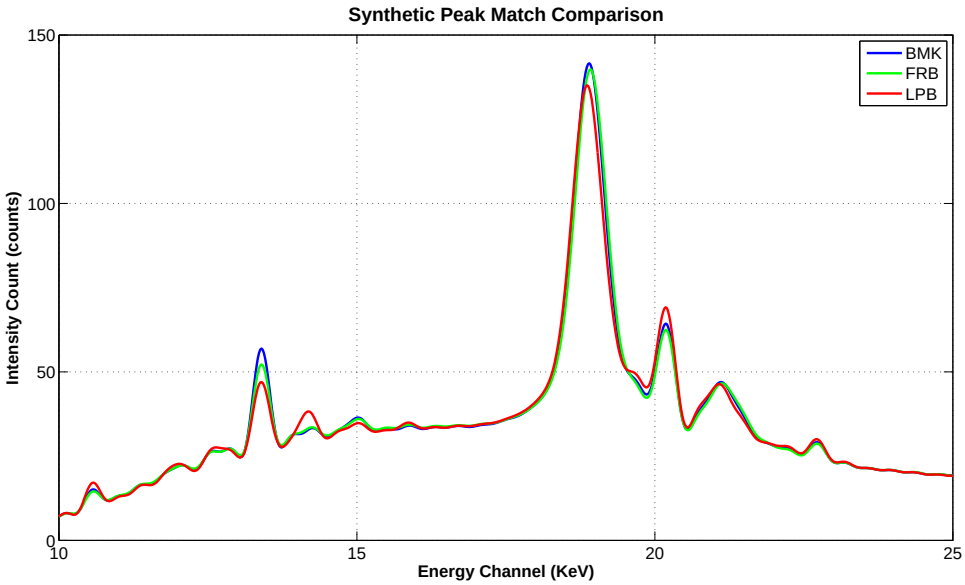

Figure 58: Synthetic spectra generated from the BMK carpet sample as reference to match the FRB and LPB carpet series

The final step in generating the synthetic characteristic peak is to determine the synthetic peak area with respect to the reference peak and obtain the Gaussian function parameters associated with the peak. The synthetic peak area, P_1, can be determined from the characteristic peak area and its background in the peak energy channel, denoted by P_0 and P_{B0}, respectively, along with the original background in the peak energy channels of the blank carpet before background matching, P_{B1}. The synthetic peak area for the blank carpet then can be calculated using the following relationship:

$$P_1 = \sqrt{\frac{P_{B1}}{P_{B0}}} P_0 \tag{38}$$

Since the location of the peak, c, is well defined for all elements, the width of the peak, b, can be considered constant across all the carpet samples studied in this research as is reported in A. Finally, the peak height, A, can be determined using the formula

$A = P_1/(c\sqrt{2\pi})$. Once these parameters are determined, the synthetic peak can be generated and superimposed on the compensated background to generate the final synthetic XRF spectrum.

Examples of the synthetic peak generation and their performance evaluations are presented in Section 6.5 and Appendix E.

6.5 Practical Example

For the methodology introduced in this chapter, this section demonstrates how to synthetically generate XRF spectra for carpet calibration using only stock solutions and blank carpet samples. This example assumes that each carpet manufacturer has samples of their fluorochemical stock solution with at least two taggant concentration levels. These solution samples and their corresponding XRF measurements should be obtained and archived in advance. An XRF measurement of a blank, new carpet will be obtained for the calibration process. This section specifically demonstrates synthetic spectrum generation using the MAR-995-3.5-LPB series carpet samples.

For this example, all instrument and measurement settings are set according to Table 4, and the signal processing algorithms were as listed in Table 26. These algorithms were chosen to ease implementation, since none are computational demanding. In addition, the single chemical taggant utilized in this example is Rubidium (Rb). A targeted standard Rb concentration of 100 ppm on the final carpet samples was specified for this example.

The overall process to generate synthetic carpet spectra and perform calibration using these synthetic spectra can be described as the following steps. First, existing XRF measurements from fluorochemical stock solution are processed using a set of pre-defined signal processing algorithms. Next, the XRF measurements from the blank carpet are acquired using the same measurement settings and processed through the same algorithms. Then, the background matching process is performed

Table 26: Signal processing algorithms and their corresponding parameters used to generate synthetic spectra

Algorithm	Algorithm Name	Parameters
Smoothing Algorithm	Low-statistics Filter	Channel Width = 3 Base Degree = 10 Cut-Off A = 75 Slope Constraint = 1.3
Background Removal	Peak Stripping Method	Channel Width = 5 Iteration = 50
Peak Searching Algorithm	Top-hat Peak Search	Intensity Threshold = 50 Sensitivity Factor = 4 Central Window = 9 Side Window = 5
Curve Fitting Function	Gaussian	

on those stock solution spectra to match them to the blank carpet samples. Finally, the characteristic peak properties from the solution sample are added to the XRF measurements of the blank carpet samples, and the final calibration curve may now be calculated. For this example, Rb-tagged stock solutions of 0, 25, 50, and 100 ppm of Rb were previously applied onto carpet samples by the manufacturer and these are used as the calibration control samples.

The first step to the entire process is to obtain XRF measurements from both the fluorochemical solutions and blank carpet samples (LPB_00RB). All spectra were processed through the same signal processing algorithms listed in Table 26. Then, the processed spectra were matched to the blank LPB carpet sample as described in Section 6.3, and the results are plotted in Figure 59. The actual Rb concentration in the solution and its average Rb peak counts from background matched results are shown in Table 27.

The total background intensity counts in the Rb K_α region were calculated both for the LPB blank carpet and the background matched spectra from stock solution

Table 27: Actual Rb concentration in stock solution and the peak counts resulting from background matched to LPB carpet

Targeted Rb Concentration On Carpets (ppm)	Actual Rb Concentration In Stock Solution (ppm)	Average Rb Counts (counts)
25	208	598
50	417	1271
100	833	2293

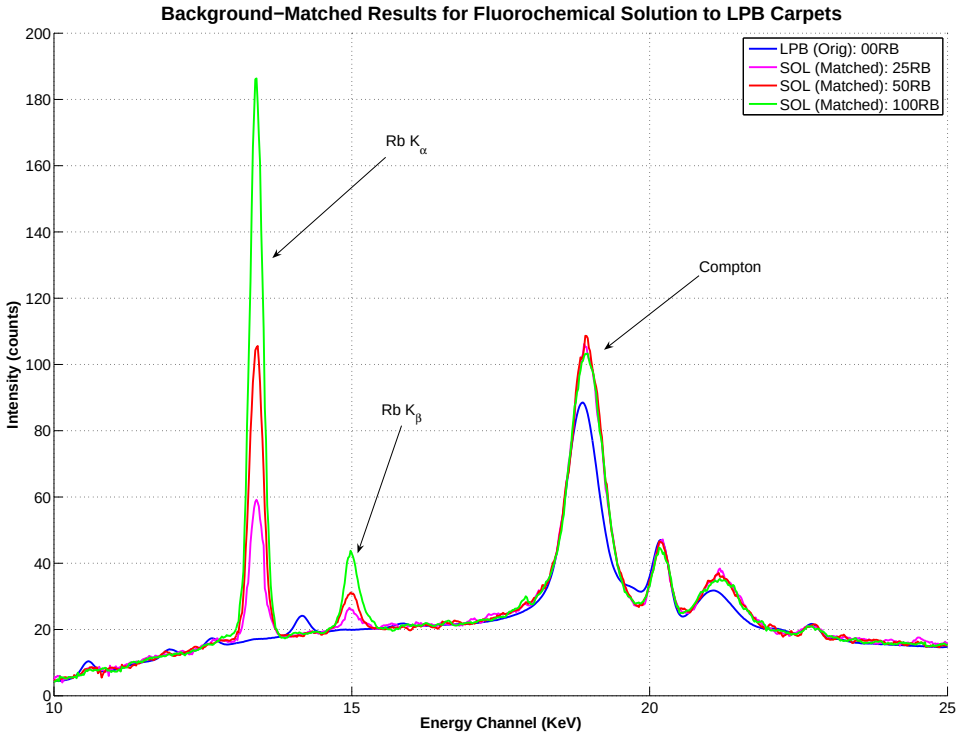

Figure 59: Results from matching Rb-tagged fluorochemical samples to the blank LPB carpet

samples. The results are shown in Table 28. The background match results in background intensity counts of synthetic spectra that are within 10% of the reference LPB carpet background.

The solution calibration procedure was then performed based on the results in Table 27. The resulting calibration curve is

$$C = 0.37I - 29.91 \tag{39}$$

Table 28: Total background intensity counts in Rb K_α region for an actual LPB carpet and the stock solution samples resulting from background matched to LPB carpet

Targeted Rb Concentration On Carpets (ppm)	LPB Carpet (counts)	Backgrond-Matched Stock Solution(counts)	Error (%)
25	676	684	1.18
50	676	707	3.55
100	676	736	8.88

with a fitting score of 1.00. Once this calibration curve is obtained, the Rb peak area corresponding to 25, 50, and 100 ppm of Rb can be easily calculated. These peaks lead to the last step in generating synthetic spectra for carpet samples, which is the peak matching procedure. Due to the scattering effect from carpet fibers, Rb K_α peaks in carpet samples are slightly wider than those from stock solution samples as studied in Appendix A. The Rb peak width (FWHM) for all the carpet in this series have an average value of 0.38 KeV. The corresponding peak height can be determined from the height and width parameters for a Gaussian peak fit to the characteristic Rb peak using the relationship $\sqrt{\pi}A\sigma$, where A and σ are parameters for Gaussian peak height and width, respectively. The results from generating the Rb K_α peaks are shown in Figure 60, 61, and 62 for 25, 50, and 100 ppm Rb-tagged carpet, respectively.

For verification purposes, three control carpet samples in the same carpet series were measured. These were manufactured with the targeted Rb concentrations of 25, 50, and 100 ppm. Using the same measurement procedures, twenty five XRF measurements were acquired from these samples from the same five locations as the blank carpet samples. The average of these spectra were also processed through the same signal processing algorithms. Once the Compton background for these average spectra are matched with LPB_00RB, XRF measurements are obtained and processed in the same manner as for the LPB_00RB carpet sample. The average characteristic peak counts obtained from these carpets will be used to predict the

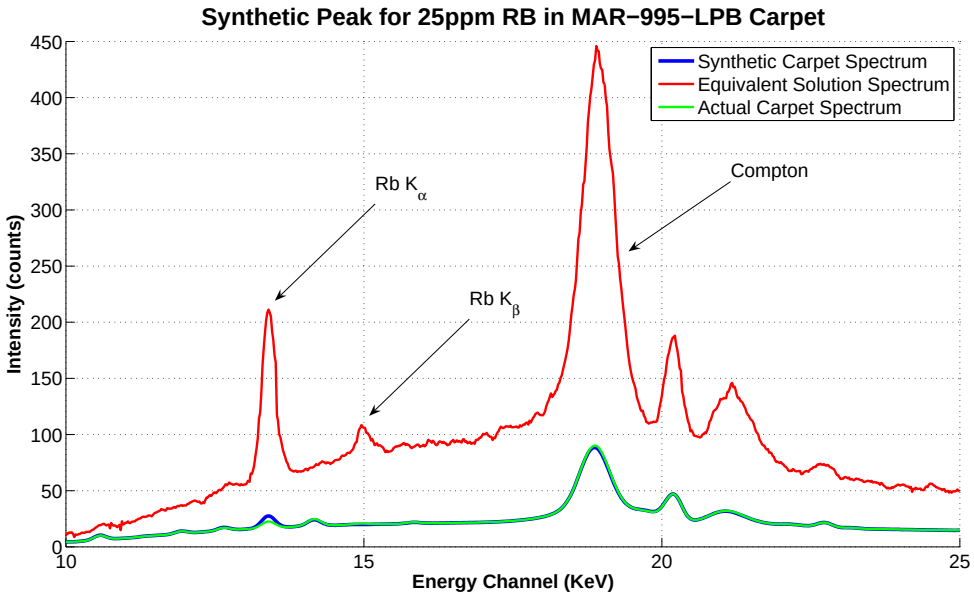

Figure 60: Synthetic and actual Rb K_α peak from carpet and stock solution for 25 ppm Rb

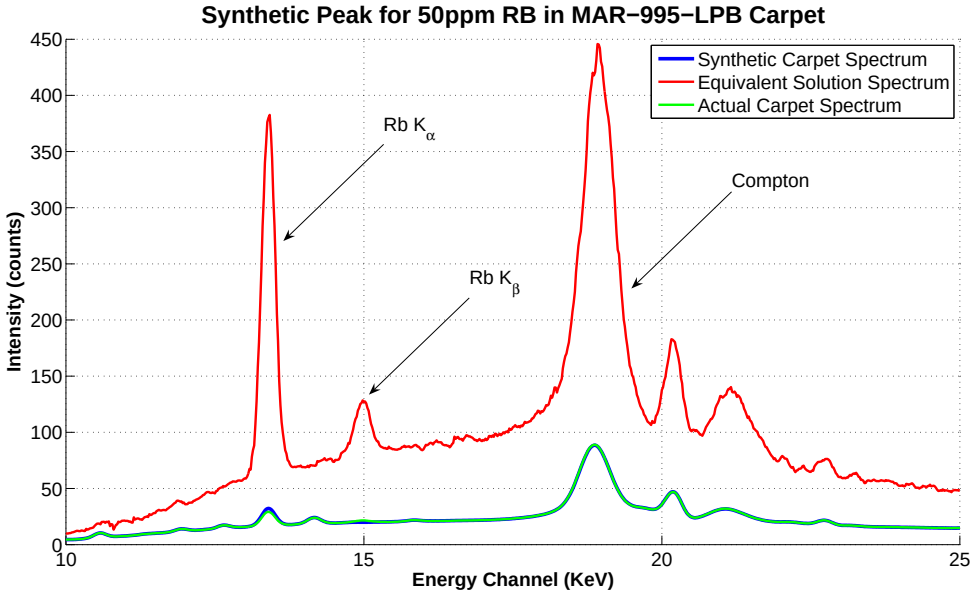

Figure 61: Synthetic and actual Rb K_α peak from carpet and stock solution for 50 ppm Rb

actual fluorochemical concentration on these control carpet samples and those results will then be compared to the AATCC test results as a final performance evaluation.

In an effort to compare the compatibility of the XRF measurements and the

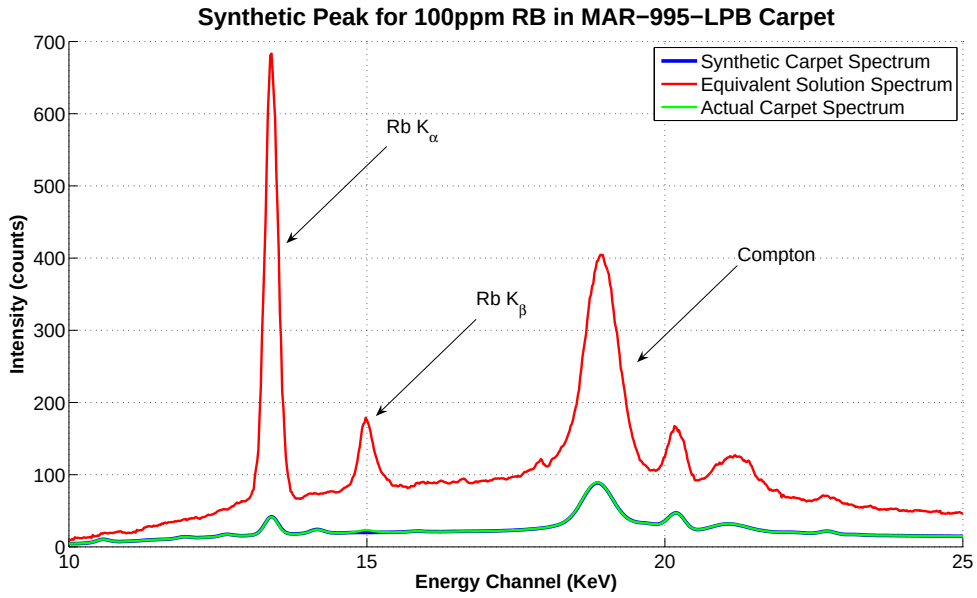

Figure 62: Synthetic and actual Rb K_α peak from carpet and stock solution for 100 ppm Rb

industry standard AATCC test, a random sample of each carpet in the LPB series was also taken to a professional test laboratory to perform the standard AATCC test to determine the actual levels of fluorochemicals. The results from these burn tests are shown in Table 29 will be used to determine the accuracy of the synthetic spectra generation methodology.

Table 29: Targeted and actual fluorochemical (F) and its translated taggant (Rb) concentration on LPB carpets using AATCC test

Carpet Sample	Targeted Rb (ppm)	Targeted F (ppm)	Actual F (ppm)	Translated Rb (ppm)
LPB_00RB	0	0	31	0
LPB_25RB	25	75	95	44
LPB_50RB	50	150	135	57
LPB_100RB	100	300	421	160

Table 30 shows the results from the entire process described above. The estimated fluorochemical concentration obtained from XRF measurements are listed against those obtained from AATCC test. The difference between the estimated and targeted

fluorochemical concentration are listed as an error. From this table, one can notice a systematic error, a drift, in the error column. To improve the performance of the calibration process using synthetic spectra, we recommend to add or replace at least one carpet sample with known fluorochemical concentration from AATCC test. Table 31 assumes that standard Rb tagged samples are available with 50ppm Rb and 150ppm F, along with the AATCC test results. XRF measurement results from this last sample can be added to the previous calibration to substantially reduce measurement errors. Specifically, by approximately 50% for this example.

Table 30: Performance evaluation for synthetic peak generation for MAR-995-LPB carpet series without AATCC correction

Targeted Rb (ppm)	Actual Rb (ppm)	Translated F (ppm)	AATCC F (ppm)	Error (ppm)
25	2.54	7.62	95.00	-67.38
50	36.83	110.50	135.00	-39.50
100	100.07	300.22	421.00	0.22

Table 31: Performance evaluation for synthetic peak generation for MAR-995-LPB carpet series with AATCC correction

Targeted Rb (ppm)	Actual Rb (ppm)	Translated F (ppm)	AATCC F (ppm)	Error (ppm)
25	14.72	44.15	95.00	-30.85
57	45.37	136.12	135.00	-13.88
100	101.90	305.70	421.00	5.70

Appendix E shows additional results from using fluorochemical solutions and blank carpet XRF measurements to effect synthetic XRF spectra for to two additional carpet types. Although the final calibration results are within the acceptable range of $\pm$50ppm accepted by most carpet manufacturers, carpet samples are still recommended with known fluorochemical concentrations as established from the industry standard AATCC burn test.

CHAPTER VII

RECOMMENDATIONS FOR CARPET INDUSTRY APPLICATIONS

The on-line XRF measurement system reported by this study is intended for near-real-time measurement of the fluorochemical content on carpet fibers. There are two aspects to the fluorochemical content analysis on carpet fibers: concentration and distribution measurements. The concentration aspect of the measurements focuses on assuring a targeted fluorine concentration of 150 ± 50 ppm, while the distribution aspect of the measurements concerns not only the fluorine concentration, but also its corresponding distribution across the entire carpet sample. This chapter summarizes the general guidelines for both aspects of these measurements.

In general, the overall steps required to establish a successful fluorochemical measurement system using portable XRF device can be summarized as the following:

1. Select a chemical taggant and establish calibration standards.
2. Select a location in the manufacturing line to perform XRF measurement.
3. Select a set of instrument settings that will enhance the taggant detection and extend the continuous on-line operating time of the XRF instrument.
4. Determine required measurement time required to achieve a desired accuracy.
5. Determine required measurement number and locations required to accurately identify fluorochemical concentrations.
6. Select a set of signal processing algorithms to be used in all calibration and analysis processes.

Step 1: Taggant Selection The first and most important step in setting up the XRF measurement system for the fluorochemical content measurement on carpet fibers is to determine a chemical taggant suitable for the application. Section 3.3 describes the ideal properties of a good chemical taggant. Since different carpet manufacturers have slightly different chemical compositions for their carpet backings and fibers, an ideal chemical taggant may have to vary from one manufacturer to another. Figure 63 shows XRF spectra obtained from different carpet samples. These carpets contain similar elements commonly found in carpet fibers as well as in carpet backings, such as Ti, Fe, Cu, and Sr.

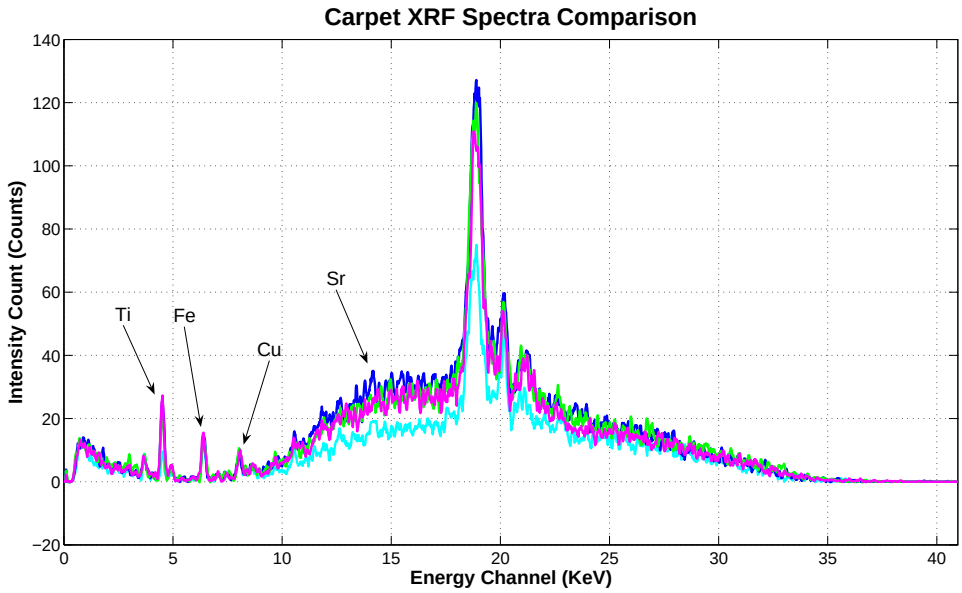

Figure 63: XRF spectra from different carpet samples

Since all K_α characteristic peaks belonging to elements found in carpet fibers and backing are in same energy channel range targeted for taggants, 6 - 18 KeV, specific characteristics of the background XRF spectra from manufacturer to manufacturer will affect their choices of a chemical taggant. As shown in Figure 64, any taggant chosen for the fluorochemical application should have the most prominent characteristic peak (K_α) within the energy channel range above. Further, from the varieties of

carpets studied in this research, most characteristic peaks generated from the actual carpet samples were located in the energy range between 6 -10 KeV, leaving elements with characteristic peaks from energy channel 10-18 KeV (Ga - Mo) more suitable for the chemical taggants.

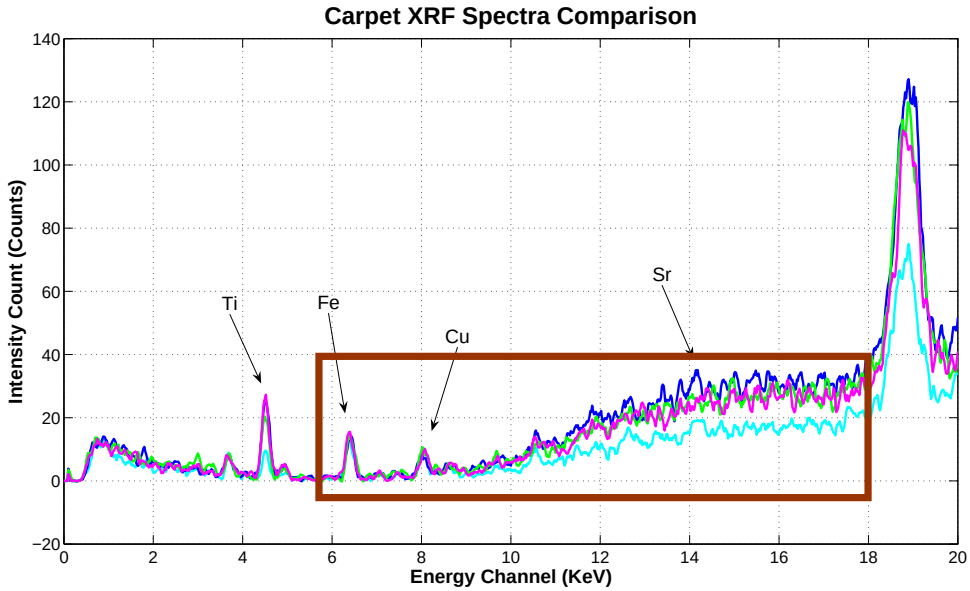

Figure 64: Possible energy channel range in XRF spectra for ideal chemical taggant

In addition to the location of the chemical taggant characteristic peak, other chemical properties should also be considered to select a suitable taggant for a particular carpet manufacturer, such as inter-element effects, bonding properties between the taggant and fluorochemicals, and effects of the taggant on the performance of the carpets. The chemical properties of the taggant such as the bonding properties and the effects of the selected taggant on carpet performance are beyond the scope of this research study. However, the inter-element effects were described early on in this research. Ideally, for the simplicity of the calibration process, we want to find a chemical taggant that does not interfere with any other elements in the carpet samples; however, if carefully calibrated, compensation can be made for inter-element effects. Inter-element effects were only partially studied in this research.

In this research, Rubidium (Rb) was chosen to be the chemical taggant of interest because the K_α peak is located at the energy channel 13.39 KeV, far away from other elements present in the carpet fibers and backing. The lower limit of detection (LLD) for Rb in a carpet sample is approximately 25 ppm based on the study in Section 4.1. If a standard Rb concentration of 50 ppm is used to represent 150 ppm of fluorine on carpet fibers, then the acceptable fluorochemical concentration range of 150 ± 50 ppm can be translated to the acceptable Rb concentration of 50 ± 16.7 ppm.

Step 2: XRF Measurement Location Although there is a great deal of similarity, carpet manufacturing processes differ between carpet manufacturers. These processes are summarized in Figure 65. During the carpet manufacturing process, tufted carpets are continuously moving along the production line. The fluorochemical application is usually before the backing is applied and before the finished carpets are moved through a drying oven. Once these carpets are rolled out of the oven and thus dried, the carpet fibers are sheared to a desired pattern. Last, the carpets are rolled out flat for final inspection, which typically consists of a technician performing a final visual inspection. Since the carpet is stationary for this visual inspection, this is the location where an XRF measurement system might be implemented.

In the final inspection area, a linear, single-axis, scanner holding the portable XRF device could be constructed to freely move across the carpet in a direction transverse to the carpet moving direction, i.e., across the web of the carpet. The overall XRF and scanner system should be programed so that it travels to pre-determined locations across the carpet to obtain desired XRF measurements while the carpet is stationary during the visual inspection. Since the final carpet normally stays stationary in this location for several minutes, allowing the technicians to walk across and perform visual inspections, this will allow a reasonable amount of time for the XRF measurements. However, it should be noted that this time frame will be suitable

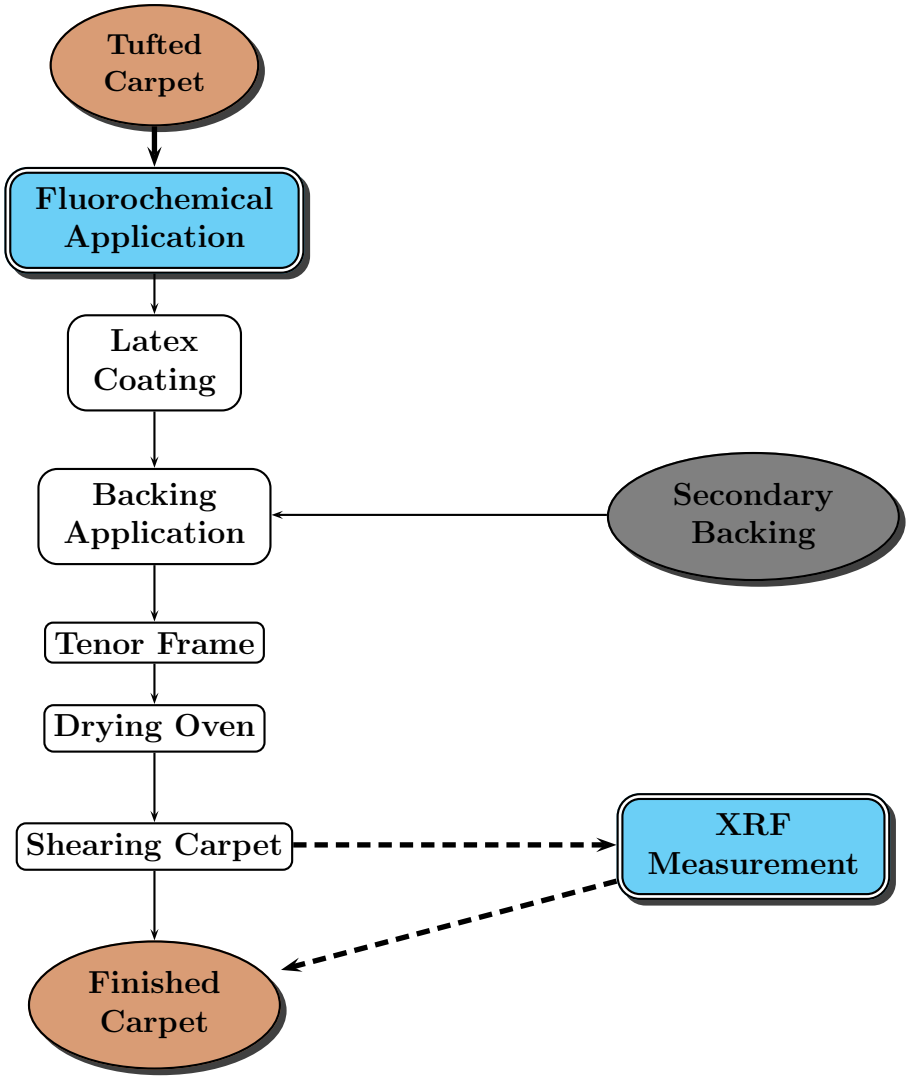

Figure 65: Fluorochemical application and recommended XRF locations during carpet manufacturing process

for concentration verification process only. The fluorochemical distribution analysis should be performed off-line due to the large number of measurements required to complete the task. The details for each type of analysis are discussed in this chapter.

Step 3: Instrument Settings: XRF instrument settings can be adjusted to enhance the detection of the chemical taggant in carpet samples while reducing background noise from other elements as much as possible. To generate sufficient intensity counts from the low concentration taggants in carpet samples, within the limited time

to take measurements on the manufacturing line, XRF instrument should be set at its highest operating power, i.e., highest X-ray tube voltage and current, with the fastest duty cycle without having to place it off-line for a cool down period between measurements.

Besides the X-ray tube voltage and current, the primary beam filter can help to further effectively eliminate XRF counts in unwanted regions while maintaining counts around the energy channels containing the characteristic peaks of the selected taggant. For our XRF measurements on carpet samples with Rb taggant, filters listed in Table 2 were sufficient to obtain reasonable measurement results. Based on our test results shown in Figure 66, the 300 μm Al and 25 μm filter, filter No. 1, was the most effective for reducing the XRF continuum near the Rb characteristic peaks locations of 13.39 and 14.96 KeV for K_α and K_β peaks, respectively. These results were also shown in Figure 17 filter No. 1.

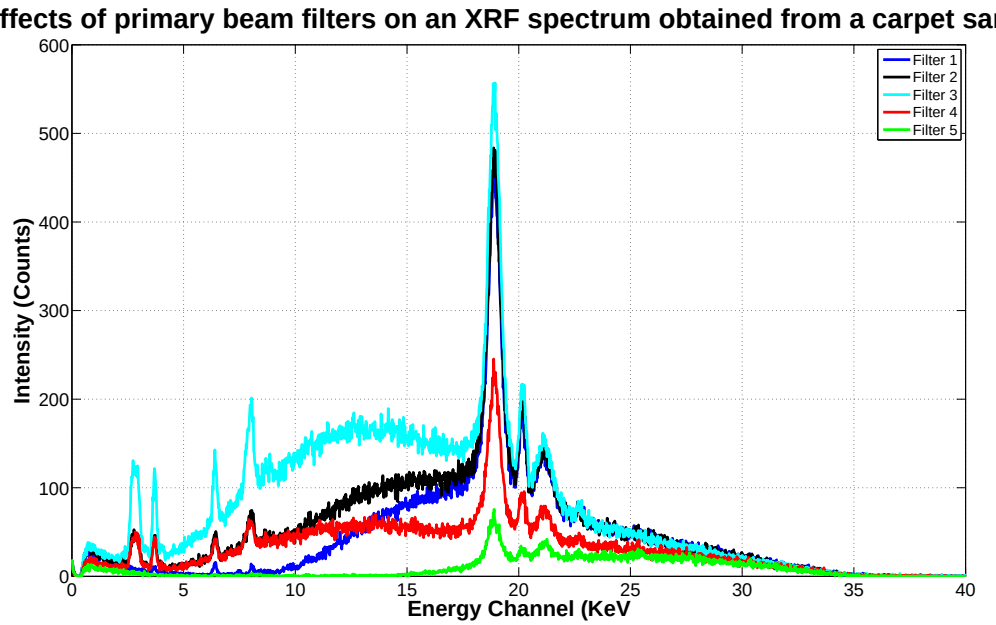

Figure 66: Effects of all primary beam filters equipped in S1 TRACeR on a typical carpet spectrum

The Compton peak locations in XRF spectra generated from different XRF instruments vary based on the hardware components of each instrument. Shifting these peak locations can reduce the interference between the background continuum generated from the Compton peak and the taggant characteristic peaks. However, this step can only be accomplished by consulting with the XRF instrument manufacturers.

The recommended measurement settings listed in Table 4 are specifically for the S1 TRACeR portable XRF instrument. It is expected that XRF instruments from different manufacturers, with different hardware components, will have different optimal settings and filter selections for optimizing detection of taggant characteristic peaks.

Step 4: Measurement Time Measurement time can significantly improve the accuracy of the XRF measurements. However, due to time constraints for the brief period of time when the carpet is stationary for visual inspection, the measurement time has to be selected to be as short as possible without compromising the accuracy of the measurements. In Section 3.5.4, the effects of the measurement time on the accuracies of XRF measurements were reported for various samples. A summary of the relative standard deviation of ten measurements collected from both carpet and fluorochemical solution samples are shown in Figure 67.

The overall recommendation for the measurement time is summarized in Table 32. In the case of Rb-tagged carpet samples, we judged that a relative standard deviation of 3% is required. Thus, a measurement time of 30 seconds is recommended for each individual measurement.

Step 5: Number of Measurements The number of measurements is an important key in accurately determining fluorochemical concentrations on carpet samples. The limited time the carpet stays stationary for visual inspection combined with the minimum measurement time to ensure measurement accuracy dictates the maximum

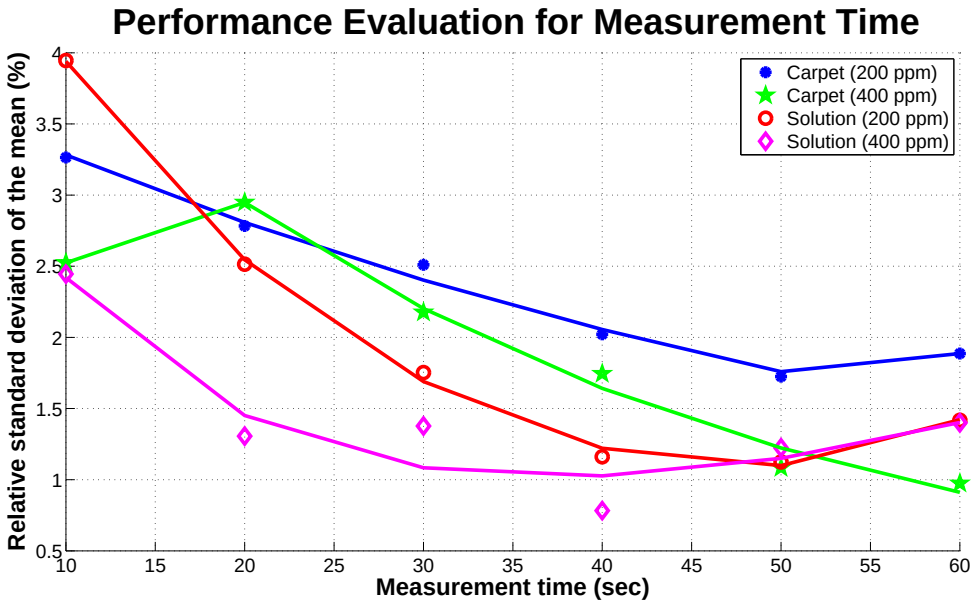

Figure 67: Effect of the measurement time on the XRF measurement accuracy

Table 32: Recommended measurement time for fluorochemical measurements

Minimum Measurement Time (seconds)	Minimum RSD (%)
10	4.00
20	3.00
30	2.75
40	2.25
50	1.75
≥60	1.90

number of measurements allowable across the carpet samples. There are two aspects to consider for the measurement number. First, how many locations across the carpet sample should be considered for measurements. Second, for each location, the minimum measurement number required per location to ensure the desired accuracy.

Appendix B summarizes the experiment which investigates the effects of the number of measurements on the accuracy of the measurements. The number of measurements per location improved the accuracy of the measurement result as can be seen in Figure 68. However, data from various locations on carpet samples should be collected

to obtain a representative concentration for the carpet. The studies in Appendix B suggests that in order to achieve a minimum of 10% relative standard deviation, a minimum of three measurements per location will be required.

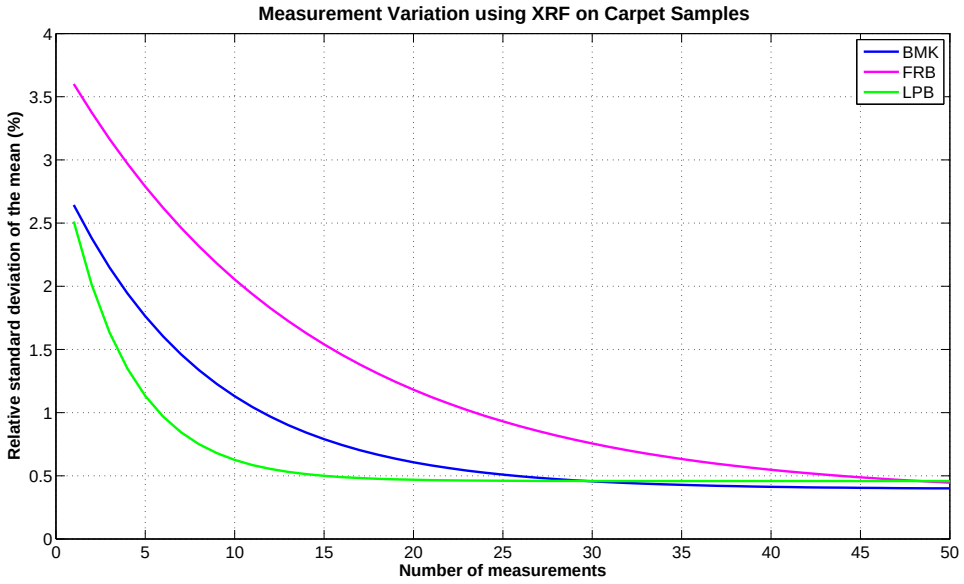

Figure 68: Measurement variation with relation to measurement numbers

Table 33 summarizes the recommended instrument settings of the Bruker S1 TRACeR for the on-line measurements. Due to the measurement time and the number of required measurements necessary to achieve sufficient accuracy, the XRF measurements should be made at several positions while it is stationary, but cannot be used to measure concentration across the entire cross section of the carpet. Since the spray application systems for fluorochemicals on the carpet manufacturing line can consist of multiple spray nozzles across the carpet as shown in Figure 69, the application of the fluorochemicals may not be uniform across the carpet. The location of the XRF measurement position should include the maximum, minimum, and the average value locations from the expected nozzle pattern.

Step 6: Signal Processing Algorithm Selection Measurement noise and deviation can be further reduced using appropriate signal processing algorithms. These

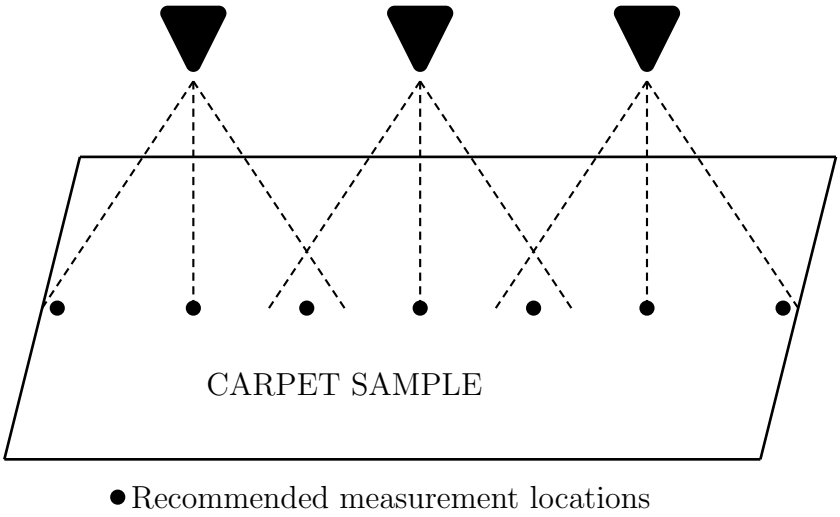

Figure 69: Fluorochemical distribution profile from spray application

Table 33: Recommended measurement and instrument settings for fluorochemical measurement on carpet fibers using S1 TRACeR

Category	Value
Tube Voltage	40 KeV
Tube Current	2.8 μA
Primary Beam Filter	Layer 1: Al (300 μm)
	Layer 2: Ti (25 μm)
Measurement Time	30 s
Pause Time between Measurements	30 s
Measurement Number per location	5
Measurement Number per nozzle	3

algorithms and their corresponding parameters should be investigated and selected prior to the calibration process. Furthermore, these algorithms have to be kept consistent throughout the validation and calculation of the remaining samples. These algorithms should be selected such that they minimize the on-line processing time and the standard deviation of the overall taggant peak counts.

The signal processing algorithms have to be consistent for both the calibration and on-line measurements. From the results of this research, the recommended signal

processing algorithms suitable for real-time analysis of the XRF spectra obtained from carpet samples are listed in Table 9. Depending on the chemical taggant and its corresponding nominal concentration applied to the fluorochemical solution, some adjustments to these algorithms may be required.

Step 7: Calibration As mentioned in Section 3.5, the measurement setup and the sample characteristics play an significant impact in the resulting XRF spectra. To improve the performance of the proposed methodology, reference XRF spectra used to generate calibration spectra are recommended to be as similar to the actual analysis samples as possible. In addition, they should be easy and economical to fabricate. We have demonstrated that properly tagged fluorochemical solutions are suitable samples to be utilized as reference samples. It will be required that the carpet manufacturers maintain a minimal database of tagged carpet samples prepared from carefully controlled stock solutions. Further, AATCC burn test should be performed on all of these samples to adjust the XRF calibration results.

In summary, the steps to effect a reasonable calibration are as follows:

1. Select the corresponding chemical taggant from the database.

2. Select the instrument and the measurement settings intended for the on-line XRF measurements.

3. Perform the calibration using the Lucas-Tooth and Price algorithm summarized in Section 2.5.2 using a properly tagged stock solution.

4. For any new unknown carpets, record the corresponding fiber and backing weight and take XRF measurements based on the instrument and measurement settings defined in Step 2.

5. Synthetically generate calibration spectra for the unknown carpet.

6. Add a few data points from the AATCC laboratory test to adjust the overall calibration as required.

CHAPTER VIII

CONCLUSIONS AND RECOMMENDATIONS FOR FUTURE WORK

Throughout this research, experiments were performed to investigate the suitability of using XRF to measure the amount of fluorochemicals on carpet fibers. Observations from these results are summarized in this chapter. Recommendations for future work in the fluorochemical application in carpet manufacturing are also listed at the end of this chapter.

8.1 Conclusions

A recommended set of the measurement settings used for on-line measurement of fluorochemical concentration on carpet fibers was identified in this research. XRF is sensitive to characteristics of samples as well as well as measurement settings. This research demonstrated that carpet pile height, yarn density, and backing materials affect the overall XRF spectra and the resulting characteristic peak areas used to deduce fluorochemical concentration. Experiments showed that the carpet pile height is inversely proportional to XRF intensity counts. No correlations were found between yarn density and carpet backing materials versus XRF intensity counts. Additionally, measurement settings including X-ray tube voltage and current, primary beam filter, measurement time, and measurement numbers can effectively enhance the detection of the chemical taggant in carpet samples.

This study showed that multiple XRF measurements are required to effectively determine the fluorochemical concentration on carpet fibers. To achive a relative

standard deviation of less than 5% of each XRF measurement, a minimum of 5 measurements are required. Additionally, the fluorochemical spray nozzles can introduce slight wave pattern in flurochemical distribution in carpet samples. To determine the overall fluorochemical concentration on each carpet sample, a minimum set of $2s + 1$ measurements at predetermined locations is required, where s is the number of nozzle spray heads in the manufacturing line. Time permitting, a set of $4s+1$ measurements is recommended to determine fluorochemical concentration at extreme locations as well as intermediate points.

A continuous scanning method was investigated to assist in fluorochemical distribution measurements. The results showed that the maximum speed in which the XRF instrument can be moved and still collect valid amount of intensity counts is 3 cm/s. Thus,a carpet web width of approximately 400 cm will require a measurement time of 2.5 minutes, which also means that the XRF instrument requires approximately this same amount of time to cool down its internal temperature before starting another measurement sequence. Results from the continuous scanning method suggested that this scanning method can provide the overall, average fluorochemical concentration over the measurement path, but it is not sufficient to detect specific distribution patterns. The continuous scanning method should be used in conjunction with measurements at the $4s + 1$ locations described above to provide a complete analysis of the fluorochemical distribution of a carpet on the manufacturing line.

XRF calibration performed using actual fluorochemical solution and carpet samples tagged with Rb showed that given the availability of reference carpet samples of the same type, i.e. backing materials, pile height, and density, the fluorochemical concentration on an unknown carpet sample can be determined to the accuracy of within ± 30 ppm of fluorine, which is within the allowable ± 50 ppm of fluorine used in the carpet industry. Unfortunately, manufacturing carpet samples with various taggant concentrations is expensive, and failure to produce reference carpet samples

will result in inaccurate determination of the fluorochemical concentration.

To overcome the reference sample fabrication, this research introduced a new methodology to synthetically generate required reference XRF spectra for use in the calibration process. This methodology generates a desired XRF spectrum for a particular carpet sample by combining the characteristic peak data of the desired taggant from fluorochemical solutions and an XRF spectrum obtained from the carpet sample without any taggant. The process involved in synthetic peak generation first selected an energy range of interest based on the chemical taggant used. Next, the background continuum in this energy region from the fluorochemical solution is matched to the blank carpet sample, and finally proper characteristic peak width and height are adjusted to match the new background continuum and the net peak area is calculated for calibration. This study showed that the synthetically generated XRF spectra alone were not always sufficient to guarantee the confidence interval required by the certified AATCC test.

The errors in carpet calibration using only synthetically generated spectra could be reduced dramatically by adding one or more reference spectra from an actual carpet sample with its fluorochemical concentration verified using the AATCC burn test. The error margin of ± 100 ppm of F could possibly be reduced down 50% to approximately ± 50 ppm of F just by adding AATCC test results from one carpet sample. Due to the error margin potentially present in the calibration using only synthetic XRF spectra, the on-line measurement of the fluorochemical concentration on carpet fibers using XRF should be adjusted as necessary using the chemical burn test specified by AATCC. Further, XRF measurements can rapidly select questionable carpet samples for further off-line analysis.

8.2 Recommendations for Future Work

Fabricating carpet samples with specific taggant concentrations is an expensive process and requires careful preparation to achieve optimal XRF calibration results. The lack of samples prevents the studies of the following subjects, which should be further investigated to improve the accuracy of the synthetically generate XRF spectra:

- Investigate the effects of carpet characteristics on XRF spectra, i.e., how the measured XRF intensity counts change with respect to carpet pile height, yarn density, and turn-per-inch.
- Investigate the effect of embedding multiple taggants in carpet samples not only for the measurement of fluorochemical concentration, but also for authentication purposes.
- Investigate the accuracy of synthetically generated XRF spectra from a large variety of carpets with different known backing materials.
- Investigate the use of the industry standard AATCC test results to improve the accuracy of XRF calibration

APPENDIX A

CHARACTERISTIC PEAK EVALUATIONS

In this appendix, three sets of experiments are used to investigate the characteristic peak differences between various chemical taggants, instruments, and sample materials. For all of the experiments presented in this appendix, the measurement settings and the signal processing algorithms employed followed Tables 4 and 26. Since the characteristic peak of interest is the K_α peak of the chemical taggant Rb, the results shown in this appendix are only for this peak.

The first sets of the experiments explores the similarities of the Gaussian peak characteristics of different elements in same base material. This set of experiments were performed early on in this study using the TRACeR II instrument. For this set of experiements, Cu-, Zn-, and Rb-tagged solution samples, each with various taggant concentrations, were prepared. For each sample, three measurements were acquired and processed using the algorithms defined in Table 26. The estimated Gaussian peak width, center, and height for each sample are displayed in Tables 34, 35, and 36.

The parameters of the Gaussian peaks for the Cu, Zn, and Rb tagged solution samples were all accurately determined using the TRACeR II XRF instrument. All peak centers are accurately located at 8.5, 8.64, and 13.3 KeV, which are the K_α locations for Cu, Zn, and Rb, respectively. Likewise, the peak widths remained constant within a small variation. The peak widths observed for Cu, Zn, and Rb using the TRACeR II are 0.60, 0.58, and 0.64 KeV with standard deviations of 4.55E-02, 1.21E-02, 1.47E-02, respectively. As a result, we conclude that the overall characteristic peak widths remain constant regardless of the concentration, whereas peak heights and areas are directly related to the chemical concentration of these

elements.

The second set of experiments explored the effect of the portable XRF instrument on the Gaussian peak characteristics. To investigate instrument dependance, both TRACeR II and S1 TRACeR were used to obtain measurements from the same Rb-tagged solution sample. The results are listed in Tables 36 and 37 for the measurements obtained using TRACeR II and S1 TRACeR instruments, respectively. Although the peaks are correctly located at the same energy channel of 13.3 KeV, the peak, the peak width and height are very different for the two instruments. Thus, we conclude that the choice of instrument affects all peak parameters except perhaps the location of the peak for a Rb-tagged solution sample.

The last set of experiments investigated any differences of the characteristic peak parameters when the same chemical taggant was embedded in different sample materials. In this set of experiments, both solution and carpet samples tagged with various Rb concentrations were used. From a stock solution sample, fluorochemical solutions of 25, 50, 100 ppm Rb were prepared. These target values are the ppm level that would result if these solutions were applied to carpet samples. The actual Rb concentrations in these stock solution are listed in Table 27. Three series of carpet samples were manufactured using fluorochemical solutions tagged with the same four levels of Rb concentration. These samples were manufactured using the same carpet backing and fiber materials, but styles varied as listed in Table 16.

In this set of experiments, five XRF measurements were acquired for each sample using the S1 TRACeR portable XRF instrument with the same measurement settings as the previous set of experiments. These spectra are then processed using the same algorithms as summarized in Table 9. The results for Rb K_α peak characteristics in fluorochemical solution samples are shown in Table 38. Compared to the results obtained from the aqueous solutions listed in Table 37 for the same instrument, Rb peaks widths remained relatively constant with width values of 0.36 and 0.37 KeV, and

with standard deviation values of 2.99E-02 and 8.26E-03 for Rb tagged fluorochemical solution and carpet samples, respectively.

Tables 39, 40, and 41 show similar results for the Rb K_α peak characteristics in the BMK, FRB, and LPB carpet series, respectively. From the Gaussian peak parameters obtained from these carpet samples, the peak centers are consistently located at the 13.3 KeV, while the widths are approximately 0.38 KeV with a worst case standard deviation value of 2.38E-02 from the LPB-series carpets. Thus, the Rb characteris peaks obtained from the carpet samples are slightly wider than those obtained from the solution samples. This effect is most likely caused by the scattering of the incident X-ray beam within carpet samples due to the uneven surface of the carpet fibers.

Table 34: Cu characteristic peak in Cu-tagged aqueous solution using TRACeR II

Cu Concentration (ppm)	**Cu K_α Peak Characteristic**			
	Center (KeV)	**Height** (counts)	**FWHM** (KeV)	**Area** (counts)
174.49	8.05	9	0.67	7
	8.05	9	0.54	5
	8.05	11	0.82	10
Average	**8.05**	**10**	**0.68**	**7**
STD	**0**	**1.1**	**0.14**	**2.3**
348.98	8.05	14	0.73	11
	8.05	13	0.81	12
	8.05	21	0.48	11
Average	**8.05**	**16**	**0.68**	**11**
STD	**0**	**4.3**	**0.17**	**0.4**
697.95	8.05	35	0.53	20
	8.05	34	0.58	21
	8.05	26	0.57	16
Average	**8.05**	**31**	**0.56**	**19**
STD	**0**	**5.2**	**0.03**	**2.9**
1395.91	8.05	35	0.65	24
	8.05	54	0.52	30
	8.05	82	0.52	45
Average	**8.05**	**56**	**0.56**	**33**
STD	**0**	**24**	**0.08**	**11.0**
2791.82	8.05	82	0.64	56
	8.05	130	0.53	73
	8.05	90	0.59	56
Average	**8.05**	**101**	**0.58**	**61**
STD	**0**	**25.6**	**0.06**	**9.6**
5583.63	8.05	206	0.57	126
	8.05	167	0.57	102
	8.05	226	0.54	130
Average	**8.05**	**200**	**0.6**	**119**
STD	**0**	**29.8**	**0.02**	**15.1**
8375.45	8.05	187	0.64	128
	8.05	289	0.57	175
	8.05	466	0.48	236
Average	**8.05**	**314**	**0.56**	**180**
STD	**0**	**141.0**	**0.08**	**54.0**

Table 35: Zn characteristic peak in Zn-tagged aqueous solution using TRACeR II

Zn Concentration (ppm)	**Zn K_α Peak Characteristic**			
	Center (KeV)	**Height** (counts)	**FWHM** (KeV)	**Area** (counts)
179.74	8.64	10	0.63	7
	8.64	12	0.62	8
	8.64	10	0.64	6
Average	**8.64**	**10**	**0.63**	**7**
STD	**0**	**1.6**	**0.01**	**1.0**
359.47	8.64	21	0.55	12
	8.64	23	0.60	15
	8.64	15	0.59	10
Average	**8.64**	**19**	**0.58**	**12**
STD	**0**	**4.1**	**0.03**	**2.5**
718.95	8.64	38	0.65	27
	8.64	42	0.57	26
	8.64	44	0.56	26
Average	**8.64**	**41**	**0.6**	**26**
STD	**0**	**2.7**	**0.05**	**0.4**
1437.89	8.64	74	0.57	45
	8.64	73	0.56	44
	8.64	75	0.60	48
Average	**8.64**	**73**	**0.58**	**46**
STD	**0**	**0.9**	**0.02**	**1.9**
2875.79	8.64	177	0.56	105
	8.64	179	0.56	107
	8.64	173	0.59	108
Average	**8.64**	**176**	**0.57**	**107**
STD	**0**	**3.1**	**0.01**	**1.3**
5751.57	8.64	270	0.57	164
	8.64	289	0.55	168
	8.64	276	0.56	165
Average	**8.64**	**278**	**0.56**	**166**
STD	**0**	**9.6**	**0.01**	**2.5**
8627.36	8.64	383	0.58	237
	8.64	388	0.55	228
	8.64	389	0.56	230
Average	**8.64**	**387**	**0.56**	**232**
STD	**0**	**3.2**	**0.02**	**4.4**

Table 36: Rb characteristic peak in Rb-tagged aqueous solution using TRACeR II

Rb Concentration (ppm)	**Rb K_α Peak Characteristic**			
	Center (KeV)	**Height** (counts)	**FWHM** (KeV)	**Area** (counts)
62.5	13.30	28	0.60	18
	13.30	30	0.57	19
	13.30	29	0.61	19
Average	**13.30**	**28**	**0.59**	**18**
STD	**0**	**1.2**	**0.02**	**0.4**
125	13.30	53	0.59	34
	13.30	56	0.65	39
	13.30	58	0.67	41
Average	**13.30**	**55**	**0.6**	**37**
STD	**0**	**2.3**	**0.04**	**3.9**
250	13.30	101	0.57	61
	13.30	107	0.62	71
	13.30	83	0.66	58
Average	**13.3**	**96**	**0.62**	**63**
STD	**0**	**12.8**	**0.05**	**6.7**
500	13.30	188	0.57	114
	13.30	193	0.63	130
	13.30	188	0.59	119
Average	**13.30**	**190**	**0.60**	**121**
STD	**0**	**3.2**	**0.03**	**8.5**
1000	13.30	334	0.65	231
	13.30	350	0.62	231
	13.30	350	0.64	237
Average	**13.30**	**345**	**0.64**	**233**
STD	**0**	**9.0**	**0.01**	**3.6**
2000	13.30	563	0.67	401
	13.30	565	0.68	406
	13.30	579	0.66	404
Average	**13.30**	**569**	**0.67**	**404**
STD	**0**	**8.6**	**0.01**	**2.4**
3000	13.30	721	0.74	565
	13.30	734	0.71	552
	13.30	724	0.71	549
Average	**13.30**	**726**	**0.72**	**555**
STD	**0**	**6.7**	**0.16**	**8.5**

Table 37: Rb characteristic peak in Rb-tagged aqueous solution using S1 TRACeR

Rb Concentration (ppm)	**Rb K_α Peak Characteristic**			
	Center (KeV)	**Height** (counts)	**FWHM** (KeV)	**Area** (counts)
62.5	13.30	110	0.41	49
	13.30	101	0.30	33
	13.30	100	0.33	35
Average	**13.30**	**104**	**0.35**	**39**
STD	**0**	**5.7**	**0.57**	**8.5**
125	13.30	196	0.40	83
	13.30	186	0.39	77
	13.30	179	0.35	66
Average	**13.30**	**187**	**0.38**	**75**
STD	**0**	**8.8**	**0.03**	**8.9**
250	13.30	354	0.33	125
	13.30	338	0.39	140
	13.30	363	0.41	156
Average	**13.30**	**351**	**0.38**	**140**
STD	**0**	**12.7**	**0.04**	**15.8**
500	13.30	676	0.37	263
	13.30	691	0.40	292
	13.30	653	0.37	256
Average	**13.30**	**673**	**0.38**	**270**
STD	**0**	**19.2**	**0.02**	**19.0**
1000	13.30	1250	0.33	443
	13.30	1330	0.33	463
	13.30	1250	0.33	444
Average	**13.30**	**1284**	**0.3**	**450**
STD	**0**	**43.6**	**0**	**11.3**
2000	13.30	2360	0.39	965
	13.30	2400	0.36	912
	13.30	2410	0.36	932
Average	**13.30**	**2391**	**0.37**	**936**
STD	**0**	**29.5**	**0.01**	**26.6**
3000	13.30	3140	0.36	1210
	13.30	3260	0.35	1220
	13.30	3190	0.38	1290
Average	**13.30**	**3202**	**0.36**	**1248**
STD	**0**	**57.1**	**0.01**	**43.8**

Table 38: Rb characteristic peak in Rb-tagged fluorochemical solution

Rb Concentration (ppm)	**Rb K_α Peak Characteristic**			
	Center (KeV)	**Height** (counts)	**FWHM** (KeV)	**Area** (counts)
25	13.30	151	0.37	42
	13.30	145	0.36	40
	13.30	144	0.39	43
	13.30	151	0	41
	13.30	147	0.36	40
Average	**13.30**	**148**	**0.37**	**41**
STD	**0**	**3.1**	**0.01**	**1.2**
50	13.30	303	0.37	85
	13.30	307	0.38	87
	13.30	293	0.39	85
	13.30	297	0.37	81
	13.30	294	0.38	83
Average	**13.30**	**299**	**0.38**	**84**
STD	**0**	**5.9**	**0.01**	**2.0**
100	13.30	562	0.37	157
	13.30	556	0.37	155
	13.30	572	0.37	159
	13.30	575	0.37	159
	13.30	573	0.37	160
Average	**13.30**	**568**	**0.37**	**158**
STD	**0**	**8.1**	**0**	**2.0**

Table 39: Rb characteristic peak in Rb-tagged MAR-995-BMK carpet series

Rb Concentration (ppm)	**Rb K_α Peak Characteristic**			
	Center (KeV)	**Height** (counts)	**FWHM** (KeV)	**Area** (counts)
25	13.30	63	0.39	19
	13.30	74	0.37	21
	13.30	58	0.40	17
	13.30	42	0.40	13
	13.30	52	0.35	14
Average	**13.30**	**57**	**0.38**	**16**
STD	**0**	**11.9**	**0.02**	**3.3**
50	13.30	83	0.38	24
	13.30	94	0.38	27
	13.30	99	0.38	29
	13.30	75	0.39	22
	13.30	76	0.38	22
Average	**13.30**	**85**	**0.4**	**24**
STD	**0**	**10.9**	**0**	**3.1**
100	13.30	153	0.38	44
	13.30	154	0.38	45
	13.30	115	0.38	33
	13.30	109	0.38	31
	13.30	137	0.38	40
Average	**13.30**	**134**	**0.38**	**38**
STD	**0**	**21.1**	**0**	**6.0**

Table 40: Rb characteristic peak in Rb-tagged MAR-995-6.0-FRB carpet series

Rb Concentration (ppm)	**Rb K_α Peak Characteristic**			
	Center (KeV)	**Height** (counts)	**FWHM** (KeV)	**Area** (counts)
25	13.30	52	0.38	15
	13.30	40	0.38	12
	13.30	49	0.38	14
	13.30	45	0.39	13
	13.30	42	0.39	12
Average	**13.30**	**45**	**0.38**	**13**
STD	**0**	**4.9**	**0**	**1.3**
50	13.30	106	0.39	31
	13.30	93	0.38	27
	13.30	80	0.40	24
	13.30	79	0.37	22
	13.30	93	0.38	27
Average	**13.30**	**90**	**0.38**	**26**
STD	**0**	**11.1**	**0.01**	**3.4**
100	13.30	70	0.38	20
	13.30	87	0.39	25
	13.30	94	0.38	27
	13.30	94	0.38	27
	13.30	98	0.39	28
Average	**13.30**	**88**	**0.38**	**25**
STD	**0**	**11.1**	**0**	**3.3**

Table 41: Rb characteristic peak in Rb-tagged MAR-995-3.5-LPB carpet series

Rb Concentration (ppm)	**Rb K_α Peak Characteristic**			
	Center (KeV)	**Height** (counts)	**FWHM** (KeV)	**Area** (counts)
25	13.30	49	0.38	14
	13.30	33	0.38	9
	13.30	30	0.38	9
	13.30	32	0.38	9
	13.30	27	0.39	8
Average	**13.30**	**34**	**0.38**	**9**
STD	**0**	**8.78**	**0.01**	**2.4**
50	13.30	55	0.37	15
	13.30	62	0.34	16
	13.30	48	0.40	15
	13.30	49	0.43	16
	13.30	55	0.34	14
Average	**13.30**	**54**	**0.38**	**15**
STD	**0**	**5.69**	**0.04**	**0.8**
100	13.30	102	0.40	31
	13.30	104	0.35	27
	13.30	85	0.38	24
	13.30	102	0.41	31
	13.30	53	0.37	15
Average	**13.30**	**88**	**0.38**	**25**
STD	**0**	**21.7**	**0.02**	**6.7**

APPENDIX B

PERFORMANCE EVALUATION: MEASUREMENT NUMBERS

Common to all measurement systems, increasing the number of measurements in an experiment, increases the confidence in the result such that the average value will lie closer to the population true mean value. However, in a near-real-time measurement system, time is limited, which prohibits obtaining an unlimited number of measurements. Experiments described here were intended to determine the required measurement number necessary to achieve any given measurement accuracy.

Three types of carpet samples are described in Table 16 as tagged with different Rubidium (Rb) concentrations, and these were used for this experiment. For each carpet type, four different levels of taggant concentrations were considered: 0, 25, 50, and 100 ppm, making a total of twelve carpet samples for this experiment. For each carpet sample, a 17×30 grid with a 5mm pitch between each locations was used to define the measurement locations. Five measurements were taken at each location for a total of 2550 measurements per carpet sample. The XRF instrument and measurement settings were in accordance to Table 4. The XRF instrument was placed on an automated scanner and set for a 30-second measurement, followed by a 30-second cool down period to keep the instrument's internal temperature within the recommended operating range.

From the set of 2550 measurements obtained from each carpet sample, sets of 2, 3, 4, ..., 100 measurement numbers were randomly selected from the entire population pool. Next, relative standard deviation of the mean was calculated for each measurement set. Multiple trials were performed and an overall average was obtained

to represent the average measurement numbers for any given sample. The results of the averages from all trials for all carpet samples are plotted in Figures 70 through 81 and displayed in Tables 42, 43, and 44 for BMK, FRB, and LPB carpet series, respectively.

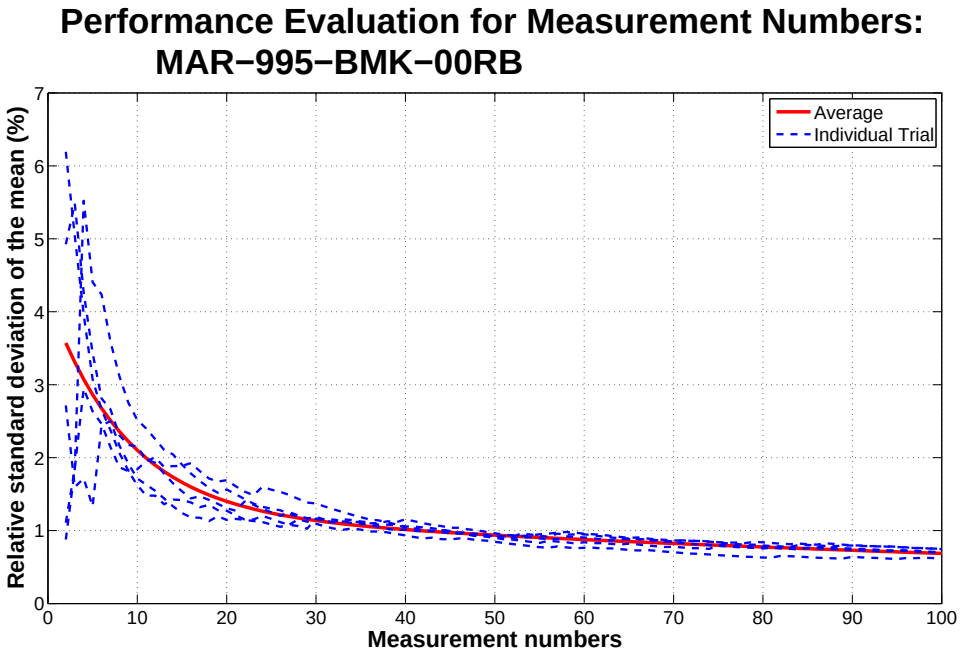

Figure 70: Measurement numbers and measurement accuracy analysis for carpet MAR-995-BMK series with no taggant

Increasing number of XRF measurements per sample can reduce the measurement uncertainty. As one can see from the results in this appendix, five XRF measurements are sufficient to guarantee 5% standard deviation in most carpet samples, 3% in some carpet samples. A small subset of carpet samples may require up to 10 measurements to obtain less than 5% relative standard deviation. One observation seen from these results is that the high intensity counts result in high standard deviations. Thus, for higher intensity counts, additional measurements are required to maintain the same relative standard deviation.

Table 42: Average relative standard deviation of the mean for carpet MAR-995-BMK series

Measure.	MAR-995-BMK RSDM				Measure.	MAR-995-BMK RSDM			
Number	00RB	25RB	50RB	100RB	Number	00RB	25RB	50RB	100RB
2	3.57	5.78	8.74	6.08	51	0.93	1.11	2.35	2.22
3	3.31	4.67	7.78	5.83	52	0.92	1.10	2.32	2.20
4	3.07	3.88	6.99	5.60	53	0.92	1.08	2.30	2.18
5	2.86	3.30	6.35	5.39	54	0.91	1.07	2.27	2.16
6	2.68	2.89	5.82	5.19	55	0.91	1.06	2.25	2.14
7	2.51	2.59	5.38	5.00	56	0.90	1.04	2.23	2.12
8	2.36	2.37	5.03	4.83	57	0.89	1.03	2.21	2.10
9	2.22	2.21	4.73	4.67	58	0.89	1.02	2.18	2.08
10	2.10	2.09	4.48	4.52	59	0.88	1.01	2.16	2.06
11	1.99	1.99	4.27	4.38	60	0.88	0.99	2.14	2.05
12	1.90	1.92	4.10	4.25	61	0.87	0.98	2.12	2.03
13	1.81	1.86	3.95	4.12	62	0.87	0.97	2.09	2.01
14	1.73	1.82	3.82	4.01	63	0.86	0.96	2.07	1.99
15	1.66	1.78	3.71	3.90	64	0.86	0.95	2.05	1.98
16	1.60	1.74	3.62	3.80	65	0.85	0.93	2.03	1.96
17	1.54	1.71	3.54	3.70	66	0.84	0.92	2.01	1.94
18	1.49	1.69	3.46	3.61	67	0.84	0.91	1.99	1.93
19	1.44	1.66	3.40	3.53	68	0.83	0.90	1.97	1.91
20	1.40	1.64	3.34	3.45	69	0.83	0.89	1.95	1.90
21	1.36	1.61	3.28	3.37	70	0.82	0.88	1.93	1.88
22	1.33	1.59	3.24	3.30	71	0.82	0.87	1.91	1.87
23	1.30	1.57	3.19	3.24	72	0.81	0.86	1.89	1.85
24	1.27	1.55	3.15	3.17	73	0.81	0.85	1.87	1.84
25	1.24	1.53	3.11	3.11	74	0.80	0.84	1.85	1.82
26	1.22	1.51	3.07	3.06	75	0.80	0.83	1.83	1.81
27	1.19	1.49	3.03	3.00	76	0.79	0.82	1.81	1.79
28	1.17	1.48	2.99	2.95	77	0.79	0.81	1.79	1.78
29	1.15	1.46	2.96	2.90	78	0.78	0.80	1.78	1.76
30	1.14	1.44	2.93	2.86	79	0.78	0.79	1.76	1.75
31	1.12	1.42	2.89	2.81	80	0.78	0.78	1.74	1.74
32	1.11	1.40	2.86	2.77	81	0.77	0.77	1.72	1.72
33	1.09	1.39	2.83	2.73	82	0.77	0.76	1.70	1.71
34	1.08	1.37	2.80	2.69	83	0.76	0.75	1.69	1.70
35	1.07	1.35	2.77	2.66	84	0.76	0.74	1.67	1.68
36	1.06	1.34	2.74	2.62	85	0.75	0.73	1.65	1.67
37	1.04	1.32	2.71	2.59	86	0.75	0.72	1.64	1.66
38	1.03	1.30	2.69	2.56	87	0.74	0.71	1.62	1.64
39	1.02	1.29	2.66	2.52	88	0.74	0.70	1.60	1.63
40	1.01	1.27	2.63	2.49	89	0.73	0.69	1.59	1.62
41	1.01	1.26	2.60	2.47	90	0.73	0.69	1.57	1.61
42	1.00	1.24	2.58	2.44	91	0.73	0.68	1.55	1.59
43	0.99	1.23	2.55	2.41	92	0.72	0.67	1.54	1.58
44	0.98	1.21	2.52	2.38	93	0.72	0.66	1.52	1.57
45	0.97	1.20	2.50	2.36	94	0.71	0.65	1.51	1.56
46	0.97	1.18	2.47	2.33	95	0.71	0.65	1.49	1.55
47	0.96	1.17	2.45	2.31	96	0.70	0.64	1.48	1.53
48	0.95	1.15	2.42	2.29	97	0.70	0.63	1.46	1.52
49	0.94	1.14	2.40	2.26	98	0.70	0.62	1.45	1.51
50	0.94	1.12	2.37	2.24	99	0.69	0.61	1.43	1.50
					100	0.69	0.61	1.42	1.49

Table 43: Average relative standard deviation of the mean for carpet MAR-995-FRB series

Measure.	MAR-995-FRB RSDM				Measure.	MAR-995-FRB RSDM			
Number	00RB	25RB	50RB	100RB	Number	00RB	25RB	50RB	100RB
2	3.98	4.83	10.13	5.51	51	1.06	1.13	3.84	1.13
3	3.17	4.20	8.37	4.44	52	1.05	1.12	3.80	1.11
4	2.65	3.70	7.35	3.69	53	1.04	1.11	3.76	1.10
5	2.30	3.30	6.74	3.16	54	1.03	1.09	3.73	1.08
6	2.07	2.98	6.38	2.79	55	1.02	1.08	3.69	1.07
7	1.92	2.72	6.14	2.52	56	1.01	1.07	3.66	1.06
8	1.81	2.52	5.99	2.32	57	1.00	1.06	3.62	1.04
9	1.74	2.35	5.87	2.18	58	0.99	1.05	3.58	1.03
10	1.69	2.22	5.78	2.08	59	0.98	1.03	3.55	1.02
11	1.65	2.11	5.71	1.99	60	0.97	1.02	3.51	1.01
12	1.62	2.02	5.64	1.93	61	0.96	1.01	3.48	0.99
13	1.59	1.94	5.58	1.88	62	0.95	1.00	3.45	0.98
14	1.57	1.88	5.53	1.84	63	0.94	0.99	3.41	0.97
15	1.55	1.83	5.47	1.80	64	0.93	0.98	3.38	0.96
16	1.53	1.78	5.42	1.77	65	0.92	0.97	3.35	0.94
17	1.51	1.74	5.36	1.74	66	0.91	0.96	3.31	0.93
18	1.50	1.70	5.31	1.72	67	0.90	0.95	3.28	0.92
19	1.48	1.67	5.26	1.69	68	0.89	0.93	3.25	0.91
20	1.46	1.64	5.21	1.67	69	0.88	0.92	3.22	0.90
21	1.45	1.62	5.15	1.65	70	0.87	0.91	3.19	0.89
22	1.43	1.59	5.10	1.63	71	0.87	0.90	3.15	0.88
23	1.42	1.57	5.05	1.60	72	0.86	0.89	3.12	0.86
24	1.40	1.55	5.00	1.58	73	0.85	0.88	3.09	0.85
25	1.39	1.53	4.96	1.56	74	0.84	0.87	3.06	0.84
26	1.38	1.51	4.91	1.54	75	0.83	0.86	3.03	0.83
27	1.36	1.49	4.86	1.52	76	0.82	0.85	3.00	0.82
28	1.35	1.47	4.81	1.51	77	0.81	0.84	2.97	0.81
29	1.33	1.46	4.76	1.49	78	0.81	0.84	2.94	0.80
30	1.32	1.44	4.72	1.47	79	0.80	0.83	2.92	0.79
31	1.31	1.42	4.67	1.45	80	0.79	0.82	2.89	0.78
32	1.29	1.41	4.63	1.43	81	0.78	0.81	2.86	0.77
33	1.28	1.39	4.58	1.41	82	0.77	0.80	2.83	0.76
34	1.27	1.37	4.54	1.40	83	0.76	0.79	2.80	0.75
35	1.25	1.36	4.49	1.38	84	0.76	0.78	2.78	0.74
36	1.24	1.34	4.45	1.36	85	0.75	0.77	2.75	0.73
37	1.23	1.33	4.40	1.34	86	0.74	0.76	2.72	0.73
38	1.22	1.31	4.36	1.33	87	0.73	0.75	2.70	0.72
39	1.20	1.30	4.32	1.31	88	0.73	0.75	2.67	0.71
40	1.19	1.28	4.28	1.29	89	0.72	0.74	2.64	0.70
41	1.18	1.27	4.24	1.28	90	0.71	0.73	2.62	0.69
42	1.17	1.25	4.19	1.26	91	0.70	0.72	2.59	0.68
43	1.15	1.24	4.15	1.25	92	0.70	0.71	2.57	0.67
44	1.14	1.23	4.11	1.23	93	0.69	0.71	2.54	0.66
45	1.13	1.21	4.07	1.21	94	0.68	0.70	2.52	0.66
46	1.12	1.20	4.03	1.20	95	0.68	0.69	2.49	0.65
47	1.11	1.18	3.99	1.18	96	0.67	0.68	2.47	0.64
48	1.10	1.17	3.95	1.17	97	0.66	0.67	2.44	0.63
49	1.09	1.16	3.92	1.16	98	0.66	0.67	2.42	0.62
50	1.07	1.15	3.88	1.14	99	0.65	0.66	2.40	0.62
					100	0.64	0.65	2.37	0.61

Table 44: Average relative standard deviation of the mean for carpet MAR-995-LPB series

Measure.	MAR-995-LPB RSDM				Measure.	MAR-995-LPB RSDM			
Number	00RB	25RB	50RB	100RB	Number	00RB	25RB	50RB	100RB
2	3.31	2.74	8.61	8.29	51	0.99	0.96	2.82	3.91
3	3.12	2.61	8.26	8.09	52	0.98	0.96	2.79	3.88
4	2.95	2.48	7.93	7.89	53	0.97	0.95	2.77	3.84
5	2.79	2.37	7.62	7.70	54	0.96	0.94	2.75	3.81
6	2.65	2.26	7.33	7.52	55	0.95	0.93	2.73	3.78
7	2.52	2.16	7.06	7.35	56	0.95	0.93	2.71	3.74
8	2.40	2.08	6.80	7.19	57	0.94	0.92	2.69	3.71
9	2.29	2.00	6.56	7.03	58	0.93	0.91	2.67	3.68
10	2.19	1.92	6.33	6.88	59	0.92	0.91	2.65	3.65
11	2.10	1.85	6.12	6.74	60	0.91	0.90	2.63	3.62
12	2.02	1.79	5.91	6.60	61	0.91	0.89	2.61	3.59
13	1.95	1.73	5.72	6.47	62	0.90	0.89	2.60	3.56
14	1.88	1.68	5.54	6.35	63	0.89	0.88	2.58	3.54
15	1.81	1.63	5.37	6.23	64	0.88	0.87	2.57	3.51
16	1.75	1.58	5.21	6.11	65	0.88	0.87	2.55	3.48
17	1.70	1.54	5.06	6.00	66	0.87	0.86	2.54	3.46
18	1.65	1.50	4.92	5.90	67	0.86	0.86	2.52	3.43
19	1.60	1.46	4.78	5.79	68	0.85	0.85	2.51	3.40
20	1.56	1.43	4.66	5.70	69	0.85	0.84	2.50	3.38
21	1.52	1.40	4.54	5.60	70	0.84	0.84	2.48	3.35
22	1.48	1.37	4.42	5.52	71	0.83	0.83	2.47	3.33
23	1.45	1.34	4.32	5.43	72	0.83	0.83	2.46	3.30
24	1.42	1.32	4.22	5.35	73	0.82	0.82	2.45	3.28
25	1.39	1.29	4.12	5.27	74	0.81	0.81	2.43	3.26
26	1.36	1.27	4.03	5.19	75	0.81	0.81	2.42	3.23
27	1.34	1.25	3.95	5.12	76	0.80	0.80	2.41	3.21
28	1.31	1.23	3.87	5.05	77	0.79	0.80	2.40	3.19
29	1.29	1.21	3.79	4.98	78	0.79	0.79	2.39	3.16
30	1.27	1.19	3.72	4.91	79	0.78	0.79	2.38	3.14
31	1.25	1.18	3.65	4.85	80	0.77	0.78	2.37	3.12
32	1.23	1.16	3.58	4.79	81	0.77	0.78	2.36	3.10
33	1.21	1.15	3.52	4.73	82	0.76	0.77	2.35	3.08
34	1.19	1.13	3.46	4.67	83	0.76	0.77	2.34	3.06
35	1.18	1.12	3.41	4.61	84	0.75	0.76	2.33	3.03
36	1.16	1.11	3.36	4.56	85	0.74	0.76	2.32	3.01
37	1.15	1.10	3.31	4.51	86	0.74	0.75	2.31	2.99
38	1.13	1.08	3.26	4.46	87	0.73	0.75	2.30	2.97
39	1.12	1.07	3.22	4.41	88	0.73	0.74	2.29	2.95
40	1.11	1.06	3.17	4.36	89	0.72	0.74	2.29	2.93
41	1.09	1.05	3.13	4.31	90	0.72	0.73	2.28	2.91
42	1.08	1.04	3.09	4.27	91	0.71	0.73	2.27	2.89
43	1.07	1.03	3.06	4.22	92	0.70	0.72	2.26	2.87
44	1.06	1.02	3.02	4.18	93	0.70	0.72	2.25	2.86
45	1.05	1.01	2.99	4.14	94	0.69	0.71	2.24	2.84
46	1.04	1.00	2.96	4.10	95	0.69	0.71	2.24	2.82
47	1.03	1.00	2.93	4.06	96	0.68	0.70	2.23	2.80
48	1.02	0.99	2.90	4.02	97	0.68	0.70	2.22	2.78
49	1.01	0.98	2.87	3.98	98	0.67	0.69	2.21	2.76
50	1.00	0.97	2.84	3.95	99	0.67	0.69	2.20	2.74
					100	0.66	0.68	2.20	2.73

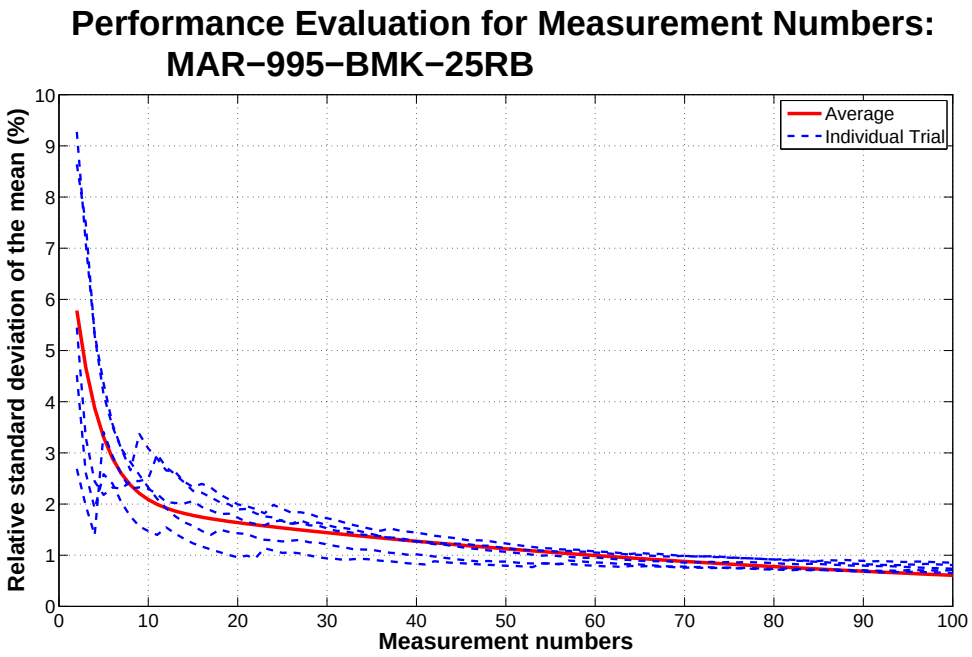

Figure 71: Measurement numbers and measurement accuracy analysis for carpet MAR-995-BMK series with 25ppm Rb

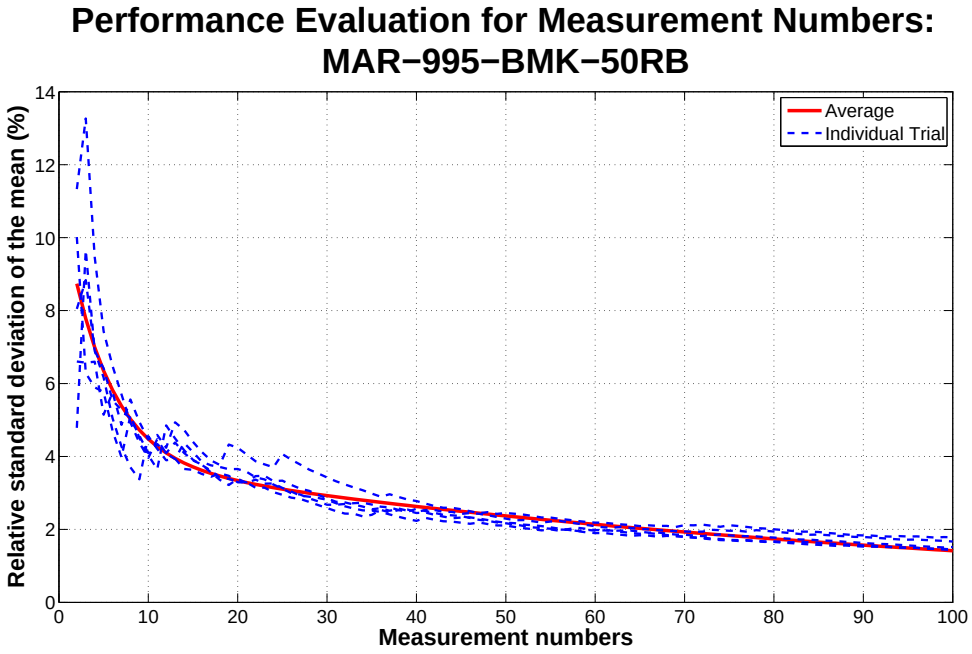

Figure 72: Measurement numbers and measurement accuracy analysis for carpet MAR-995-BMK series with 50ppm Rb

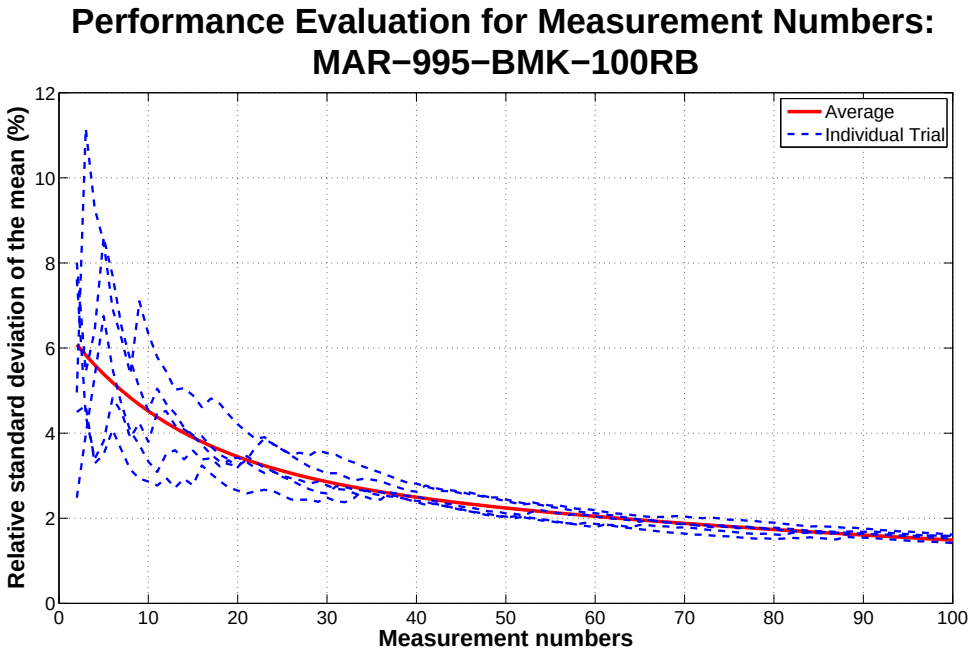

Figure 73: Measurement numbers and measurement accuracy analysis for carpet MAR-995-BMK series with 100ppm Rb

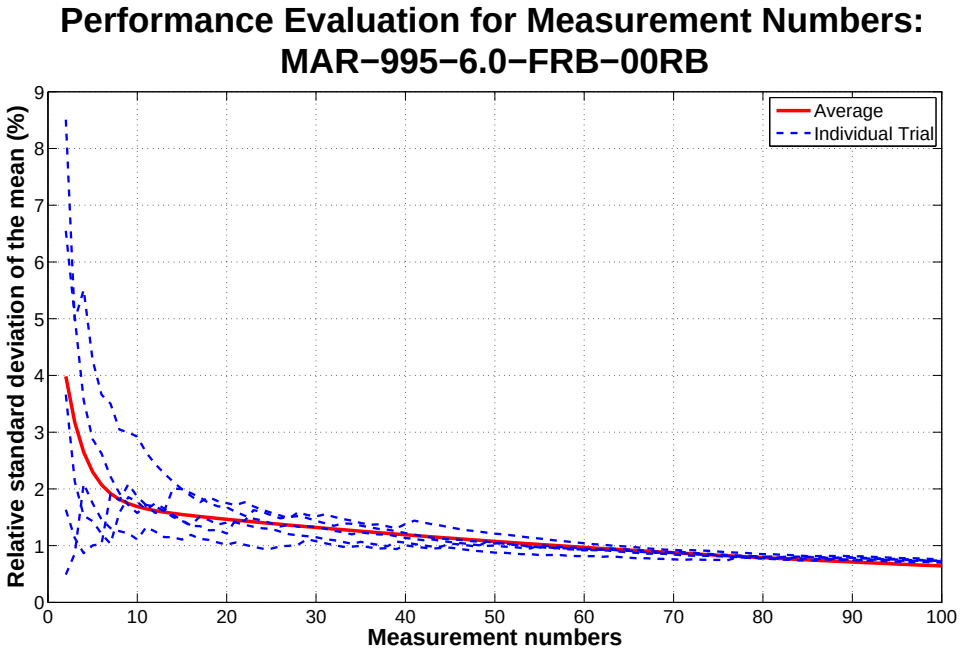

Figure 74: Measurement numbers and measurement accuracy analysis for carpet MAR-995-6.0-FRB with no taggant

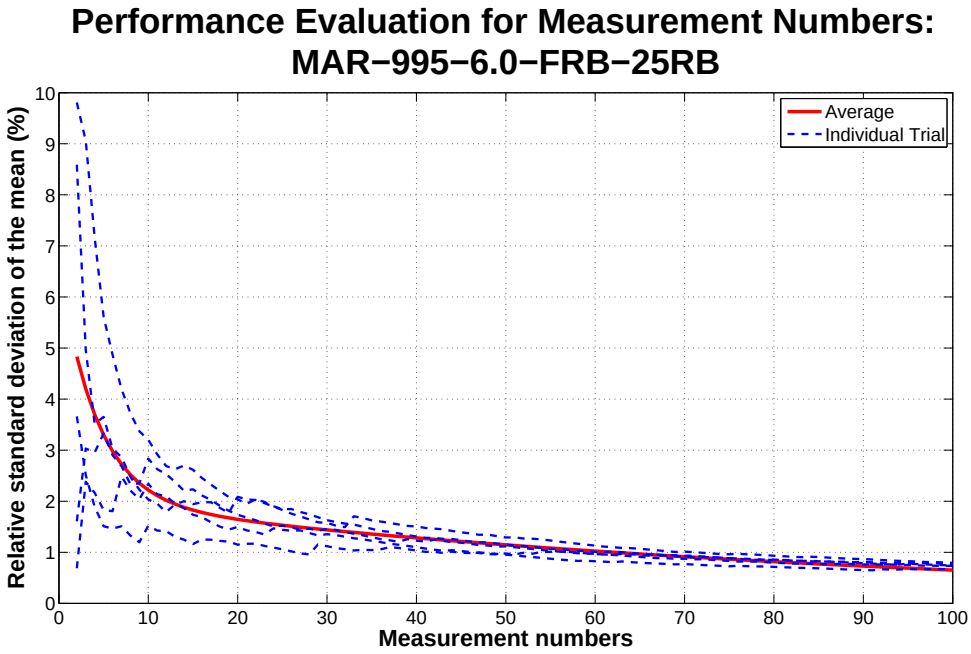

Figure 75: Measurement numbers and measurement accuracy analysis for carpet MAR-995-6.0-FRB with 25ppm Rb

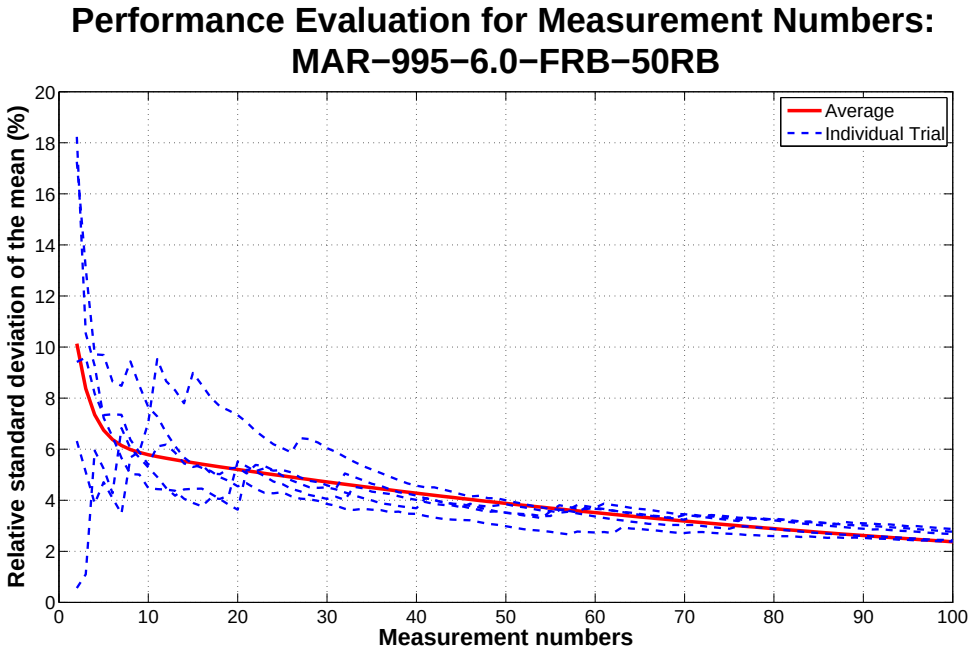

Figure 76: Measurement numbers and measurement accuracy analysis for carpet MAR-995-6.0-FRB with 50ppm Rb

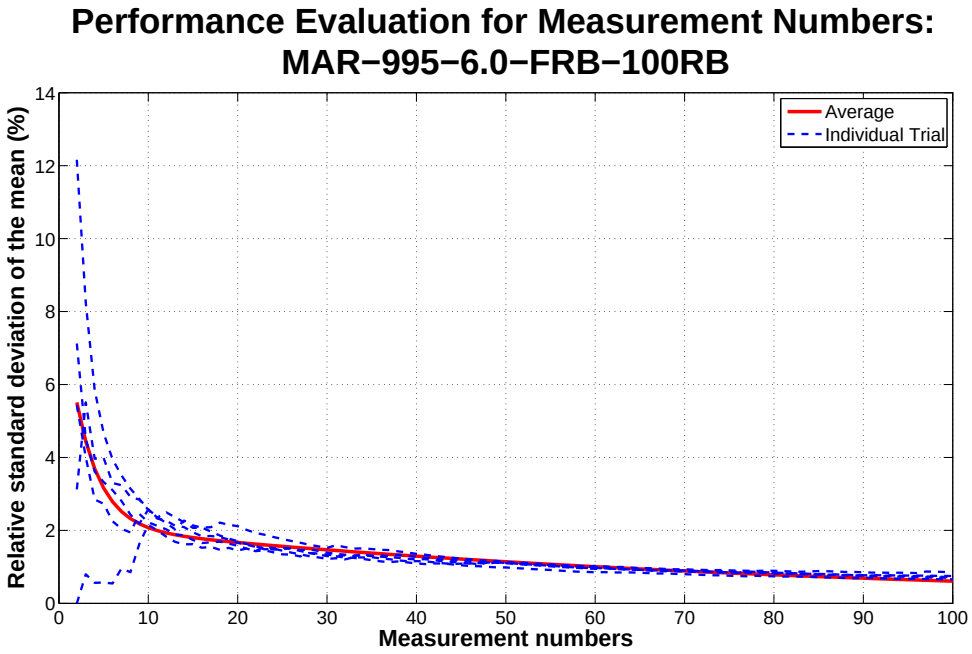

Figure 77: Measurement numbers and measurement accuracy analysis for carpet MAR-995-6.0-FRB with 100ppm Rb

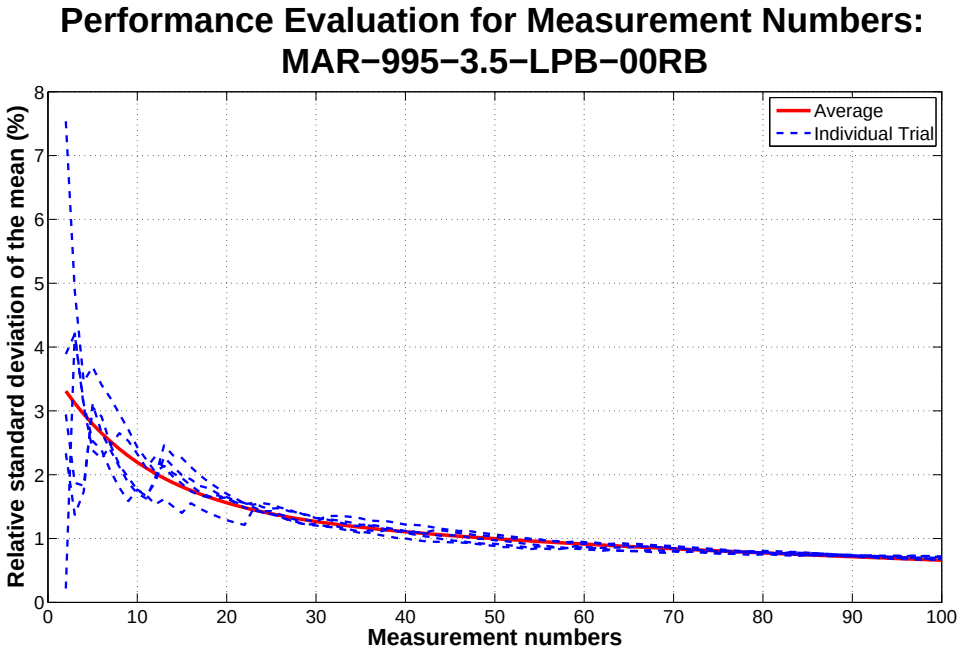

Figure 78: Measurement numbers and measurement accuracy analysis for carpet MAR-995-3.5-LPB with no taggant

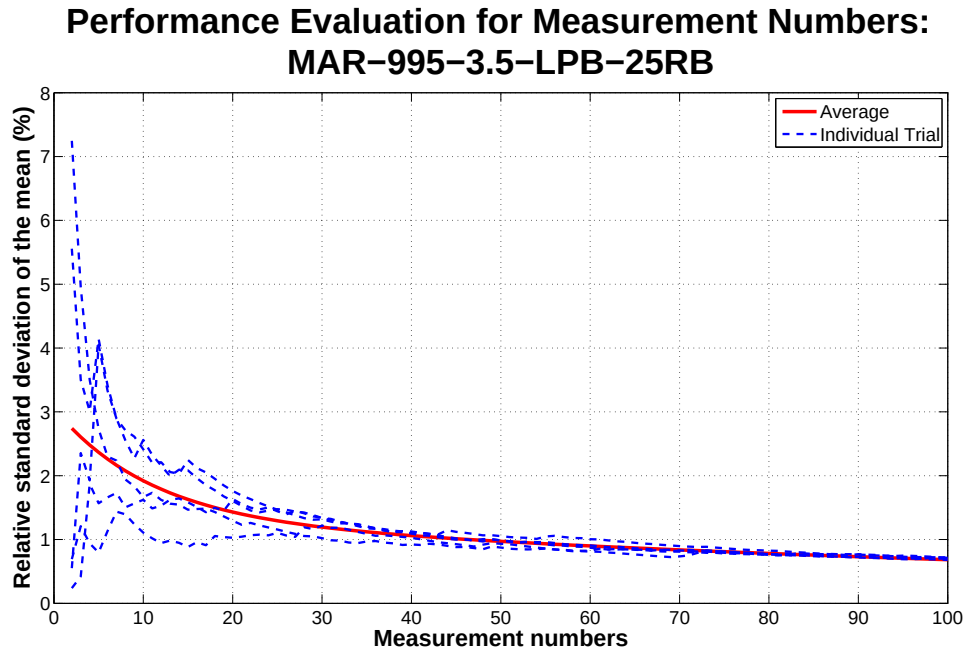

Figure 79: Measurement numbers and measurement accuracy analysis for carpet MAR-995-3.5-LPB with 25ppm Rb

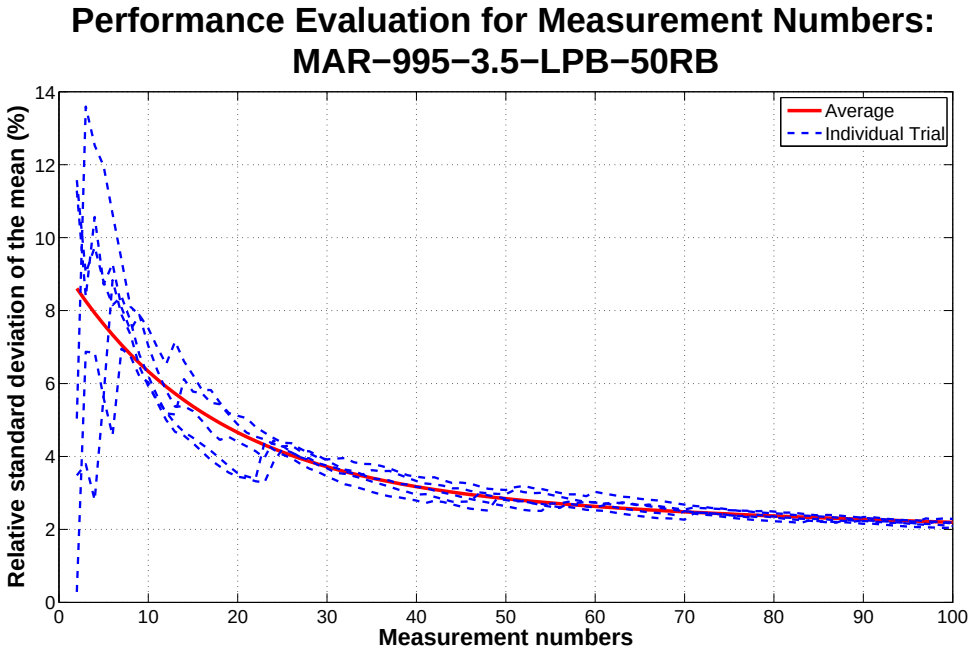

Figure 80: Measurement numbers and measurement accuracy analysis for carpet MAR-995-3.5-LPB with 50ppm Rb

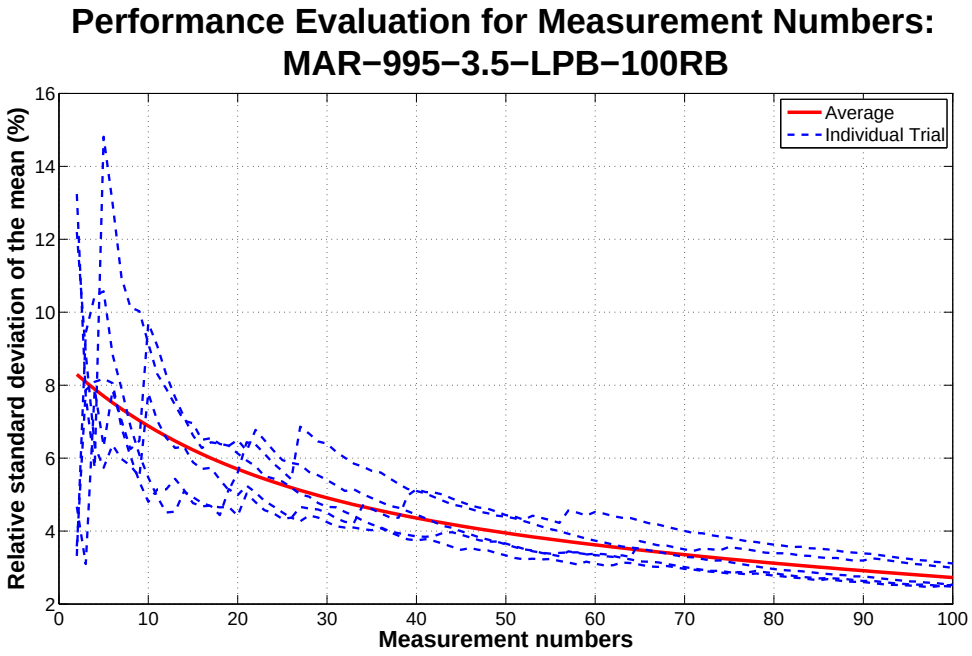

Figure 81: Measurement numbers and measurement accuracy analysis for carpet MAR-995-3.5-LPB with 100ppm Rb

APPENDIX C

PERFORMANCE EVALUATION: CONTINUOUS SCANS

Section 3.1.2 introduces two types of XRF measurement scanning methods, stationary and continuous. The stationary scanning method acquires XRF measurements at specific locations while the instrument is held stationary during the measurement at each position. This method provides a mean to obtain fluorochemical concentrations at a specific locations on the carpet sample, but does not provide XRF measurements between the discrete measurement positions. An important assumption made in the stationary scanning process is that the XRF measurement locations selected for this scanning process should represent the best and the worst possible locations for the fluorochemical concentration, i.e. that all possible variations from the nozzle spray pattern are represented by the choice of measurement locations.

For continuous scanning method, the XRF instrument is continuously moved across the carpet sample during the measurement process. This method offers the possibility of obtaining the average fluorochemical concentration for the entire cross section of a carpet sample. Ideally, the continuous scanning method requires that the XRF instrument reports real-time count rates per unit time rather than the total XRF counts within the measurement period. However, due to the limitation of the data collection capability of the portable EDXRF instruments, only the total counts are available. This chapter investigates the accuracy and the compatibility of the scanning approach compared to the stationary approach.

The first set of experiments investigated the effect of scanning speed on the XRF measurements. Three carpet types were used, BMK, FRB, and LPB, and each was tagged with 50 ppm of Rb. Each carpet sample was approximately 200 cm wide

by 100 cm long. The XRF instrument was moved at seven constant speeds ranging from 0 cm/s, i.e., stationary, to a relatively fast speed of 3 cm/s. The direction was across the width dimension of each carpet sample, and the duration for each measurement was 30 seconds. Ten measurements were collected for each speed set. For the stationary position measurements, 0 cm/s, ten measurements were acquired from ten successive locations on the same path as the continuous scan with 10 cm between each location. The average Rb peak counts and their corresponding relative standard deviations were calculated and are listed in Table 45.

Table 45: XRF measurements from the scanning approach

Speed	MAR-995-BMK		MAR-995-6.0-FRB		MAR-995-3.5-LPB	
(cm/s)	Average	RSD	Average	RSD	Average	RSD
0.0	446	9.5	386	10.2	179	8.6
0.5	429	9.6	395	10.9	176	10.1
1.0	431	8.8	397	11.0	165	10.2
1.5	452	9.6	382	10.2	142	10.0
2.0	421	9.4	327	11.6	147	9.6
2.5	387	9.3	243	15.5	89	10.7
3.0	167	10.5	115	12.8	N/A	N/A

Results from Table 45 show that average Rb intensity counts collected when the scanner is moving at speeds less than or equal to 1.5 cm/s are within 20 counts of the stationary scanning method (0 cm/s). For scanning speeds greater or equal to 1.5 cm/s, a significant decrease in the average Rb intensity counts can be observed. The overall decline in average intensity counts with the increase of the scanner speed results from the fact that some characteristic intensities were not captured by the XRF instrument detector as the instrument was moved across the sample. Additionally, for the FRB carpet, which has the lowest fiber density, scanning speeds more than 3 cm/s resulted in intensity counts that were below the minimum level specified by the safety mechanism of the S1 TRACeR instrument. Thus, the upper limit of the scanning speed was limited to 3 cm/s for the studies reported here.

The second set of experiments investigated the ability of the continuous scanning method to detect any inconsistencies of the fluorochemical distribution across carpet samples. Two carpet samples, tagged with 0 and 50 ppm Rb, from each carpet type, BMK, LPB, and FRB, were selected for this experiment. These are the same samples that were utilized previously and results using the stationary measuring method were reported in Table 18.

The sample pair of each carpet type, i.e., with 0 and 50 ppm Rb, were positioned next to each other and a total scan distance of 30 cm was selected which covered different lengths from each carpet sample as shown in Figure 82. For each length combination, ten 30-second measurements were acquired using S1 TRACeR moving at a speed of 1 cm/s and the average Rb intensity counts along with their corresponding relative standard deviations are listed in Table 46

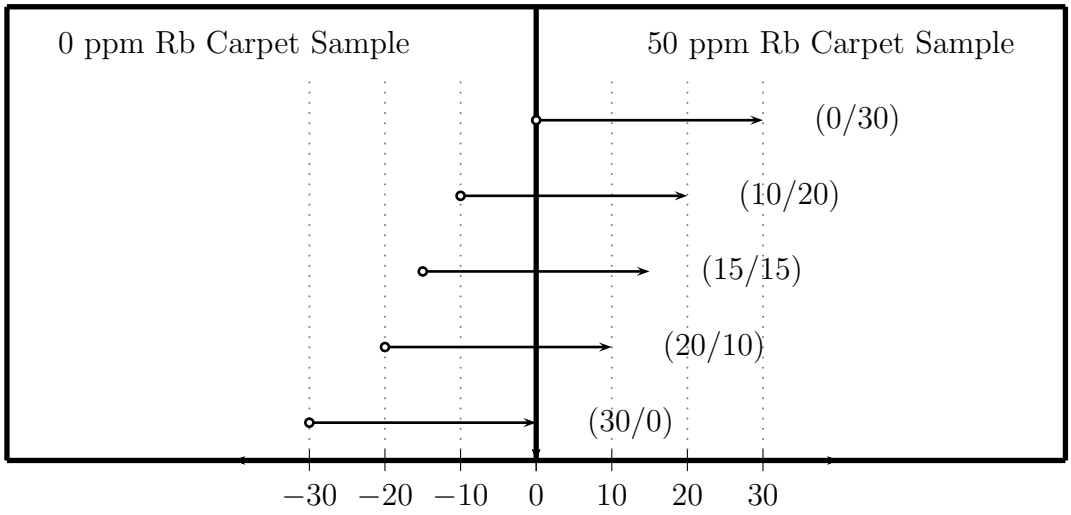

Figure 82: Continuous scanning setup using two carpet samples with different chemical taggant to detect inconsistencies in taggant distribution (Two numbers in the parenthesis correspond to the scanning length for carpet tagged with 0 and 50 ppm of Rb, respectively)

The results in Table 46 show that the average Rb intensity counts are consistent with the average Rb concentration over the entire length where XRF measurements

Table 46: Scanning measurements from carpet pairs with different concentrations

Carpet Set	0ppm	50ppm	Average	RSD
BMK	0	30	446	9.36
	10	20	317	10.23
	15	15	212	9.95
	20	10	152	10.74
	30	0	34	10.06
FRB	0	30	386	9.38
	10	20	246	9.74
	15	15	193	9.25
	20	10	138	10.03
	30	0	22	10.27
LPB	0	30	179	8.39
	10	20	127	8.75
	15	15	91	9.26
	20	10	55	8.01
	30	0	12	9.68

were captured. For example, the Rb intensity counts obtained from scanning across equal distances of the 0 and 50 ppm Rb tagged carpet sample pairs in a single scan were consistently half of the intensity counts obtained from separate scans of the 50 ppm Rb tagged samples of the same type. Additionally, the Rb intensity counts obtained from two other sets of measurements were directly proportional to the distance of the scans across the 50 ppm Rb tagged sample.

Acquiring XRF measurements using the continuous scanning method for on-line analysis requires sufficient measurement time to allow the XRF instrument to slowly move across the entire carpet sample. From measurements reported in this chapter, the fastest speed that the S1 TRACeR instrument can be utilized for this type of measurement without a significant drop in the detected counts is 3 cm/s. At this speed for a typical carpet manufacturing line, i.e., a web width of approximately 400 cm, a time of approximately 2.5 minutes would be required to scan across the entire carpet section.

Additionally, the experiments reported in this appendix also suggested that the continuous scanning method can only provide the overall, average fluorochemical concentration over the measurement path. Thus, the continuous scanning method alone is not appropriate for determining the distribution of fluorochemicals across a carpet sample.

APPENDIX D

FLUOROCHEMICAL DISTRIBUTION ANALYSIS

Fluorochemicals are typically applied to carpets during the manufacturing process using spray nozzles or foam applicators. The spray-on method is used mainly for residential carpets, and this was the method used to prepare samples for this research. A general diagram of a fluorochemical application using a spray system is shown in Figure 83. These systems typically consists of several nozzle spray heads attached to a distribution tube, through which fluorochemicals are supplied. These nozzle spray heads are evenly located across the web of the carpet. To ensure the coverage of the fluorochemicals across carpets during manufacturing process, the spray nozzles are placed so that the coverage areas slightly overlaps from two adjacent nozzles, and this results in a wave pattern of fluorochemical concentration across the carpet as illustrated in the bottom of Figure 83.

In this chapter, a series of experiments are described to investigate the sensitivity of the XRF measurements for measuring the above mentioned wave pattern. To explore the measurement sensitivity to the distribution of fluorochemical concentration, three sets of carpet types with four levels of fluorochemical concentrations were measured for a total of twelve carpet samples. For each carpet sample, a 17×30 measurement grid with a pitch of 5cm between neighboring locations was used. For each location, five XRF measurements were obtained and finally the average Rb peak counts from each location are plotted to show any fluorochemical concentration differences across on the carpet sample.

For the distribution analysis, color maps showing the fluorochemical concentration distribution for each carpet sample are plotted. To generate the distribution color

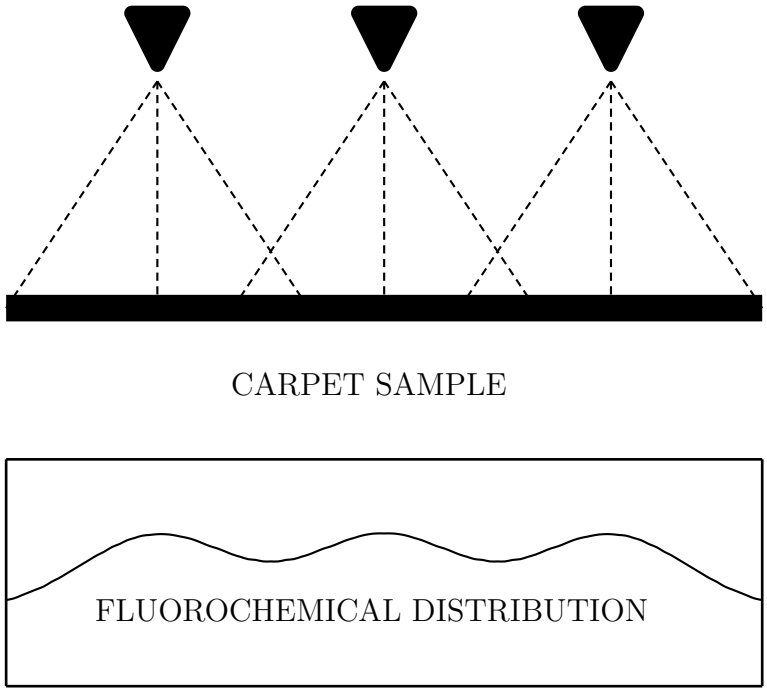

Figure 83: Fluorochemical distribution profile from spray application

map, XRF measurements obtained from all locations on each carpet were processed through the recommended signal processing algorithms listed in Table 9. The overall average from all Rb counts from each carpet served as a population mean for the corresponding carpet sample. These population mean values are then used to perform the Rb calibration and translate the predicted Rb concentration to its equivalent fluorochemical concentration. Then the average of the five measurements acquired at each location in the 17×30 grid is translated to the fluorochemical concentration based on the proper calibration curve and the color map is generated.

The calibration results from the the MAR-995-BMK carpet samples, tagged with Rb concentration levels of 0, 25, 50, and 100ppm, are shown in Table 47. The overall population mean was utilized in this calibration process. Once the calibration was established, the average XRF measurements from each location were then processed and translated to the corresponding fluorochemical concentration values. Finally, the

fluorochemical concentrations from each location within the same carpet samples are plotted as a color map. Results for each these carpet samples are shown in Figures 84 through 87.

Table 47: Calibration results for carpet MAR-995-BMK series

Carpet Name	Actual F Concentration (ppm)	Intensity Count (counts)	Predicted Rb Concentration (ppm)	F Concentration (ppm)	Counting Method
00RB	33	434	7	48	
25RB	110	510	22	85	Raw
50RB	146	661	50	159	Peak
100RB	355	1060	125	352	Count
00RB	33	42	1	31	
25RB	110	184	26	97	Gaussian
50RB	146	338	54	169	Peak
100RB	355	718	123	347	Count

From the distribution map results for all carpet samples in the MAR-995-BMK series, we observed an uneven fluorochemical distribution across the carpet samples. The variation in the fluorochemical concentration increases as the fluorochemical concentration on the carpet sample increases. The blank carpet sample, which contains 33ppm of fluorochemical concentration, has approximately 80ppm in fluorochemical concentration variation. This number increases to approximately a value of 300ppm for the variation in fluorochemical concentration variation for the 100ppm Rb-tagged carpet sample in the same carpet series. In addition, we can discern the fluorochemical distribution pattern. Although the wave pattern was not clearly detected, both sides of the carpet and some area in between show maximum and minimum values of concentration at the same consistent regions on the carpet samples.

The same experimental procedures were repeated for the carpet MAR-995-3.5-LPB and the MAR-995-6.0-FRB series. The population mean for each carpet type were again obtained to calculate the calibration curves for each carpet series. The

overall measurement results for the FRB and LPB series are listed in Tables 48 and 49, respectively. Similarly, the concentration distribution maps for all carpet in these two series were obtained and plotted in Figures 88 through 95. As we can observed from all these distribution maps, locations of the maximum and minimum concentration to those observed from the MAR-995-BMK carpet series are also present in the distribution map for carpets from the FRB and LPB series.

Table 48: Calibration results for carpet MAR-995-FRB series

Carpet Name	Actual F Concentration (ppm)	Intensity Count (counts)	Predicted Rb Concentration (ppm)	F Concentration (ppm)	Counting Method
00RB	34	443	8	39	
25RB	104	487	15	59	Raw
50RB	117	814	71	201	Peak
100RB	347	1040	110	302	Count
00RB	34	43	-2	15	
25RB	104	196	27	88	Gaussian
50RB	117	380	61	175	Peak
100RB	347	692	119	323	Count

The scan results for the LPB carpet type are shown in Figure 92 through 95. Results from the scan of a carpet sample with 50ppm Rb, Figure 94, exhibit some stripping of the data from line to line. This effect was noted but not investigated as to the cause. The LPB carpet type also had the shortest cut pile height of all carpets tested and was the least dense, which made it more sensitive to carpet backing effects and more difficult to test. Note that Figure 92a is a scan of the carpet without any applied taggant, and variations picked up from the carpet backing are detected as two distinct bands on the plot. Figure 92b shows the same data set after signal processing to remove background effects.

These observations lead to the conclusion that XRF measurements from multiple locations are needed to determine the overall fluorochemical distribution across

Table 49: Calibration results for carpet MAR-995-LPB series

Carpet Name	Actual F Concentration (ppm)	Intensity Count (counts)	Predicted Rb Concentration (ppm)	F Concentration (ppm)	Counting Method
00RB	31	256	0	0	
25RB	95	351	43	113	Raw
50RB	135	407	72	187	Peak
100RB	421	563	153	393	Count
00RB	31	29	0	0	
25RB	95	98	34	93	Gaussian
50RB	135	173	73	191	Peak
100RB	421	330	154	396	Count

a carpet. The recommended grid location numbers required to determine the fluorochemical distribution on a carpet sample is $4s + 1$, where s is the number of nozzle spray heads on the manufacturing line. $2s+1$ of these grids should be located directly under each nozzle spray head, at the locations between nozzle spray heads where the spaying paths are overlapped, and locations half way between these two sets of locations. For an actual carpet manufacturing line where there are several nozzle spray heads are installed across the carpet, taking XRF measurements at all locations for fluorochemical distribution analysis is very time consuming and may not possible for on-line measurements.

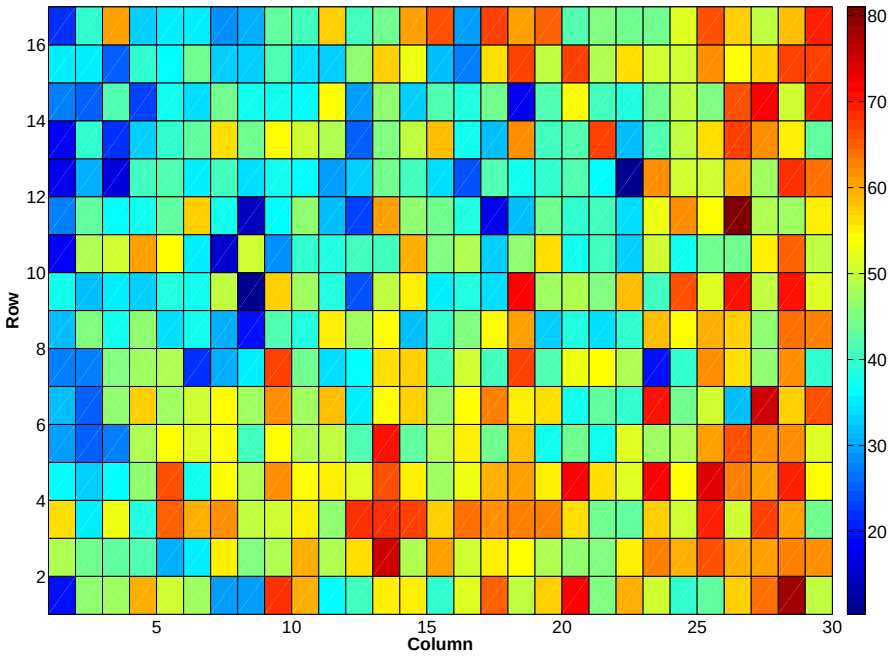

(a) Fluorochemical distribution without signal processing

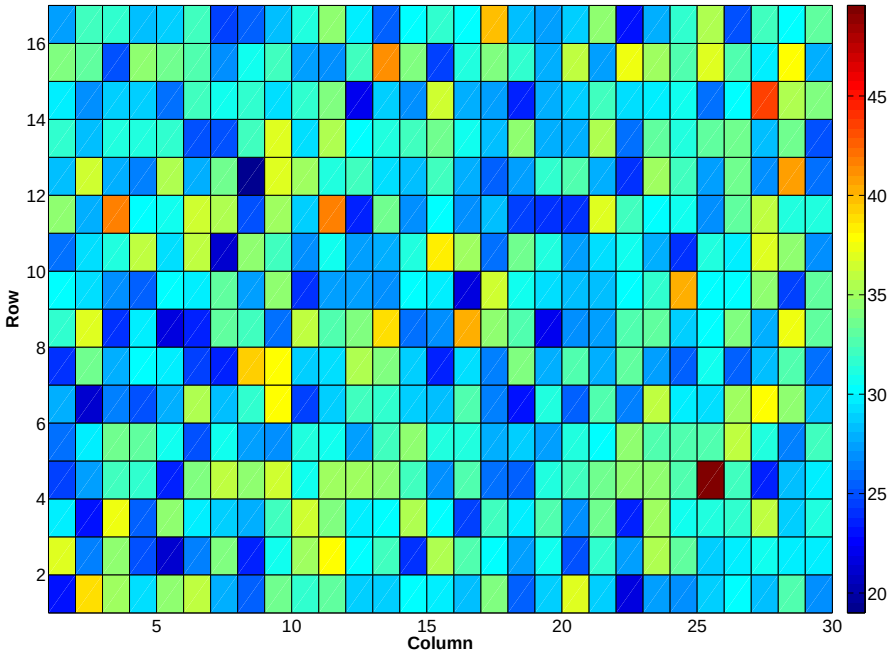

(b) Fluorochemical distribution with signal processing

Figure 84: Fluorochemical distribution profile for carpet MAR-995-BMK series with no taggant

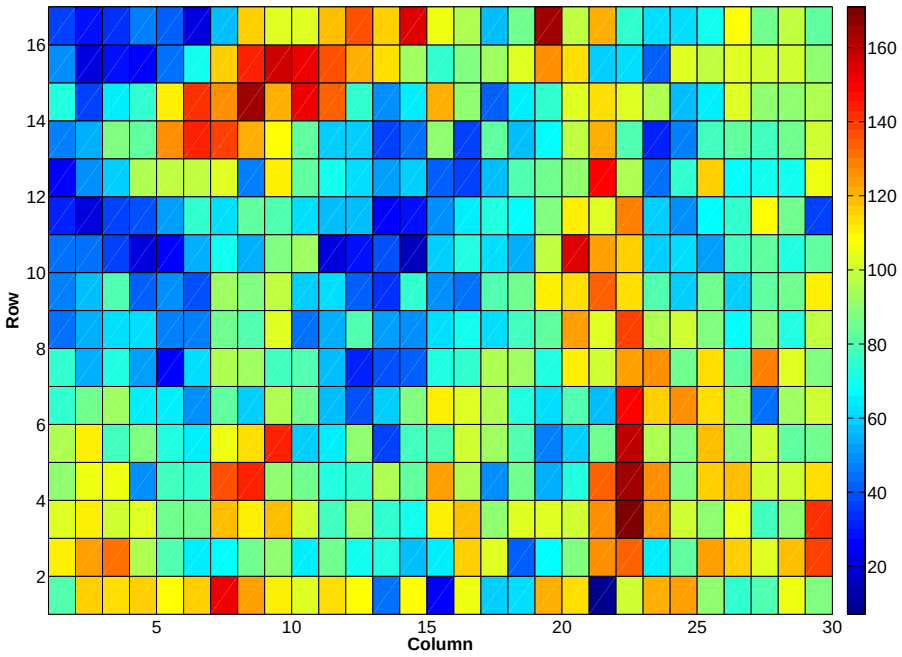

(a) Fluorochemical distribution without signal processing

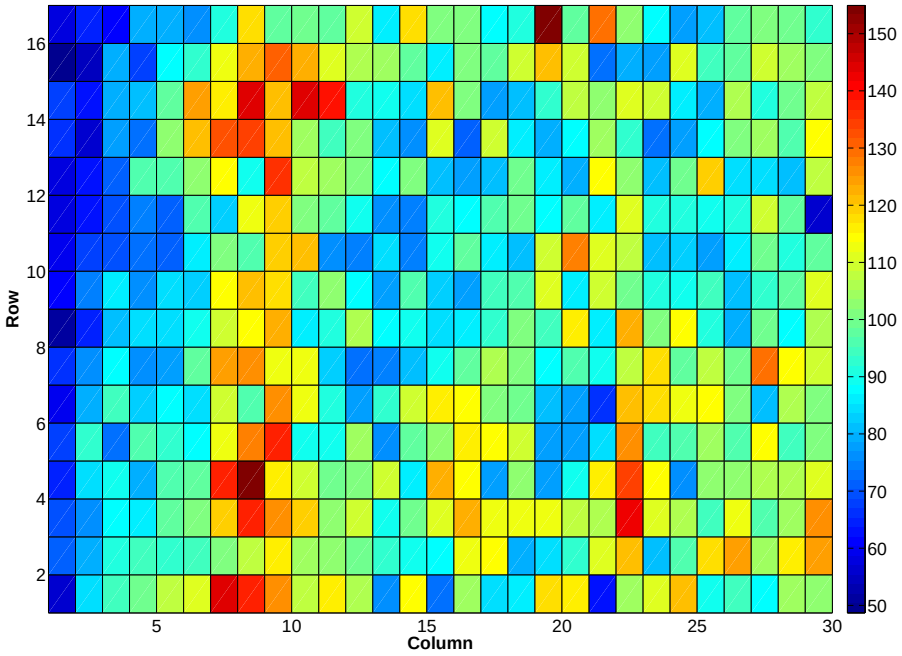

(b) Fluorochemical distribution with signal processing

Figure 85: Fluorochemical distribution profile for carpet MAR-995-BMK series with 25ppm Rb

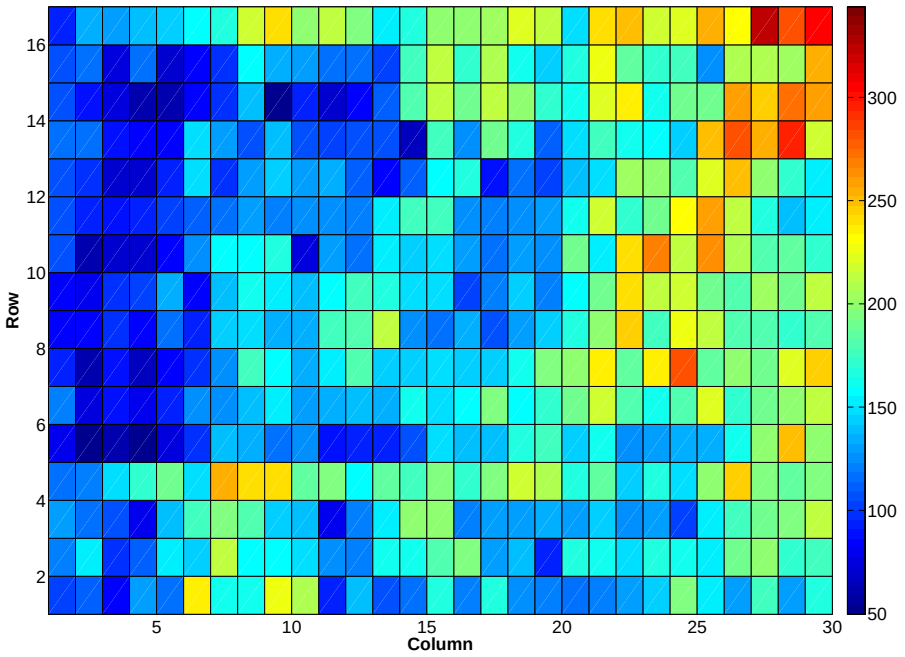

(a) Fluorochemical distribution without signal processing

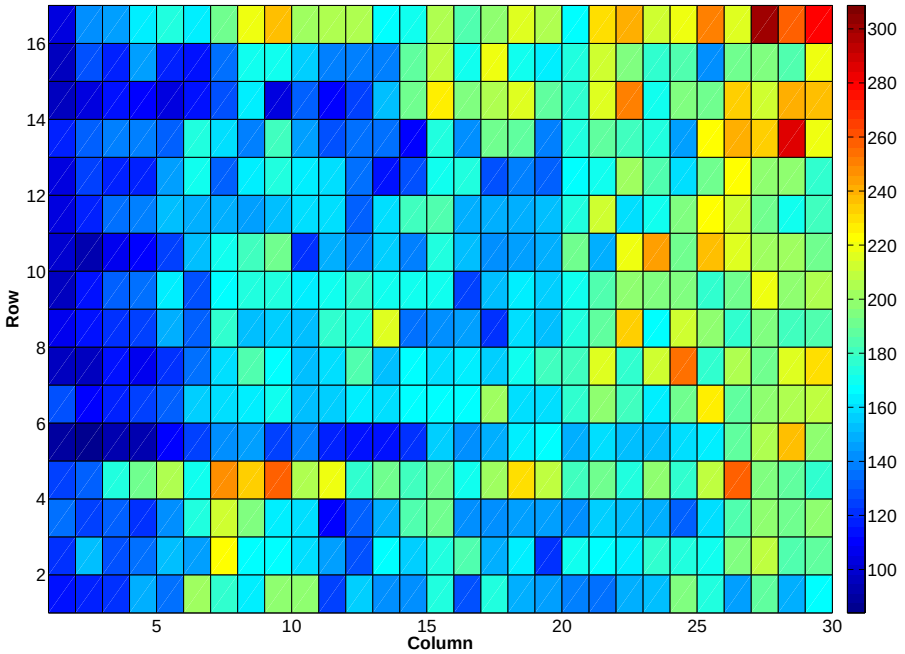

(b) Fluorochemical distribution with signal processing

Figure 86: Fluorochemical distribution profile for carpet MAR-995-BMK series with 50ppm Rb

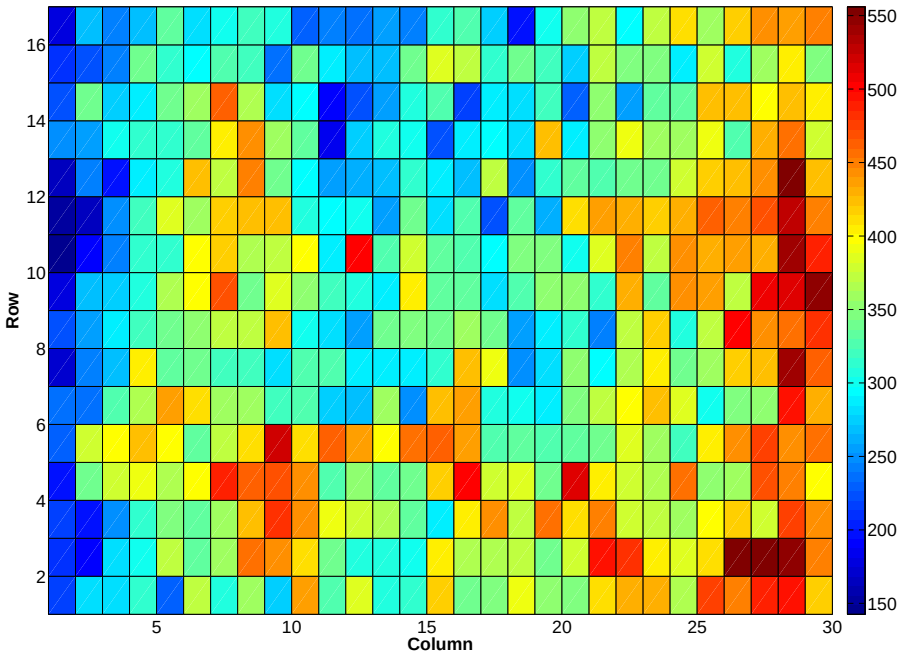

(a) Fluorochemical distribution without signal processing

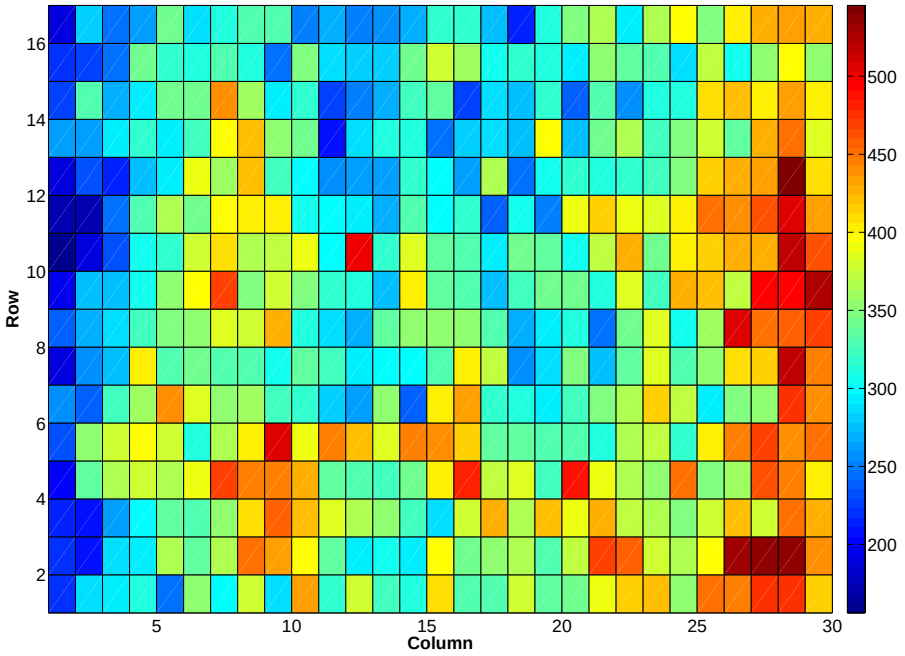

(b) Fluorochemical distribution with signal processing

Figure 87: Fluorochemical distribution profile for carpet MAR-995-BMK series with 100ppm Rb

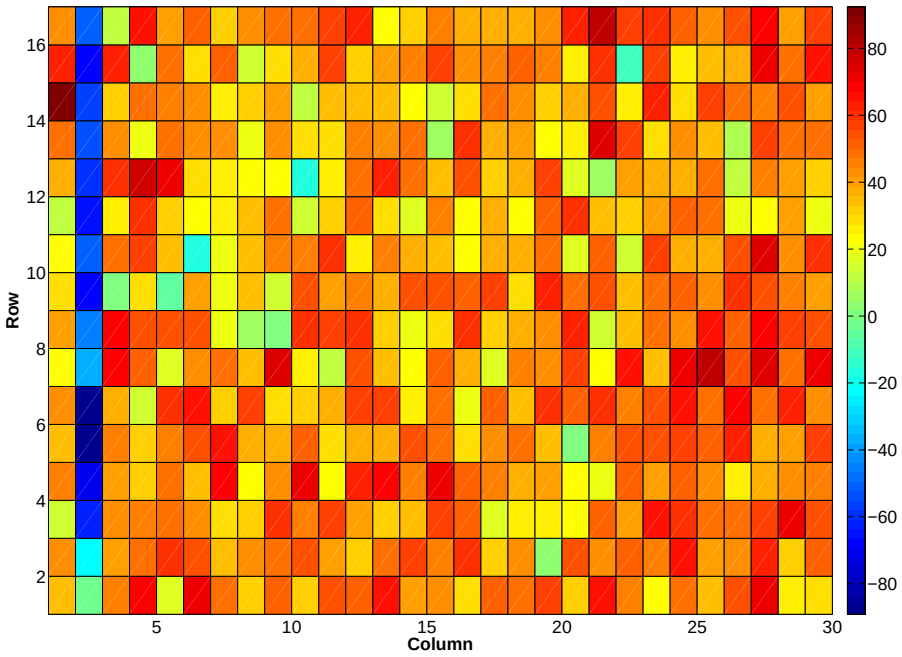

(a) Fluorochemical distribution without signal processing

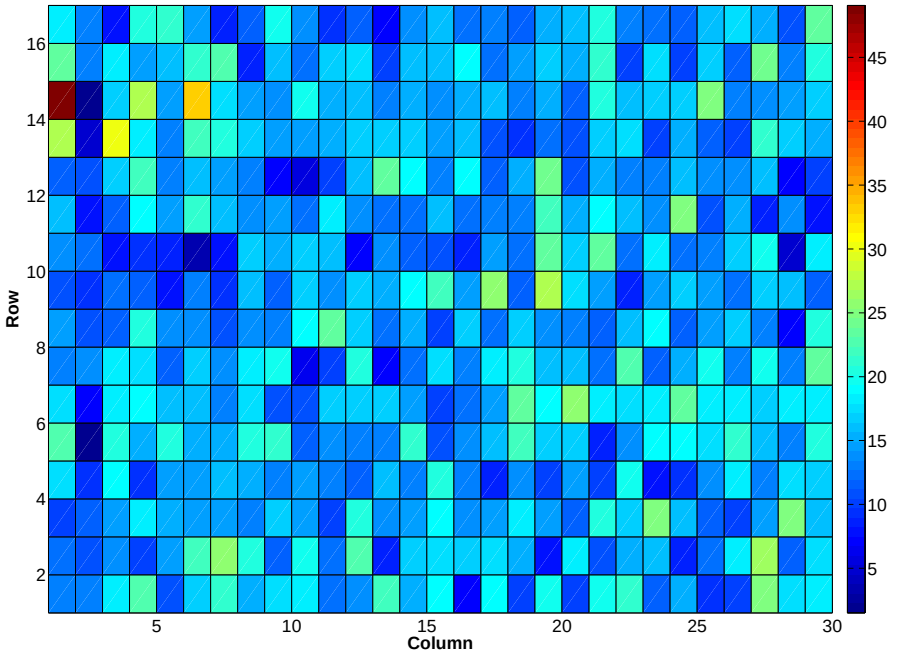

(b) Fluorochemical distribution with signal processing

Figure 88: Fluorochemical distribution profile for carpet MAR-995-3.5-FRB series with no taggant

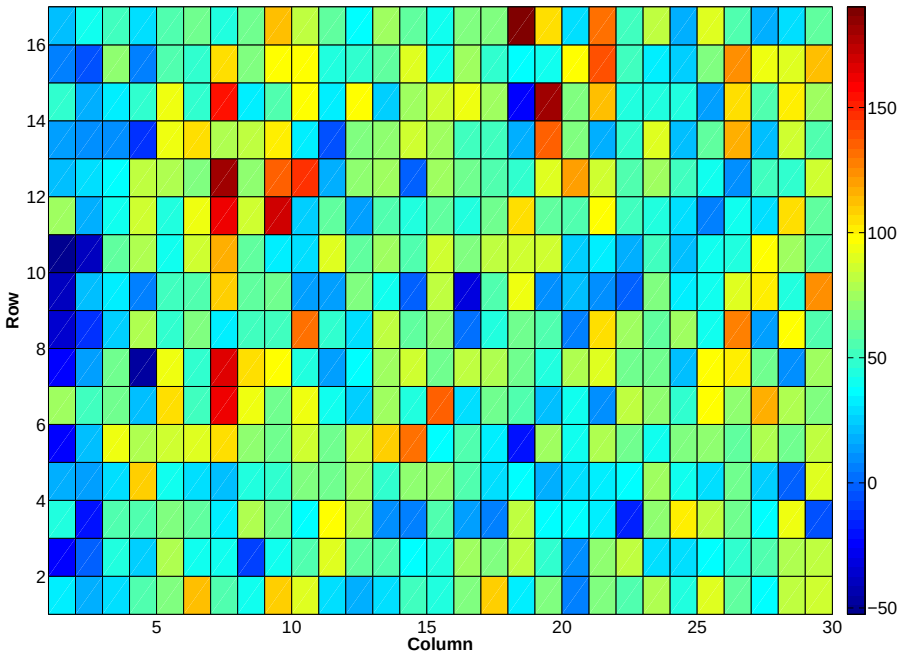

(a) Fluorochemical distribution without signal processing

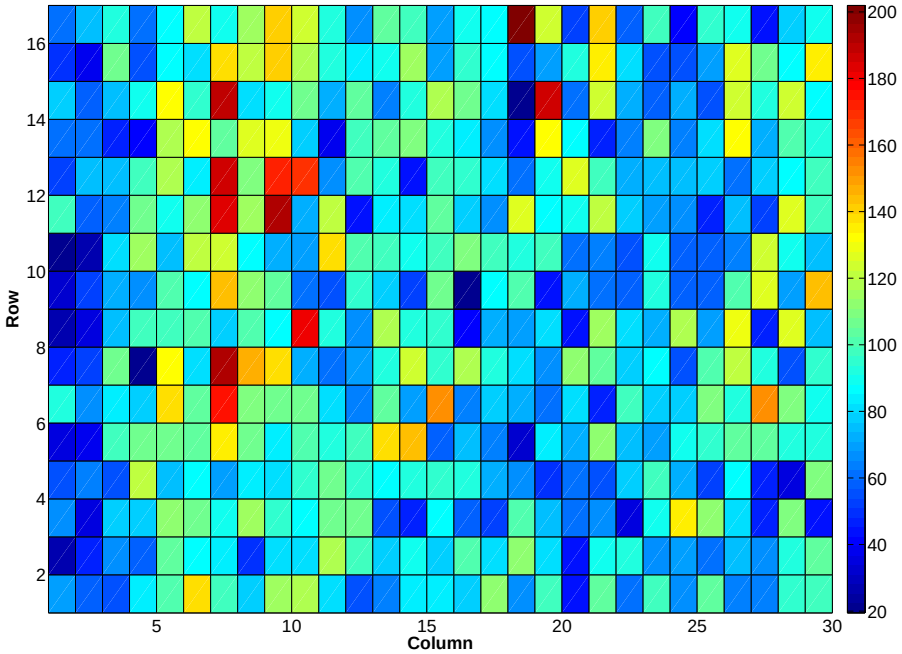

(b) Fluorochemical distribution with signal processing

Figure 89: Fluorochemical distribution profile for carpet MAR-995-3.5-FRB series with 25ppm Rb

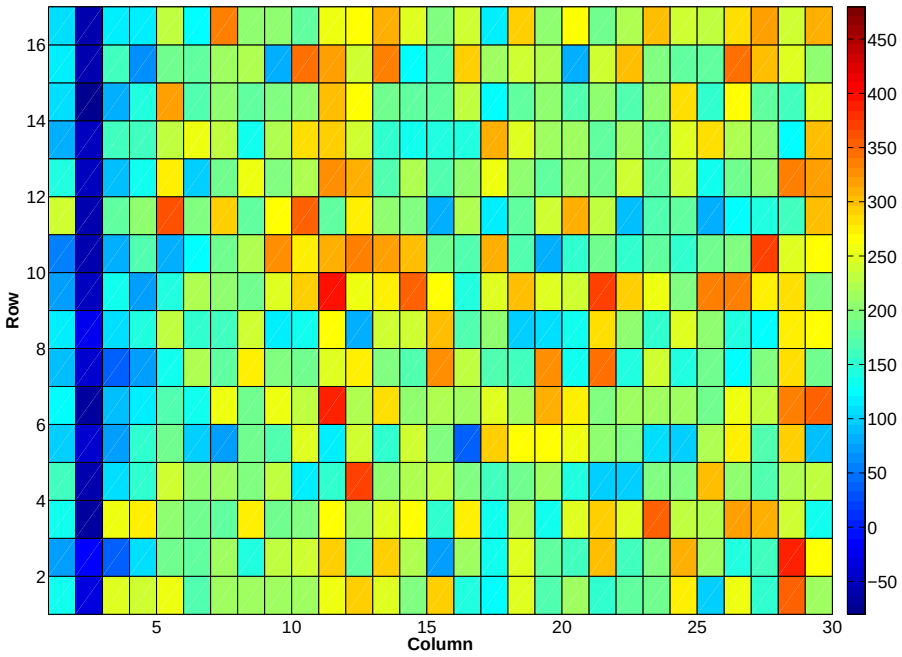

(a) Fluorochemical distribution without signal processing

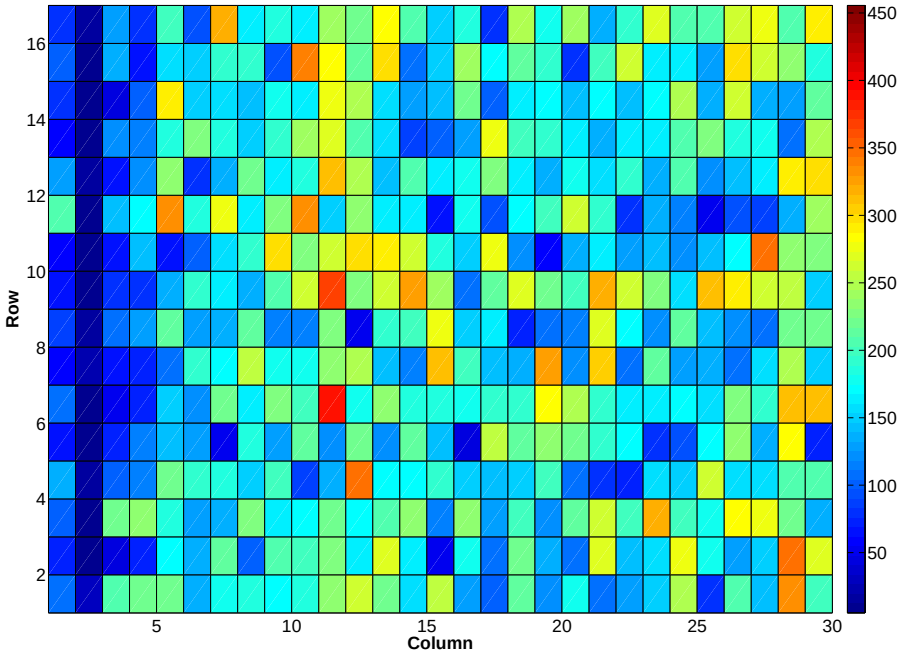

(b) Fluorochemical distribution with signal processing

Figure 90: Fluorochemical distribution profile for carpet MAR-995-3.5-FRB series with 50ppm Rb

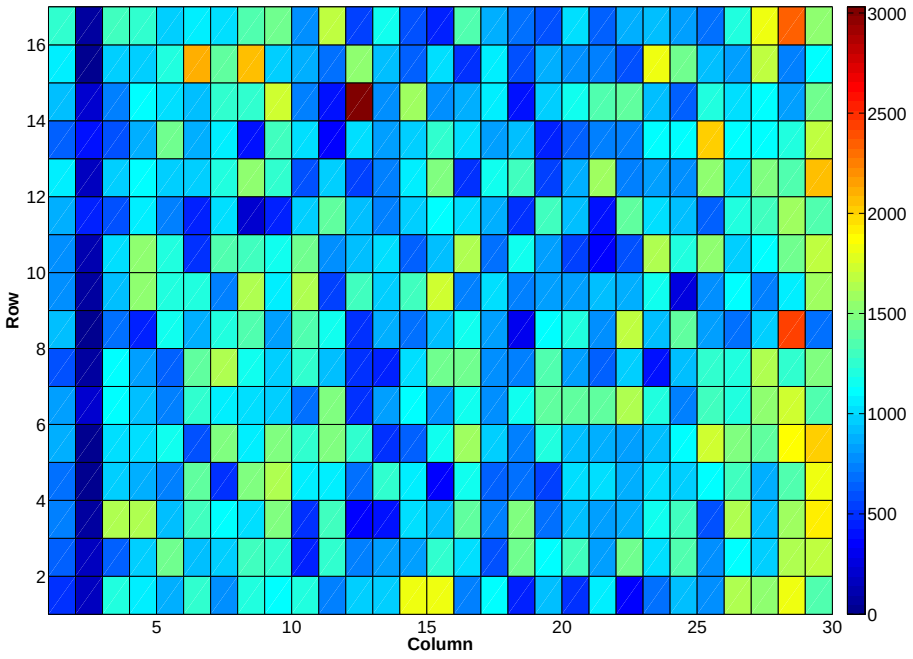

(a) Fluorochemical distribution without signal processing

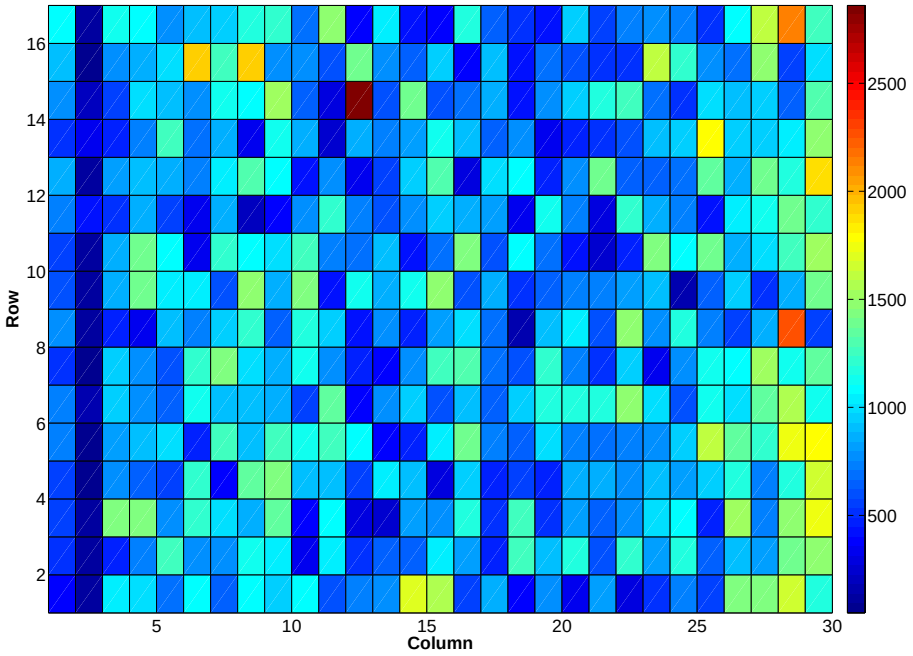

(b) Fluorochemical distribution with signal processing

Figure 91: Fluorochemical distribution profile for carpet MAR-995-3.5-FRB series with 100ppm Rb

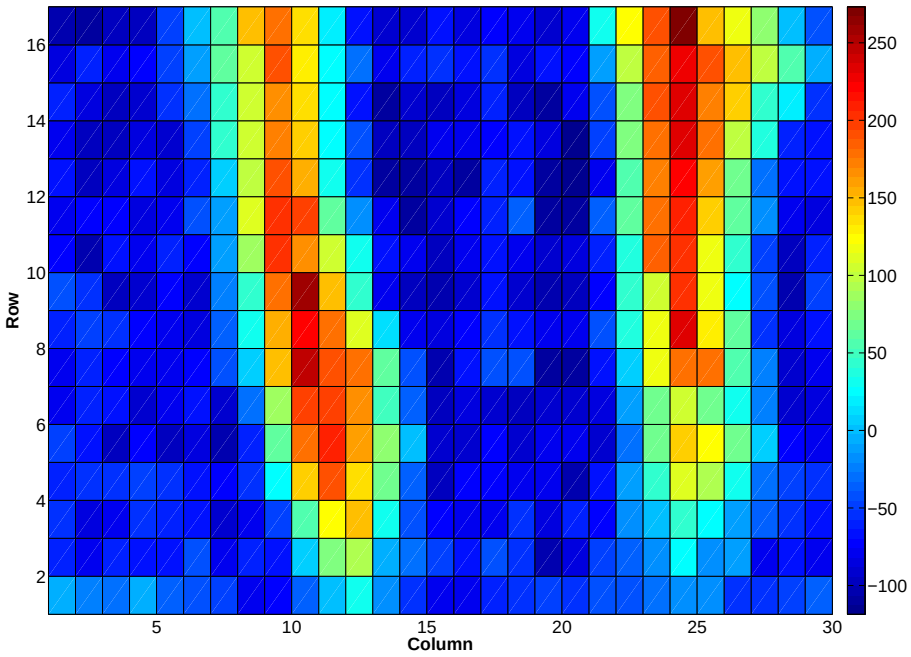

(a) Fluorochemical distribution without signal processing

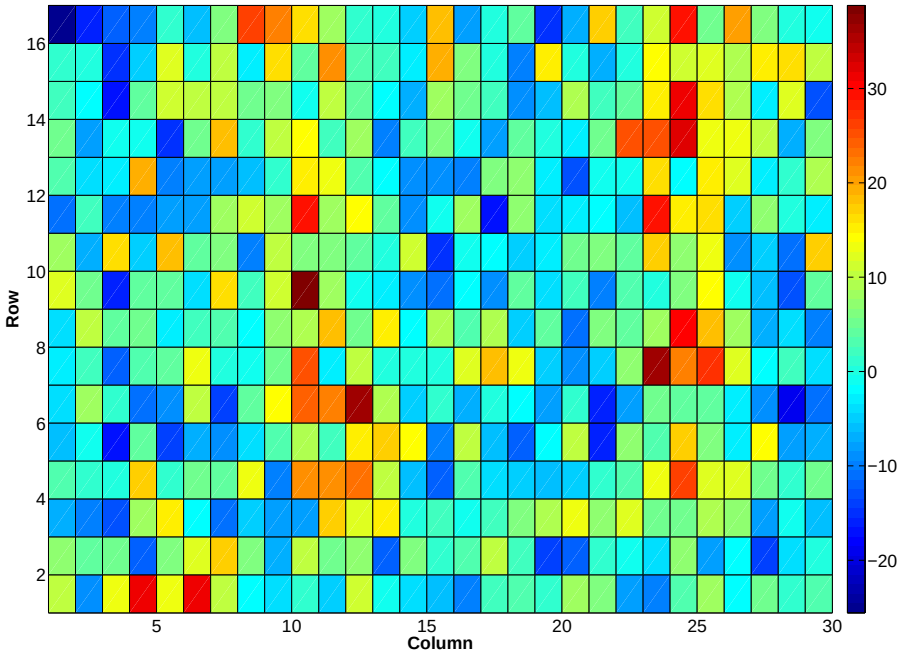

(b) Fluorochemical distribution with signal processing

Figure 92: Fluorochemical distribution profile for carpet MAR-995-6.0-LPB series with no taggant

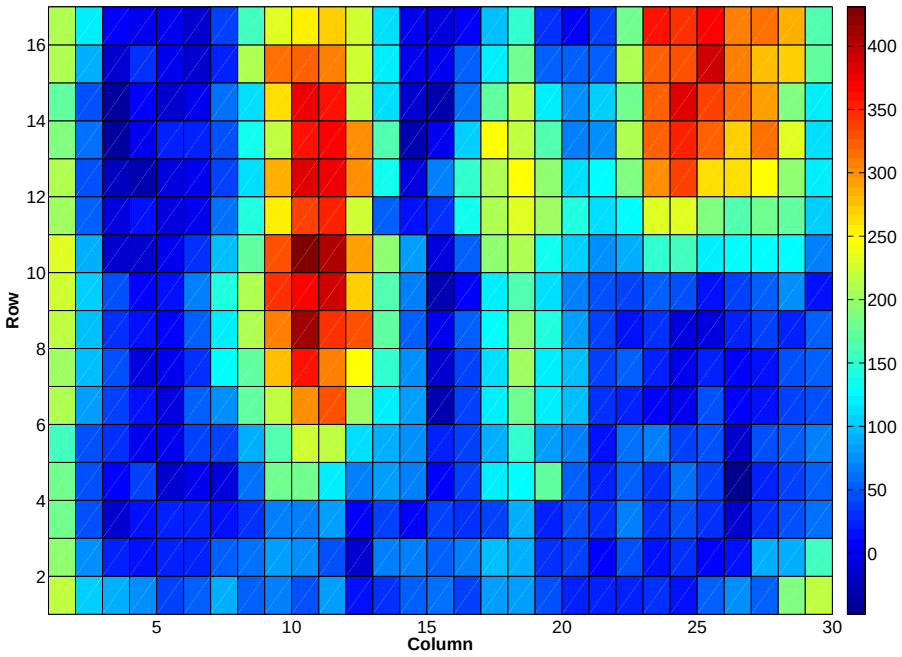

(a) Fluorochemical distribution without signal processing

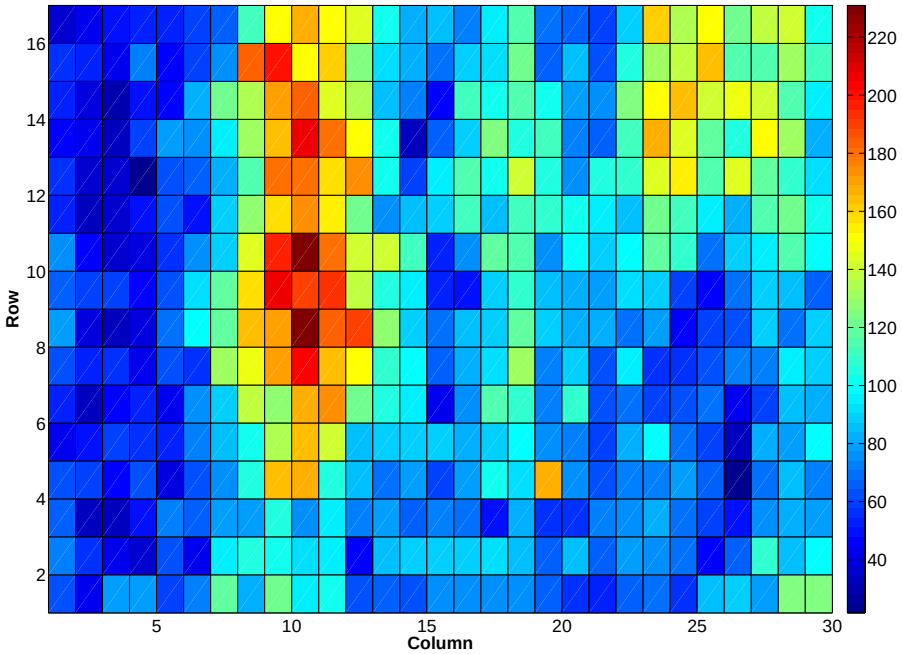

(b) Fluorochemical distribution with signal processing

Figure 93: Fluorochemical distribution profile for carpet MAR-995-6.0-LPB series with 25ppm Rb

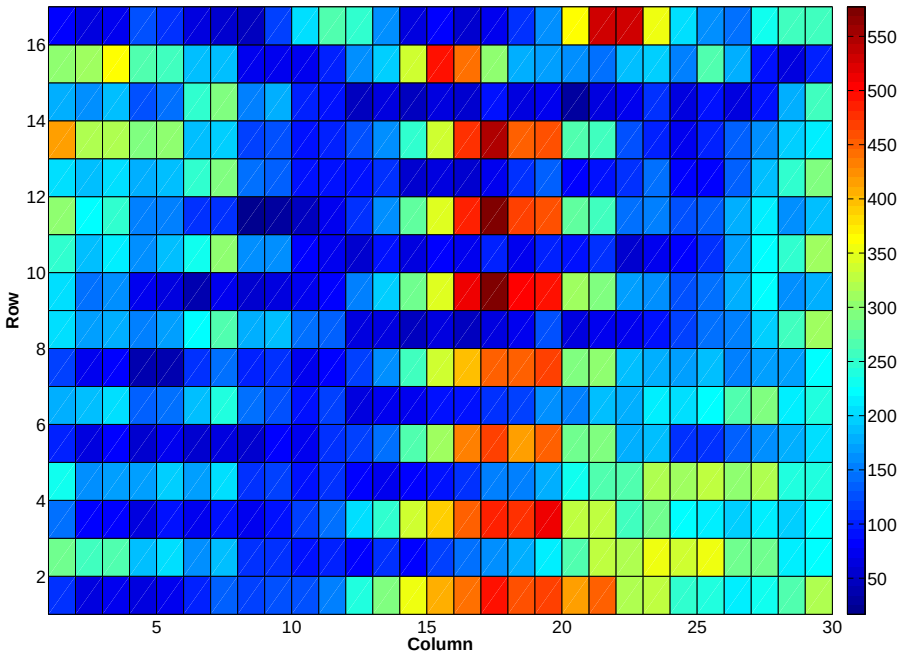

(a) Fluorochemical distribution without signal processing

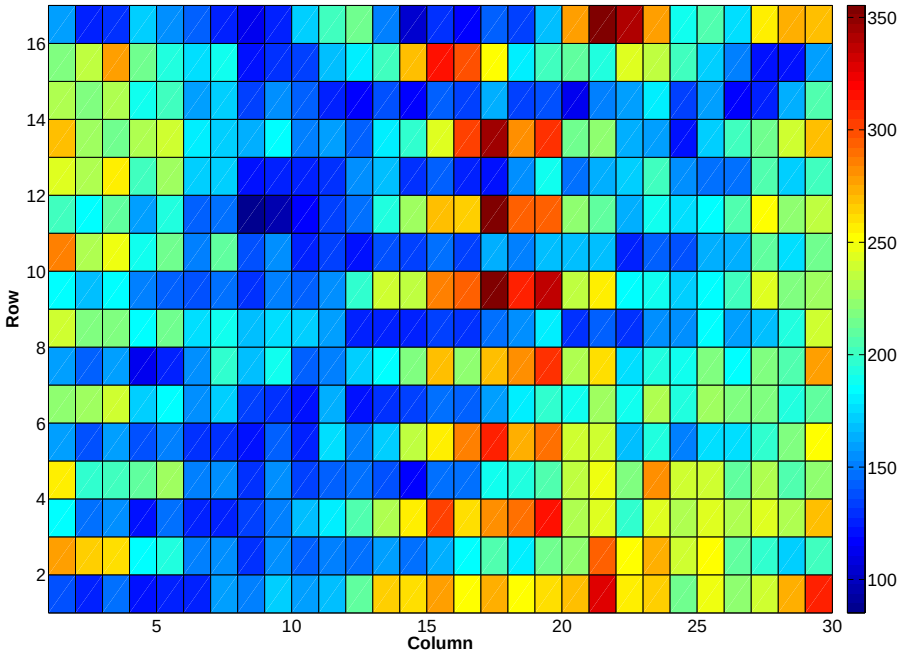

(b) Fluorochemical distribution with signal processing

Figure 94: Fluorochemical distribution profile for carpet MAR-995-6.0-LPB series with 50ppm Rb

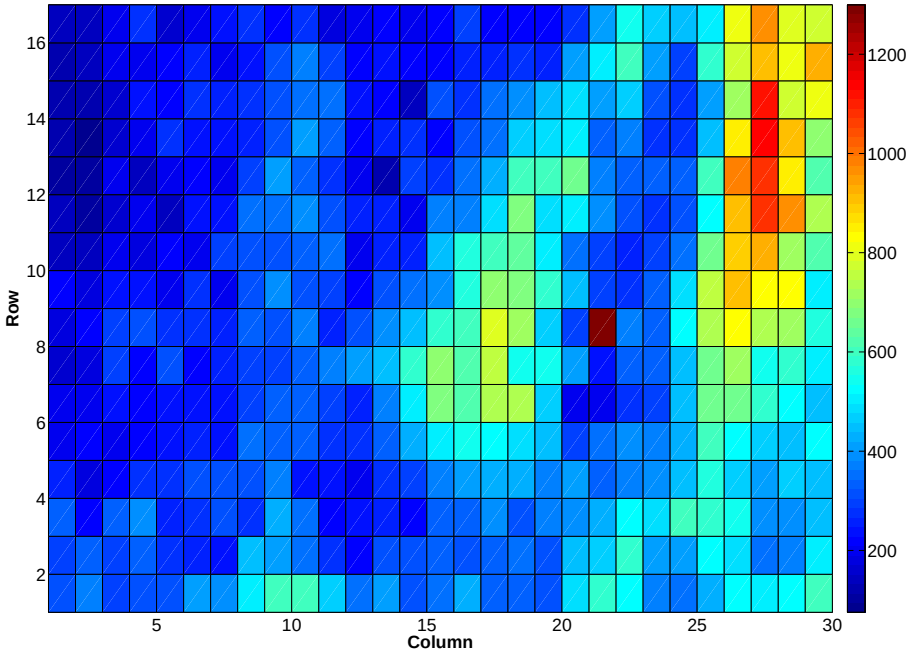

(a) Fluorochemical distribution without signal processing

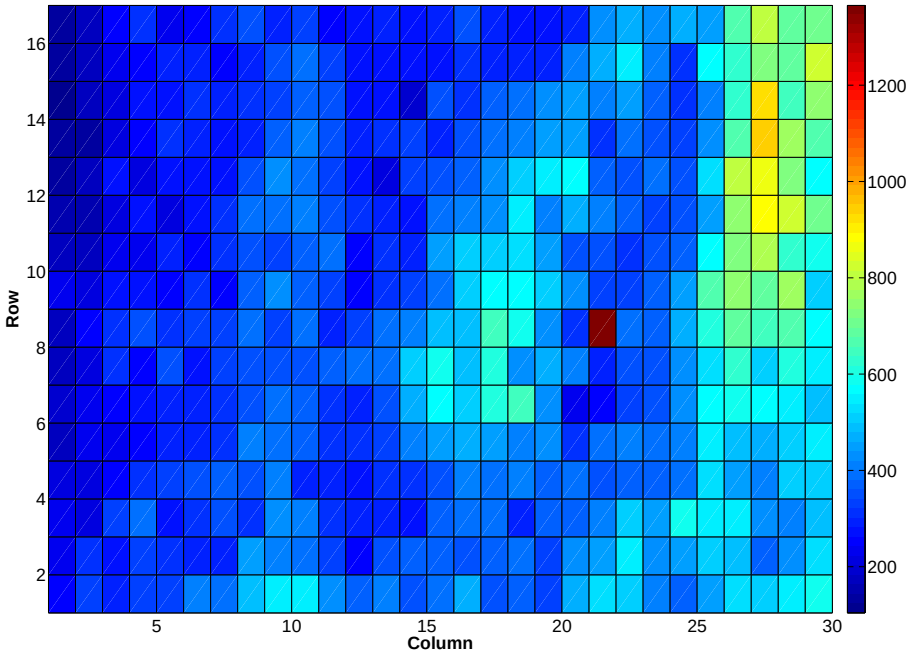

(b) Fluorochemical distribution with signal processing

Figure 95: Fluorochemical distribution profile for carpet MAR-995-6.0-LPB series with 100ppm Rb

APPENDIX E

SYNTHETIC PEAK CALIBRATION PROCEDURE

In Section 6.5, a practical example was presented for synthetically generating XRF spectra for carpet samples. Specifically, spectra that would suffice as calibration standards for the actual quality control of determining fluorochemical concentrations during the carpet manufacturing process. This appendix provides two additional sets of synthetic XRF spectra for each of three other types of carpet to explore the feasibility of the proposed algorithms introduced by this study. Using the same set of measurement settings and signal processing algorithms as in Section 6.5, the same set of fluorochemical stock solution samples were used as reference samples.

The carpet type first used here to demonstrate the feasibility of generating synthetic spectra is the MAR-995-BMK series carpet, which were manufactured with 0, 25, 50, and 100 ppm of Rb. For each sample, twenty five XRF measurements were obtained using the same methodology as described in Section 6.5. The average of these spectra for each sample was processed using the same signal processing algorithms shown previously in Table 26. Matching the fluorochemical spectra background to the blank BMK carpet sample yields the characteristic peak counts shown in Table 50. These spectra are also plotted in Figure 96.

Table 50: Actual Rb concentration in stock solution and the peak counts resulting from background matched to BMK carpet

Targeted Rb Concentration On Carpets (ppm)	Actual Rb Concentration In Stock Solution (ppm)	Average Rb Counts (counts)
25	208	1018
50	417	2148
100	833	3890

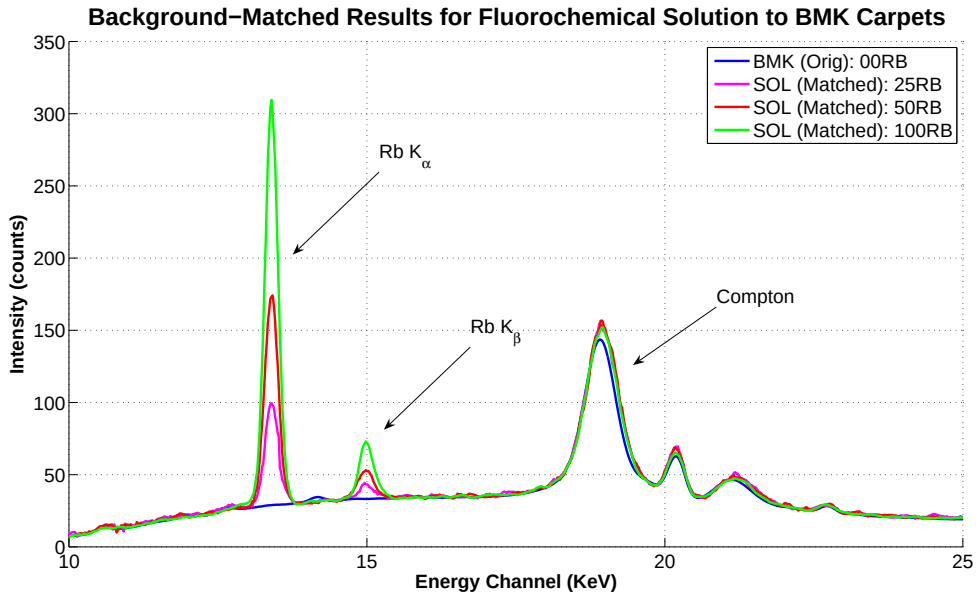

Figure 96: Results from matching Rb-tagged fluorochemical samples to the blank BMK carpet

These new synthetic peak counts generate a new calibration curve of $C = 0.22I - 29.98$ with the fitting factor of 1.00. To follow the same methodology in Section 6.5, the characteristic peak width and height are adjusted to match those from the BMK carpet samples, the results for these synthetic spectra are compared with the actual carpet spectra shown in Figure 97, 98, and 99 for 25, 50, and 100 ppm Rb-tagged carpet, respectively.

XRF spectra were also acquired and processed from three additional carpet samples in the BMK carpet series, which were tagged with 25, 50, and 100 ppm Rb by the manufacturer. The same procedures described above were used for measurements and processing of spectra data. The industrial standard AATCC tests were also performed on samples from these carpets and results shown in Table 51. Table 52 shows the performance evaluation for this above set of synthetically derived XRF calibration spectra.

The same procedures were repeated for the MAR-995-FRB carpet series and the fluorochemical solution calibration curve, based on the background matching results

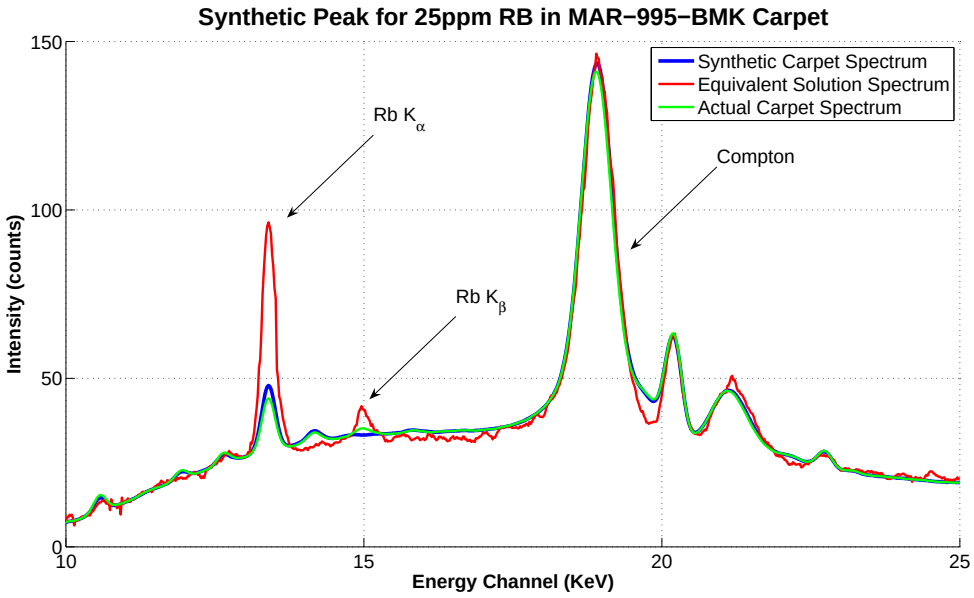

Figure 97: Synthetic and actual Rb K_α peak from carpet and stock solution for 25 ppm Rb

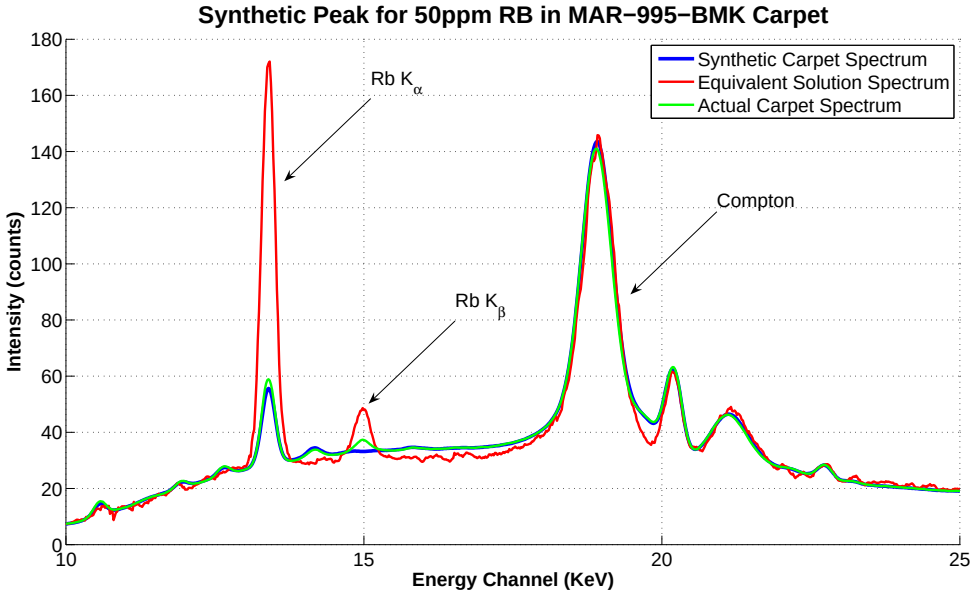

Figure 98: Synthetic and actual Rb K_α peak from carpet and stock solution for 50 ppm Rb

shown in Table 54, is $C = 0.22I - 30.05$ with a fitting score of 1.00. The characteristic peak width and height were adjusted to match those from the FRB carpet samples, and the results for these synthetic spectra are compared with the actual measured

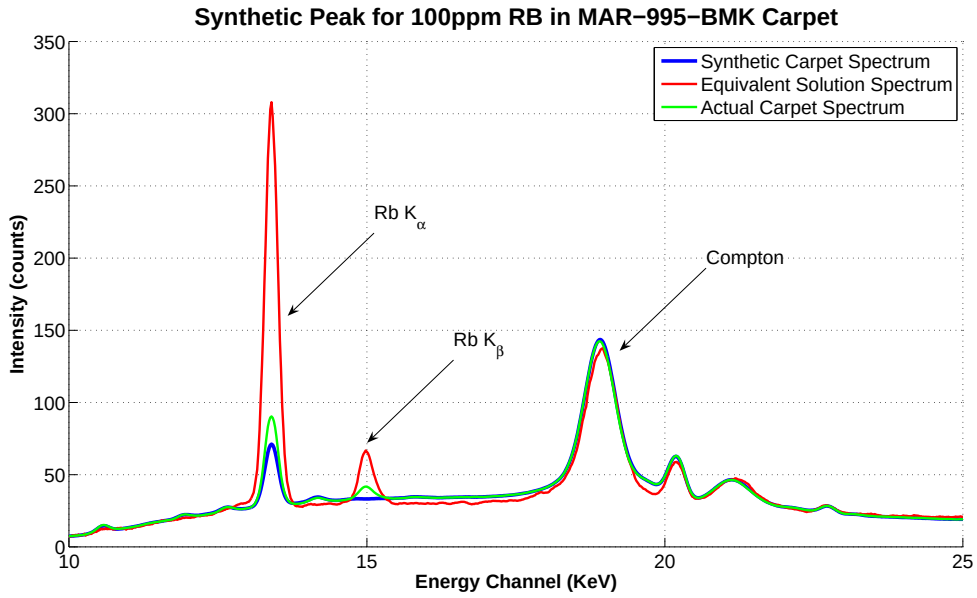

Figure 99: Synthetic and actual Rb K_α peak from carpet and stock solution for 100 ppm Rb

Table 51: Targeted and actual fluorochemical (F) and its translated taggant (Rb) concentration on BMK carpets using AATCC test

Carpet Sample	Targeted Rb (ppm)	Targeted F (ppm)	Actual F (ppm)	Translated Rb (ppm)
BMK_00RB	0	0	33	0
BMK_25RB	25	75	110	34
BMK_50RB	50	150	146	45
BMK_100RB	100	300	355	125

Table 52: Performance evaluation for synthetic peak generation for MAR-995-BMK carpet series without correction

Targeted Rb (ppm)	Actual Rb (ppm)	Translated F (ppm)	AATCC F (ppm)	Error (ppm)
25	21.10	63.29	110.00	-46.71
50	67.79	203.37	146.00	57.37
100	164.45	493.34	355.00	138.34

carpet spectra in Figure 101, 102, and 103 for 25, 50, and 100 ppm Rb-tagged carpet, respectively.

Table 53: Performance evaluation for synthetic peak generation for MAR-995-BMK carpet series with correction

Targeted Rb (ppm)	Actual Rb (ppm)	Translated F (ppm)	AATCC F (ppm)	Error (ppm)
25	15.75	47.25	110.00	-62.75
49	61.33	183.99	146.00	37.99
100	155.69	467.06	355.00	112.06

Table 54: Actual Rb concentration in stock solution and the peak counts resulting from background matched to FRB carpet

Targeted Rb Concentration On Carpets (ppm)	Actual Rb Concentration In Stock Solution (ppm)	Average Rb Counts (counts)
25	208	1037.08
50	417	2187.45
100	833	3962.50

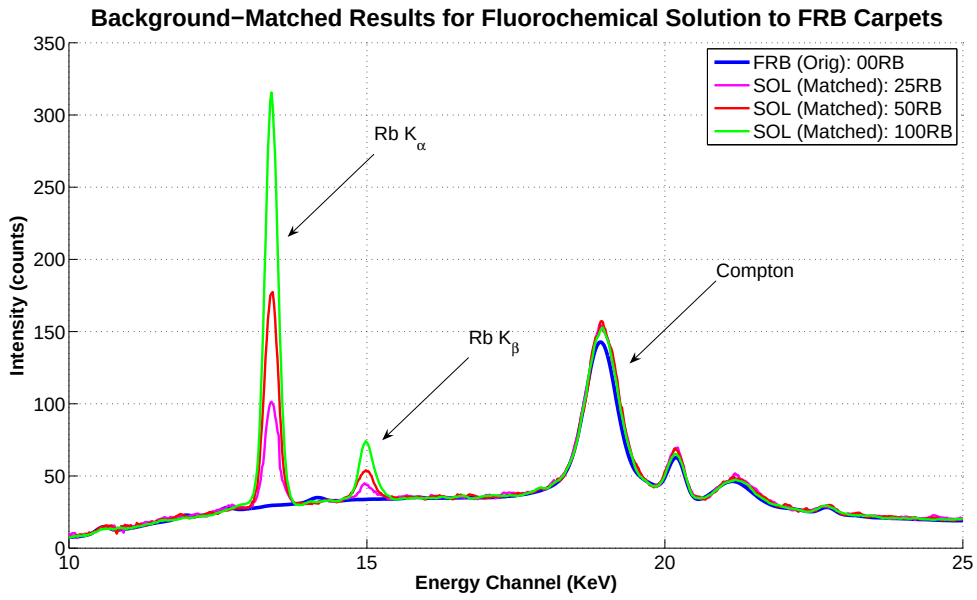

Figure 100: Results from matching Rb-tagged fluorochemical samples to the blank FRB carpet

Following the same procedures, XRF spectra from three additional carpets in the FRB carpet series, which were tagged with 25, 50, and 100 ppm Rb by the manufacturer, were acquired and processed. The results from the AATCC tests performed on

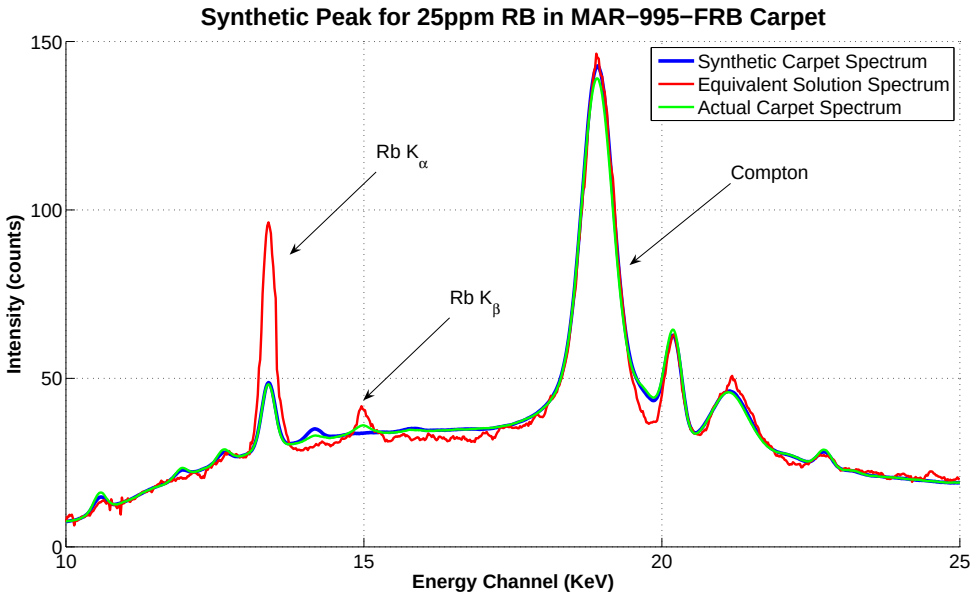

Figure 101: Synthetic and actual Rb K_α peak from carpet and stock solution for 25 ppm Rb

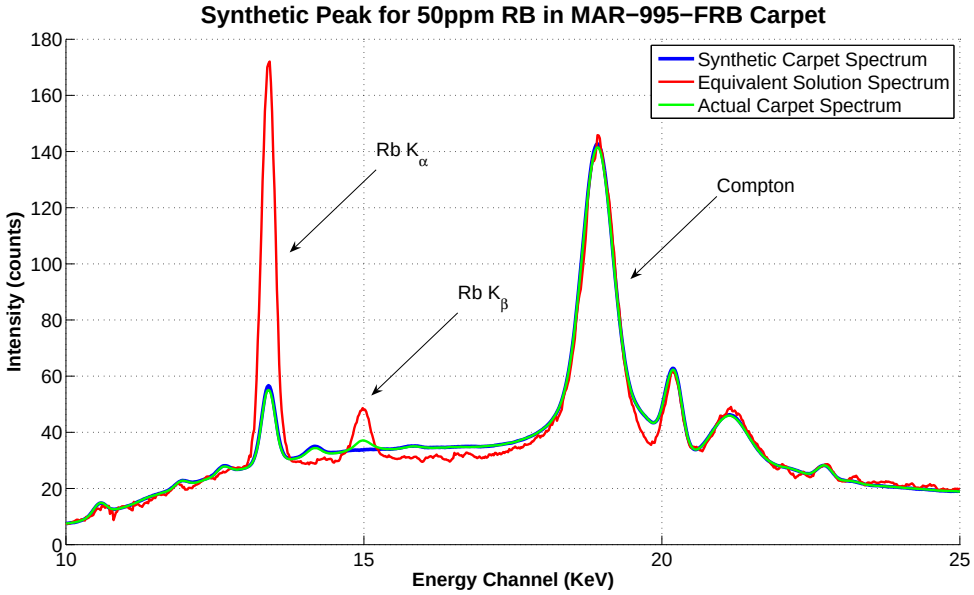

Figure 102: Synthetic and actual Rb K_α peak from carpet and stock solution for 50 ppm Rb

these carpets are shown in Table 55 and the performance evaluations for the synthetically derived calibration are shown in Table 56.

In all carpet calibration examples using synthetically generated reference spectra,

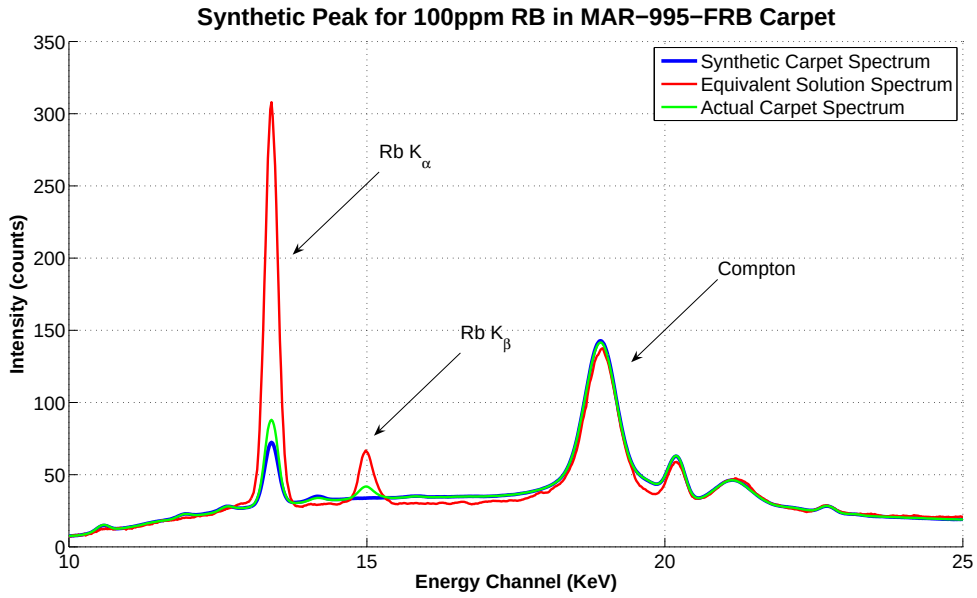

Figure 103: Synthetic and actual Rb K_α peak from carpet and stock solution for 100 ppm Rb

Table 55: Targeted and actual fluorochemical (F) and its translated taggant (Rb) concentration on FRB carpets using AATCC test

Carpet Sample	Targeted Rb (ppm)	Targeted F (ppm)	Actual F (ppm)	Translated Rb (ppm)
FRB_00RB	0	0	33	0
FRB_25RB	25	75	103	34
FRB_50RB	50	150	133	45
FRB_100RB	100	300	374	125

Table 56: Performance evaluation for synthetic peak generation for MAR-995-FRB carpet series without correction

Targeted Rb (ppm)	Actual Rb (ppm)	Translated F (ppm)	AATCC F (ppm)	Error (ppm)
25	31.15	93.46	103.00	-9.54
50	53.07	159.22	133.00	26.22
100	151.62	454.85	347.00	107.85

the additional reference data obtained from an actual AATCC burn test can reduce the overall errors of the calibration. The calibration results shown in this appendix

Table 57: Performance evaluation for synthetic peak generation for MAR-995-FRB carpet series with correction

Targeted Rb (ppm)	Actual Rb (ppm)	Translated F (ppm)	AATCC F (ppm)	Error (ppm)
25	27.96	83.89	103.00	-19.11
49	50.27	150.81	133.00	17.81
100	150.56	451.67	347.00	104.67

suggest that more than one calibration data point from standard AATCC burn test is required to further reduce the error of the XRF calibration process using synthetically generated spectra.

REFERENCES

[1] Von Moody and Howard L. Needles. *Tufted Carpet: Textile Fibers, Dyes, Finishes, and Processes*. William Andrew Publishing, Norwich, New York, 2004.

[2] AATCC Committee RA57. Fluorine content of carpet fibers. Technical report, American Association of Textile Chemists and Colorists (AATCC), Research Triangle Park, NC, 2007.

[3] M. Mantler and N. Kawahara. How accurate are modern fundamental parameter methods? *The Rigaku Journal*, 21(2):17–25, 2004.

[4] K. Hamalainen V. Honkimaki and S. Manninen. Quantitative X-ray fluorescence analysis using fundamental parameters: application to gold jewelry. X-*ray spectrometry*, 25(25):215–220, 1996.

[5] Rudolf O. Muller. *Spectrochemical Analysis by* X-*ray Fluorescence*. Plenum Publishing Corporation, New York, New York, 1972.

[6] J. A. Bearden. X-ray wavelengths and W-ray atomic energy levels. *Reviews of Modern Physics*, 31(1), 1967.

[7] Ron Jenkins, R. W. Gould, and Dale Gedcke. *Quantitative* X-*ray Spectrometry*. Marcel Dekker, Inc, New York, New York, 1981.

[8] J. H. Hubbell and S. M. Seltzer. Tables of X-ray mass attenuation coefficients and mass energy-absorption coefficients from 1 KeV to 20 MeV for elements z = 1 to 92 and 48 additional substances of dosimetric interest. Web site database, October 2010. http://www.nist.gov/pml/data/xraycoef/index.cfm.

[9] Rene E. Van Grieken and Andrzej A. Markowicz. *Handbook of* X-*ray Spectrometry: Method and Techniques*. Marcel Dekker, Inc, New York, New York, 1992.

[10] D. H. Wilkinson. Breit-Wigners viewed through Gaussians. *Nuclear Instruments and Methods*, 95(1):295–364, August 1971.

[11] R. Gunnink. An algorithm for fitting Lorentzian-broadened, K-series X-ray peaks of the heavy elements. *Nuclear Instruments and Methods*, 143(1):145–149, May 1977.

[12] Reinhold Schlotz and Stefan Uhlig. *Introduction to* X-*ray Fluorescence (*XRF*)*. Bruker AXS Inc., Madison, Wisconsin, 2000.

[13] J. W. Criss, L. S. Birks, and J. V. Gilfrich. Versatile X-ray analysis program combining fundamental parameters and empirical coefficients. *Analytical Chemistry*, 50(1):33–37, January 1978.

[14] J. U. Jordanov, T. S. Tsanov, R. Stefanov, and N. Jordanov. Problems of automatic qualitative X-ray fluorescence analysis: Part one. X-*ray Spectrometry*, 16(6):255–259, November 1987.

[15] A. Rindby. Software for energy-dispersive X-ray fluorescence. X-*ray Spectrometry*, 18:113–118, 1989.

[16] Richard M. Rousseau. Detection limit and estimation of uncertainty of analytical XRF results. *The Rigaku Journal*, 18(2):33–47, 2001.

[17] IAEA. *QXAS: Quantitative* X-*ray Analysis System.* IAEA Laboratories Seibersdorf, Seibersdorf, Austria, 2005.

[18] E. L. Torres, M. V. Fuentes, and E. D. Greaves. SAX, software for the analysis of X-ray fluorescence spectra. X-*ray Spectrometry*, 27:161–165, 1998.

[19] P. H. Abbott and M. J. Adams. AXIS: Automated XRF interpretation of spectra. X-*ray Spectrometry*, 26:125–131, 1997.

[20] S. Steenstrup. A simple procedure for fitting a background to a certain class of measured spectra. *Journal of Applied Crystallography*, 14(4):226–229, August 1981.

[21] Mike J. Adams. *Chemometrics in Analytical Spectroscopy.* Royal Sciety of Chemistry, Cambridge, United Kingdom, 2nd edition, 2004.

[22] Ron Jenkins. X-*ray Fluorescence Spectrometry.* John Wiley & Sons, Inc, New York, New York, 2nd edition, 1999.

[23] A. Likar and T. Vidmar. A peak-search method based on spectrum convolution. *Journal of Physics D: Applied Physics*, 36:1903–1909, 2003.

[24] J. de Donder J. Hertogen and R. Gijbels. Experimental data on photopeak integration methods in activation analysis. *Nuclear instruments and methods*, 115(1):197–212, February 1974.

[25] H. J. Lucas-Tooth and B. J. Price. A mathematical method for the investigation of inter-element effects in X-ray fluorescent analyses. *Metallurgia*, 64(383):149–152, September 1961.

[26] H. J. Lucas-Tooth and C. Pyne. The accurate determination of major constituents by X-ray fluorescent analysis in the presence of large interelement effects. *Advances in* X-*ray Analysis*, 7:523–541, 1963.

[27] Jacob Sherman. The theoretical derivation of fluorescent X-ray intensities from mixtures. *Spectrochimica Acta*, 7:283–306, 1955.

[28] J. W. Criss. Fundamental-parameters calculations on a laboratory microcomputer. *Advance X Ray Anal*, pages 93–97, 1980.

[29] Richard M. Rousseau and Jacques A. Boivin. The fundamental algorithm: A natural extension of the Sherman equation part i: Theory. *The Rigaku Journal*, 15(1):13–28, 1998.

[30] J. W. Criss and L. S. Birks. Intensity formulae for computer solution of multicomponent electron probe specimens. *Proceedings of The First National Symposium on The Electron Microprobe*, pages 217–236, 1966.

[31] J. W. Criss and L. S. Birks. Calculation methods for fluorescent X-ray spectrometry. *Analytical Chemistry*, 40(7):1080–1086, June 1968.

[32] W. K. de Jongh. X-ray fluorescence analysis applying theoretical matrix corrections. stainless steel. *Norelco Reporter*, 23(1):26–31, April 1976.

[33] G. R. Lachance and R. J. Traill. A new approach to X-ray spectrochemical analysis. *Geological Survey of Canada*, (64):57–79, 1965.

[34] S. D. Rasberry and K. F. J. Heinrich. Calibration for interelement effects in X-ray fluorescence analysis. *Analytical Chemistry*, 46(1):81–89, 1974.

[35] P. Lemberge and P. J. Van Espen. Quantitative energy-dispersive X-ray fluorescence analysis of liquid using partial least-squares regression. X-*ray Spectrometry*, 28:77–85, 1999.

[36] Yongdong Wang, Xinna Zhao, and Bruce R. Kowalski. X-ray fluorescence calibration with partial least-squares. *Applied Spectroscopy*, 44(6):998–1002, July 1990.

[37] M. I. M. S. Bueno I. Facchin, C. Mello and R. J. Poppi. Simultaneous determination of lead and sulfur by energy-dispersive X-ray spectrometry. comparison between artificial neural networks and other multivariate calibration methods. X-*ray Spectrometry*, 28:173–177, 1999.

[38] E. Kowalska and P. Urbanski. XRF full-spectrum calibration technique using artificial neural network. *Nukleonika*, 42(4):879–887, 1997.

[39] Liqiang Luo. An algorithm combining neural networks with fundamental parameters. X-*ray Spectrometry*, 31:332–338, 2002.

[40] Ron Jenkins and J. L. De Vries. *Practical* X-*ray Spectrometry*. Springer - Verlag New York, Inc, New York, New York, 2nd edition, 1999.

[41] S. Uhlig, K.-E. Mauser, and G. Granacher. Multi-element analysis by modern X-ray fluorescence analysis. *Bruker Report*, (145):17–19, 1998.

[42] Y. Hasakawa. Online element analysis by energy distributed fluorescence X-ray method. *Instrumentation*, 29(12):51–58, December 1986.

[43] D. Wegrzynek E. Chinea Cano S. A. Bamford R. Padilla Alvarez, A. Markowicz and D. Hernandez Torres. Quality management and method validation in EDXRF analysis. X-*ray Spectrometry*, 36:27–34, 2007.

[44] John Baliga. RoHS verification using XRF. *Semiconductor International*, 28(13):32, 2005.

[45] Scott OConnell Puneet Shrivastava and Allen Whitley, editors. *Handheld X-ray fluorescence: practical application as a screening tool to detect the presence of environmentally-sensitive substances in electronic equipment, number = 17, series =.*

[46] Olli Haavisto, Jani Kaartinen, and Heikki Hytyniemi. Optical spectrum based estimation of grades in mineral flotation. *Proceedings of the* IEEE *International Conference on Industrial Technology*, pages 2529–2534, December 2006.

[47] Itzhak Mazor Avishai KeptenC Roey Shavivc Yosi Shacham-Diamanda, Boris Yokhin and Ayelet Gabaic. At-line X-ray fluorescence metrology of metals and ultra-thin barrier layers for ULSI applications. SPIE *Conference on In-line Characterization Techniques for Performance and Yield*, 3509:88–94, 1998.

[48] M. Wickham and C. Hunt. XRF equipment as a RoHS screening tool. *Circuits Assembly*, 19:26, 28, 30, 32, February 2008.

[49] William B. Davis Robert D. Giauque Daniel Turler, Murat Karaca and Deborah Hopkins. Improved process control through real-time measurement of mineral content. Conference: Society of mining engineering annual meeting and exhibit, Phoenix, AZ, November 2001. USDOE Assistant Secretary for Energy Efficiency and Renewable Energy. Office of Industrial Technologies (US).

[50] Oliver Hahn Wolfgang Malzer and Birgit Kanngiesser1. A fingerprint model for inhomogeneous ink-paper layer systems measured with micro-X-ray fluorescence analysis. X-*ray Spectrometry*, 33:229–233, 2004.

[51] T. Calligaro G. Demortier A. Hautojarvi M. Mader L. Martinot M. Schreiner T. Tuurnala C. Neelmeijer, I. Brissaud and G. Weber. Paintings - a challenge for XRFand PIXE analysis. X-*ray Spectrometry*, 29.

[52] Christopher J. Scolese. TRACeR helps identify materials and authenticate parts. Technical report, National Aeronautics and Space Administration (NASA), Washington, DC, 2007.

[53] Robert Kravitz. How science fiction resulted in better carpet extractors. Cleaning & Restoration Magazine, October 2006. www.ascr.org.

[54] Ravi Yellepeddi and Robert Thomas. New developments in wavelength- dispersive XRF and XRD for the analysis of foodstuffs and phamaceutical materials. *Spectroscopy*, 21(9):36–41, 2006.

[55] Samuel Floyd Carl Selavka Gerald Zeosky Norman Gahn Timothy McClanahan Jeffrey Schweitzer, Jacob Trombka and Thomas Burbine. Portable generator-based XRF instrument for non-destructive analysis at crime scenes. *Nuclear Instruments and Methods in Physics Research*, 241:423–427, 2005.

[56] V. I. Kazimirov, A. D. Zorin, and V. F. Zanozina. Application of X-ray fluorescence analysis to investigation of the composition of gunshot residues. *Journal of Applied Spectroscopy*, 73:359–365, 2006.

[57] Laurent Mahuteau. *Study of algorithms for analysis of* XRF *spectra to automate inspection of carpets.* Master thesis, Georgia Institute of Technology, School of Electrical and Computer Engineering, 2008.

[58] AutoItScript. AutoItScript: Automation and scripting language. http://www.autoitscript.com/site/autoit/. Last retrieved: August 12, 2010.

[59] Bruker AXS. *Bruker* S*1* TRACeR *Portable* XRF *Analyzer (User Manual).* Bruker AXS Inc., Kennewick, WA, 2007.

[60] Eugene P. Bertin. *Principles and Practice of* X*-ray Spectrometric Analysis.* Plenum Press, New York, New York, 2nd edition, 1975.

[61] C. G. Ryan, E. Clayton, W. L. Griffin, S. H. Sie, and D. R. Cousens. SNIP, a statistics-sensitive background treatment for the quantitative analysis of PIXE spectra in geoscience applications. *Nuclear Instruments & Methods in Physics Research, Section B (Beam Interactions with Materials and Atoms)*, B34(3):396–402, September 1988.

[62] V. V. Monakhov, P. A. Naumenko, and O. A. Chashinskaya. An envelope method for removing background from X-ray fluorescence spectra. *Instruments and Experimental Techniques*, 49(1):56–60, 2006.

[63] Antonio Brunetti. Removal of the continuum of X-ray spectra using morphological operators. IEEE *Transactions on Nuclear Science*, (5):2281–2287, 1998.

[64] Frederick H. Schamber. Curve fitting techniques and their application to the analysis of energy dispersive spectra. *Proceedings of the Workshop on Energy Dispersive* X*-ray Spectrometry*, pages 193–231, April 1979.

[65] A. J. Antolak M. L. Hildner and G. S. Bench. Improved fitting of PIXE spectra: the Voigt profile and Si(Li) detector modeling. *Nuclear instruments and methods*, 373:124–130, 1995.

[66] R. L. Myklebust C. E. Fiori and K. Gorlen, editors. *Sequential* SIMPLEX*: A procedure for resolving spectral interference in energy dispersive* X*-ray spectrometry", series =.*

[67] G. R. Lachance and R. J. Traill. A practical solution to the matrix problem in X-ray analysis, part 1: Method. *Canadian Spectroscopy*, pages 43–48, March 1966.

[68] G. R. Lachance and R. J. Traill. A practical solution to the matrix problem in X-ray analysis, part 2: Application to a multicomponent alloy system. *Canadian Spectroscopy*, pages 63–71, May 1966.

[69] Kevin Ashley and Mary E. McKnight. Lead abatement in buildings and related structures. *Stadardization News*, 21(12):32–29, 1993.

[70] L. S. Birks. X-*ray Spectrochemical Analysis*. Interscience Publisher, INC., New York, New York, 1959.

[71] A. Buhler and A. Seyfarth. X-ray fluorescence analysis for process control in the minerals and mining industries. *Bruker Report*, (145):20–22, 1998.

[72] Z. W. Chen, Berry Beumer Danhong Li, Kai Xin, and Jay Burdett. Online total chlorine analysis using monochromatic wavelength-dispersive XRF for crude oil. *Proceedings of the Annual ISA Analysis Division Symposium, 2008, Proceedings of AD 2008 - 53rd Analysis Division Symposium on Analytical Solution for Process Control and Compliance*, April 2008.

[73] J. E. Fernandez and A. Tartari. EDXRF procedure for quantitative analysis matching theoretically generated reference spectra to measured spectra. X-*ray Spectrometry*, 24:277–282, 1995.

[74] Gene S. Hall and Julie Tinklebberg. Determination of Ti, Zn, and Pb in lead-based house paints by EDXRF. *Journal of Analytical Atomic Spectrometry*, 18(7):775–778, July 2003.

[75] J. P. Willis and G. R. Lachance. Comparison between some common influence coefficient algorithms. X-*ray spectrometry*, 33:181–188, February 2004.

[76] G. R. Lachance. Demystification of algorithms and influence coefficients in quantitative XRF analysis. *International Centre for Diffraction Data*, pages 718–731, 1999.

[77] P. Mazurkiewicz. A fast and inexpensive product screening method for R.O.H.S. compliance. ISTFA *2005. Proceedings of the 31st International Symposium for Testing and Failure Analysis*, pages 451–456, 2005.

[78] F. M. V. Pereira and M. I. M. Bueno. Calibration of paint and varnish properties: potentialities using X-ray spectroscopy and partial least squares. *Chemometrics and Intelligent Laboratory Systems*, 92(2):131–137, 2008.

[79] Richard M. Rousseau. The fundamental algorithm: An exhaustive study of the Claisse-Quintin algorithm and the Tertian and Lachance identities part ii: Application. *The Rigaku Journal*, 15(1):14–25, 1998.

[80] Richard M. Rousseau. Debate on some algorithms relating concentration to intensity in XRF spectrometry. *The Rigaku Journal*, 19(1):25–34, 2002.

[81] Richard M. Rousseau. Corrections for matrix effects in X-ray fluorescence analysis - a tutorial. *Spectrochimica Acta - Part B Atomic Spectroscopy*, 61(7):759–777, 2006.

[82] Richard M. Rousseau, James P. Willis, and Andrew R. Duncan. Practical XRF calibration procedures for major and trace elements. X-*ray Spectrometry*, 25:179–189, 1996.

[83] F. Schimidt, L. Cornejo-Ponce, M. I. M. S. Bueno, and R. J. Poppi. Determination of some rare earth elements by EDXRF and artificial neural networks. X-*ray Spectrometry*, 32(6):423–427, November 2003.

[84] M. A. Short and E. J. Bonner. X-ray bremsstrahlung spectra. X-*ray Spectrometry*, 18:183–186, 1989.

[85] A. D. Sokolov, D. Docenko, E. Bliakher, O. Shirokobrod, and J. Koskinen. Online analysis of chrome-iron ores on a conveyor belt using X-ray fluorescence analysis. X-*ray Spectrometry*, 34(5):456–459, September 2005.

[86] J. Swerts, A. Aerts, N. De Biscop, F. Adams, and P. Van Espen. Age determination of chinese porcelain by X-ray fluorescence and multivariate analysis. *Chemometrics and Intelligent Laboratory Systems*, 22(1):97–105, January 1994.

[87] V. Vigneron, J. M. Martinez, A. C. Simon, and R. Junca. Measurement of uranium quantities by X-ray fluorescence using neuronal techniques. *Proceedings of 17th Symposium on Safeguards and Nuclear Material Management*, pages 715–722, May 1995.

[88] G. J. Weltje and R. Tjallingii. Calibration of XRF core scanners for quantitative geochemical logging of sediment cores: theory and application. *Earth and Planetary Science Letters*, 274(3):423–438, October 2008.

[89] Margaret West, Andrew T. Ellis, Peter Kregsamer, Phillip J. Potts, and Christina Streli. Atomic spectrometry update. X-ray fluorescence spectrometry. *Journal of Analytical Atomic Spectrometry*, 23:1409–1437, 2008.